HIGHWAY RESEARCH RECORD

Number 343

Design of Traffic Safety Barriers

10 Reports

Subject Areas

22 Highway Design
27 Bridge Design
51 Highway Safety

HIGHWAY RESEARCH BOARD
DIVISION OF ENGINEERING NATIONAL RESEARCH COUNCIL
NATIONAL ACADEMY OF SCIENCES—NATIONAL ACADEMY OF ENGINEERING
WASHINGTON, D.C. 1971

ISBN 0-309-01849-8

Price: $4.00

Available from

Highway Research Board
National Academy of Sciences
2101 Constitution Avenue
Washington, D.C. 20418

GROUP 2—DESIGN AND CONSTRUCTION OF TRANSPORTATION FACILITIES

John L. Beaton, California Division of Highways, Sacramento, chairman
William G. Gunderman, Highway Research Board staff

SECTION A—GENERAL DESIGN

F. A. Thorstenson, Minnesota Department of Highways, St. Paul, chairman
Lawrence F. Spaine, Highway Research Board staff

Committee 4—Traffic Safety Barriers and Sign, Signal and Lighting Supports
Eric F. Nordlin, California Division of Highways, Sacramento, chairman
Verdi Adam, W. C. Anderson, William C. Burnett, Edward M. Conover, James J. Crowley, Albert L. Godfrey, Sr., Malcolm D. Graham, Alf H. Hansen, Wayne Henneberger, Robert N. Hunter, Jack E. Leisch, Edwin C. Lokken, Jarvis D. Michie, Gilbert E. Morris, Jr., Robert M. Olson, John M. Quigg, Edmund R. Ricker, Neilon J. Rowan, Frank G. Schlosser, Paul C. Skeels, Flory J. Tamanini, James A. Thompson, Charles Y. Warner, M. A. Warnes, Earl C. Williams

SECTION C—BRIDGE

Arthur L. Elliott, California Division of Highways, Sacramento, chairman
Lawrence F. Spaine, Highway Research Board staff

Committee 1—Bridge Design
Richard J. Posthauer, New York State Department of Transportation, Albany, chairman
William L. Armstrong, Neal H. Bettigole, Louis M. Bjorn, J. N. Clary, Arthur L. Elliott, Frede Gloersen, George C. Goble, Theodore R. Higgins, Nelson C. Jones, Robert J. McDonagh, Robert M. Olson, Adrian Pauw, Donald A. Recchio

FOREWORD

Traffic barriers are installed to protect errant vehicles from roadside hazards that cannot be eliminated or to prevent head-on collisions on divided highways having narrow medians. The strength and safety characteristics of traffic barriers may be evaluated by subjecting prototype designs to full-scale collisions by vehicles, by computer simulation of collisions, or by scale-model tests. Traffic safety barriers on bridges, shoulders, and in medians must have compatible strength and geometric characteristics, and energy-absorbing devices are required at certain locations. Highway engineers having responsibility for designing, constructing, and maintaining traffic safety barriers will find the ten papers contained in this RECORD to be of interest.

The first paper describes a computer program for simulating automobile collisions with barriers. Powell presents results for two barriers and describes the procedure used to synthesize and solve the problem. Input data are obtained from experimental data, and output predictions are compared with available test data.

Warner and Walker report on tests comparing a contemporary guardrail with a similar barrier equipped with energy-absorbing cartridges constructed of lightweight concrete. The authors conclude that these prototype cartridges, which are described in detail, can reduce decelerations on vehicles by 20 to 30 percent and provide other safety characteristics as well as provide a favorable cost-benefit ratio.

In the third paper, Michie, Gatchell, and Duke discuss experiments on guardrail posts using an instrumented pendulum to obtain data on more than 100 timber and several steel specimens. They evaluated the information collected and concluded that "Peak force, average force, and fracture energy are...a direct and linear function of moment of inertia."

Six full-scale crash tests were conducted to evaluate timber weak-post guardrail systems by Bronstad and Burket, who found that "...a $\frac{1}{4}$-in. diameter steel bolt and a pipe insert provide proper attachment of rail to post." The results of a test on a transition between the developmental system and the Ohio Department of Highways standard design are also presented.

A series of tests on bridge barriers by the California Division of Highways is described by Nordlin, Woodstrom, Folsom, and Hackett, who report the results of five full-scale crash tests on a 27-in. high reinforced concrete parapet with a traffic-side contour similar to the New Jersey median barrier. A 12-in. high steel tube rail is mounted on top of the parapet. Tests at speeds of 45 to 66 mph and impact angles of 7, 15, and 25 deg indicate that high-speed impacts produce negligible vehicle damage at angles up to 7 deg, moderate damage as impact angles approach 15 deg, and severe damage at angles of 25 deg.

Two researchers at the University of Denver conducted a scale-model test of a crash cushion barrier. Fay and Wittrock found that the model test agreed well with results from a full-scale test of the prototype. Modeling techniques are presented, and similitude requirements for scale modeling of car and barrier are included.

Warner and Free of Brigham Young University report the results of computer simulation of a water-plastic impact cushion and compare the model predictions with results from full-scale tests. The model was also

employed to predict vehicle response, and the authors conclude that "Predictions show that the water-plastic unit provides good performance across the spectrum of impacting vehicle momenta, and that it provides a response that takes advantage of almost all the available stopping distance for impacts between 30 to 70 mph, employing vehicles weighing from 2,000 to 6,000 lb."

Performance of water-filled plastic tubes based on the results of five crash tests is discussed by Hayes, Ivey, and Hirsch. Vehicles ranging in weight from 1,680 to 4,650 lb struck the crash cushion head-on at speeds of 59 to 64 mph. One 59-mph collision at 20 deg with the cushion center line was included. It was found that the cushions performed satisfactorily.

The final two papers by Nordlin, Woodstrom, and Doty describe dynamic tests conducted on two energy-absorbing barriers. The first series consisted of four collisions with water-filled plastic cells that were placed between plywood panels to form a barrier 19.5 ft in length. A 4,700-lb automobile struck the barrier on the nose and side at speeds near 60 mph, and the authors conclude that this barrier configuration, as modified, is recommended for operational installation on a trial basis.

The second series consisted of three crash tests into a barrier constructed of 55-gal steel drums. Automobiles weighing 4,700 lb traveling at 54 to 64 mph collided with the barrier at 0, 9, and 11 deg. The authors state, "The results of the three tests indicate that the barrier effectiveness in reducing the severity of most impacts is such that it should be used operationally on an experimental basis. However, future refinements in the design need to be made, particularly with regard to the method used to redirect vehicles that collide with the side of the barrier."

—Robert M. Olson

CONTENTS

GENERAL COMPUTER PROGRAM FOR ANALYSIS OF AUTOMOBILE BARRIERS

Graham H. Powell, Department of Civil Engineering, University of California, Berkeley

A computer program developed to predict the behavior of an automobile striking a protective barrier is described. The barrier is idealized as a structural framework of arbitrary configuration and the automobile as a body surrounded by a cushion of springs. Large displacements and inelastic behavior, including hysteresis effects on unloading, are considered in the barrier structure. The automobile slides along the barrier, and the effects of normal forces, friction forces, and wheel drag forces are considered in determining its motion. Input data to the program consist of the configuration of the barrier, the properties of the barrier members and automobile, and the trajectory of the automobile before impact. Output consists of time histories of automobile positions, velocities and accelerations, barrier deflections, and barrier member forces. The paper describes the procedure used to solve the problem, discusses the capabilities and limitations of the program, and presents results for two example barriers.

•THE INTERACTION of an automobile with a barrier system is exceptionally difficult to simulate on a computer. Dynamic effects, extremely large displacements, and inelastic behavior must all be considered. Dynamic loads are not explicitly specified but must be determined by satisfying force equilibrium and displacement compatibility between the automobile and barrier.

The objective of the study described in this report has been the development of a computer program to predict the behavior of a wide variety of automobile barrier systems. Because of the complexity of the problem, it has not been possible to develop a computer program that is applicable to all barriers. Nevertheless, barriers of many different types and configurations can be analyzed. The features and limitations of the program are essentially as follows:

1. The barrier is idealized as a two-dimensional structural framework of arbitrary shape.
2. Seven different types of structural members may be specified in any combination. These are beams, cables, springs, ideal columns, viscous damping links, friction damping links, and posts. Two- and three-dimensional elements are not available but can be simulated by equivalent lattices of bars.
3. Nonlinear modes of behavior are assigned to the structural members, and hysteresis effects in yielding members are taken into account. Bilinear elastic-plastic behavior is assumed for each yielding member, but, by combining members in parallel, a variety of more complex force-deformation characteristics can be represented.
4. The automobile is idealized as a rigid body of arbitrary shape surrounded by a cushion of inelastic springs. The automobile boundary is defined by a series of discrete points at which interaction with the barrier may occur.
5. The barrier must possess a clearly defined interface, or series of interfaces, along which interaction with the automobile points takes place. The automobile slides along the barrier interface. Normal and tangential (friction) forces are transmitted.

Sponsored by Committee on Traffic Safety Barriers and Sign, Signal and Lighting Supports and presented at the 50th Annual Meeting.

6. The analysis is two-dimensional in the horizontal plane. Out-of-plane effects, which include vertical displacements of both the automobile and the barrier, are not considered.

The computer program should provide valuable information at two different stages in the evaluation of barrier systems, as follows:

1. At the initial design stage, the program can be used to compare design concepts and to assist in the prototype design; and
2. At the testing stage, if it is shown that the program gives good results for the ranges of parameters considered in the tests, the behavior can be predicted for other values of the parameters, and the number of tests can be reduced.

In all cases, however, the results of the computer analyses should be interpreted cautiously. This is because it is necessary to estimate the structural properties of the barrier members before analyses can be carried out, and it will be found that it is frequently difficult to obtain accurate estimates of these properties. Also, the behavior of a barrier system may be governed as much by the design details of the barrier as by its overall configuration. That is, barriers that may be idealized identically for the purposes of analysis may perform quite differently in actual tests because of differences in their structural details. Final evaluations must therefore be obtained from field tests of actual designs.

In this paper, a brief description of the solution procedure is presented, the idealization of the barrier and automobile structures is explained, and two example analyses are discussed. A more detailed description of the technique, with additional examples, is presented elsewhere (1).

SOLUTION PROCEDURE

A dynamic step-by-step analysis is carried out in which linear structural behavior of the barrier and automobile is assumed within any time step. The conditions at the beginning of any step are known, including the following: (a) the positions, velocities, and accelerations of all points on the automobile and barrier; (b) the magnitudes and directions of the normal and friction forces exerted between the automobile and barrier, and the positions at which they act; and (c) the axial forces and bending moments in the barrier members. The problem is to find these quantities at the end of the time step so that the computation can be continued. A simplified description of the procedure is given in the following.

Step 1. The axial forces and bending moments in the barrier members are examined, and it is determined whether each member is in an elastic or yielded condition at the beginning of the step.

Step 2. A stiffness matrix for the barrier structure, in its deformed configuration, is assembled member by member, taking into account the condition of each member. A yielded member is assigned essentially zero stiffness. This stiffness matrix is then modified to account for inertia, viscous damping, and structural stability effects.

Step 3. The solution of the interaction problem is initiated by allowing the automobile and barrier to move as independent dynamic systems, each under constant load. The loads are the interaction forces at the end of the previous time step. The changes in automobile and barrier positions are determined by structural analysis procedures.

Step 4. Because the automobile and barrier have been permitted to move independently, gaps or overlaps will generally have developed at the automobile-barrier interface. That is, the geometric compatibility condition required for solution of the interaction problem will generally be violated. This must ultimately be corrected, but a further error resulting from allowing the automobile and barrier to move independently is first considered. This error results from the fact that, as the vehicle moves along the barrier interface, the positions of the interaction forces on the barrier change, although their magnitudes may remain constant. That is, the dynamic nature of the loading is due not only to changes in the magnitudes of the loads but also to changes in their positions. The effect of change in position is taken into account as follows: The

;eometrical relationships at the automobile-barrier interface at the end of Step 3 are ɔxamined. New locations on the barrier interface are determined for all automobile ɔoints that were in contact with the barrier at the beginning of the time step. New nor-nal and tangential directions to the barrier are also determined at each of these points. Γhe change in barrier load resulting from change in automobile position is therefore ɗetermined by removing the normal and tangential forces from the barrier at their ɔositions at the beginning of the time step and by reapplying them in their new positions. Γhe barrier displacements resulting from this load change are determined and added to ɕhe displacements computed in Step 3. New automobile positions are also determined, allowing for the slight changes in direction of the normal and tangential forces.

Step 5. The automobile and barrier positions at the end of Step 4 have been determined on the assumption that the interaction forces remain constant in magnitude and, as noted previously, will generally not satisfy the geometric compatibility requirement at the interface. Changes in magnitude of the forces must therefore be determined such that compatibility is reestablished. The geometrical relationships at the automobile-barrier interface at the end of Step 4 are examined, and locations are determined for all automobile points potentially in contact with the barrier. Those automobile points overlapping the barrier interface are assumed to be potential contact points. In addition, those points that were in contact with the barrier at the end of the previous time step are potential contact points, although some of these points may not overlap the barrier interface. The normal and tangential directions for each potential contact point are determined, together with the normal distance from each point to the barrier interface. The magnitudes of these normal distances are a measure of the extent to which compatibility is violated. Changes in the interaction forces must be determined such that these distances are reduced to zero.

To determine the required force changes, a flexibility method of analysis is used. Unit normal forces, with tangential forces of appropriate magnitude, depending on the coefficient of friction and the direction of slip along the interface, are applied to the barrier and automobile at each contact point, and the changes in normal distance are determined. These changes constitute a set of dynamic flexibility coefficients, which can be used to determine the changes in the interaction forces required to reduce the normal overlap distances to zero. These force changes are determined by solving a set of linear simultaneous equations.

The solution of the interaction problem is now nearly complete except that the force changes computed for some automobile points may be such that the total interaction forces at these points are tension rather than compression. If this occurs, the solution of the simultaneous equations must be repeated, with an imposed condition that the force changes at each such point must be equal and opposite to the previous interaction force at the point so that the net force is zero. This step is complete when all interaction forces are either compression or zero. The automobile points with compression forces are the contact points at the beginning of the next time step. If all interaction forces are zero for a specified number of successive time steps, the automobile is assumed to have separated from the barrier.

Step 6. The analysis for the time step is finally completed by summing the position changes of the automobile and barrier calculated in Steps 4 and 5 to obtain the total changes during the time step. The changes in velocity and acceleration of the automobile and barrier can then be determined, and the changes in axial force and bending moment in the barrier members can be calculated. The computations are then repeated from Step 1 for the next time step.

The solution of the interaction problem is essentially a two-cycle iteration procedure and does not ensure exact satisfaction of equilibrium and compatibility at the end of each time step. However, the procedure is such that errors are not accumulated from time step to time step, and thus the errors should not be significant. The accuracy with which the interaction problem is solved increases as the time step is made shorter. However, for practical use of the programs, a compromise must be reached between required accuracy and cost of the analysis because the number of steps, and thus the solution time, increases as the time step is reduced.

BARRIER IDEALIZATION

Barrier Structure

The barrier is idealized as a framework of arbitrary shape lying in the horizontal plane. The geometry of the structure is defined by specifying the coordinates of the joints between members of the framework and by specifying which joints are connected by members. The properties of the members are also specified.

Available Structural Members

Seven different types of members can currently be specified, as follows: beam members, possessing extensional and flexural strength and stiffness; cable members, possessing only tensile extensional strength and stiffness; column members, possessing tensile and compressive extensional strength and stiffness (in tension the strength is governed by yielding and in compression by elastic buckling); springs, possessing tensile and compressive extensional strength and stiffness; friction damping members, which slip extensionally at prescribed forces; viscous damping members, which possess velocity-dependent extensional resistance; and posts, which provide resistance to movement at single joints of the structure.

The members can be assigned nonlinear force-deformation characteristics, as explained in the following sections. In all cases the strength and stiffness properties are assigned by the user of the programs. Members with more complex characteristics than those of the basic members can be constructed by placing two or more basic members, of the same or different types, in parallel.

Beam Members—Beam members are assumed to be of uniform cross section and to have bilinear elastic-plastic properties both flexurally and extensionally. The moment-curvature and force-extension relationships are as shown in Figure 1. After yielding, the member unloads around a hysteresis loop as shown. Shearing deformations are ignored.

Interaction between the bending moment and axial force is ignored. That is, a beam member is treated as a combination of a purely flexural member and a purely extensional member, both of which are parallel and independent. Both members are assumed to be infinitely ductile with negligible strain hardening. However, strain-hardening effects can be included by setting up composite members. The extensional member is assumed to yield over its full length when the axial force exceeds the yield force. The flexual member is assumed to yield by forming localized plastic hinges at either end of the member or at both ends.

Cable Members—Cable members are assumed to have bilinear elastic-plastic properties in tension and to possess virtually no stiffness in compression. The force-extension relationship is therefore as shown in Figure 2. Energy is lost during yielding in tension, and the cable may go slack in compression and subsequently retighten. Infinite ductility with negligible strain hardening is assumed after yielding.

Column Members—Column members are assumed to have bilinear elastic-plastic properties in tension and to buckle elastically in compression at a specified force.

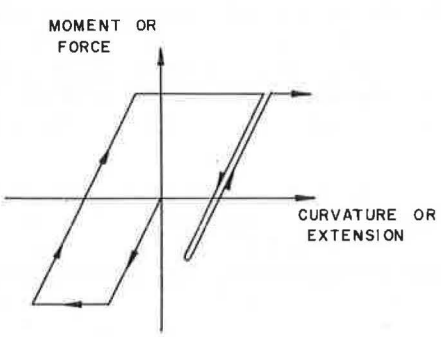

Figure 1. Typical moment-curvature or force-extension relationship.

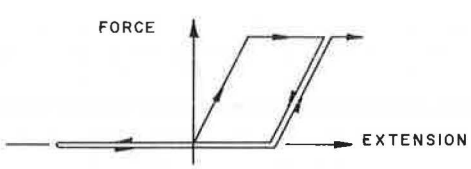

Figure 2. Typical force-extension relationship for a member going slack in compression.

The force-extension relationship is therefore as shown in Figure 3. If a member of a structure may buckle inelastically, or if the buckling load may be increased by inertial resistance, the member must be treated as a series of beam members.

Spring Members—Spring members are assumed to be perfectly elastic, but they have been assigned a "bottoming" feature that permits their stiffnesses to change at specified extensions, as shown in Figure 4. The stiffness may be either increased or decreased at bottoming.

Coulomb Dampers—Coulomb (friction) dampers may be specified to be reversible, to operate in tension only while going slack in compression, or to operate in compression only while going slack in tension. The force-extension relationship for a reversible damper is shown in Figure 1, and the relationship for a damper operating in tension only is shown in Figure 2. A damper operating in compression only has the relationship shown in Figure 2 but with tension and compression reversed.

It is assumed that coulomb dampers can extend indefinitely after slipping. However, bottoming at specified limits of travel can be achieved by placing a spring in parallel with each damper.

Viscous Dampers—Viscous dampers are assigned constant viscous damping coefficients and may be specified to be reversible, to operate in tension only, or to operate in compression only.

Posts—Posts are assigned stiffnesses and yield strengths for displacements in two principal directions at right angles. These stiffnesses are assigned if the post is behaving elastically. Elasto-plastic behavior is assumed to commence when the applied loads on the post are such that the following interaction condition is satisfied:

$$\left(\frac{F_A}{F_{yA}}\right)^2 + \left(\frac{F_B}{F_{yB}}\right)^2 = 1 \qquad (1)$$

in which F_A, F_B are the applied loads along the principal directions and F_{yA}, F_{yB} are the specified yield strengths along the principal directions. In the yielded condition an elasto-plastic stiffness corresponding to elastic-perfectly plastic behavior is determined. It should be noted that the forces F_A and F_B may change after a post enters the elasto-plastic range. However, in order to satisfy the yield condition, if one force increases, the other must decrease. If the post reenters the elastic range, unloading along a hysteresis loop is assumed to take place, essentially as shown in Figure 1.

Limiting deflections are also specified, at which the post will fail completely. Failure is assumed to take place when the following condition is satisfied:

$$\left(\frac{\Delta_A}{\Delta_{uA}}\right)^2 + \left(\frac{\Delta_B}{\Delta_{uB}}\right)^2 = 1 \qquad (2)$$

in which Δ_A, Δ_B are the deflections along the principal directions and Δ_{uA}, Δ_{uB} are the specified limiting deflections along the principal directions.

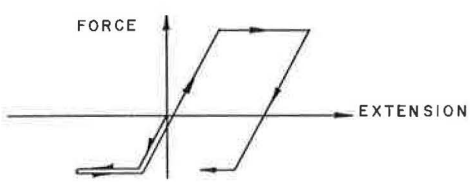

Figure 3. Typical force-extension relationship for a member buckling in compression.

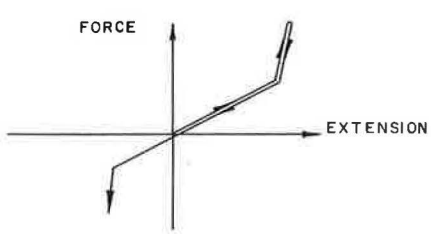

Figure 4. Typical force-extension relationship for a bottoming spring member.

When a post fails it is removed from the structure, and the load it was carrying immediately prior to failure is transferred to the remaining structure. If the failure is sudden, the post load is transferred to the structure suddenly, but, if the failure is more gradual, the load is transferred over a period of time. The failure of a real post is unlikely to be sudden, and thus in the computer program the failure is assumed to extend over the 10 time steps following initiation of failure. The post force is therefore transferred in 10 equal parts, and numerical difficulties that might arise from the sudden application of a shock load are avoided. After failure is initiated, the post contributes no stiffness to the structure, but it is still assumed to contribute mass to the structure.

Posts must be included to represent all attachments of a barrier to the ground or to a rigid object. To simulate connection to a rigid object, the post is made very stiff and strong.

AUTOMOBILE IDEALIZATION

The automobile is idealized as a body of arbitrary shape that possesses mass and rotational inertia. That part of the automobile boundary that may interact with the barrier is defined by specifying a number of points at which contact with the barrier may be made. A discrete nonlinear spring, with a force-deflection relationship of the type shown in Figure 5, is then associated with each point. The springs are assumed to have no mass and no viscous damping. Wheel positions can also be defined, and the brakes can be specified to be either on or off during the analysis. The idealized automobile is therefore shown in Figure 6. The locations of the automobile contact points and wheels are defined with respect to a coordinate system (r, s) as shown.

During the interaction of the automobile with the barrier, both normal and tangential forces are exerted. In the analysis, the normal directions are assumed to be normals to the barrier at the positions where the automobile points are in contact with the barrier. The normal forces are calculated during the solution of the interaction problem, and the tangential forces are assumed to be equal to the normal forces multiplied by coefficients of friction. As the normal forces increase, the springs compress, and thus the automobile points change position relative to the automobile center of gravity. During each analysis step, the increase in displacement of each spring point is computed, and new coordinates are determined.

The wheels may be directed parallel to the automobile axis, or at any angle to this axis. The steer angle is assumed to remain constant during the analysis.

If the brakes are specified to be on, there is a drag force at each wheel equal to a value specified by the user and acting opposite to the direction in which the wheel is traveling relative to the ground at any instant. If the brakes are specified to be off, the wheel will roll freely in the direction the wheel is pointing but will develop drag forces normal to this direction. The drag force in this case is set equal to the full drag force if the wheel moves in a direction greater than 10 deg from the direction in which the wheel is pointing and is reduced linearly for slip angles less than 10 deg.

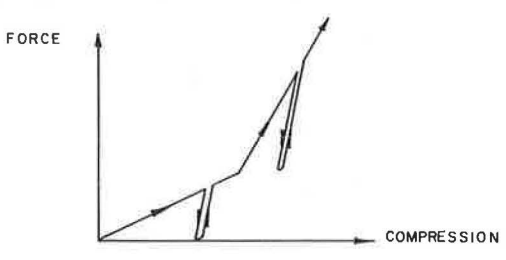

Figure 5. Typical force-compression relationship for automobile boundary spring.

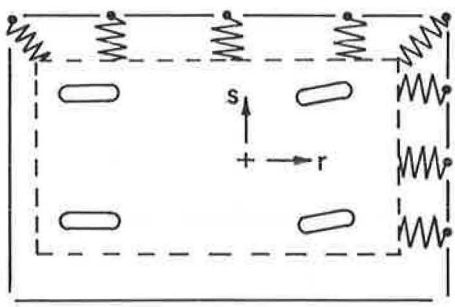

Figure 6. Idealized automobile.

It would be possible to include a sprung mass, representing a passenger, as a part of the idealized automobile, but this feature has not been included in the computer program because it is believed to be a poor idealization of an actual passenger/seat-belt system. Instead, provision has been made for the displacement, velocity, and acceleration time histories to be computed and printed at a number of specified points on the automobile. Because the mass of a passenger is small in relation to that of the automobile, the motion of a passenger will not significantly affect the automobile trajectory. Hence, the computed time history of motion at points on the automobile at which passengers may be seated can be determined and used as input to special-purpose programs for the determination of passenger response.

OUTPUT INFORMATION

A great deal of information on the state of the automobile is determined by the computer program, including positions, velocities, accelerations, details of those automobile points in contact with the barrier, and the magnitudes of the normal and tangential interaction forces. The data printed include the automobile positions and heading angles, forward and sideways velocities and accelerations, velocities and accelerations in the x, y coordinate directions, and resultant velocities and accelerations. Provision is also made for the data to be punched on cards for subsequent reentry into computer plotting routines. This option is valuable because considerable time is required to produce plots by hand.

Information on the deflections of the barrier joints and the forces in the barrier members is also printed, and data on the locations of the barrier joints and automobile points can be punched. The punched data can be used to produce computer plots of deflected shapes of the automobile and barrier.

EXAMPLES OF AUTOMOBILE-BARRIER INTERACTIONS

Two examples are considered in this section; several other example structures are discussed by the author elsewhere (1). The examples considered here are (a) a bridge rail barrier with fragmenting-tube, energy-absorption devices, for which limited test results are available (2); and (b) a multiple-interface ductile beam abutment barrier with dimensions corresponding to a detailed design developed by Cornell Aeronautical Laboratory (3).

The properties selected for the automobile have been chosen largely from information presented elsewhere (4), although a number of arbitrary assumptions have been made. The assumed plan dimensions are shown in Figure 7. The other assumed automobile properties are as follows:

1. Weight = 4,720 lb for the first example, 3,600 lb for the second example;
2. Moment of inertia = 45,000 lb-sec^2 in. for the first example, 34,000 lb-sec^2 in. for the second example;

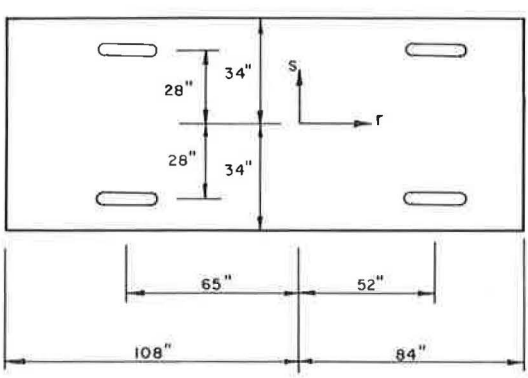

Figure 7. Dimensions of basic automobile.

3. Boundary spring stiffness for each 12 in. of perimeter tributary to any point = 0.5 k/in. for sheet metal, 3.0 k/in. after bottoming, and 4.0 k/in. on unloading;
4. Bottoming distance for boundary springs = 15 in.; and
5. Maximum drag forces between wheel and ground = 27.5 percent of weight for front wheels and 22.5 percent for rear wheels.

Fragmenting Tube Bridge Rail

Tubes that fragment on being forced into a die have been investigated as energy-absorbing devices for barrier

structures. The tubes behave as coulomb damping devices with predictable and essentially constant slip forces. A preliminary report on a series of tests of a bridge rail system incorporating fragmenting tubes has been prepared at the Texas Transportation Institute (2). Data for the computer program have been prepared from details given in that report.

The computed motion of the automobile for a typical analysis (impact at 25 deg and 54.8 mph) is shown in Figure 8. The computed time histories of forward and transverse accelerations at the automobile centroid are shown in Figure 9 and compared with accelerometer values determined by Hirsch, Stocker, and Ivey (2). The agreement between theory and experiment is far from exact but is nevertheless encouragingly close considering the complexity of the problem. Both theory and experiment predict two deceleration peaks, the second corresponding to impact of the rear of the automobile on the barrier, and the predicted decelerations are quite close to the measured ones. It should be noted that the test accelerometers were not mounted at the automobile centroid, and that their positions were not known at the time the analyses were carried out. Other analyses (not shown) have demonstrated that the accelerations change substantially from point to point on the automobile. The test results also appear to contain a large oscillation superimposed on a basic deceleration pattern, and this accounts for a large part of the difference between theory and experiment. These oscillations probably result from vibrations of the automobile structure or instrument assembly and would not be experienced by a passenger in the automobile.

The analysis predicted departure of the automobile from the barrier at 28.8 mph at an angle of 14 deg. This is significantly below the test value of approximately 33 mph at an unknown angle. The departure velocity depends substantially on the coefficient of friction between the automobile and barrier, which was assumed to be 0.6 in the analysis. Further investigations are necessary to determine suitable coefficients for use in analysis.

A strength of 12.5 k was assigned to each fragmenting tube. This is larger than the value of approximately 10 k indicated by Hirsch, Stocker, and Ivey (2). Similar automobile deceleration results were obtained with an assumed strength of 10 k, but with

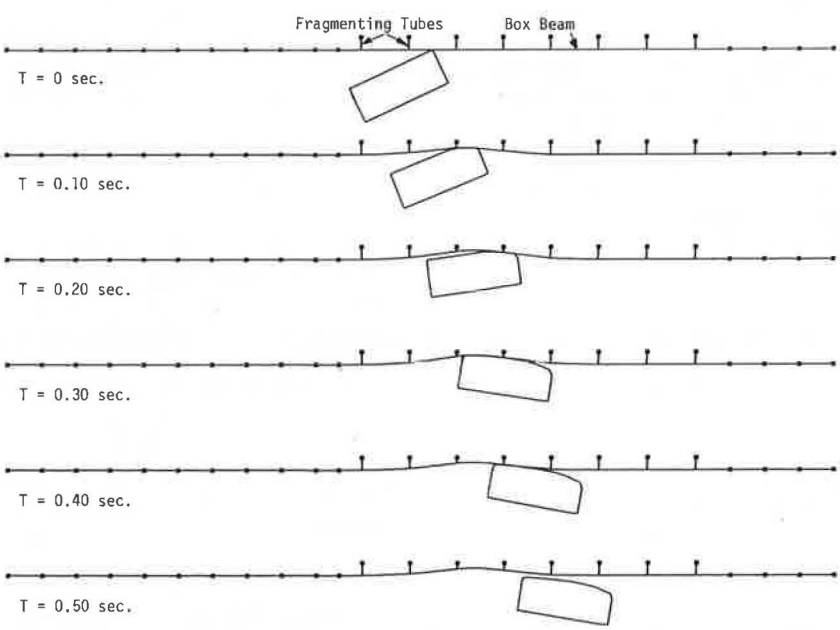

Figure 8. Deflected shapes of fragmenting-tube bridge rail.

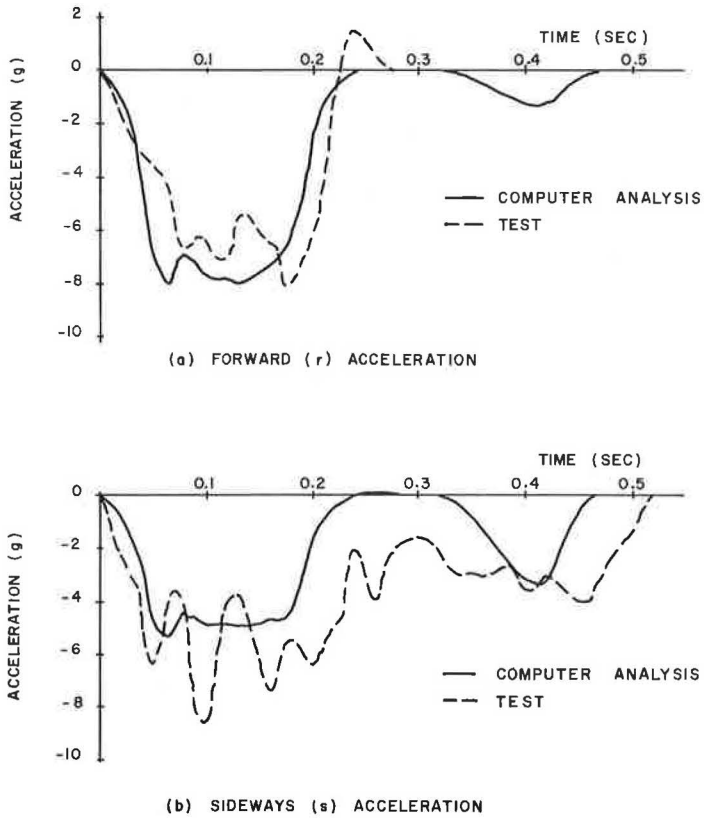

Figure 9. Fragmenting-tube bridge rail (forward and sideways automobile accelerations).

this strength the computed barrier deflections were substantially larger than the measured deflections. The measured and computed amounts of shortening of the five fragmenting tubes in the impact region were as follows:

Tube No.	Test (in.)	Tube Strength of 12.5 k (in.)	Tube Strength of 10 k (in.)
1	0.1	0	0
2	6.0	3.6	4.8
3	14.8	16.0	18.9
4	10.0	12.0	17.0
5	0.1	0.7	3.8

Ductile Beam Abutment Barrier

The geometry of an abutment barrier designed by Cornell Aeronautical Laboratory (3) is shown in Figure 10. The concept of the barrier is that an automobile is decelerated by each of the arch "layers" in turn. The resisting force of the outer layer is not so large that a light automobile is decelerated too rapidly, yet the inner layers

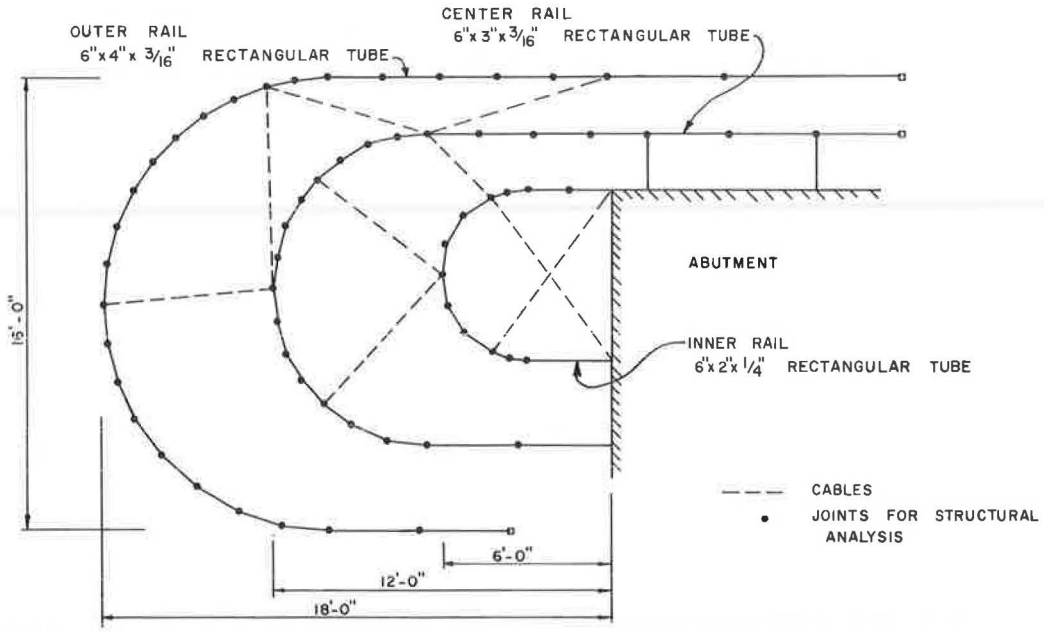

Figure 10. Geometry of ductile beam abutment barrier.

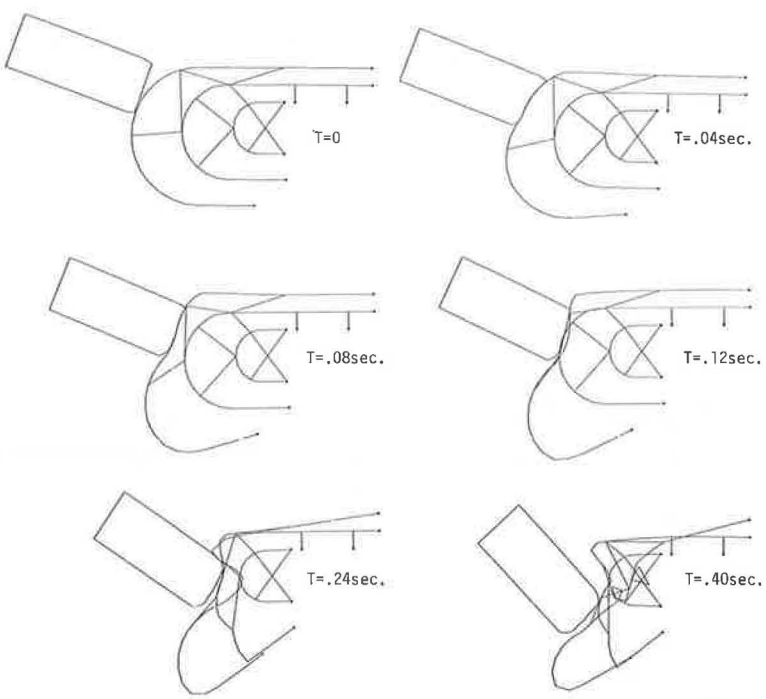

Figure 11. Deflected shapes of ductile beam abutment barrier.

prevent total penetration by a heavy automobile. No test results for this type of barrier are available.

Deflected shapes of the barrier for a head-on impact at 50 mph are shown in Figure 11. Time histories of automobile decelerations are shown in Figure 12. The following points may be noted:

1. The peak decelerations at approximately 0.04 and 0.13 sec correspond to development of the maximum strengths of the outer and first inner barriers respectively. The deceleration at the second peak is large, although the peak is of short duration.
2. After yielding and buckling, the computed resistances of the barrier layers decrease substantially. However, strain hardening was ignored in the analysis, and, if strain-hardening effects are present, the post-yield strength could be significantly increased. Strain-hardening effects can be included in the analysis if desired.
3. The outer barrier layers overlap the inner layers when the displacements are large. In an actual barrier, the design may be such that the layers cannot overlap, and in such a case the behavior might be substantially different. However, provision for barrier-to-barrier contact in the computer program is impractical. The errors introduced by ignoring this contact must be determined by prototype testing.
4. At 0.38 sec the barrier buckled away from the automobile and contact was lost, although the automobile was still moving at 8.0 mph. Ater 15 subsequent steps, contact had not been reestablished, and the computation was terminated. The very large deformations of the barrier toward the end of the analysis should particularly be noted.

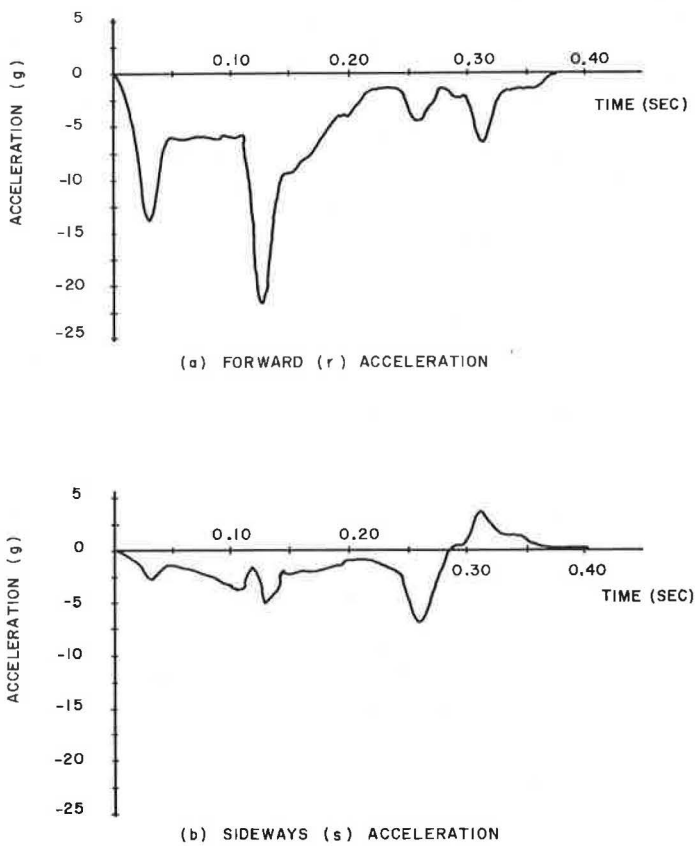

Figure 12. Ductile beam abutment barrier (forward and sideways automobile accelerations).

Solution Times

The computer program is written in FORTRAN IV and operates entirely in core. The author's analyses have been carried out on the CDC 6400 computer at the University of California, Berkeley. The program requires 27300 K decimal for execution and can be run on any machine with adequate capacity, although double precision arithmetic would be essential on machines with short word lengths.

The solution times for the examples considered in this paper were as follows:

Example 1—113 joints in barrier (339 barrier equations to be solved in each time step), 151 structural members; central processor time = 1.74 sec per time step, 365 sec for complete analysis (210 time steps of 0.0025 sec each).

Example 2—69 joints (207 equations, but with larger bandwidth than example 1), 83 members; central processor time = 3.23 sec per time step, 646 sec for complete analysis (200 time steps of 0.002 sec each). The peripheral processor times vary with the problem size and amount of output but are generally small.

CONCLUSION

From the limited series of examples discussed in this paper and elsewhere (1), it appears that the computer program should be a valuable aid for the investigation of barrier systems. The agreement with the few available sets of experimental data is encouraging, the program is fairly easy to use, and the solution technique is surprisingly stable in view of the complexity of the problem. It is obvious, however, that further study, both analytical and experimental, is needed to test the accuracy of the program and to determine its range of application.

A series of barrier structures for which reliable physical data and experimental results are available should be selected and then idealized in different ways for analysis. The range of member types available to the program permits considerable flexibility in the idealization procedure. The effects of varying the idealization should then be studied, and the effects of varying such parameters as automobile size and stiffness, coefficient of friction, and time step should also be investigated for each idealization. The accuracy of the computer results could then be determined, and recommendations on idealization procedures could be made. Until such an investigation has been completed, it is not possible to make detailed recommendations of the use of program or to draw definite conclusions on its accuracy.

ACKNOWLEDGMENT

This research investigation was conducted under the sponsorship of the Federal Highway Administration. The opinions, findings, and conclusions expressed are those of the author and not necessarily of the sponsor.

REFERENCES

1. Powell, G. H. Computer Evaluation of Automobile Barrier Systems. Dept. of Civil Engineering, Univ. of California, Berkeley, Aug. 1970.
2. Stocker, A. J., Ivey, D. L., and Hirsch, T. J. Energy Absorbing Bridge Rail (Fragmenting Tube). Texas Transportation Institute, Texas A&M University, Feb. 1970; also, Full-Scale Crash Tests of the Fragmenting-Tube-Type Energy-Absorbing Bridge Rail. Highway Research Record 302, 1970, pp. 28-37.
3. Shoemaker, N. E. Research and Design of an Impact Absorbing Barrier for Fixed Highway Objects. Cornell Aeronautical Laboratory, Inc., Rept. VJ-2501-V-1, June 1968.
4. Development of an Analytical Approach to Highway Barrier Design and Evaluation. New York Dept. of Public Works, Bureau of Physical Research, Res. Rept. 63-2, April 1963.

CRASH TEST PERFORMANCE OF A PROTOTYPE LIGHTWEIGHT CONCRETE ENERGY-ABSORBING GUARDRAIL SYSTEM

Charles Y. Warner, Brigham Young University; and
Grant W. Walker, Dynamic Research and Manufacturing, Inc., Sacramento, California

This paper presents the results of a series of crash tests that compare the performance of standard G4 guardrail with that of a similar guardrail equipped with energy-absorbing cartridges constructed of lightweight concrete. Test results indicate that the cartridges can reduce acceleration loads on vehicles by 20 to 30 percent, improve resistance to pocketing and overriding, and reduce maintenance costs in some instances. Cartridge design is compatible with existing hardware and is adaptable to special needs. The low cost of the cartridges suggests a favorable cost-benefit ratio.

•PROTECTION of motorists from roadside hazards that cannot economically be removed commonly results in the placement of guardrail systems. With proper design and installation, guardrails provide redirection and prevent penetration of errant vehicles (1, 2).

Some recent effort has been directed toward energy-absorption systems used in conjunction with deflecting guardrails to improve vehicle dynamics and reduce accident costs. One such study evaluated a fragmenting-tube absorber system (3). Lightweight concrete barriers have been tested with some success for vehicle barriers at gores (4). This paper deals with tests of a guardrail system that combines these concepts, substituting energy-absorbing cells of lightweight concrete for the wood blockout already in common use in many states (1).

The cost of this system is such that the energy-absorbing components can be substituted for the rigid blocks in a new G4 installation for an additional cost of about 40 cents per foot, or less than 10 percent additional cost.

A test guardrail incorporating vermiculite concrete cartridges is shown before and after a 55-mph test in Figure 1. Seven-in. diameter, spiral-wrapped lightweight vermiculite concrete cylinders with 3-in. diameter holes were used to make an energy-absorbing cartridge for each guardrial post, as shown in Figures 2 and 3. Response of the cylinders is controlled by the geometry of the block, the strength and flow characteristics of the matrix, and the spacing of the spiral wrap wire.

The initial failure of the cylinder fills the center hole progressively from the weak front boundary. As the center hole fills, the apparent pressure within the crushed cylinder increases, causing the crushed matrix to flow through the spiral wrap wire. The pressure within the cylinder can be carefully controlled for a given loading rate by increasing or decreasing the spacing of the spiral wrap wires.

The cylinder response is similar in time sensitivity to that of a hydraulic cylinder in that higher rates of loading increase the apparent pressure within the cylinder, which causes a greater resisting force. The crushed vermiculite matrix flowing through the spiral wrap wire can be controlled in a way similar to the orifice control on a hydraulic

Sponsored by Committee on Traffic Safety Barriers and Sign, Signal and Lighting Supports and presented at the 50th Annual Meeting.

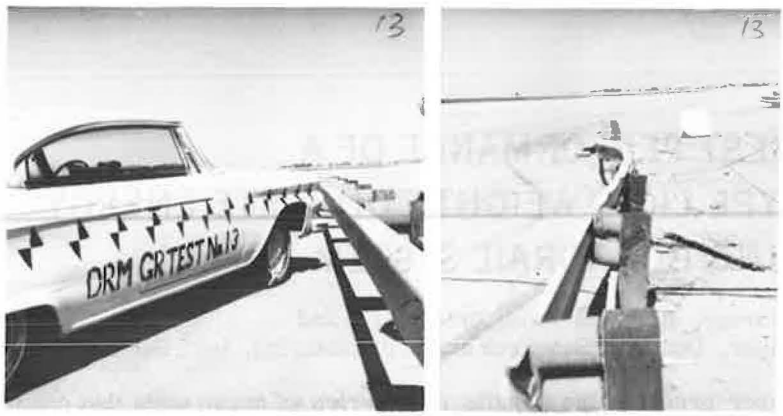

Figure 1. Guardrail system before and after 55-mph, 28-deg impact.

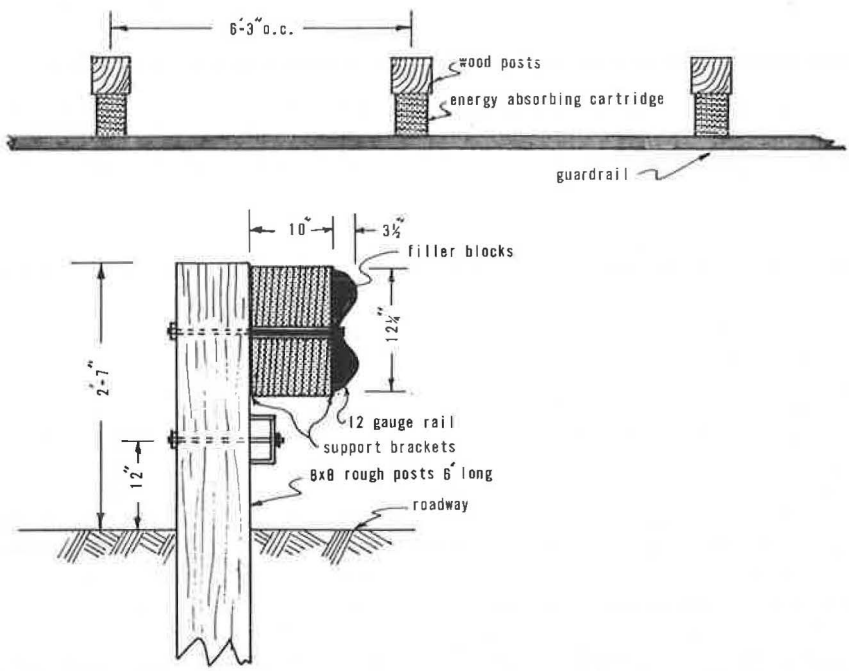

Figure 2. Schematic of energy-absorbing guardrail.

cylinder. As the spacing of the wire increases, the apparent pressure within the cylinder decreases for a given rate of loading. The front half of the cylinder was made softer by increasing the wire spacing. Wire spacing was decreased from $1\frac{1}{4}$ in. over the front half of the cylinder to less than $\frac{3}{4}$ in. over the back part of the cylinders, providing a continuously increased resistance from front to back. The effect of slight mix variations and casting techniques is minimized by the great influence of the spiral wrap wire on the overall character of the cell.

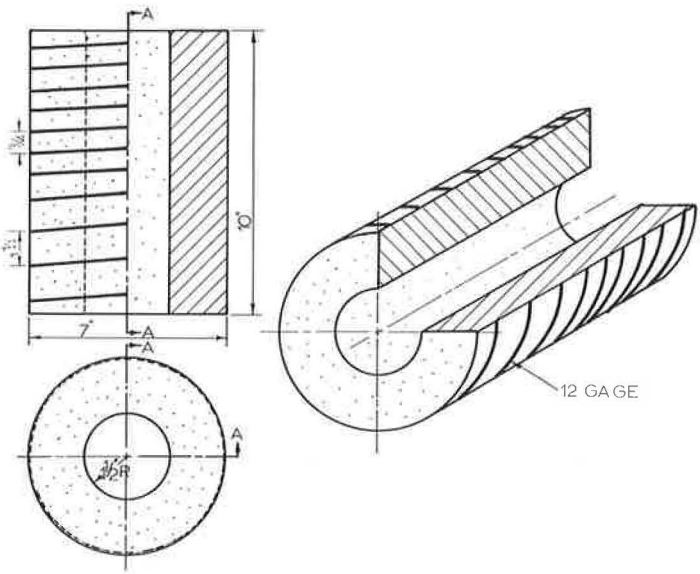

Figure 3. Energy-absorbing lightweight concrete cylinder.

Each cartridge is composed of two hollow cylinders of lightweight concrete fastened to plywood headers. Each cylinder is precast, cured, and wound with steel reinforcing wire before assembly (Fig. 3). Completed cells are weatherproofed by a sealant coating before installation.

TEST PROCEDURE

A series of full-scale vehicle crashes has been conducted during the progress of development and feasibility analysis for this device. Four tests are presented here that compare the performance of the G4 standard rail (1) with that of a modified G4 rail in which the energy-absorbing vermiculite concrete (VC) cartridges are substituted for the standard wood blockout.

Vehicles of the same year and model were chosen for each comparison to provide a uniform basis. Barrier posts were buried in fresh 45-in. deep, 12-in. diameter holes in a hard clay soil and held firmly by a well-compacted sand fill. Impact points were established to prevent any post that shifted due to test loads from being subjected to direct impact loads in a subsequent test.

Visual data were gathered by high-speed movie cameras placed strategically around the impact site. Vehicle accelerations at the left-rear floor pan were measured electronically by two accelerometers connected by hardline to a recorder in a mobile in-

TABLE 1

OVERALL CONDITIONS OF TEST

Test No.	Barrier Type	Impact Speed (mph)	Vehicle Weight (lb_f)	Impact Angle (deg)	Kinetic Energy ($ft\text{-}lb_f \times 10^{-5}$)
14	G4 with VC cartridge	39.8	4,600	28	2.45
15	G4 with wood blockout	39.6	4,600	26.5	2.41
13	G4 with VC cartridge	55.0	3,500	28	3.52
16	G4 with wood blockout	59.5	3,600	27	4.27

TABLE 2

TEST OUTCOMES

Test No.	Duration of Contact (msec)	Maximum Dynamic Lateral Penetration		Accelerations, G				Speed Change During Contact (mph)	Exit Angle (deg)	Trajectory Distances	
				Longitudinal		Lateral					
		Top of Post (in.)	Rail (in.)	Peak	Average	Peak	Average			Reentry (ft)	Stop (ft)
14	336	6	14.8	-5.6	-1.65	5.0	2.4	11.5	12.0	30	120[a]
15	372	8.7	13.3	-8.4	-2.0	7.4	3.0	15.3	10.0	50	208
13	397	11.9[b]	21.9	-12.0	-3.7	10.0	2.3	32.3	7.0	55	136
16	242	34.7[c]	26.7	-17.0	-6.0	8.8	4.2	31.6	8.5	45	69

[a]Bumper pressed against wheel, braking car after hit. [b]Soft footing for this post. [c]Post shattered.

strument van. Redundant measurements of accelerations were recorded by an Impactograph.

Camera framing speeds were established by reference to synchronous clocks in the field of view during the tests. Duration of vehicle-barrier contact was established by visual reference to the high-speed movies. Velocity-change calculations from the film were compared with those obtained from integrating longitudinal-axis accelerometer traces and the average value reported. In most cases, these figures agreed within 1 mph; in no case with the difference greater than 2.2 mph, which reconfirmed confidence in the data.

Impact velocity was measured by a digital clock actuated by fixed switches on the approach run, which also fired flashbulbs visible in the high-speed movies, allowing correlation of electronic and film data. Photographic and manually measured records of vehicle and barrier damage were summarized for comparison of results.

TEST RESULTS

Tables 1, 2, and 3 give the conditions, measurements, and damage resulting from the four tests (all tests having impact angles greater than 26 deg). The first two rows of the tables compare G4 and modified guardrails at about 40 mph. The last two rows

TABLE 3

DAMAGE REPORT

Test No.	Residual Lateral Rail Deflection (in.)	Damage Codes		Results of Test
		Vehicle[a]	Barrier[b]	
14	8	0111	2321	Bumper bent against right front tire, acting as brake
15	11	2121	3231	Two wood blocks split
13	18	2122	4554	Wheel climbed channel, causing post to split, then shatter
16	24	2232	4343	1 post split, 3 wood blocks split

[a]Vehicle condition after test–XXXX:

1st digit–wheel and tire condition
- 0, intact
- 1, tire blown
- 2, rim torn

2nd digit–suspension hardware
- 0, intact
- 1, bent
- 2, torn loose

3rd digit–main vehicle frame
- 0, intact
- 1, minor bending
- 2, moderate distortion
- 3, severe distortion
- 4, broken or torn

4th digit–body parts
- 0, minor deformation
- 1, major deformation
- 2, structural parts torn off

[b]Barrier condition after test–XXXX:

1st digit–number of posts disturbed or broken
2nd digit–number of blockouts destroyed
3rd digit– number of 6 ft 3 in. lengths of guardrail deformed or destroyed
4th digit–number of 6 ft 3 in. lengths of channel rub-rail destroyed or bent

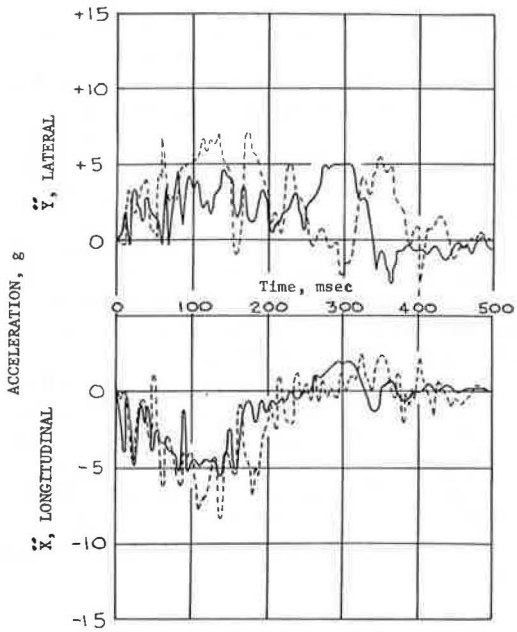

Figure 4. Acceleration histories: Test 14 (solid line)—39.8 mph, 28 deg, VC cartridge; test 15 (broken line)—39.6 mph, 26.5 deg, wood blockout.

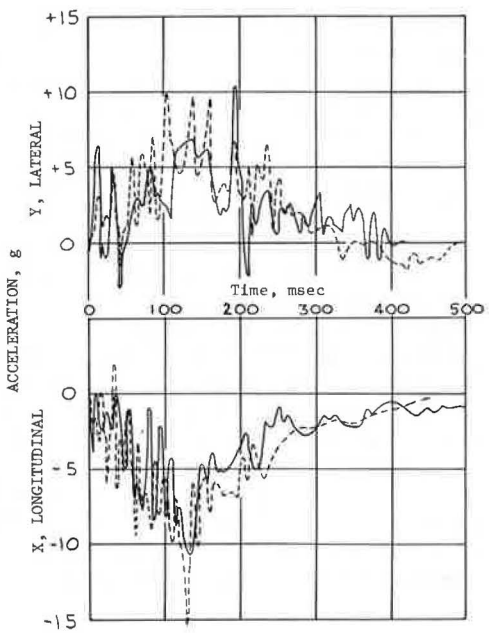

Figure 5. Acceleration histories: Test 13 (solid line)—55 mph, 28 deg, VC cartridge; test 16 (broken line)—59.5 mph, 27 deg, wood blockout.

make a similar comparison at about 60 mph (test controls failed to establish a 60 mph speed in test 13; however, the steep angle partially compensated for this). Figures 4 and 5 show acceleration histories for comparable tests.

DISCUSSION OF RESULTS

Table 2 gives data showing that the initial exit trajectory of the vehicle is not greatly different in either case. In the low-speed test pair, the durations do not differ significantly, while a notable difference in speed change occurs. This is also borne out in the presentation of acceleration measurements, showing the standard G4 system to subject the vehicle to greater loads for the duration of impact. In the high-speed series the velocity change is comparable, but the shorter duration of the wood-block impact again leads to higher average loads. In both series, peak accelerations were found to be higher in the wood-block tests.

It was intended that all tests be made at different impact points on the test guardrail to ensure undisturbed soil conditions for each test. This condition was achieved for all except test 16. Because of a guidance error, the impact point of test 16 was nearly the same as that for test 13 thus making the soil conditions softer for test 16. The loads on the car would probably have been more severe during test 16 if the soil conditions had been undisturbed, as they were for test 13.

The maximum dynamic deflections of rail and posts demonstrate the effect of the VC cartridges. Although the rail deflection is roughly the same for the tests in each pair, the accompanying post deflection is much smaller in the case of the vermiculite blocks. This indicates a reduction in maintenance costs per impact, substituting cartridge compression for post disturbance.

The effect of the energy-absorbing distances provided by the VC cartridges is further illustrated in the comparison of vehicle decelerations, as given in Table 2 and shown in Figures 4 and 5. Both peak and average decelerations are reduced by substitution of the cartridges. Reductions of 20 to 30 percent are typical.

Table 3 gives a summary of the damage inflicted on vehicle and barrier for each test. The lesser residual lateral rail deflection, in the case of the VC cartridge test in each pair, suggests that the rail is given freedom to deform more gradually over a greater distance. This should lead to a decreased friction between rail and vehicle and is probably a deterrent to pocketing.

The damage codes given in Table 3 are meant to condense qualitative photographic impressions and measurements from the vehicle and barrier after test. Generally, the higher numbers indicate greater damage.

In the low-speed series, serious damage to tire and suspension was averted in test 14, resulting in a smooth runout, although the bumper was pressed against the tire. Test 15 caused significant tire-wheel damage, resulting in a rough runout that was significantly more hazardous. Two wood blockouts were split in this test, and three posts were displaced, whereas test 14 caused displacement of only two posts.

In the high-speed series, damage to the vehicle was somewhat more severe in test 16, primarily in the degree of distortion at frame and suspension parts. The barrier damage in these tests was roughly equivalent. It was noted in several tests using the VC cartridges that the guardrail, after the cartridges were partially crushed, appeared to rise and fall rather freely with the vehicle. The decrease of vertical stiffness in the overall guardrail system provided by the VC cartridge blockout allowed the W-beam to move vertically in unison with the vehicle. This apparently provided greater resistance to overrunning the guardrail system.

CONCLUSIONS

The following statements appear to be warranted by the results of these preliminary tests:

1. The presence of the VC cartridges has at least five beneficial effects: (a) impact acceleration loads can be reduced by 20 to 30 percent; (b) at moderate speed, vehicle rideout trajectory and control may be improved because vehicle suspension and frame damage is reduced; (c) post deflections were significantly reduced by the energy-absorbing VC cartridges during the test series (deflection of the posts accounted for the major part of the energy absorbed by the rail when wood blocks were used); (d) guardrail maintenance problems are reduced, at least at the lower speeds; and (e) the tendency of the vehicle to produce pockets in the guardrail beam is reduced.
2. The low cost, modular construction, quick-change features, and compatibility with hardware already in use suggest a favorable cost-benefit ratio in new construction. Modification and updating of existing guardrail systems can be readily and inexpensively accomplished.
3. The ease of controlling the geometry and the dynamic properties of the VC cartridge suggest broad adaptability to specialized needs, such as gradual stiffening at bridge rail transitions.

REFERENCES

1. Michie, J. D., and Calcote, L. R. Location, Selection, and Maintenance of Highway Guardrails and Median Barriers. NCHRP Rept. 54, 1968.
2. Olson, R. M., Post, E. R., and McFarland, W. F. Tentative Service Requirements for Bridge Rail Systems. NCHRP Rept. 86, 1970.
3. Stocker, A. J., Ivey, D. L., and Hirsch, T. J. Full-Scale Crash Tests of the Fragmenting-Tube-Type Energy-Absorbing Bridge Rail. Highway Research Record 302, 1970, pp. 28-37.
4. Ivey, D. L., Buth, E., and Hirsch, T. J. Feasibility of Lightweight Cellular Concrete for Vehicle Crash Cushions. Highway Research Record 306, 1970, pp. 50-57.

DYNAMIC EVALUATION OF TIMBER POSTS FOR HIGHWAY GUARDRAILS

Jarvis D. Michie, Southwest Research Institute;
Charles J. Gatchell, Forest Product Marketing Laboratory; and
Theodore J. Duke, American Wood Preservers Institute

An experimental program was performed on guardrail posts to learn the more significant dynamic properties. A special pendulum impact facility was used to subject test specimens to dynamic loading that simulated a vehicle-guardrail installation collision. One hundred specimens of Douglas fir, southern pine, red oak, and red pine wood were evaluated; for comparison 6B8.5 and 3I5.7 steel members were tested. Sizes of wood posts ranged from 4 by 4 in. to 8 by 8 in. in cross section. The post specimens were rigidly secured in a base fixture, and the dynamic load was applied 24 in. above grade. Basic test data include a complete load resistance-post deflection determination for each specimen. The dynamic properties of peak resistance force, average resistance force, and fracture energy are reported for the four wood species and steel members. Test results show that, while data scatter exist within a wood species and size test group, the average values of such groups can be plotted in a manner to give meaningful trends. Peak force, average force, and fracture energy are shown to be a direct and linear function of moment of inertia.

•IN RECENT YEARS, highway engineers have had two main objectives in the design of guardrail and median barrier systems: first, to redirect errant vehicles in such a manner that the occupants survive the impact, and, second, to ensure that the redirected vehicle presents a minimum hazard to following and adjacent traffic. Analytical design of a system to perform these dynamic functions is a complex task for which no rigorous procedures are available. As a result, highway engineers have been compelled to develop effective guardrail systems by a trial-and-error procedure in which candidate systems are selected on the basis of individual judgment and intuition and then evaluated by full-scale crash testing. This method has proved to be slow and expensive.

More recently, analytical procedures have been developed that can characterize the vehicle-guardrail impact with excellent precision, provided that the dynamic properties of the system are known. Although meaningful results can be generated by these procedures, their widespread use has been curtailed due to insufficient information on the properties of barrier materials—in particular, on the dynamic properties of guardrail posts.

The objective of this program was to determine experimentally performance properties of timber posts when subjected to dynamic, horizontal forces. The testing procedure was designed to closely simulate the loading of a highway guardrail post when the guardrail installation is impacted by an errant vehicle. The scope of the program involved testing to failure of red oak, red pine, Douglas fir, and southern pine wood species in sizes ranging from 4- by 4-in. to 8- by 8-in. cross sections. For reference, two typical steel guardrail post shapes were also tested. The reference steel posts were 6B8.5 and 3I5.7 members.

Sponsored by Committee on Traffic Safety Barriers and Sign, Signal and Lighting Supports and presented at the 50th Annual Meeting.

EXPERIMENTATION PROCEDURE

The test apparatus and procedures were designed to subject specimens to a loading similar to that induced in highway guardrail posts when the guardrail system is hit by a typical passenger car. The test program was composed of four wood species and two steel post shapes. The specimens for each geometry evaluated are given in Table 1.

Facility

The Southwest Research Institute pendulum impact test facility consists of a pendulum, its operating equipment, and the test-control and data-acquisition instrumentation. An overall view of the facility is shown in Figure 1. A 4,000-lb mass is suspended in such a manner that it remains horizontal throughout the normal swing arc of a 26-ft radius.

Impact velocity is programmed by adjusting the vertical fall of the mass, and is calculated by the expression $V_I = \sqrt{2gh}$ where V_I is impact velocity in feet per second, g is acceleration due to gravity (32.2 ft/sec^2), and h is the mass drop height in feet. Impact velocities ranging from 0 to 40 feet per second (fps) are obtainable within the available 25-ft drop height. Other weights and mass geometrics can be used; however, the 4,000-lb mass is normally used because it represents the weight of a medium-size passenger car. A half section of an 8-in. diameter steel pipe, filled with concrete and rigidly attached to the mass, serves as the contact surface or "bumper".

Figure 1. Southwest Research Institute pendulum impact tester.

Test specimens are stationed at the lowest point of the pendulum arc where the kinetic energy (i.e., velocity) of the mass is maximum. The specimens are secured in a rigid fixture or they may be embedded in soil for cases in which the integral post-soil behavior is to be studied. Features of the post specimen and fixtures are shown in Figure 2. A firm elastomer cushion, inserted in the fixture at grade level, helps to distribute the resisting force of the fixture over the specimen width. Although the cushion reduces the degree of fixity, its purpose is to improve test simulation of the soil-embedded guardrail post by (a) permitting the specimen to deform laterally (i.e., Poisson effect) and (b) eliminating the chance of a sharp fixture edge cutting into the specimen.

The instrumentation consists of a velocity sensor and an accelerometer. A photocell, located immediately upstream from the specimen, is triggered by light-reflecting

TABLE 1

TEST SPECIMENS

Material	Dimensions (in. by in.)					
	4 by 4	4 by 6	6 by 6	6 by 8	8 by 8	9-in. Diameter
Douglas fir	8	8	—	8	8	—
Red oak	8	8	5	8	—	—
Red pine[a]	—	—	—	—	—	—
Southern pine	—	4	6	—	8	4
Steel 3I5.7	4					
Steel 6B8.5	4					

[a]16 round posts ranging in diameter from 6 to 9¾ in.

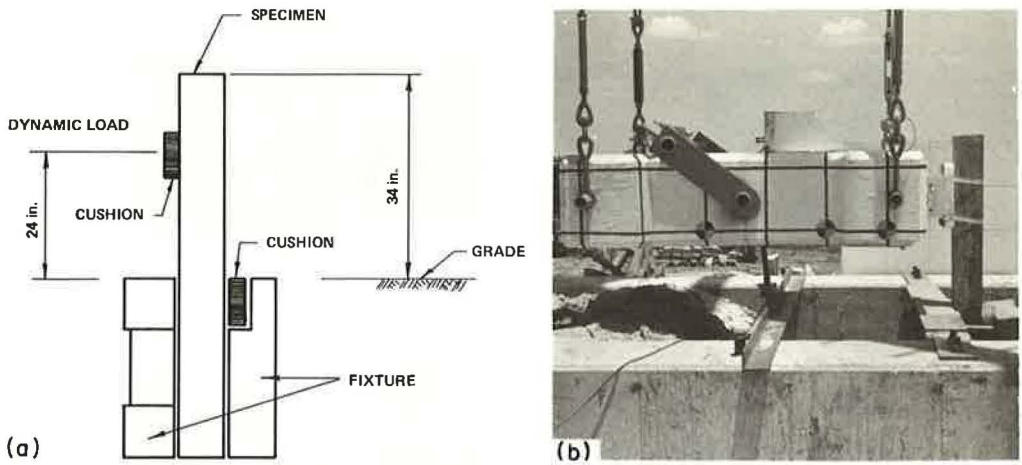

Figure 2. Features of specimen boundary conditions: (a) schematic, and (b) view prior to test.

strips attached to the lower surface of the pendulum mass. As the pendulum mass moves past the photocell, signal pulses are produced by the incrementally spaced strips. A linear strain-gage accelerometer (CEC Type No. 4-202-001, a ±25-g range), rigidly mounted to the pendulum mass at the bumper, senses the magnitudes of the pendulum mass deceleration caused by the specimen's resistance to breaking. Thus, the post's resisting force can be calculated and plotted at each instant throughout impact by multiplying mass deceleration at a particular instant by the mass weight. Signals from the velocity photocells and accelerometer are continuously recorded on a CEC VR-3300 data tape recorder. During each test, a visual record (i.e., strip chart from a Honeywell 906 C Visicorder) of the raw data is also produced to provide preliminary information and to ensure that instrumentation systems are functioning properly. A typical impact sequence is shown in Figure 3.

Procedure

After post specimens are inspected to ensure their conformance to limitations on knots, splits, and other large surface discontinuities, test numbers are assigned and the specimens' dimensions are recorded. Each specimen is inserted into the fixture with 34 in. extending above grade (Fig. 2). A firm elastomer cushion at grade level provides lateral support. Another cushion is attached to the specimen at the point of load application to attenuate the rate of force onset.

Mechanics of the test are simple. Instrumentation systems are energized and calibrated. The mass is pulled away from the impact point to an elevation calculated to provide the proper impact velocity. On signal from the test engineer, the mass is released by means of a quick-release mechanism. Instrumentation signals are continously recorded from the time of mass release, through impact, and until swing-through has been achieved. Duration of impact usually ranges from 10 to 100 msec.

Originally, an impact velocity of 30 fps was planned for all program tests. However, it became evident early in the program that only a small quantity of energy is expended in breaking the smaller posts. Consequently, the pendulum mass velocity change during impact with the smaller posts is small and difficult to measure with precision. By decreasing the impact velocity from 30 fps to 20 and 15 fps for a majority of the tests, a more discernible velocity change is effected. It was anticipated that the kinetic energy dissipated would be insensitive to this change in impact velocity. Also, the "inertia" peak in the typical force vs. time data plot is attenuated by a reduction in impact velocity. This peak, which is associated with the impulse required to accelerate the test specimen to impact velocity, is a dynamic characteristic of the specimen relating to density (i.e., mass) and is not necessarily an index of the post

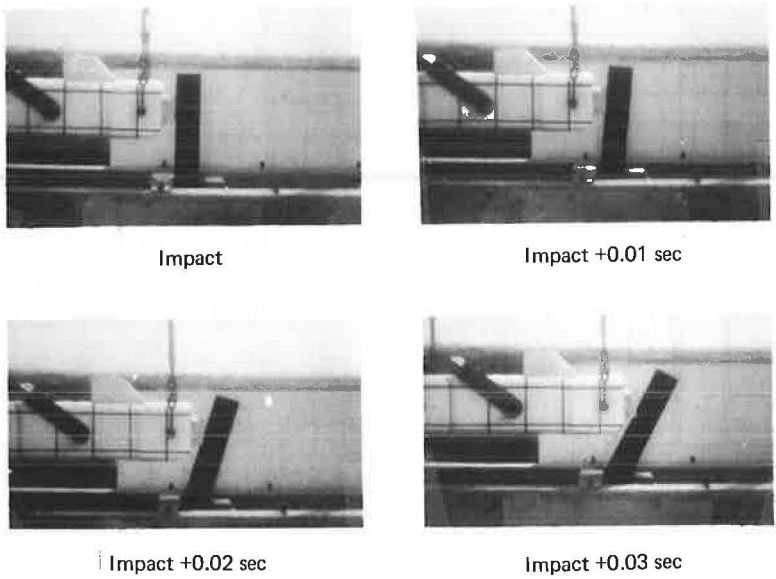

Figure 3. Pendulum specimen impact sequence.

strength. It may be of interest to note that the effect of varying the impact velocity from 30 to 15 fps is not readily apparent from the test results (i.e., post strength factors are not velocity-sensitive for these test conditions).

After the test, a section of the specimen at least 1 in. long was cut from near the failed area and weighed immediately for determination of specific gravity and moisture content. Moisture content and dry specific gravity of Douglas fir, red oak, and red pine specimens were determined by Forest Product Marketing Laboratory personnel. Although the southern pine posts were creosote-treated, the American Wood Preservers Bureau, Inc., determined the moisture content and dry specific gravity from samples taken from the failed post specimens.

FINDINGS

The types of experimental data acquired in the program, selected for the purpose of defining the post failure characteristics, were (a) peak force Fp, (b) average force F, and (c) fracture energy FE. These characteristics greatly influence the dynamic behavior of a highway guardrail installation when impacted by a fast-moving vehicle. Peak force defines the breakaway value for posts in a "weak-post" guardrail system; it also provides an input for predicting peak declerations that are induced in a vehicle during redirection. Average force is an idealized value used in the theoretical analysis of the interaction between the vehicle and the guardrail. Fracture energy of guardrail posts, in addition to other guardrail performance characteristics, is directly related to the vehicle kinetic energy dissipated during impact. These properties are shown in Figures 4 and 5 for typical timber and steel posts respectively; sample data-reduction calculations are given in the Appendix.

Findings from the experimental program are given in Tables 2, 3, 4, and 5 for red oak, red pine, southern pine, and Douglas fir timber species respectively. Data from dynamic tests performed on typical steel guardrail posts are given in Table 6 for reference.

Variation of the peak resistance force is shown in Figure 6 for Douglas fir posts. The average of data from each post size is indicated by a darkened symbol; a straight

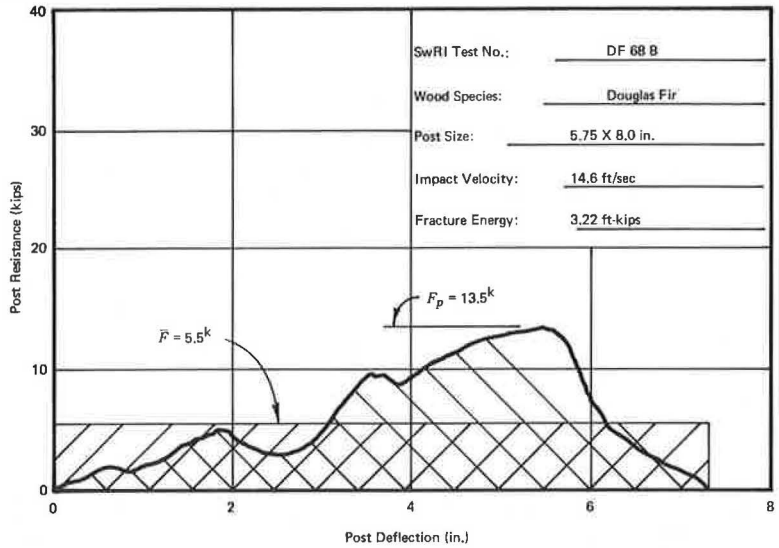

Figure 4. Typical dynamic force-deflection plot of timber specimen.

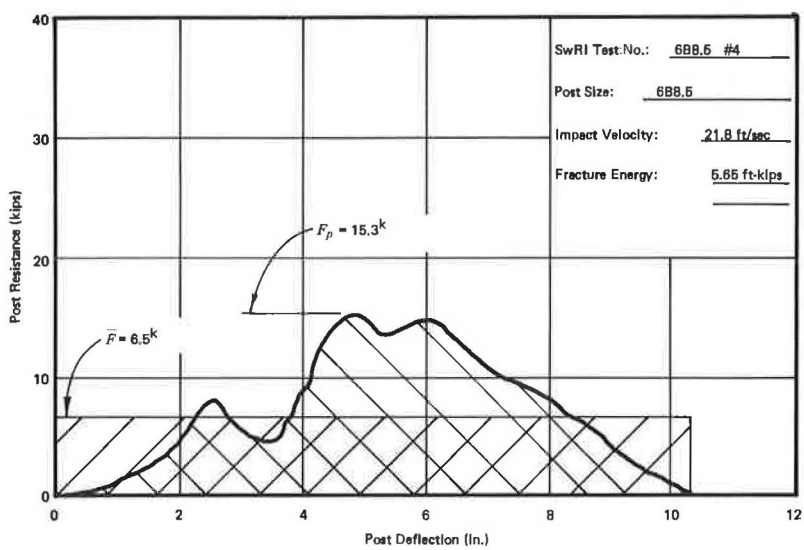

Figure 5. Typical dynamic force-deflection plot of steel specimen.

line is extended through these points. It is to be noted that the extended curve does not intersect the zero ordinate point. This anomaly may be attributed to inertia effects of the post.

Other plots of the test data are shown in Figures 7, 8, 9, and 10. The points represent the average value for the particular post specimen geometry for red oak, southern pine, and Douglas fir. For red pine, however, the specimen sizes were random, and a straight curve was statistically fitted to the data points.

TABLE 2

SUMMARY OF TEST RESULTS OF RED OAK POSTS

Specimen No.	Width (W, in.)	Depth (D, in.)	Area (A, $in.^2$)	Moment of Inertia (I, $in.^4$)	Section Modulus (S, $in.^3$)	Moisture Content (C, percent)	Specific Gravity	Impact Velocity (V_I, fps)	Impact Duration (t, msec)	Impulse (MV, lb-sec)	Fracture Energy (FE, ft-kips)	Peak Force (F_p, kips)	Average Force ($\bar{F}$, kips)
RO 44													
A	3.80	4.00	15.2	20.2	10.1	16.1	0.65	14.8	58	128	1.78	4.8	2.2
B	3.80	4.10	15.6	21.7	10.6	17.8	0.71	15.0	74	243	3.48	5.8	3.3
C	3.90	4.20	16.4	24.1	11.5	19.2	0.68	14.4	54	183	2.55	7.1	3.4
D	3.80	4.20	15.9	23.5	11.2	15.7	0.66	14.7	56	182	2.60	6.4	3.2
E	4.00	4.25	17.0	25.5	12.0	14.5	0.65	14.8	60	149	2.11	5.7	2.5
F	3.75	3.80	14.2	17.1	9.0	16.1	0.72	14.9	51	121	1.79	5.5	2.4
G	3.80	4.00	15.2	20.2	10.1	16.4	0.70	15.7	56	134	2.07	5.2	2.4
H	3.80	4.00	15.2	20.2	10.1	13.9	0.71	14.8	50	79	1.08	3.3	1.6
Average			15.59	21.56	10.58	16.21	0.685	14.89	57.4	152.4	2.182	5.5	2.62
RO 46													
A	3.90	6.00	23.4	70.2	23.4	18.3	0.58	15.0	52	231	3.16	8.4	4.4
B	4.00	6.20	24.8	79.4	25.6	18.0	0.68	14.9	59	361	4.84	11.5	6.1
C	4.00	6.00	24.0	72.0	24.0	15.1	0.74	14.9	44	278	3.77	8.7	6.3
D	4.00	6.20	24.8	79.4	25.6	16.2	0.70	15.3	48	322	4.52	10.2	6.7
E	3.80	5.90	22.4	64.9	22.0	16.4	0.75	15.5	56	326	4.58	14.1	5.8
F	4.00	6.10	24.4	75.6	24.8	15.8	0.74	15.2	53	267	3.69	11.1	5.0
G	4.00	5.90	23.6	68.7	23.3	13.3	0.75	15.7	59	348	4.98	12.3	5.9
H	3.90	5.75	22.4	61.8	21.5	15.6	0.77	15.2	50	205	2.86	11.1	4.1
Average			23.72	71.50	23.78	16.09	0.714	15.21	52.6	292.2	4.050	10.9	5.54
RO 66													
A	5.80	6.00	34.8	104	34.8	17.2	0.68	14.6	63	584	7.16	17.5	9.3
B	6.00	6.25	37.5	122	39.1	19.4	0.61	14.5	52	128	1.74	6.5	2.5
D	5.75	5.75	33.1	91	31.7	19.6	0.65	14.5	50	233	3.20	10.9	4.7
E	6.00	6.10	36.6	114	37.2	18.8	0.72	14.4	48	214	2.86	10.3	4.4
F	5.80	6.00	34.8	104	34.8	18.2	0.68	14.5	44	203	2.72	10.9	4.6
Average			35.36	107.0	35.5	18.52	0.672	14.50	51.4	272.4	3.536	11.6	5.10
RO 68													
A	5.75	8.17	46.9	261	64.0	21.6	0.68	29.6	27	202	5.73	20.4	7.5
B	5.67	7.75	43.9	220	56.8	21.4	0.62	30.1	42	280	7.92	19.0	6.7
C	6.00	8.00	48.0	256	64.0	23.6	0.68	29.9	35	335	9.58	25.9	9.6
D	6.00	8.25	49.5	281	68.1	18.7	0.67	29.8	27	209	6.11	21.4	7.7
E	5.87	7.87	46.2	238	60.6	18.1	0.64	29.2	29	230	6.32	19.2	7.9
F	5.87	8.00	46.9	250	62.6	18.6	0.67	29.7	37	333	9.51	24.8	9.0
G	6.17	7.87	48.6	251	63.7	19.2	0.75	29.7	35	330	9.17	27.2	9.4
H	5.75	7.75	44.6	223	57.6	18.7	0.70	29.6	31	172	5.03	18.2	5.5
Average			46.82	247.5	62.18	19.99	0.676	29.70	32.9	261.4	7.421	22.0	7.91

TABLE 3

SUMMARY OF TEST RESULTS OF RED PINE POSTS

Specimen No.	Diameter (d, in.)	Moment of Inertia (I, $in.^4$)	Moisture Content (C, percent)	Specific Gravity	Impact Velocity (V_I, fps)	Impact Duration (t, msec)	Impulse (MV, lb-sec)	Fracture Energy (FE, ft-kips)[a]	Peak Force (F_p, kips)[b]	Average Force ($\bar{F}$, kips)[c]
A1	6.10	68.0	13	0.34	15.1	38	60.7	0.92	4.1	2.2
A5	6.50	87.6	16	0.32	15.1	48	142.5	1.99	7.9	3.9
A4	6.60	93.2	17	0.38	15.1	42	81.9	1.28	5.7	2.8
A2	6.75	101.9	16	0.37	15.1	50	136.0	1.99	8.0	3.8
A3	7.25	135.7	22	0.34	15.1	54	253.0	3.50	12.0	6.5
A9	8.60	268.6	18	0.36	15.1	52	326.0	4.45	16.0	9.1
A8	9.10	336.7	19	0.35	15.1	62	417.0	5.66	17.1	10.3
A7	9.30	367.3	23	0.39	15.1	63	611.0	7.65	21.4	9.8
B4	6.50	87.6	14	0.33	15.1	48	131.5	1.81	8.1	3.6
B7	7.00	117.9	15	0.36	15.1	56	250.5	3.50	11.1	6.3
B3	7.00	117.9	14	0.33	15.1	47	122.8	1.81	6.5	2.7
B10	7.25	135.7	15	0.36	15.1	51	145.0	2.16	7.4	2.9
B6	7.75	177.1	17	0.38	15.1	66	491.0	6.50	16.8	11.7
B8	8.15	216.6	17	0.33	15.1	54	285.5	3.99	13.2	7.6
B9	8.50	263.3	18	0.37	15.1	90	930.0	10.57	21.3	20.5
B5	9.75	443.7	17	0.37	15.1	59	467.0	6.23	19.8	12.4

[a]Statistical curve fit to data: FE = 0.73 + 0.017 I. [b]Statistical curve fit to data: F_p = 3.96 + 0.044 I. [c]Statistical curve fit to data: $\bar{F}$ = 1.56 + 0.030 I.

TABLE 4

SUMMARY OF TEST RESULTS OF SOUTHERN PINE POSTS

Specimen No.	Width (W, in.)	Depth (D, in.)	Area (A, $in.^2$)	Moment of Inertia (I, $in.^4$)	Section Modulus (S, $in.^3$)	Moisture Content (C, percent)	Specific Gravity	Impact Velocity (V_I, fps)	Impact Duration (t, msec)	Impulse (MV, lb-sec)	Fracture Energy (FE, ft-kips)	Peak Force (F_p, kips)	Average Force ($\overline{F}$, kips)
SP 46													
A	3.88	6.00	23.3	65.4	21.8	12.4	0.46	15.4	53	209	3.07	8.9	3.9
B	3.88	6.00	23.3	65.4	21.8	11.3	0.50	14.8	38	133	1.94	7.9	3.5
C	3.88	6.00	23.3	65.4	21.8	10.0	0.46	15.2	38	141	2.00	7.6	3.7
D	3.88	6.00	23.3	65.4	21.8	11.5	0.50	15.3	50	166	2.37	8.5	3.3
Average			23.30	65.40	21.80	11.30	0.480	15.2	44.8	162.2	2.345	8.2	3.60
SP 66													
A	6.00	6.12	36.7	115	37.5	11.6	0.46	15.0	47	126	1.80	7.7	2.7
B	5.75	6.06	34.8	107	35.2	11.4	0.41	15.2	38	103	1.46	7.8	2.7
C	6.00	6.00	36.0	108	36.0	10.8	0.52	15.1	58	309	4.30	12.0	5.3
D	6.00	6.12	36.7	115	37.5	12.3	0.62	15.1	67	359	4.92	14.3	5.4
E	6.00	6.00	36.0	108	36.0	10.9	0.47	15.1	52	183	2.67	9.3	3.5
F	6.00	6.00	36.0	108	36.0	11.3	0.47	15.1	41	118	1.64	8.9	2.9
Average			36.03	110.2	36.37	11.38	0.491	15.10	50.5	199.7	2.798	10.0	3.75
SP 88													
A	7.88	8.38	66.0	386	92.2	14.0	0.53	19.9	55	637	11.7	22.0	11.6
B	8.25	8.38	69.1	405	96.6	17.7	0.51	29.8	68	637	17.3	24.3	9.4
C	8.06	8.12	65.4	360	88.6	13.1	0.53	29.4	43	506	13.9	25.9	11.8
D	8.06	8.50	68.5	413	97.1	13.3	0.50	27.6	32	233	6.3	29.4	7.3
E	8.00	8.12	64.9	357	87.9	10.7	0.56	27.6	43	470	12.1	25.2	10.9
F	8.12	8.38	68.0	398	95.0	11.2	0.46	29.6	43	452	12.4	28.4	10.5
G	7.94	8.31	65.9	380	91.4	15.1	0.54	29.2	40	366	9.9	28.0	9.2
H	8.12	8.25	66.9	380	92.1	12.8	0.58	27.6	43	424	10.9	25.4	9.9
Average			66.84	384.9	92.61	13.49	0.526	27.59	45.9	465.6	11.81	26.1	10.08
AP 9R													
A	8.38		55.1	242	57.8	9.5	0.53	20.9	34	209	4.24	14.4	6.1
B	8.75		60.1	288	65.8	12.4	0.63	20.2	44	373	6.97	20.8	8.5
C	8.00		50.2	201	50.3	11.2	0.52	20.1	43	313	5.85	17.3	7.3
D	8.38		55.1	242	57.8	11.1	0.52	20.2	35	243	4.77	15.6	6.9
Average			55.12	243.2	57.9	11.05	0.550	20.35	39.0	284.5	5.458	16.8	7.20

Note: Post specimens were creosote-treated. Specific gravity and moisture content were determined by the American Wood Preservers Bureau, Inc.

TABLE 5

SUMMARY OF TEST RESULTS OF DOUGLAS FIR POSTS

Specimen No.	Width (W, in.)	Depth (D, in.)	Area (A, $in.^2$)	Moment of Inertia (I, $in.^4$)	Section Modulus (S, $in.^3$)	Moisture Content (C, percent)	Specific Gravity	Impact Velocity (V_I, fps)	Impact Duration (t, msec)	Impulse (MV, lb-sec)	Fracture Energy (FE, ft-kips)	Peak Force (F_p, kips)	Average Force ($\overline{F}$, kips)
DF 44													
A	3.88	3.88	15.0	18.8	9.7	13.0	0.50	14.8	44	63	0.90	3.7	1.4
B	3.94	4.00	15.8	21.0	10.5	14.4	0.45	15.0	44	84	1.27	4.7	1.9
C	3.88	4.12	15.9	22.7	11.0	12.7	0.46	14.9	40	82	1.27	4.7	2.0
D	4.12	4.12	16.9	23.9	11.6	13.6	0.49	15.0	36	51	0.73	3.3	1.4
E	3.88	4.06	15.8	21.5	10.6	14.5	0.50	14.8	42	78	1.08	4.4	1.8
F	3.88	4.00	15.5	20.6	10.3	14.1	0.57	15.2	53	122	1.83	5.5	2.3
G	3.75	4.12	15.4	21.8	10.6	13.8	0.43	14.7	31	35	0.54	2.9	1.1
H	3.94	4.12	16.2	22.9	11.1	14.0	0.52	14.9	44	102	1.44	5.6	2.3
Average			15.81	21.65	10.68	13.76	0.490	14.91	41.8	77.1	1.132	4.35	1.78
DF 46													
A	4.00	6.00	24.0	72.0	24.0	15.0	0.48	15.0	36	159	2.32	10.0	4.4
B	4.12	6.00	24.7	74.1	24.7	13.0	0.50	14.8	43	182	2.61	10.5	4.2
C	3.88	6.00	23.3	69.9	23.3	17.2	0.47	14.9	48	112	1.61	6.5	2.3
D	4.25	6.00	25.5	76.5	25.5	15.8	0.44	15.0	49	137	1.98	7.4	2.8
E	4.12	6.12	25.2	78.6	25.7	15.6	0.47	15.1	50	174	2.50	7.5	3.5
F	4.25	5.88	24.9	72.0	24.5	13.8	0.44	15.0	47	97	1.45	5.9	2.1
G	4.00	6.00	24.0	72.0	24.0	15.5	0.44	14.8	46	98	1.43	5.9	2.1
H	4.00	6.00	24.0	72.0	24.0	14.7	0.46	14.8	35	90	1.25	6.8	2.6
Average			24.45	73.39	24.46	15.08	0.462	14.92	44.2	131.1	1.894	7.56	3.00
DF 68													
A	6.00	8.00	48.0	256	64.0	14.6	0.56	14.5	55	360	4.70	17.9	6.5
B	5.75	8.00	46.0	245	61.3	14.0	0.47	14.6	42	233	3.22	13.5	5.5
C	5.75	8.00	46.0	245	61.3	13.6	0.49	14.9	50	247	3.45	15.5	4.9
D	6.00	7.75	46.5	233	60.1	14.3	0.46	14.6	54	430	5.59	18.2	8.0
E	5.80	7.75	44.9	225	58.1	16.0	0.60	14.6	45	202	2.74	12.3	4.5
F	5.75	7.80	44.8	227	58.3	16.8	0.63	14.6	67	715	8.43	21.5	10.7
G	5.80	7.75	44.9	233	60.1	16.1	0.49	14.6	64	622	7.52	18.0	9.7
H	5.80	8.00	46.4	248	61.9	14.8	0.58	14.7	48	235	3.25	13.3	4.9
Average			45.94	239.0	60.64	15.02	0.535	14.64	53.1	380.5	4.862	16.28	6.84
DF 88													
A	7.60	8.00	60.8	324	81.1	14.2	0.43	15.0	61	596	7.52	22.1	9.8
B	7.60	7.88	59.9	310	78.6	14.8	0.45	14.7	77	531	6.70	16.9	6.9
C	7.75	8.00	62.0	331	82.7	14.5	0.47	14.9	63	596	7.45	21.5	9.5
D	7.60	7.88	59.9	310	78.6	14.1	0.46	14.7	67	483	6.18	17.5	7.2
E	7.60	7.88	59.9	310	78.6	15.9	0.51	15.0	58	537	6.86	20.9	9.2
F	7.60	7.75	58.9	295	76.1	16.1	0.51	14.8	63	664	8.00	23.0	10.5
G	7.75	7.75	60.1	301	77.6	14.6	0.53	14.8	65	689	8.23	22.1	10.6
H	7.60	7.88	59.9	310	78.6	15.1	0.45	14.9	63	561	7.07	19.0	8.9
Average			60.18	311.4	78.99	14.91	0.477	14.85	64.6	582.1	7.251	20.38	9.08

TABLE 6

TEST RESULTS FROM TYPICAL STEEL GUARDRAIL POSTS

Specimen No.	Section Modulus (Sx, in.^{3})	Section Modulus (Sy, in.^{3})	Impact Velocity (V_I, fps)	Impulse (MV, lb-sec)	Fracture Energy (FE, ft-kips)	Impact Duration (t, msec)	Peak Force (F_p, kips)	Average Force ($\bar{F}$, kips)
3I5.7								
1	1.7	0.40	14.8	248	3.43	74	4.9	3.4
2	1.7	0.40	14.7	264	3.56	75	5.0	3.5
3	1.7	0.40	20.8	152	3.01	53	5.5	2.9
4	1.7	0.40	14.9	336	4.55	74	6.5	4.5
Average			16.3	333	3.635	69.0	5.5	3.58
6B8.5								
1	5.07	0.96	19.7	258	4.86	37	14.3	7.0
2	5.07	0.96	14.6	506	6.40	61	15.5	8.3
3	5.07	0.96	19.8	400	7.23	50	16.0	8.0
4	5.07	0.96	21.8	273	5.65	42	15.3	6.5
Average			19.0	359	6.035	48	15.3	7.4

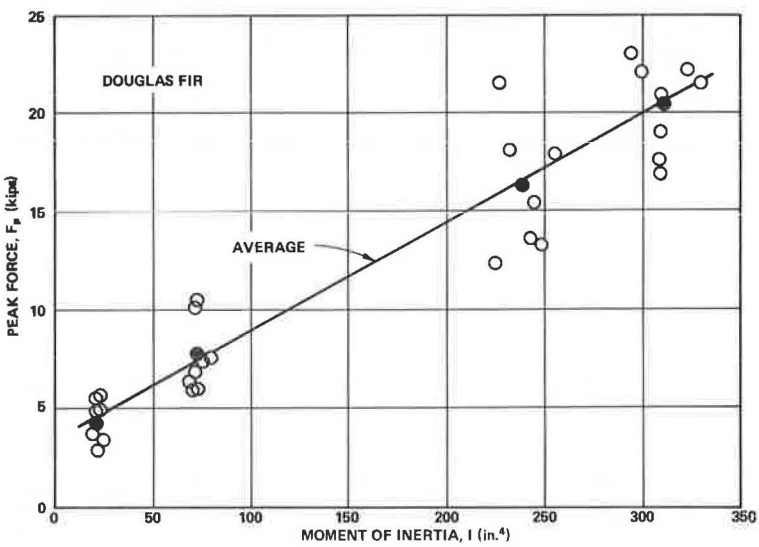

Figure 6. Variation of Douglas fir peak force with moment of inertia.

Peak resistance force plotted against moment of inertia is shown in Figure 7. Each point is the average of the four to eight tests conducted on the various sizes and wood species. With the exception of the 4- by 6-in. red oak group and the 8- by 8-in. southern pine group, the points fall quite near their respective straight lines. Douglas fir and southern pine exhibit approximately the same strength property, whereas red oak is the highest strength species and red pine the lowest strength species.

In Figure 8, average post resistance is plotted against moment of inertia. As expected, the resistance increases with moment of inertia for all species. The curves are approximately parallel with the red pine and red oak materials indicating the highest strength; the southern pine and Douglas fir curves almost coincide. It is to be noted that the shape of the post (i.e., round or rectangular) appears to have modest effect on the curves as evidenced by the 9-in. diameter southern pine specimen group point that falls on the basic curve. Clear round wood is normally 18 percent stronger in static flexure than clear rectangular wood. One point on the red oak appeared to be high and was neglected.

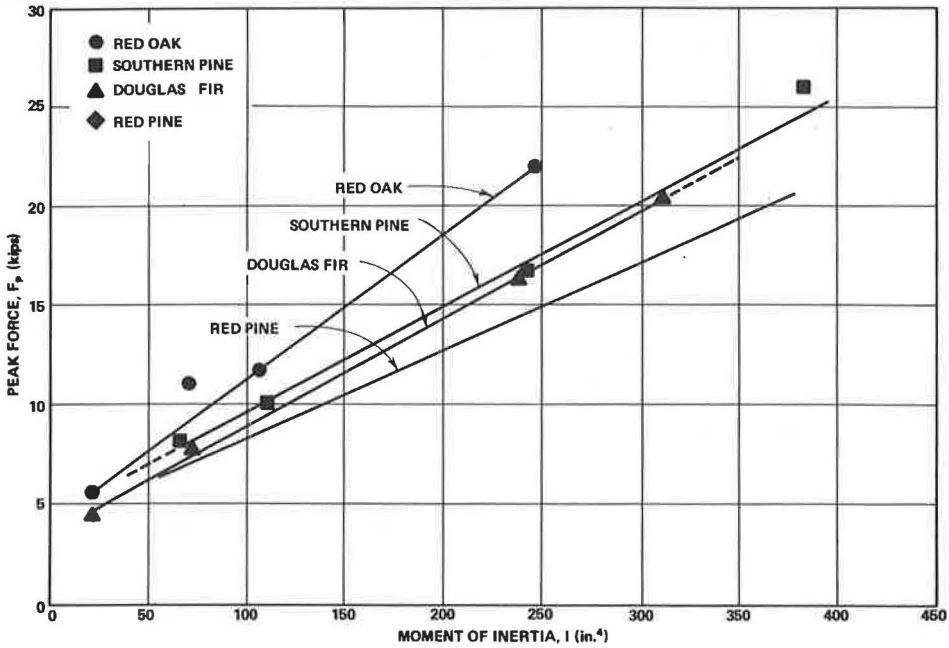

Figure 7. Variation of peak force with moment of inertia.

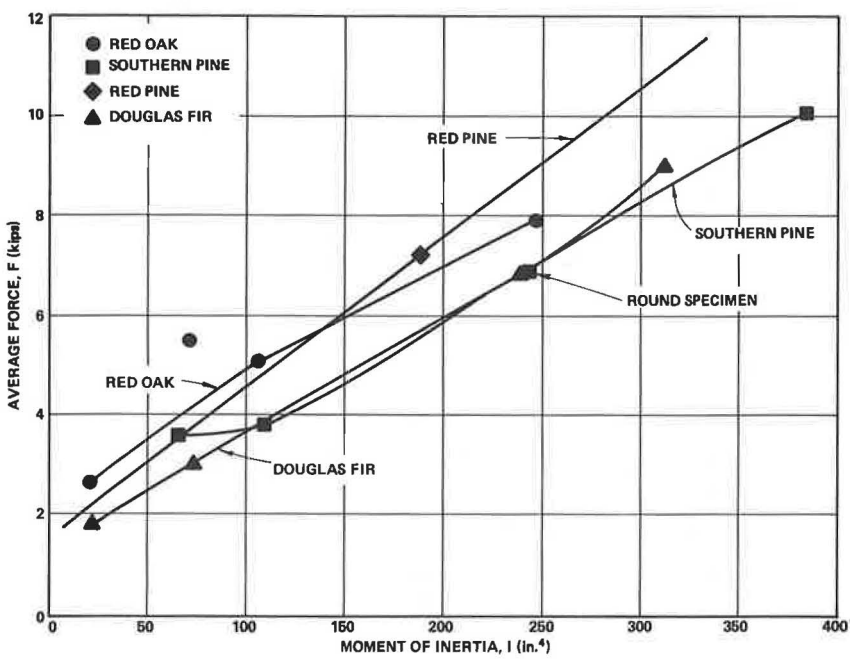

Figure 8. Variation of average force with moment of inertia.

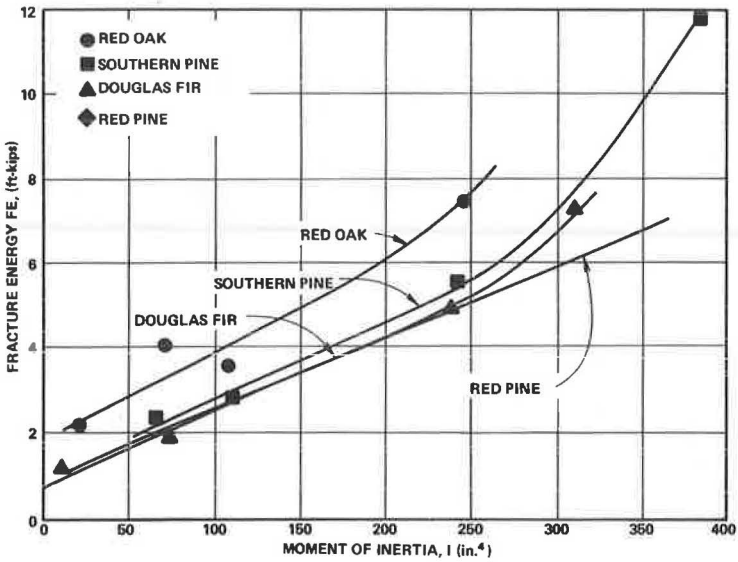

Figure 9. Variation of fraction energy with moment of inertia.

Fracture energy is plotted against moment of inertia for the four timber species in Figure 9. Red oak species possess the highest fracture energy for a given moment of inertia. The fracture energy of the other species is approximately the same. Below a moment of inertia I of 200 in.^{4}, the curves appear to be nearly linear. Above an I of

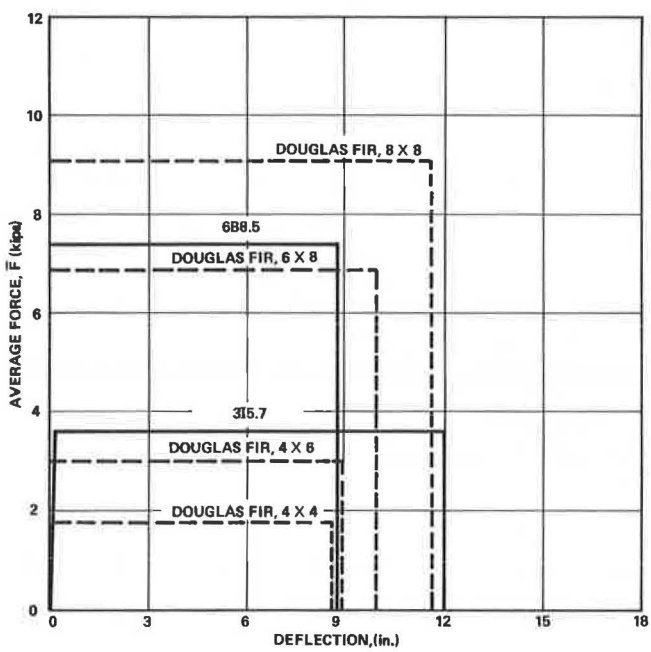

Figure 10. Average force versus deflection for typical guardrail posts.

250 in.^{4}, fracture energy indicates a tendency to increase at a more pronounced rate, particularly for Douglas fir and southern pine. It is to be noted that the shape of the southern pine specimens appears to have negligible effect on fracture energy as the round specimen group points fall on the curve connecting the rectangular-shaped specimen groups.

In Figure 10, average force is plotted against post deflection and displayed for some typical guardrail post specimens. Plots of Douglas fir specimens (4 by 4 in., 4 by 6 in., 6 by 8 in., and 8 by 8 in.) are shown with those of 6B8.5 and 315.7 steel members. In all tests, the specimens were rigidly fixed. The timber specimens fractured at the cantilever point, while the steel members twisted and bent about their weak axis. It is to be noted that the Douglas fir specimens of 6 by 8 in. and 4 by 6 in. are comparable to the 6B8.5 and 315.7 steel specimens respectively.

DISCUSSION OF FINDINGS

Several points from the program findings seem worthy of discussion and emphasis.

Test Procedure

For this program, the specimens were rigidly secured in a base fixture and then impacted with a mass possessing sufficient kinetic energy to break the specimen. Except for the so-called weak-post guardrail systems (1), guardrail posts seldom break under vehicle impact but, instead, deflect in the soil. As shown in Figure 11, in case I, the post is sufficiently embedded in the soil to develop the post strength, and it breaks prior to significant soil deformation. Cases II and III demonstrate the strong-post system in which soil failure occurs at a force on the post that is less than the post's breaking strength. Because the purpose of the program was to generate guardrail post properties and not the more complex post-soil composite properties, the soil-embedment effect was eliminated by securing the specimens in a rigid fixture.

Test Data Variation

Although there is a variation in the data of an individual specimen from its species and size group average, the average values of peak force, average force, and fracture

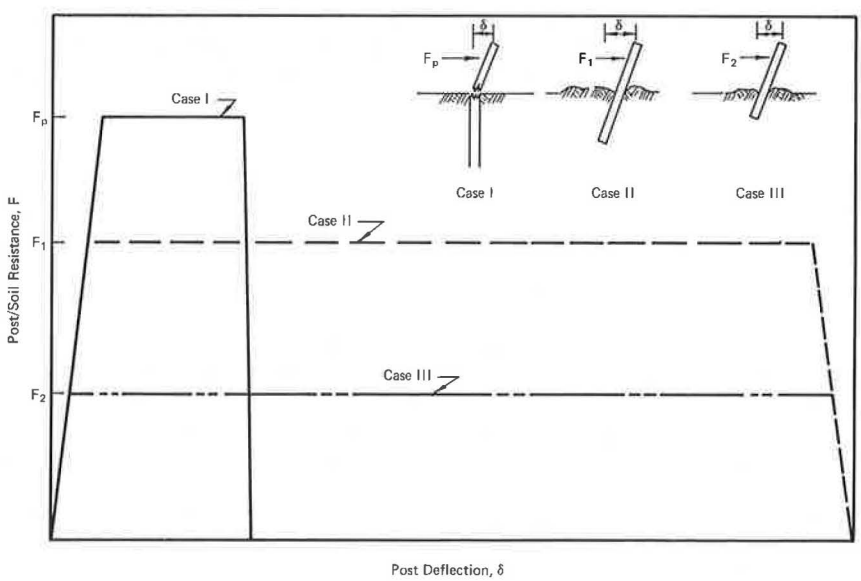

Figure 11. Idealized post-soil reactions.

energy, plotted as a function of moment of inertia, fall on or near a linear curve. This would suggest that the variation within a species and size test group has a normal distribution. On examination of the failed specimens, the variation can generally be attributed to any of several specimen imperfections such as knots, checks, shakes, worm holes, and rot located in the failure zone. Also, a portion of the data scatter is attributed to variation of ring density and specific gravity. Effects of moisture content (i.e., within normal service range) and preservative treatment on the dynamic properties of guardrail post are unknown but are surmised to be small.

Dynamic Properties

One of the three most important post dynamic properties is considered to be peak (or breaking) force. Peak force is a critical factor in the design of weak-post guardrail systems. If the post breaking force is too large, the impacting vehicle will snag on the post and spin out. Hence, higher strength is not necessarily a prerequisite of post materials for a guardrail system. On the contrary, it is suspected that the lower strength wood species may exhibit superior performance in the weak-post systems. On the other hand, if the breaking force is too small, the entire guardrail installation will collapse at initial vehicle impact. In the strong-post systems, it is necessary to provide a post strength slightly in excess of the soil resistance force (F_1 or F_2 in cases II and III respectively, Fig. 11).

The magnitude of dynamic peak force, average force, and fracture energy is a function of (a) specimen geometry and (b) wood species. As shown in Figures 7, 8, and 9, these properties vary directly with moment of inertia. (These properties also vary directly with the section area and section modulus, but the curves are nonlinear.) Specimen sectional shape does not appear to be a critical factor as square, rectangular, and round specimen data can be displayed on the same curve (Figs. 7, 8, and 9). This suggests that the engineer can use sawed or round material and expect equal performance for equal moments of inertia.

Concerning wood species, red oak, in general, exhibited the highest dynamic property values followed by Douglas fir and southern pine and then red pine. For the average force property, the red pine values were comparable to those of the red oak species. Ring density and specific gravity, possible subgroup characteristics of each wood species, appear, as one might expect, to have a meaningful influence on the properties. However, no definite conclusion on the magnitude of this effect can be deduced from the test results. Moisture content and preservative treatment also may affect dynamic properties, but results from static tests by others suggest these effects would be small. The presence of a significant degree of imperfections such as knots, checks, shakes, holes, and rot in the failure zone could significantly reduce the dynamic properties.

Application of Results

Several potential uses are suggested for the data and findings developed in the program:

1. Alternate materials may be specified for guardrail posts. By selecting a proper sectional area, the posts of alternate material will develop dynamic characteristics equivalent to those of the standard posts.
2. Dimensional tolerances for posts can be established on the basis of design performance. For instance, if a post is being selected to break within a certain dynamic force range, then the post dimensions can be established with tolerances consistent with the force range. It is to be noted that tolerances on section depth may be more critical than section width in cases where moment of inertia is a design factor.
3. Initial design of posts for new guardrail systems can be based on the experimental data.
4. The findings can be utilized in various mathematical models of a vehicle-barrier collision to improve correlation between the theoretical and physical events.
5. The findings may serve as a base line for exploring new and improved methods to convert existing strong-post systems and pole designs to breakaway designs.

REFERENCE

1. Michie, J. D., and Calcote, L. R. Location, Selection, and Maintenance of Highway Guardrails and Median Barriers. NCHRP Rept. 54, 1968.

Appendix

SAMPLE CALCULATIONS

The following calulations are used in scaling, converting, and processing experimental data from the pendulum impact facility. The basic data consist of a continuous recording of accelerometer output during specimen impact.

1. Determine acceleration magnitude of pendulum mass at time t

$$A_t = \left(\frac{d_t}{d_c}\right) A_c \tag{1}$$

where d_c is the Visicorder trace deflection (in.) resulting from the reference calibration signal corresponding to A_c acceleration (g), and d_t is the Visicorder trace deflection (in.) at any time t during test.

Example: For case where d_c, A_c, and d_t are 2.98 in., 5.2 g, and 0.75 in. respectively, then

$$A_t = \left(\frac{0.75}{2.98}\right)(5.2) = 1.31 \text{ g}$$

2. Determine magnitude of force acting on pendulum mass at time t (note that this is equal to but in the opposite direction of the force acting on the post)

$$F_t = ma_t \tag{2}$$

where m is pendulum mass (lb-sec^2/ft) and a_t (ft/sec^2) is acceleration (or deceleration) of mass.

Example: For case where pendulum weighs 4,000 lb and a_t is 1.31 g,

$$F_t = \left(\frac{4{,}000}{g}\right)(1.31 \text{ g}) = 5{,}240 \text{ lb}$$

3. Determine velocity of pendulum mass after impact. By Newton's second law of motion, the linear impulse is equal to the change in linear momentum of the pendulum mass

$$\int_{t_o}^{t_f} F_{x_t} dt = m(v_f - v_o) \tag{3}$$

where F_{x_t} is the resultant force acting on the pendulum mass in the x-direction at time t, m is the pendulum mass, and v_o and v_f are the initial and final velocities of the mass in the x-direction. A typical force-time curve is shown in Figure 12. (By definition linear impulse is equal to the area under the curve.)

Example: If the time scale in Figure 12 is 20 msec/in. and the force scale is 20,800 lb/in., then 1.0 sq in. of area represents a linear impulse of 0.020 x 20,800 or 416

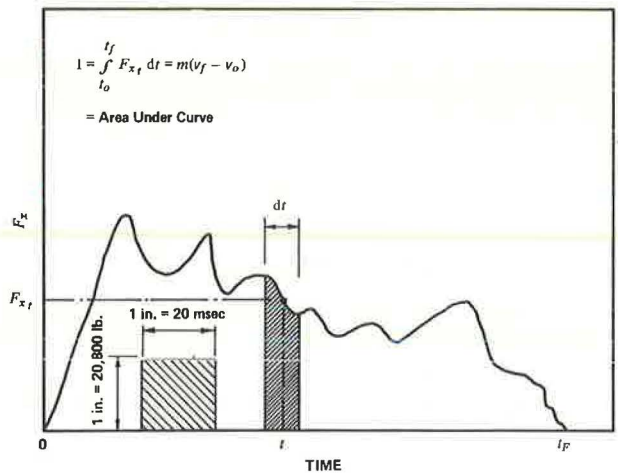

Figure 12. Pendulum mass linear impulse determination.

lb-sec/in.^{2}. If the area under the curve is determined to be 6.50 sq in., initial velocity of the mass is 30.3 fps, and the mass weighs 4,000 lb, then the final velocity can be calculated as

$$\int_{t_o}^{t_f} F_{x_t} dt = (\text{area})(K) = m(v_f - v_o)$$

$$-(6.50)(416) = \frac{4{,}000}{32.2}(v_f - 30.3)$$

$$v_f = (30.3 - 21.8) = 8.5 \text{ fps}$$

4. Determine the energy dissipated in fracturing the post specimen. The work ΔU done by force F_X on the pendulum mass during movement d_X is equal to the change in kinetic energy ΔT of the mass; this is also the fracture energy of the post specimen:

$$\Delta U = \Delta T \tag{4}$$

$$\int_0^x F_x dx = \frac{1}{2} m(v_f^2 - v_o^2)$$

Example: Initial and final velocities are 30.3 and 8.5 fps respectively. Then the change in kinetic energy (fracture energy) is

$$\Delta T = \frac{1}{2} m(v_f^2 - v_o^2) = \frac{4{,}000}{2(32.2)}\left[(8.5)^2 - (30.3)^2\right] = 52{,}500 \text{ ft-lb}$$

5. Calculate post displacement during impact. Assume mass velocity changes linearly with time; thus

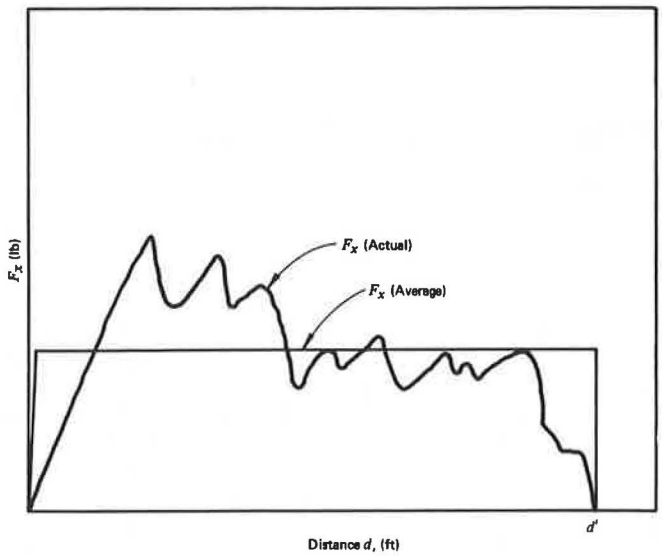

Figure 13. Relationship between actual and average force.

$$d' = \left(\frac{v_f + v_o}{2}\right)(t_f - t_o) \tag{5}$$

where v_f, v_o, t_f, and t_o are respectively final and initial velocities and final and initial time.

Example: Let v_f and v_o be 30.3 and 8.5 fps and t_f and t_o be 200 and 0 msec; then

$$d = \left(\frac{8.5 + 30.3}{2}\right)(200 - 0) = 3.88 \text{ ft}$$

6. Calculate the average force during specimen displacement

$$\int_0^x F_x dx = \overline{F}_x d' = \Delta U \tag{6}$$

where $\overline{F}_x$ is an idealized constant force that acts through distance d′ (Fig. 13).

Example: Let ΔU be 52,500 ft-lb and d′ be 3.88 ft; then

$$\overline{F}_x = \left(\frac{U}{d'}\right) = \left(\frac{52,500}{3.88}\right) = 13,520 \text{ lb}$$

EVALUATION OF TIMBER WEAK-POST GUARDRAIL SYSTEMS

Maurice E. Bronstad, Southwest Research Institute; and
Robert B. Burket, Ohio Department of Highways

Six full-scale vehicle crash tests were conducted on guardrail systems to evaluate the effectiveness of substituting timber posts for the standard 3I5.7 steel posts specified in a current guardrail standard. Results of the tests indicate that timber is a suitable post material for the "weak-post" concept. Although there was some difficulty in determining the proper rail attachment to the post, solutions to the problem are suggested in this report. Basically, the timber post design calls for a 12-gage flexural beam mounted on 6- by 7-in. or 5½-in. diameter pine posts spaced at 12.5-ft centers. A ¼-in. diameter steel bolt and a pipe insert provide proper attachment of rail to post. The sixth test of the series provided an evaluation of the effectiveness of a continuous installation composed of the new timber weak-post system and the department's strong-post system. The test results indicated that the transition design between the two systems was satisfactory, but design changes could improve performance.

•PRIOR TO 1967 and publication of the Yellow Book on Highway Safety (1), Ohio's guardrail design for most projects featured a steel W-shaped rail mounted on heavy round or square sawed wood posts or on 6B8.5 steel posts spaced 12.5 ft center to center.

In 1967 the Federal Highway Administration announced that guardrails used in new construction projects had to conform to requirements for systems that had been subjected to dynamic testing. This requirement limited guardrail design at that time to those developed by California and New York. Ohio was not prepared to accept the new concepts developed by New York and elected to continue use of the universal beam rail element mounted on heavy posts and offset blocks at 6.25-ft spacings.

The Federal Highway Administration subsequently announced that existing guardrail installations must also be made to conform with current safety standards. Meanwhile, guardrail costs for new construction in Ohio increased from $2.20 per foot in 1966 for the old design to $3.62 per foot in 1968 for the new design.

It was estimated that 90 percent of the guardrails erected on the Ohio Interstate system to date could conform to the New York W-beam concept of weak posts by notching existing timber strong posts (design deflections of New York design could be tolerated). It was, therefore, considered desirable to design a guardrail system for highway shoulder applications that would take advantage of much lower costs on new construction and also lend itself to inexpensive conversion of existing systems. It was also considered desirable to permit use of a wood-post alternate on new construction because many of the posts are produced in the depressed areas of southern Ohio by low-income landowners.

Because of maintenance considerations and in order to attain a certain continuity in design, it was considered desirable to use a single rail element for all applications by varying the post stiffness and spacing to achieve a range of lateral deflections. To do

Sponsored by Committee on Traffic Safety Barriers and Sign, Signal and Lighting Supports and presented at the 50th Annual Meeting.

this it was proposed that the New York W-beam concept be used where considerable lateral deflection could be tolerated and that the California blocked-out W-beam concept be used where obstacles dictate restricted lateral deflection.

To connect the two systems where both occurred in a single run of guardrail, it was necessary to design and test a flexibility transition. A similar design could also be used as a flexibility transition between bridge parapets.

The W-beam and weak-post system concept developed by New York consists of a 12-gage steel W-beam mounted on 3I5.7 steel posts spaced at 12.5 ft; a $^{5}/_{16}$-in. diameter bolt provides the beam-to-post attachment. This system is standard G2 as reported by Michie and Calcote (2). To determine if a timber post could be substituted for the steel posts and otherwise meet the requirements of guardrail systems in Ohio, the Ohio Department of Highways contracted with the Department of Structural Research of Southwest Research Institute to conduct a full-scale crash-test program for concept evaluation. Objectives of the program were to determine (a) post size required to furnish a timber post alternate to the 3I5.7 steel post, (b) "notching" required to modify existing strong timber posts, and (c) proper rail-to-post attachment.

Although the G2 top-of-rail height had been recently raised from 30 in. to 33 in. by New York State, the rail height for this program was set at 27 in., thus conforming with the height of rail common to many existing installations in Ohio. Using the information from this test program, the Ohio Department of Highways intends to modify its installations by notching these existing strong posts. Five tests were conducted in this program to determine the optimum post size and rail-to-post attachment required to achieve desirable performance. In order to evaluate the performance of an installation incorporating a transition from a weak-post to strong-post system, a sixth test was conducted with the point of impact several feet upstream from the transition.

DISCUSSION OF TEST PROGRAM

The Ohio Department of Highways prepared a series of preliminary standard construction drawings that included a guardrail system designated as type 7. This design was similar to the G2 system mentioned previously (2) with three exceptions:

1. Wood posts were included along with the G2 standard 3I5.7 steel post;
2. The top of rail was specified as 27 in. instead of the G2 standard of 30 in.; and
3. The bolt hole in the standard washer was offset to improve support of the standard flexural beam (W-beam).

A test program was formulated to evaluate the feasibility of these changes in a proved system and to determine the size of wood post that could be substituted for the 3I5.7 steel post.

Six full-scale crash tests were conducted. All guardrail systems tested were composed of standard 12-gage steel flexural beam mounted on treated timber posts. A summary of the test series is given in Table 1. The posts were driven to grade with a

TABLE 1

SUMMARY OF TEST SERIES

Test No.	Post	Post Area (in.^{2})	Post Bolt	Vehicle Weight (lb)	Vehicle Speed (mph)	Impact Angle (deg)	Maximum Dynamic Deflection (ft)	Maximum Permanent Deflection (ft)	Guardrail Performance or Vehicle Reaction
ODH-1	4 by 4 in.	16	$^{5}/_{16}$-in. diameter steel	4,589	67.0	25.0	13+	10.0	Vehicle straddled rail, rolled 3½ times
ODH-2	4 by 6 in.	24	$^{5}/_{16}$-in. diameter steel	4,404	62.0	25.3	6.9	5.7	Vehicle straddled rail, good redirection
ODH-3	7-in. diameter	38.4	$^{5}/_{16}$-in. diameter steel with pipe insert	4,445	62.5	28.7	4.3	2.2	Vehicle pocketed, rolled over
ODH-4	6-in. diameter	28.2	$^{5}/_{16}$-in. diameter steel with pipe insert	4,242	63.1	28.3	6.5	5.2	Good redirection, vehicle rolled 15 deg but remained upright
ODH-5	6 by 6 in. (notched)	36 (30)	¼-in. diameter steel with pipe insert	4,407	70.8	26.7	7.2	2.9	Good redirection
ODH-7	—[a]	—[a]	—[a]	4,292	58.2	26.3	6.8	2.7	Some tendency to pocket, but overall good performance

[a]Transition test; see Appendix for details.

mechanical driver. Self-powered, full-size, four-door sedans were used as test vehicles. Electronic instrumentation permitted continuous recording of an anthropometric dummy's reaction to the crash-test events. Complete camera coverage included high-speed and documentary photography. The use of a motion analyzer and computer data-reduction program provided a record of time versus displacement information for the crash tests. Specific details of the test installations are shown by installation drawings in the Appendix. Several changes were incorporated as experience was gained with each test. Beginning with a post size from the preliminary Ohio Department of Highways type 7 plans, the program is described in chronological order with a discussion of the rationale for changes in the initial design. Test photographs and information summary are shown in the Appendix.

Test ODH-1

The first test in the series was conducted on a system featuring 4- by 4-in. posts. The vehicle impacted the 200-ft test installation at near midlength with a speed of 67 mph and an impact angle of 25 deg. Although the vehicle was redirected, loss of rail height and lack of sufficient post strength allowed it to straddle the rail. This contributed to multiple rollover that began as the vehicle neared the downstream terminal section. The $^{5}/_{16}$-in. diameter post bolts did not shear. Rail separation from the posts, which occurred only at the posts in the immediate impact area, was due to forcing of the bolt and rear washer through the post material. Because of camera malfunctions, high-speed movie data were unobtainable; however, accelerations measured in the dummy chest cavity registered peaks of -2 g longitudinally, -7 g laterally, and +4.5 g vertically before the multiple rollover occurred. Seat belt and shoulder harness loads were a maximum of 500 lb, also before rollover.

All posts in the installation were broken near ground level (Appendix, Figs. 8 and 9). Failure of the upstream posts clearly indicated the lack of sufficient post strength. Because of the extended contact with the system, the vehicle engaged the downstream terminal treatment, which indicated there was insufficient installation length for a general performance test.

Test ODH-2

Based on the results of the first test, 4- by 6-in. posts were installed for the test and an additional 50 ft was added to the length of the test installation. The test vehicle impacted the installation with a speed of 62 mph and an angle of 25.3 deg (Appendix, Figs. 10 and 11). Although loss of rail height after impact permitted the vehicle to straddle the rail (Fig. 1), the vehicle was contained by the system and redirected. The vehicle was launched, but remained upright and was braked to a stop with moderate vehicle damage. Peak vertical and lateral dummy accelerations were +3 and -3 g respectively. Peak vehicle accelerations were -2.8 g and -2.4 g in the lateral and longitudinal directions respectively. As in test ODH-1, the $^{5}/_{16}$-in. diameter post bolts did not shear. Rail separation from the post was accomplished by forcing the rear washer through the post material.

Although the vehicle accelerations and maximum dynamic deflection of the system were considered satisfactory for test ODH-2, two undesirable phenomena were observed that indicated a change in design to be justified:

1. The rail dropped excessively permitting the vehicle to straddle the rail; and
2. The vehicle remained in contact with the system for an extensive distance, resulting in excessive system damage.

Lack of sufficient post strength and failure of the post bolts to shear on impact were considered primary causes of these undesirable results.

Test ODH-3

It was apparent from the previous two tests that the resiliency of wood would prevent the instantaneous shearing of the $^{5}/_{16}$-in. diameter bolts. For test ODH-3, a pipe

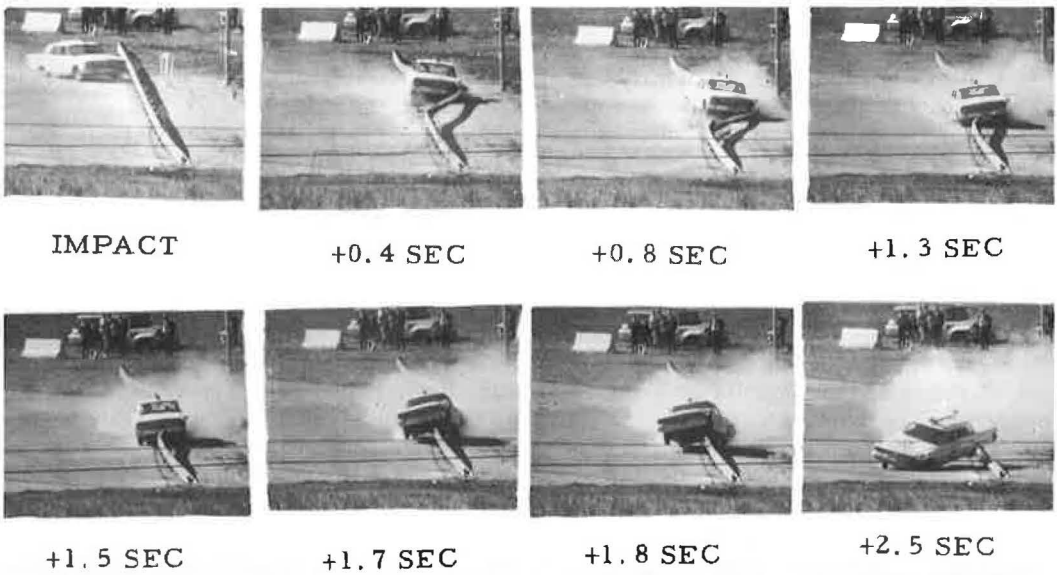

Figure 1. Sequence of events, test ODH-2.

section was inserted in the post bolt hole to provide a shearing surface similar to that provided by the steel flange of the G2 standard post. A 7-in. nominal diameter post was selected as the next size to be evaluated.

Test ODH-3 impact conditions were 62.5 mph at a 28.7-deg angle (Appendix, Figs. 12 and 13). The vehicle was initially redirected, but pocketing occurred about 30 ft from impact, and the vehicle rolled over and remained inverted (Fig. 2). Vehicle ac-

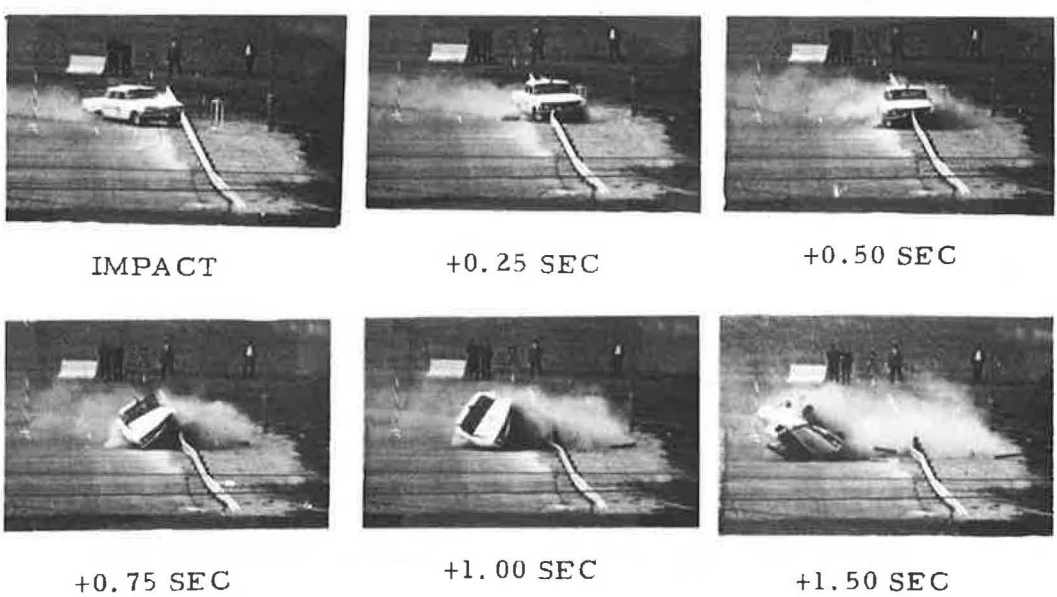

Figure 2. Sequence of events, test ODH-3.

celeration levels before rollover reached maximum values of -4 g laterally and -7.5 g longitudinally. Dummy accelerations reached maximum values of -11 g longitudinally, -8 g laterally, and -11 g vertically before rollover. Seat-belt and shoulder-harness loads reached maximum values of approximately 2,000 lb before rollover.

As indicated by the magnitude of the forces and accelerations measured prior to rollover, the 7-in. diameter posts were too formidable for the weak-post concept. Although the rollover was a clear indicator of system failure, other measured events before the rollover provided equally clear indications of the need for a weaker post. A positive result of this test was the success in achieving bolt shear in the impact area.

Test ODH-4

A 6-in. diameter post was selected for test ODH-4; all other details (including pipe inserts) were the same as for test ODH-3. The vehicle impacted the rail with a speed of 63.1 mph and an angle of 28.3 deg (Appendix, Figs. 14 and 15). The vehicle was contained and redirected by the system, but loss of rail height again occurred due to lack of bolt shear. As the rail dropped, the vehicle rolled about 15 deg but remained upright throughout; the vehicle did not straddle the rail (Fig. 3). Vehicle accelerations

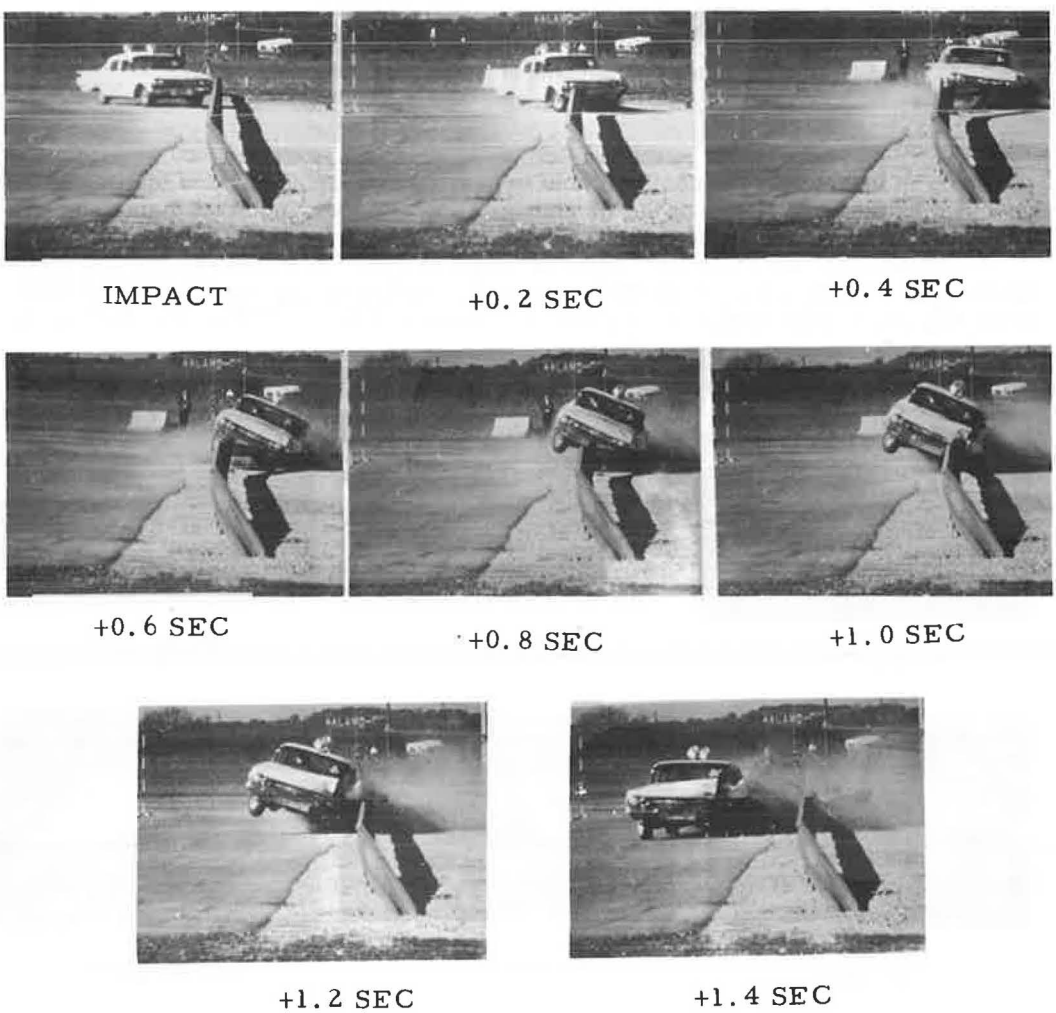

Figure 3. Sequence of events, test ODH-4.

reached maximum values of -3.8 g laterally and -3.1 g longitudinally. Maximum values of -5.0 g longitudinally, -10 g laterally, and -7 g vertically were recorded from the dummy response. Maximum seat-belt and shoulder-harness loads were 1,000 and 650 lb respectively. Failure to achieve rail separation from the posts in impact area through bolt shear was considered to be the principal cause of the rail drop.

Test ODH-5

A ¼-in. diameter bolt was substituted for the previously used $^{5}/_{16}$-in. diameter bolt. A close-fit pipe insert was selected for compatibility with the new bolt size. Because the 6-in. diameter posts from test ODH-4 were considered to be somewhat overstrength, a 6- by 6-in. post with ½-in. notches on upstream and downstream edges 2 in. above grade was selected. The vehicle impacted with a speed of 70.8 mph and an angle of 26.7 deg (Appendix, Figs. 16 and 17). Redirection of the vehicle was good, and the rail remained at an effective height throughout the test (Fig. 4). The elusive bolt shear phenomenon was attained; however, it was not confined to impact area, as all but one of the bolts sheared. Maximum vehicle accelerations were -4.6 g laterally and -3 g longitudinally. A maximum of 8.8 g laterally was recorded from the dummy; seat-belt and shoulder-harness loads reached maximum values of 1,000 and 800 lb respect respectively.

Although the test vehicle attained a speed well in excess of the desired test value, the system performed well under severe conditions. The notching of the posts had no effect on the performance, as all posts broke approximately 12 in. below ground level.

Test ODH-7

Based on the success of test ODH-5, 6- by 6-in. posts were installed as the weak-post system in line with the ODH strong-post system with a transition section between these two systems. Details of the installation are shown in the Appendix (Figs. 18 through 21). A change from test ODH-5 moved the ½-in. notches to grade level. The strong-post system as installed was composed of the 12-gage flexural beam mounted on 60 by 8-in. wood posts (6 ft 3 in. spacing) with a $^{5}/_{8}$-in. diameter post bolt and a 6- by 8-in. wood offset block. The vehicle impacted the system with a speed of 58.2 mph and an angle of 26.3 deg approximately 48 ft upstream from the first 6- by 8-in. post. The vehicle was contained and exited at this first strong post. A tendency to

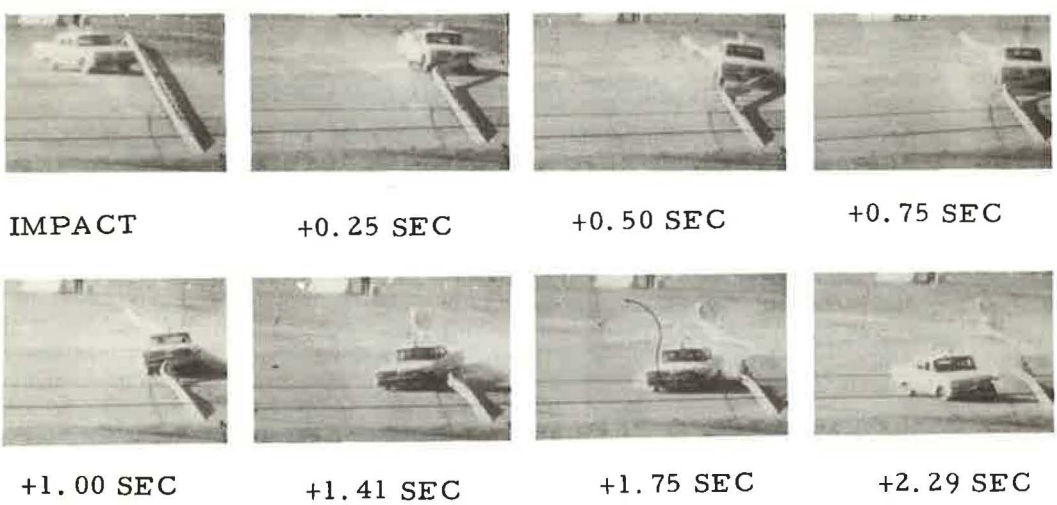

Figure 4. Sequence of events, test ODH-5.

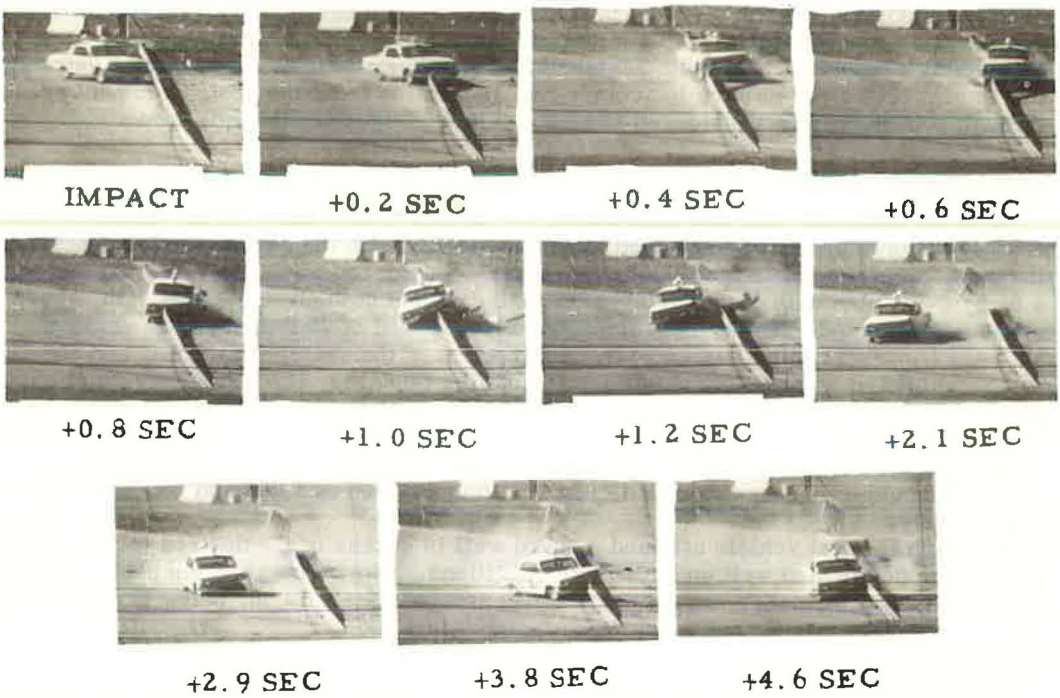

Figure 5. Sequence of events, test ODH-7.

pocket near this exit point was evident, but the vehicle ranged only about 14 ft off the rail line before the brakes were applied and a subsequent second impact with the rail system occurred (Fig. 5). Maximum vehicle accelerations from film data were -3.2 g laterally and -4.3 g longitudinally. Dummy accelerations reached maximum value of -3.0 g longitudinally, -7.5 g laterally, and -6.5 g vertically. A maximum of 1,200 lb was recorded from the right seat-belt load cell. The ¼-in. diameter bolt shear was again extensive and the effect of the notch was negated by post failure occurring below the notch line.

CONCLUSIONS AND RECOMMENDATIONS

Of the five general performance tests conducted during this test series, three installations performed successfully. After analyzing the events of test ODH-2, it could be surmised that, if the pipe insert or the ¼-in. diameter bolt or both had been used, the rail would have remained at effective height and thus prevented the vehicle from straddling the rail. The loss of rail height that occurred during test ODH-4 could possibly have been prevented through the use of ¼-in. diameter bolts or perhaps a closer fitting insert for the 5/16-in. diameter bolt. The performance of the test ODH-5 installation was good, although the extensive bolt shear and subsequent loss of rail support after impact could prove to be a maintenance problem. The other two test installations (tests ODH-1 and ODH-3) must be considered as unsatisfactory because of overall performance. The transition test (test ODH-7) is considered to be a technical success, although the tendency to pocket at the exit point should indicate that improvements are necessary.

Vehicle accelerations presented in this report can be compared to permissible vehicle accelerations that have been suggested to be within the limits of human tolerance (3). As given in Table 2, such vehicle accelerations are classified according to direction and degree of occupant restraint and are based on a duration not to exceed 0.2 sec,

TABLE 2

MAXIMUM AVERAGE VEHICLE ACCELERATIONS FOR HUMAN TOLERANCE

Restraint	Maximum Average Acceleration (g)		
	Lateral	Longitudinal	Total
Unrestrained occupant	3	5	6
Occupant restrained by seat belt	5	10	12
Occupant restrained by seat belt and shoulder harness	15	25	25

Note: Maximum average accelerations are for 200 millisecond duration.

TABLE 3

SUMMARY OF MAXIMUM AVERAGE VEHICLE ACCELERATION

Test No.	Maximum Average Acceleration (g)[a]	
	Lateral	Longitudinal
ODH-2	-2.6	-1.2
ODH-3	-3.5[b]	-5.1[b]
ODH-4	-3.4	-2.6
ODH-5	-3.9	-2.2
ODH-7	-2.9	-3.6

Note: Maximum average accelerations are for 200 millisecond duration.

[a]As measured by high-speed film analysis.

[b]Maximum average values prior to rollover.

with rate of onset not to exceed 500 g/sec. Note that the vehicle occupants are more vulnerable to lateral accelerations regardless of restraint. A summary of the maximum average acceleration values for each test is given in Table 3; it is clear that passenger restraint would be required for all tests of this series except tests ODH-2 and ODH-7, according to the criteria in Table 2.

Because all of the installations in this test series were constructed with pine posts, different post sizes would be required using other timber materials such as oak or hickory. The optimum post size for the weak-post concept indicated by the test results appears to be a 6- by 5-in. sawed rectangular post and a 5½-in. diameter round post of southern yellow pine. In all tests in this series, post strength was developed

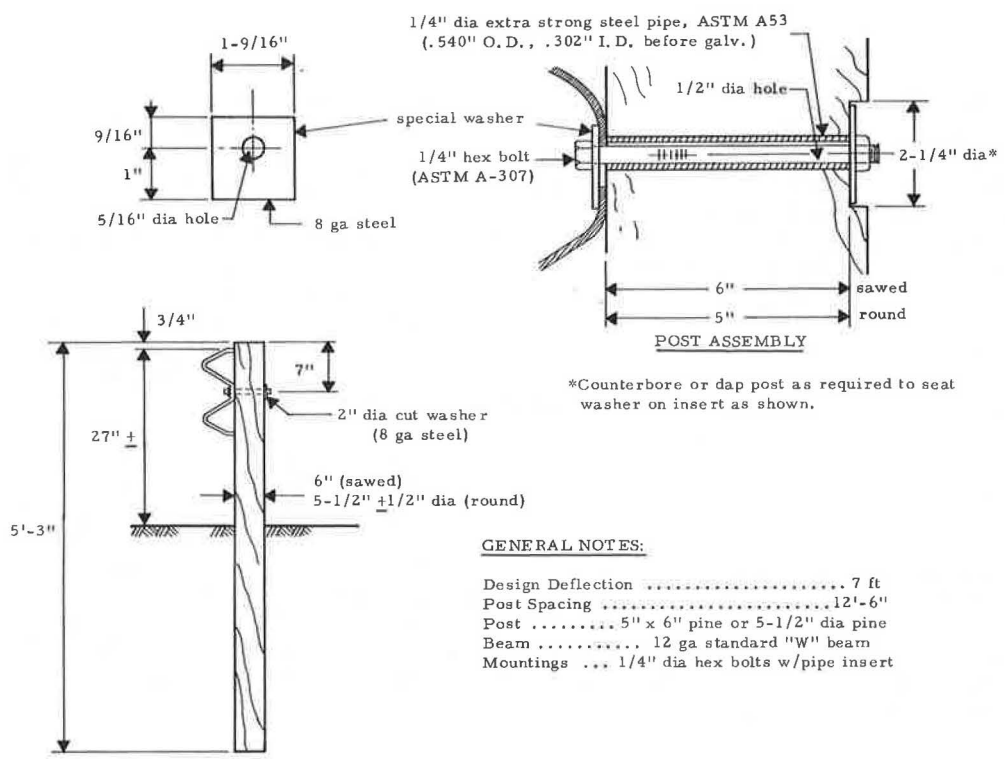

Figure 6. Timber post design for Ohio type 7 guardrail.

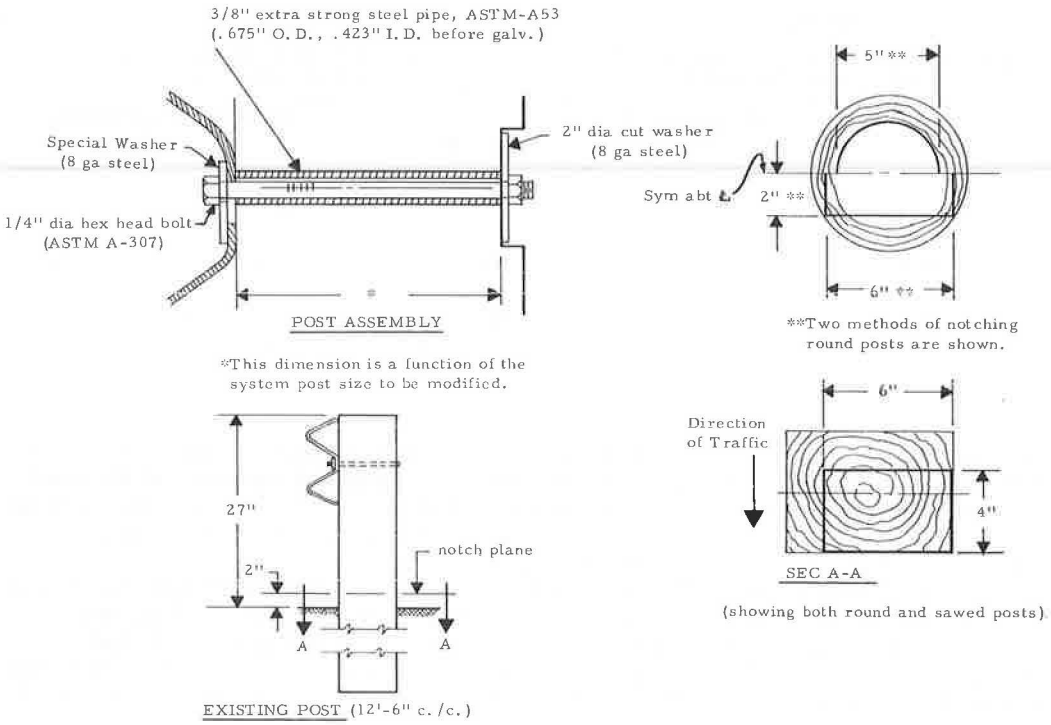

Figure 7. Recommended modification of existing strong-post systems.

by the soil; substitution of a smaller post of a stronger material than pine should be verified by test. The ODH standard washer with the offset hole proved to be of sound design. By offsetting the hole, bending of the bolt at the head during bolt tightening is eliminated. This bending normally occurs with the G2 standard washer, which has the hole in the center of the washer.

Because of problems of achieving bolt shear during this test series, a ¼-in. diameter bolt was substituted for the 5/16-in. diameter bolt initially tested. As stated previously, this ¼-in. diameter bolt could prove to be a maintenance problem of some proportion. The insert selected for the ¼-in. diameter bolt provided an extremely close fit, while the insert used with the 5/16-in. diameter bolt provided a comparatively loose fit. Should maintenance prove to be a problem with the ¼-in. diameter bolt, inserts with different inside diameters might be a solution with either the ¼-in. or the 5/16-in. diameter bolts.

Recent experience in New York has prompted this developer of the G2 system to raise the top of rail height to 33 in. Because the Ohio Department of Highways desires not only to modify its existing strong-post systems (timber posts spaced at 12.5-ft centers with top of rail 27 in. above grade) but also to formulate new standards, consideration of raising the rail height for new installations would be in order.

Design information for the suggested timber-post-system designs for ODH type 7 guardrail is shown in Figure 6. For the existing timber strong-post installations, notches cut near grade should be of sufficient depth to provide a net section of 6 by 4 in. with the 6-in. dimension normal to the roadway. As shown in Figure 7, these notches should be located 2 in. above grade.

REFERENCES

1. Highway Design and Operational Practice Related to Highway Safety. AASHO Traffic Safety Committee, Spec. Rept., Feb. 1967.
2. Michie, J. D., and Calcote, L. R. Location, Selection, and Maintenance of Highway Guardrails and Median Barriers. NCHRP Rept. 54, 1968.
3. Shoemaker, N. W., and Radt, H. S. Summary Report of Highway Barrier Analysis and Test Program. Cornell Aeronautical Laboratory, Inc., Rept. VJ-1472-V-3, July 1961.

Appendix

DETAILS OF INDIVIDUAL TESTS

The following figures contain pertinent data and photographs of the impact tests discussed in this report.

(a) Looking downstream (see insert for before test photograph)

(b) Impact area

Figure 8. Photographs of test ODH-1.

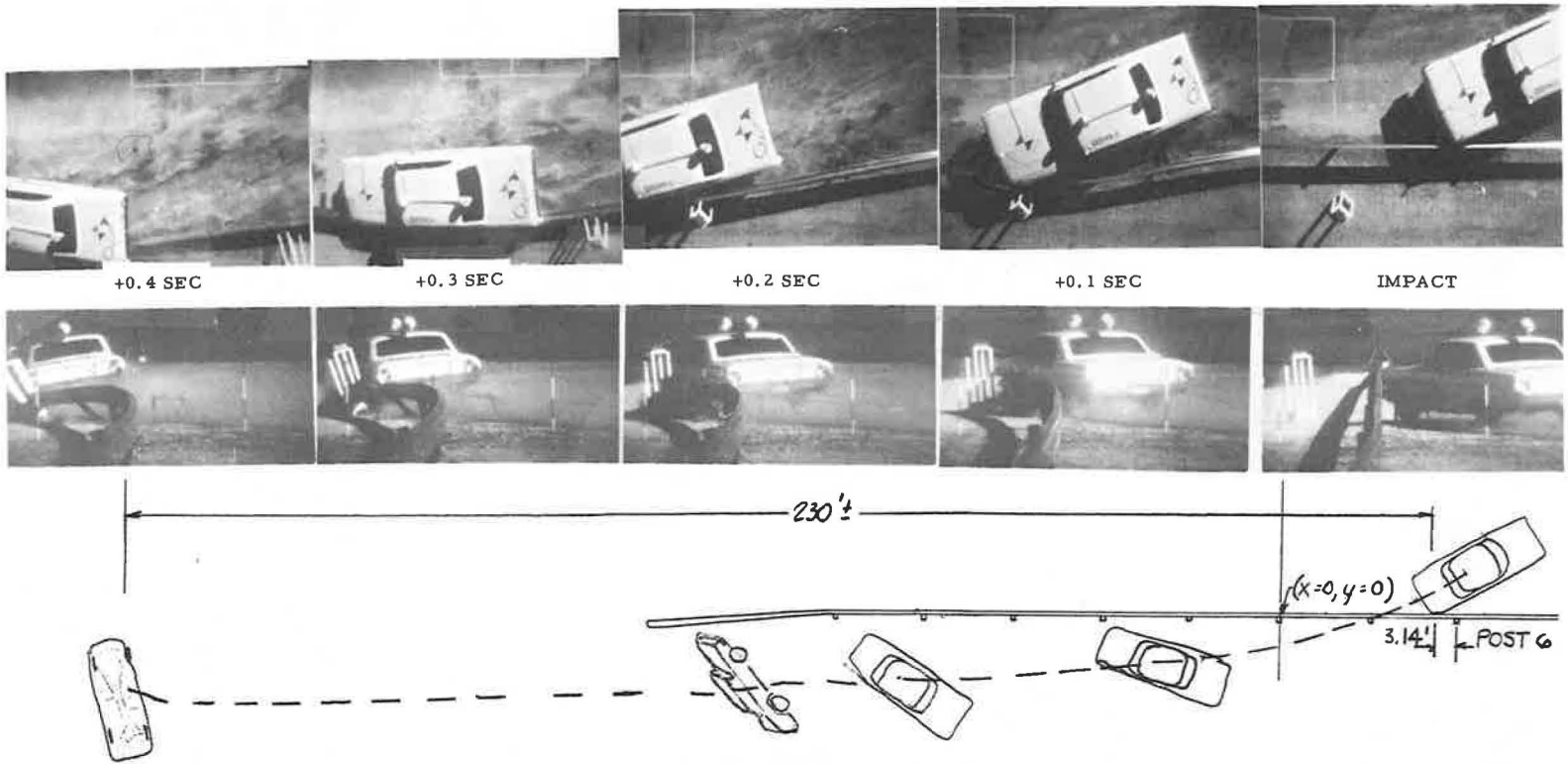

Beam Rail ..... 12 ga Galv Steel x 12'-6"	Test No. ODH-1
Post ..... 4"x4"x5'-3" SY Pine	Date 11/12/69
Post Bolt ..... 5/16 w/std ODH washer	Vehicle ..... 1964 Ford Sedan
Post Embedment ..... 35"	Vehicle Weight ..... 4589 lb
Post Spacing ..... 12'-6"	(w/dummy & instrumentation)
Height of Rail Above Grade ..... 27"	Impact Speed ..... 67 mph
Length of Installation ..... 202'	Impact Angle ..... 25°
Ground Condition ..... Damp	Exit Angle ... Vehicle rolled 3-1/2 times
Beam Rail Deflection - Max Permanent ..10'	Dummy Restraint ..... Lap Belt and
Beam Rail Deflection - Max Dynamic ... 13'+	Shoulder Strap

Figure 9. Summary of results, test ODH-1.

(a) View from vehicle approach before test

(b) Typical post

(c) Looking downstream after test

(d) View from vehicle approach after test

Figure 10. Scenes from test ODH-2.

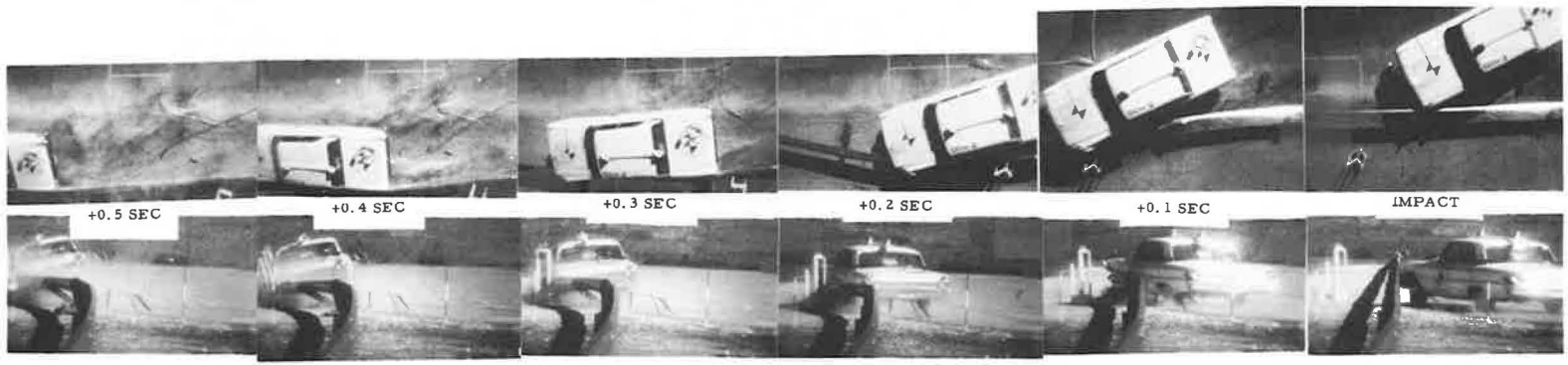

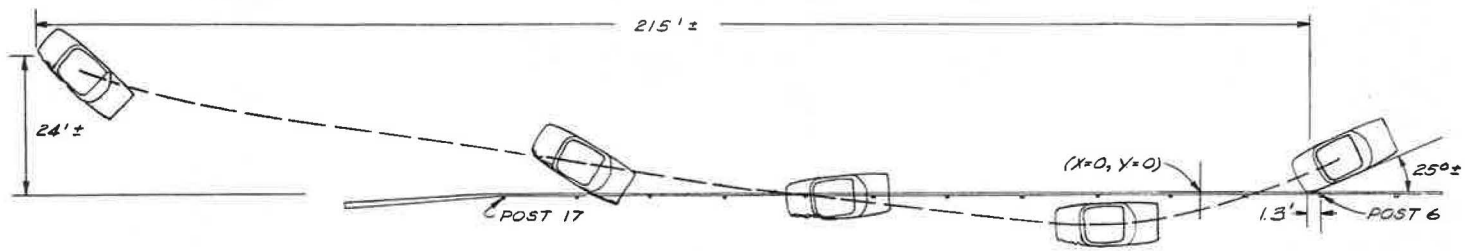

Beam Rail	12 ga Galv Steel x 12'-6"
Post	4"x6"x5'-3" SY Pine
Post Bolt	5/16 w/std ODH washer
Post Embedment	35"
Post Spacing	12'-6"
Height of Rail Above Grade	27"
Length of Installation	250'
Ground Condition	Dry
Beam Rail Deflection - Max Permanent	5.7'
Beam Rail Deflection - Max Dynamic	6.9'

Test No.	ODH-2
Date	11/20/69
Vehicle	1963 Ford Sedan
Vehicle Weight (w/dummy & instrumentation)	4404 lb
Impact Speed	62 mph
Impact Angle	25.3°
Exit Angle	-8°
Dummy Restraint	Lap Belt and Shoulder Strap

Figure 11. Summary of results, test ODH-2.

(a) View from vehicle approach

(b) Post detail

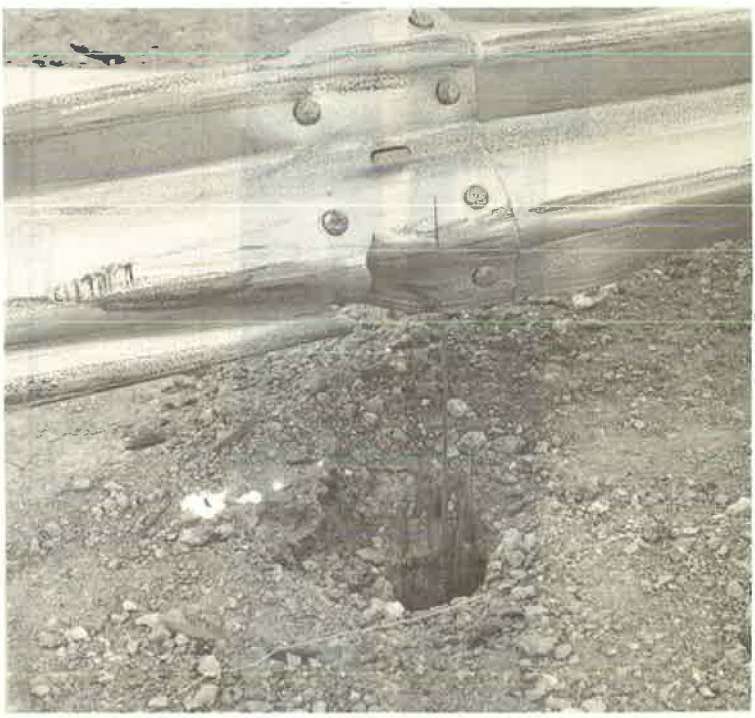

(c) Typical post failure (note tear in rail section)

(d) View from vehicle approach

Figure 12. Scenes from test ODH-3.

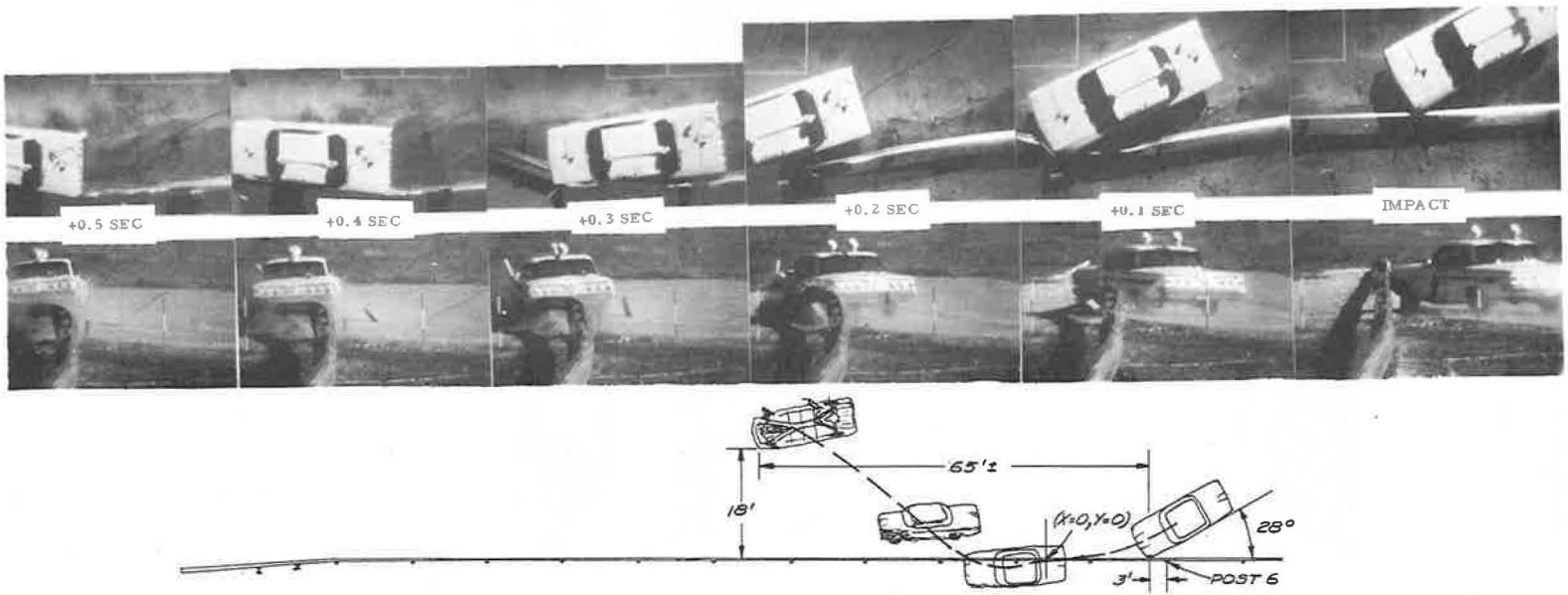

Beam Rail ..... 12 ga Galv Steel x 12'-6"	Test No. ODH-3
Post ..... 7" dia x 5'-3" SY Pine	Date 11/24/69
Post Bolt .. 5/16" dia w/ODH std washer and pipe insert	Vehicle ..... 1961 Chevrolet Sedan
Post Embedment ..... 35"	Vehicle Weight ..... 4445 lb
Post Spacing ..... 12'-6"	(w/dummy & instrumentation)
Height of Rail Above Grade ..... 27"	Impact Speed ..... 62.5 mph
Length of Installation ..... 250'	Impact Angle ..... 28.7^{0}
Ground Condition ..... Dry	Exit Angle ..... Vehicle rolled over
Beam Rail Deflection - Max Permanent..2.2'	Dummy Restraint ..... Lap Belt and
Beam Rail Deflection - Max Dynamic .. 4.3'	Shoulder Strap

Figure 13. Summary of results, test ODH-3.

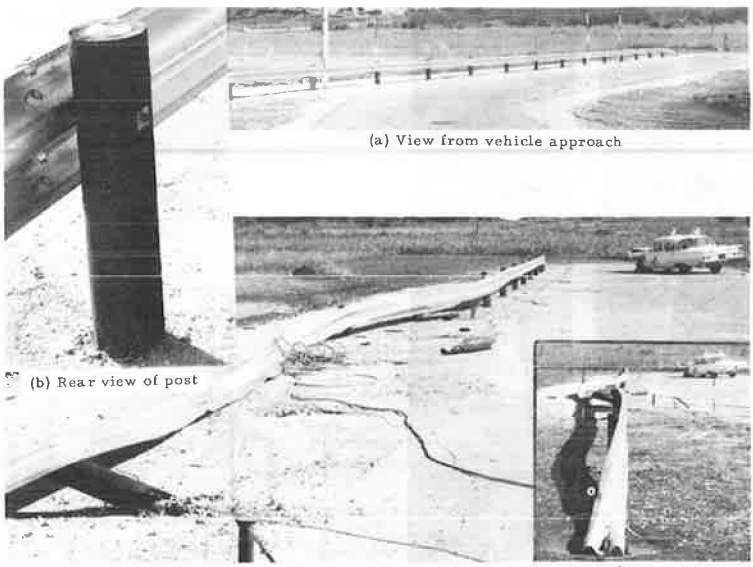

(a) View from vehicle approach

(b) Rear view of post

(c) Impact area (see insert for view looking downstream)

Figure 14. Scenes from test ODH-4.

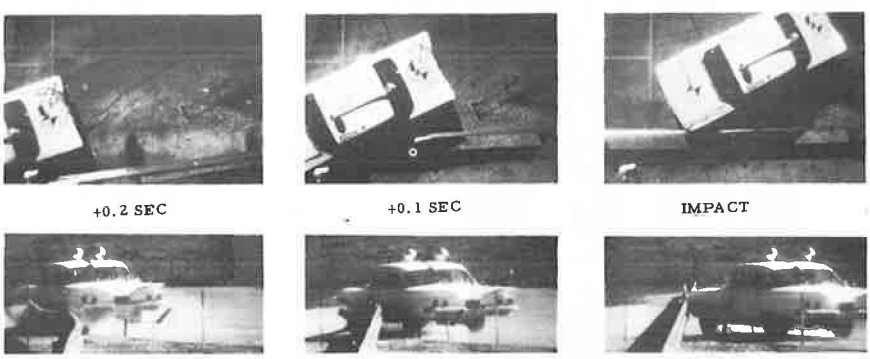

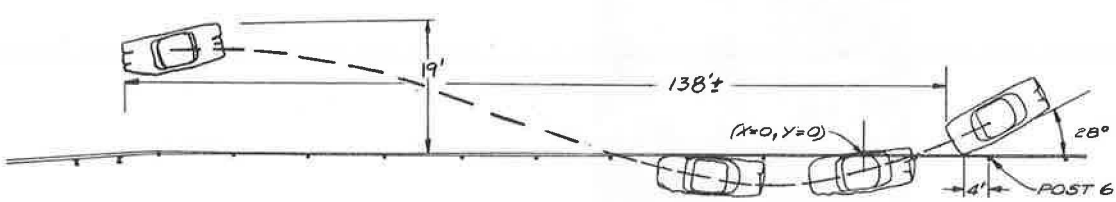

Beam Rail ..... 12 ga Galv Steel x 12'-6"	Test No. ODH-4
Post ..... 6" dia x 5'-3" SY Pine	Date 12/10/69
Post Bolt . 5/16" dia w/ODH std washer & pipe insert	Vehicle ..... 1960 Chevrolet
Post Embedment ..... 35"	Vehicle Weight ..... 4242 lb
Post Spacing ..... 12'-6"	(w/dummy & instrumentation)
Height of Rail Above Grade ..... 27"	Impact Speed ..... 63.1 mph
Length of Installation ..... 250'	Impact Angle ..... 28.3°
Ground Condition ..... Damp	Exit Angle ..... -18°
Beam Rail Deflection - Max Permanent . . 5.2'	Dummy Restraint ..... Lap Belt and
Beam Rail Deflection - Max Dynamic ...6.5'	Shoulder Strap

Figure 15. Summary of results, test ODH-4.

(a) View from vehicle approach

(b) Front view of post

(c) View from vehicle approach (see insert for overall view from upstream)

Figure 16. Scenes from test ODH-5.

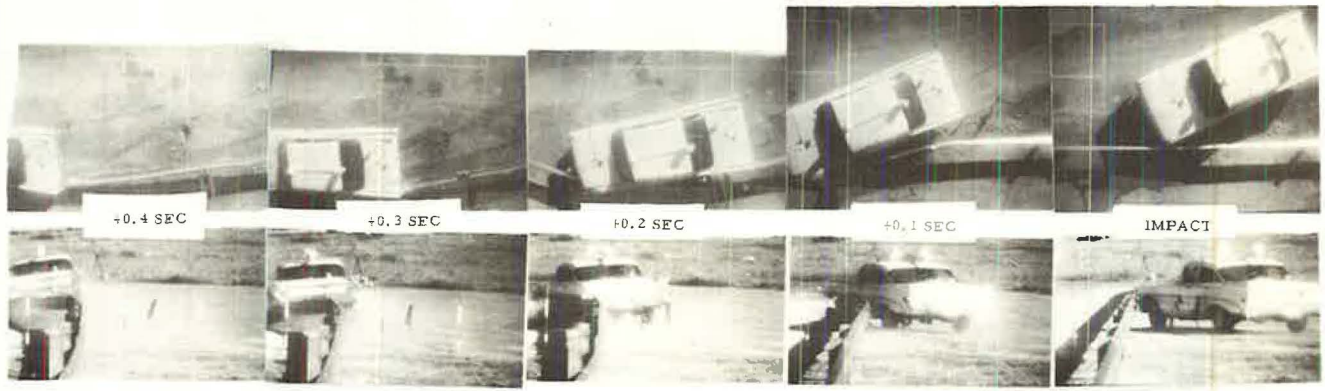

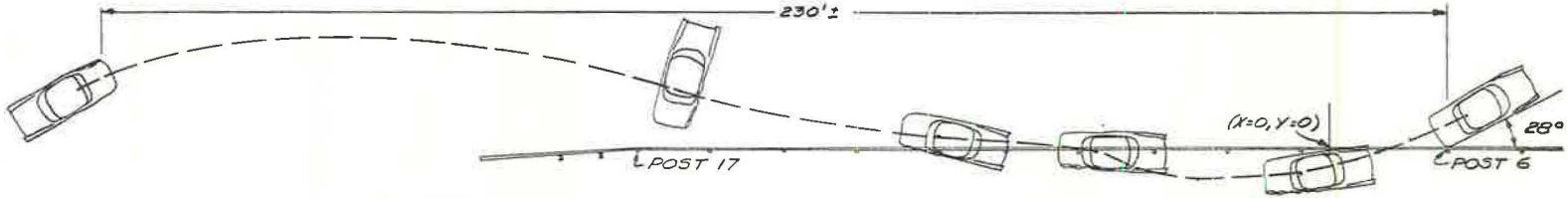

Beam Rail	12 ga Galv Steel x 12'-6"
Post	6"x6"x5'-3" SY Pine *
Post Bolt	1/4" dia w/ODH std washer & pipe insert
Post Embedment	35"
Post Spacing	12'-6"
Height of Rail Above Grade	27"
Length of Installation	250'
Ground Condition	Dry
Beam Rail Deflection - Max Permanent	2.9'
Beam Rail Deflection - Max Dynamic	7.2'

Test No.	ODH-5
Date	12/16/69
Vehicle	1959 Pontiac Sedan
Vehicle Weight (w/dummy & instrumentation)	4407 lb
Impact Speed	70.8 mph
Impact Angle	26.7°
Exit Angle	-7°
Dummy Restraint	Lap Belt and Shoulder Strap

*See installation drawing for notch details.

Figure 17. Summary of results, test ODH-5.

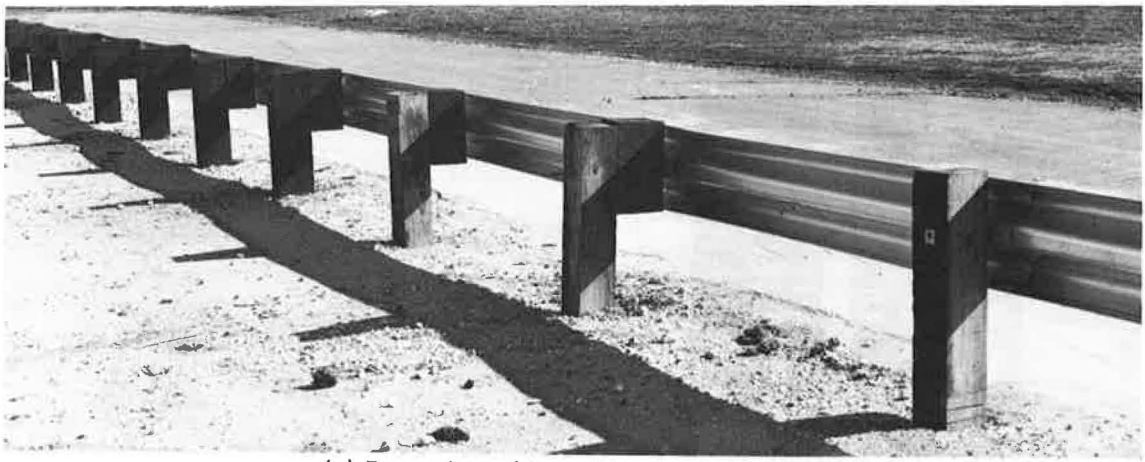

(a) Rear view of transition before test

(b) View from vehicle approach before test

(c) View from vehicle approach after test

(d) View from behind rail after test

Figure 18. Scenes from test ODH-7.

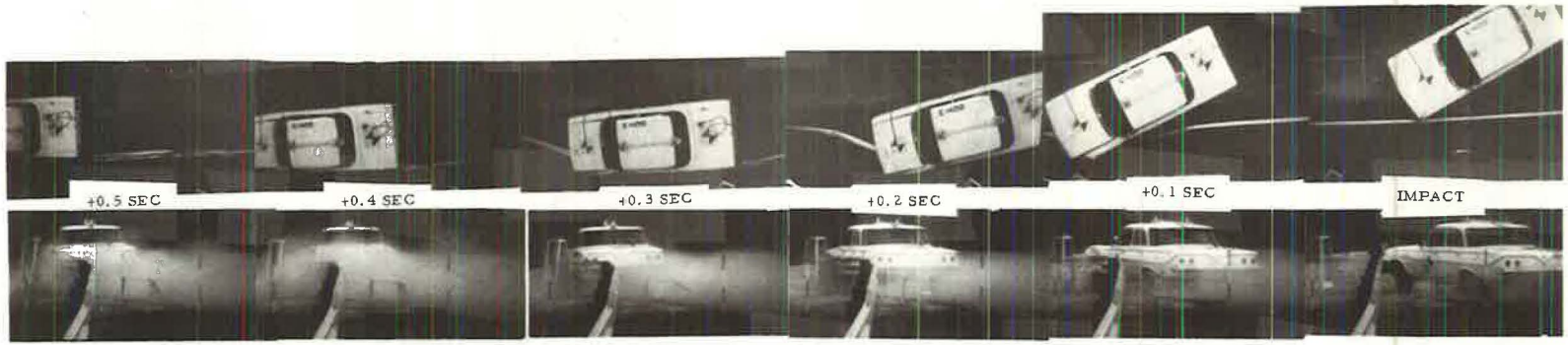

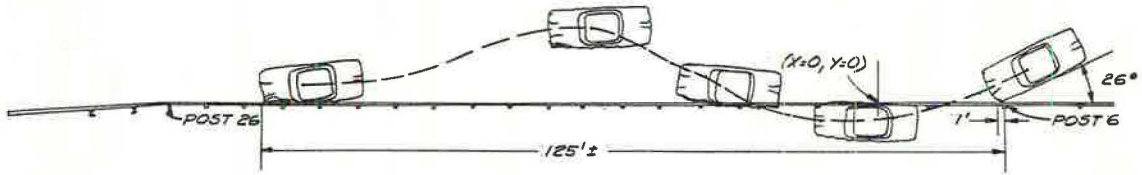

Beam Rail	12 ga Galv Steel x 12'-6"
Post	See installation drawing
Post Bolt	See installation drawing
Post Embedment	35"
Post Spacing	12'-6"
Height of Rail Above Grade	27"
Length of Installation	250'
Ground Condition	Damp
Beam Rail Deflection - Max Permanent	2.7'
Beam Rail Deflection - Max Dynamic	6.8'

Test No.	ODH-7
Date	1/12/70
Vehicle	1961 Chevrolet
Vehicle Weight (w/dummy & instrumentation)	4292 lb
Impact Speed	58.2 mph
Impact Angle	26.3°
Exit Angle	-25°
Dummy Restraint	Lap Belt and Shoulder Strap

Figure 19. Summary of results, test ODH-7.

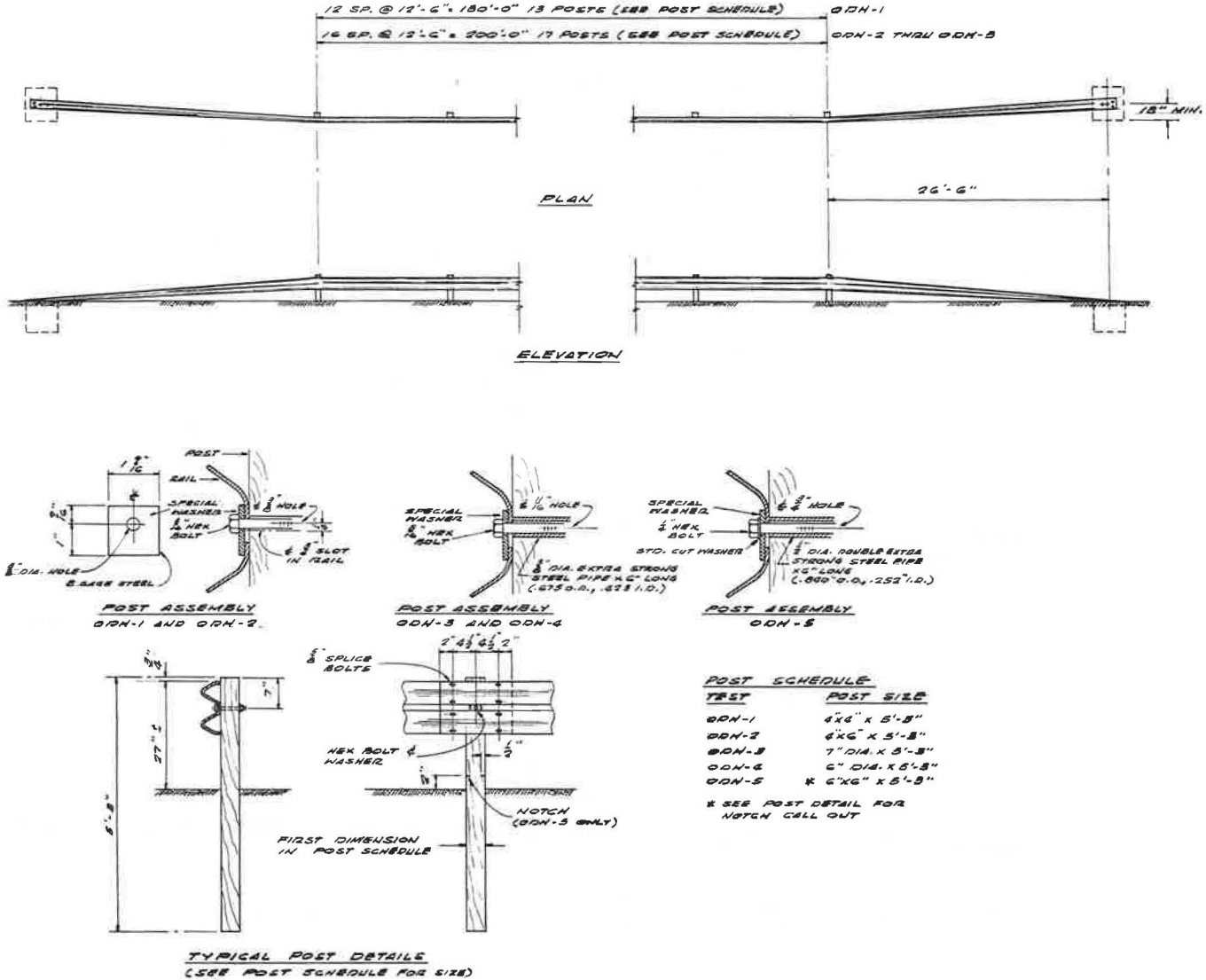

Figure 20. Installation drawing 1.

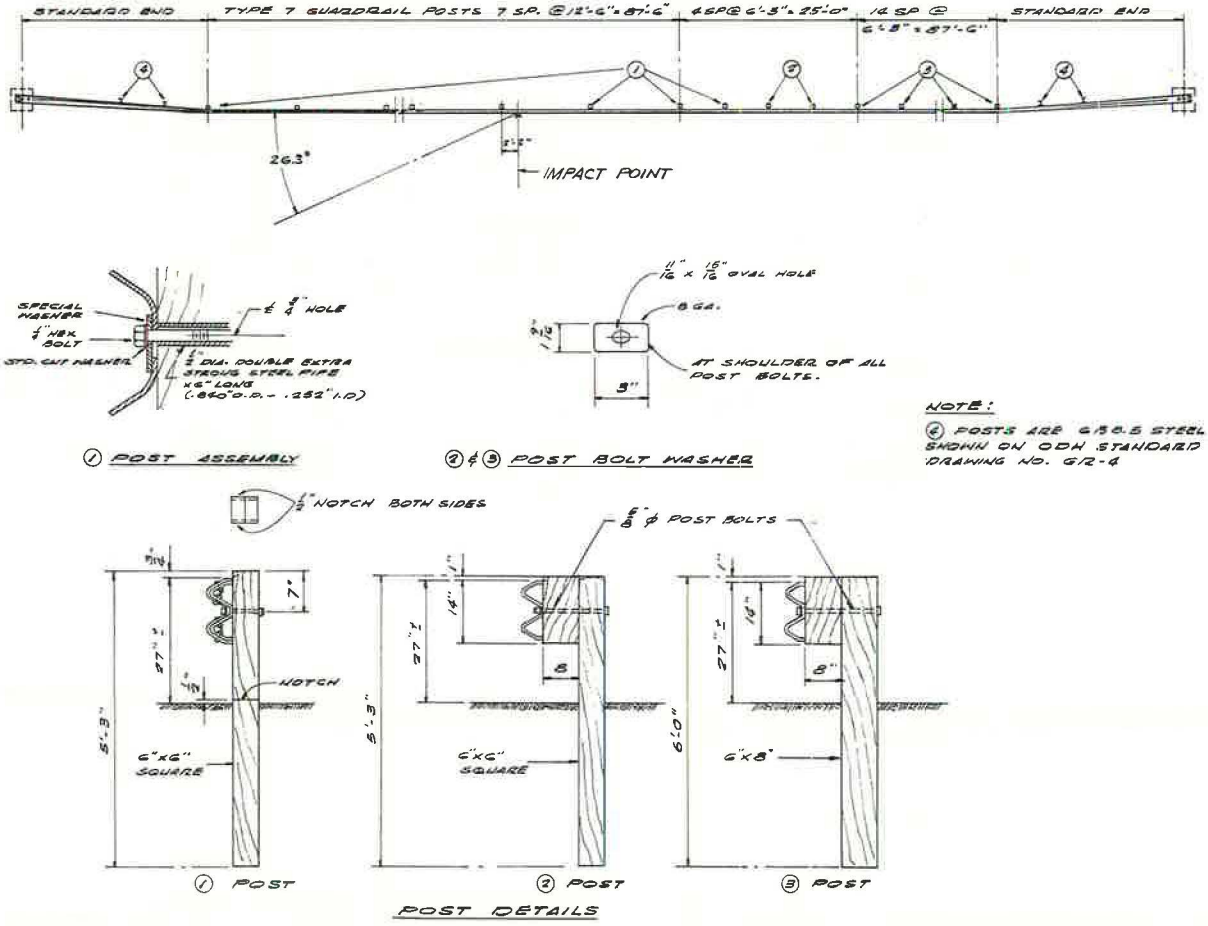

Figure 21. Installation drawing 2.

DYNAMIC TESTS OF THE CALIFORNIA TYPE 20 BRIDGE BARRIER RAIL

Eric F. Nordlin, James H. Woodstrom, Raymond P. Hackett, and J. Jay Folsom, California Division of Highways

The results of five full-scale vehicle impact tests on the California type 20 bridge rail are reported. The type 20 bridge rail is a rigid barrier system that incorporates a 27-in. high reinforced concrete parapet with a traffic-side contour very similar to that used for the New Jersey type of concrete median barrier. A 2- by 6-in. by ¼-in. thick structural steel tube rail is placed 12 in. above the top of this parapet, thus giving an overall barrier height of 39 in. Five tests were conducted at speeds of from 45 to 66 mph and at impact angles of 7, 15, and 25 deg. The test results indicated that this system will retain and redirect a 4,900-lb passenger vehicle impacting at speeds up to 65 mph and at angles of from 7 to 25 deg with the barrier. Vehicle damage varied from negligible at a 7-deg impact angle to severe at a 25-deg impact angle. The test results indicated that the vehicular decelerations sustained during 25-deg, 65-mph impacts into this system will result in occupant injuries varying from severe, if no restraints are used, to no more than moderate, if both a seat belt and a single diagonal shoulder harness are used. At impact angles of 7 deg and less, little or no injury will be sustained during a collision with this barrier regardless of the restraint system being used.

•THE FIRST vehicle impact tests of bridge barrier rails were conducted by the California Division of Highways in the mid-1950's (1, 2). These tests were initiated because of the serious operational deficiencies, primarily structural, that were developing with the bridge barrier rails then in use in California as heavier, high-speed vehicles took to the highways. As a result of these tests, the California Division of Highways adopted a design designated as the California type 1 bridge barrier rail (Fig. 1).

Subsequent vehicle impact tests of California bridge barrier rails (3, 4) have resulted in the development and adoption of the California types 8 and 9 bridge barrier rails (Figs. 2 and 3). Although these barriers have proved to be satisfactory, reports from New Jersey (5) and subsequent tests by the California Division of Highways in 1966-67 (6) indicated that the New Jersey concrete median barrier (Fig. 20, Appendix) showed definite promise of reducing the damage sustained by vehicles striking it at the more prevalent flat angles of impact. This characteristic was also reported by General Motors (7) in tests conducted on a bridge barrier containing a parapet contour similar to the New Jersey barrier (Fig. 20). The effectiveness of the lower sloped surface in reducing vehicle damage and decelerations had also been observed operationally in several experimental installations of the New Jersey concrete median barrier in California.

Sponsored by Committee on Traffic Safety Barriers and Sign, Signal and Lighting Supports and Committee on Bridge Design and presented at the 50th Annual Meeting.

Figure 1.

Figure 2.

Consequently, the Bridge Department of the California Division of Highways designed the California type 20 bridge barrier rail (Fig. 4 and Appendix Fig. 20). This design incorporates a single steel rail mounted 12 in. above the top of a 27-in. high concrete parapet. The rail is a rectangular tubing identical to that used in the type 9 design. The parapet wall has a traffic-side profile almost identical to the New Jersey median barrier.

The type 20 design provides better "see-through" characteristics than the General Motors design because the overall height is about 16 in. less, the concrete parapet is about 5 in. lower, and the steel rail is narrower. Visibility through the type 20 bridge rail is not as good as through the type 9 design. However, it appears to be adequate. Five full-scale vehicle impact tests of this type 20 bridge rail are reported herein.

OBJECTIVES

The objectives of this research were as follows:

1. Test the ability of the California type 20 bridge barrier rail to (a) retain and redirect, in a stable manner, a medium-weight passenger car traveling 60 to 65 mph and impacting at angles of from 7 to 25 deg while sustaining little or no damage; (b) minimize the damage and deceleration sustained by the impacting vehicle during these collisions so that the injuries sustained by any vehicular occupants are minimized; and

Figure 3.

Figure 4.

(c) prevent excessive rebound of the vehicle back across the traveled way or other behavior hazardous to traffic near the point of impact.

2. Evaluate the aesthetic and visibility properties of the type 20 bridge barrier railing.

TEST CONDITIONS

Barrier Design and Construction

The design of the type 20 bridge rail was developed by the Bridge Department of the California Division of Highways. Prior to the construction of the test installation, a full-scale plywood mock-up was erected on an existing bridge next to some type 1 bridge barrier railing to compare the see-through qualities of the two designs (Fig. 5). After the mock-up was reviewed, the design details for the type 20 bridge barrier railing were finalized, and the test barrier was constructed.

The type 20 design consists of the current California standard type 9 bridge barrier rail posts and rail mounted on a reinforced-concrete parapet design adapted from the New Jersey median barrier. The steel rail portion of this barrier was fabricated with a 6- by 2-in. 12.02-lb structural steel tubing conforming to the requirements of ASTM Designation A500, Grade B. The posts were fabricated using structural steel conforming to the requirements of ASTM Designation A36.

The ¾-in. welded stud rail-to-post connector and the interior sleeve rail splice, proved effective in a previous test series (4), were again used. The fabricated steel posts were spaced at 10-ft centers and were secured to the concrete parapet with one ¾-in. diameter by 8-in. long and one 1-in. diameter by 12-in. long high-strength bolt cast in the concrete. These high-strength bolts conformed to the requirements of ASTM Designation A325. The concrete portion of the barrier consisted of a 27-in. high by 67-ft long reinforced-concrete parapet constructed on a reinforced-concrete cantilevered deck. The total barrier height was 39 in. from the bridge deck to the top of the steel rail member. The deck and parapet reinforcing, as well as the other details of the type 20 bridge barrier rail design, are shown in Figure 21 in the Appendix.

This system was designed in accordance with the requirements of the Standard Specifications for Highway Bridges adopted by AASHO in 1969. The test section was built on an unused runway at a small airport near Lincoln, California.

Test Vehicles

The test vehicles used in this study were 1966 Dodge sedans weighing approximately 4,900 lb, including two anthropometric dummies and on-board instrumentation. These vehicles were retired California Highway Patrol sedans and were modified for remote radio control as described elsewhere (8). Control of the vehicle during the approach was accomplished by an operator following approximately 200 ft behind the test vehicle in a control car equipped with a tone-transmission system.

Two anthropometric dummies were placed in the front seat of the test vehicle and restrained with conventional seat belts for all five tests. The driver, "Stan", weighed about 165 lb (50th percentile male); the passenger, "Sam", weighed about 210 lb (95th percentile male).

Figure 5.

Photographic Coverage

All the tests were photographed with high-speed (250 to 400 frames per second) Photosonic cameras that were manually

actuated from a central control console. These cameras were located to the front, rear, and side of the point of impact and on a tower directly above the point of impact. Most of the Photosonic data film had red-orange timing pips projected on it at a rate of 1,000 per second. These pips were then counted to determine the frame rates of the cameras. Targets were attached to the vehicle body, and a target board was bolted to the roof of the vehicle to facilitate data reduction of the film using a Vanguard motion analyzer. Another Photosonic camera was located in the rear of the vehicle to film movement of the dummies. This camera was actuated by a switch, mounted on the rear bumper of the test vehicle, that was tripped using a 50-ft length of nylon line anchored to the pavement behind the vehicle.

Documentary coverage consisted of high-speed and normal-speed motion-picture coverage during the tests plus motion pictures, still photographs, and slides taken before and after each test. A scaffold-mounted Hulcher camera with a speed of 20 frames per second was also used for documentary coverage of the tests. Five tape switches, placed perpendicular to the vehicle path at 10-ft intervals leading into the point of impact, were actuated by the tires of the test vehicle and triggered a series of flashbulbs located in view of all the data cameras. These flashbulbs were used for correlation between all stationary cameras and for the determination of the impact velocity.

Flashbulbs mounted on top of the rear fenders of the test vehicle were used to establish the vehicle location and the time at which the brakes were applied. The bulbs also served to alert the control car driver that the test car's brakes had been applied. These flashbulbs were fired when the brake-actuating relay was closed by either radio equipment failure or the remote operator.

Instrumentation

The instrumentation system used for all five tests was the Wyle Accident Simulation Measurement System on loan from the Federal Highway Administration (9). It consisted of seven channels of FM telemetry for the crash vehicle and dummies and seven channels of hardwire equipment for the barrier. The system included seven accelerometers, two seat-belt force transducers, and all the necessary signal-conditioning equipment. The dynamic data from these transducers were recorded on a 14-channel analog magnetic tape recorder that was also a part of the system.

The location and description of the instrumentation of the test vehicle for tests 232, 234, and 235 are shown in Appendix Figure 22. The instrumentation layouts for tests 231 and 233 are not included because the accelerometer records for these tests were considered invalid.

The time at which impact occurred was established from the high-speed movies and then was located on the record of accelerometer data. The cause of accelerometer data events could then be determined, at least in some cases, through study of the vehicular and dummy kinematics recorded on the film at the same point in time.

Test Parameters

The test guidelines established by the Highway Research Board Committee on Guardrails and Guide Posts (10) specify the use of a 4,000-lb vehicle, an impact velocity of 60 mph, and impact angles of 7 and 25 deg. A heavier vehicle (4,900 lb) traveling at approximately 65 mph was used for these tests because it was felt that these higher values more nearly represented the more severe conditions now being encountered on California highways. The five tests were identical except for the differences given in Table 1.

TEST RESULTS

Descriptions of the five full-scale tests are included in the following data. In all these tests, the point of impact was within 6 ft of the concrete parapet expansion joint to test this critical point of discontinuity.

Tire skid marks and other scuff marks on the barrier parapet were studied after each test to determine vehicle behavior. After this examination, the marks were covered with white paint to prepare the barrier for the next test.

TABLE 1

TEST PARAMETERS

Test No.	Impact Speed (mph)	Angle of Impact (deg)
231	45	7
232	66	7
233	64	15
234	64	7
235	66	25

TABLE 2

DECELERATION LIMITS (g)

Occupant Restraint	Lateral	Longitudinal	Total
Unrestrained	3	5	6
Seat belt	5	10	12
Seat belt and shoulder harness	15	25	25

Note: Highest 50 msec average, vehicle passenger compartment.

The decelerations reported in the descriptions of each test are averages of the highest average decelerations sustained over a 50-msec period. The measurements were taken using Statham strain-gage accelerometers mounted on the floor of the passenger compartment and in back of the dummy chest cavity. A discussion of the processing and interpretation of these data is included elsewhere (8).

The vehicular decelerations measured during tests 232, 234, and 235 were interpreted using the tolerance limits given in Table 2. Nordlin, Woodstrom, and Hackett (8) discuss deceleration tolerances and the reasoning behind the choice of these values. These limits define what would be, in the authors' opinion, a survivable environment under almost all circumstances.

Test 231

Test 231 was conducted to evaluate the effectiveness of the type 20 bridge barrier rail when impacted at a flat approach angle and a moderate speed. The vehicle impacted the barrier approximately 27.5 ft from the upstream end at a speed of 45 mph and at an approach angle of 7 deg. After impacting the barrier, the test vehicle was smoothly redirected parallel to the barrier. Vehicle barrier contact was maintained for the remaining 40 ft of barrier, after which the vehicle traveled an additional 150 ft before coming to a stop (Appendix Fig. 23).

Maximum vehicular rise was approximately 16 in. There was minor sheet-metal damage sustained by the test vehicle and slight surface cracks sustained by the barrier (Figs. 6 and 7). No determination of the electronically measured deceleration could be made due to the poor quality of the instrumentation data.

Test 232

The same vehicle used for test 231 was used for test 232 with no repairs. Test 232 also involved a 7-deg impact, but the impact velocity was increased to 66 mph. Impact was again about 27.5 ft from the upstream end of the test barrier. After impact, the vehicle traveled along the barrier for 27 ft and then left the barrier at an exit angle of

Figure 6.

Figure 7.

Figure 8.

Figure 9.

1 deg (Appendix Fig. 24). During this test the maximum vehicle rise was 16 in. Vehicle damage was very minor, and there was no significant structural damage sustained by the barrier (Figs. 8 and 9). The damaged windshield and grill were caused by a second collision with a section of scaffold. A maximum 50-msec average deceleration of 4.8 g laterally (average of 2 data channels) was measured on the floor of the passenger compartment. This deceleration did not exceed the tolerance level for a seat-belted occupant. None of the longitudinal deceleration data was considered accurate.

Test 233

The vehicle used for tests 231 and 232 was used again for test 233, a 64-mph, 15-deg impact. Impact occurred about 27.5 ft from the upstream end of the barrier. After maintaining contact with the barrier for approximately 19 ft, the test vehicle left the barrier at an exit angle of 10 deg (Appendix Fig. 25). Vehicle rise was small; it appeared that the steel railing held the test vehicle down during the redirection. This penetration underneath the steel railing is indicative of the decreasing effect of the contoured concrete surface at larger impact angles. There was no tendency for the vehicle to roll or jump. The left front end and undercarriage of the vehicle were severely damaged (Fig. 10). Minor spalling of the concrete parapet also occurred (Fig. 11). No measurement of vehicular or dummy deceleration was obtained because of an apparent instrumentation malfunction.

Test 234

Test 234 was performed to substantiate the results of test 232. This correlation was felt necessary because the vehicular rise noted during test 232 (16 in.) was sub-

Figure 10.

Figure 11.

Figure 12.

Figure 13.

stantially less than that noted during a previous 7-deg, 65-mph test (test 161B) of the New Jersey type of concrete median barrier (6). The two tests are shown in Figures 12 and 13.

During test 234 (7 deg, 64 mph), impact was again located approximately 27.5 ft from the upstream end of the barrier. The maximum rise of the test vehicle was approximately 18 in. After impacting the barrier, the vehicle traveled along the barrier for approximately 30 ft before exiting at an angle of 1 deg (Appendix Fig. 26).

Vehicle damage was limited to minor scrapes along the left side (Fig. 14). Barrier damage was very minor (Fig. 15). The maximum 50-msec average decelerations measured on the floor of the passenger compartment were 4.8 g laterally (average of two data channels) and less than 1 g longitudinally (average of three data channels). These vehicular decelerations did not exceed the tolerance levels for a seat-belted occupant. Thus, a belt-restrained occupant would have sustained little or no injury. The maximum 50-msec dummy decelerations measured were 6.5 g laterally and 2.3 g longitudinally.

Test 235

Test 235, the most severe impact into the barrier, was conducted using the same vehicle used for test 234. The test vehicle struck the barrier 27.5 ft from the upstream

Figure 14.

Figure 15.

Figure 16.

Figure 17.

end at 66 mph and at an angle of 25 deg. After impact, the vehicle remained in contact with the barrier for approximately 12 ft before leaving the barrier at a 3-deg angle (Appendix Fig. 27). Vehicular rise was minimal as the steel rail restricted the tendency to ride up on the barrier parapet. This was also observed in test 233 (15 deg impact angle) but was not observed during tests 231, 232, and 234 (7 deg impact angle), as minimal contact with the steel rail occurred at the shallower impact angle.

Spalling of the concrete in the vicinity of impact and a slight permanent deflection (0.1 ft) of the steel railing indicated the severity of the impact (Fig. 16). The concrete portion of the barrier railing sustained a vertical crack approximately $\frac{1}{16}$ in. wide that extended from the deck to the top of the parapet. This crack was at a point just upstream from impact. Displacement of the concrete parapet was approximately $\frac{1}{8}$ in. at the top of the expansion joint. As could be expected with any 25-deg impact into a rigid barrier, vehicular damage was severe (Fig. 17).

The maximum 50-msec decelerations measured on the floor of the passenger compartment were 9.1 g laterally (average of two accelerometers) and 14.8 g longitudinally (average of four accelerometers). This lateral deceleration exceeds the tolerance level for a seat-belted occupant. Thus, an occupant restrained by a seat belt would have sustained moderate to severe injury. Both values, however, are below the tolerance level of an occupant restrained by both a seat belt and a shoulder harness and indicate that a fully restrained occupant would sustain no more than moderate injury. The maximum 50-msec average decelerations measured in the dummy driver's chest cavity were 9.2 g longitudinally and 16.9 g laterally.

Figure 18.

DISCUSSION OF RESULTS

The results of these tests indicated that the effectiveness of sloping the traffic side of the barrier parapet diminished as the angle of impact increased. This is not surprising in that the point of initial vehicle-barrier contact shifts from the tire sidewall at a 7-deg impact angle (Fig. 18) to the

body sheet metal at a 15-deg impact angle (Fig. 19).

Thus, at the greater angle, a smaller proportion of the vehicle kinetic energy is absorbed within the vehicular suspension system, and a proportionally greater amount is absorbed through deformation of the vehicle body and chassis, thus resulting in increased vehicle damage and passenger-compartment decelerations. As the impact angle approaches 25 deg, the vehicular damage sustained approaches that sustained when impacting the vertically faced type 1 bridge barrier rail. However, an excerpt in a recent study reported elsewhere (11) indicates that approximately 75 percent of the vehicles departing from the traveled way do so at an angle of 15 deg or less. Almost 60 percent depart at 10 deg or less; this indicates that, in a majority of the collisions that will probably occur with the type 20 barrier, the sloped parapet face will be beneficial.

Figure 19.

CONCLUSIONS

The following conclusions are based on an analysis of the results of the full-scale vehicle impact tests conducted during this test series:

1. The type 20 bridge barrier rail will retain and redirect a 4,900-lb passenger car impacting at speeds up to 65 mph and approach angles up to 25 deg. The vehicle will remain stable and upright during redirection, and little or no barrier damage will be sustained.
2. In the more common shallow angle impacts such as 7 deg, little or no vehicular damage will be sustained. Occupant injuries will vary from minor (seat belt and shoulder harness) to moderate (no restraint). Thus, the contoured traffic face of the type 20 bridge barrier rail parapet definitely minimizes the collision severity at shallow angles of impact. As the angle of impact increases above approximately 10 deg, the colliding vehicle will become increasingly involved with the upper surface of the barrier. When the angle of impact is 25 deg, a vehicle striking the type 20 bridge rail at a speed of 64 mph or greater will sustain severe damage, and occupant injuries will vary from minor to moderate, if a seat belt and shoulder harness are used, and to severe, if no restraints are used. The type 20 bridge barrier rail appears to offer little or no advantage over other rigid bridge barrier rails now in use in California when impacted at these larger approach angles.
3. The impacting vehicle tended to hug the bridge rail in all tests rather than rebound sharply off the rail. This was particularly true at the 7-deg impact angle. In four of the five tests, the exit angle was 3 deg or less. Thus, the type 20 rail appears to be equal or superior to other types of rigid bridge barrier rails in eliminating the secondary hazard of excessive rebound.
4. The type 20 bridge rail offers no aesthetic improvements over those types of bridge rails now in use in California, and its see-through properties are not as good as those of at least one bridge rail now in use in California. However, the use of this barrier design seems to be justified by the significantly decreased collision severity that will occur at flat impact angles.
5. No design modifications were made to the test barrier during the tests and none is recommended.

ACKNOWLEDGMENT

This work was accomplished in cooperation with the Federal Highway Administration. The opinions, findings, and conclusions expressed are those of the authors and not necessarily those of the Federal Highway Administration.

REFERENCES

1. Beaton, J. L. Full Scale Tests of Concrete Bridge Rails Subjected to Automobile Impacts. HRB Proc., Vol. 35, 1956, pp. 251-267.
2. Beaton, J. L., and Field, R. N. Dynamic Full Scale Tests of Bridge Rails. California Division of Highways, Dec. 1960.
3. Nordlin, E. F., Field, R. N., and Stoker, J. R. Dynamic Full Scale Impact Tests of Steel Bridge Barrier Rails, Series 11. California Division of Highways, June 1967.
4. Nordlin, E. F., Ames, W. H., and Hackett, R. P. Dynamic Tests of Type 9 Bridge Barrier Rail and Type 8 Bridge Approach Guardrail. Highway Research Record 302, 1970, pp. 1-20.
5. Center Barriers Save Lives. New Jersey State Highway Department, March 1965.
6. Nordlin, E. F., Field, R. N., and Stoker, J. R. Dynamic Tests of Concrete Median Barrier, Series 16. California Division of Highways, Aug. 1967.
7. Lundstrom, L. C., Skeels, P. C., Englund, B. R., and Rogers, R. A. A Bridge Parapet Designed for Safety. Highway Research Record 83, 1965, pp. 169-187.
8. Nordlin, E. F., Woodstrom, J. H., and Hackett, R. P. Dynamic Tests of the California Type 20 Bridge Barrier Rail, Series 23. California Division of Highways, Sept. 1970.
9. Nordlin, E. F., Ames, W. H., Kubel, L. G., and Chow, W. Evaluation of a Telemetry System for Use in Vehicle-Barrier Impact Tests. Materials and Research Dept., California Division of Highways, Res. Rept. 636405-1, July 1969.
10. Proposed Full-Scale Testing Procedures for Guardrails. HRCS Circular 482, Sept. 1962.
11. Highway Safety. HRB Spec. Rept. 107, 1970.

Appendix

DETAILS OF BARRIER DESIGN AND PERFORMANCE

The following figures contain pertinent data and photographs of the impact tests discussed in this report.

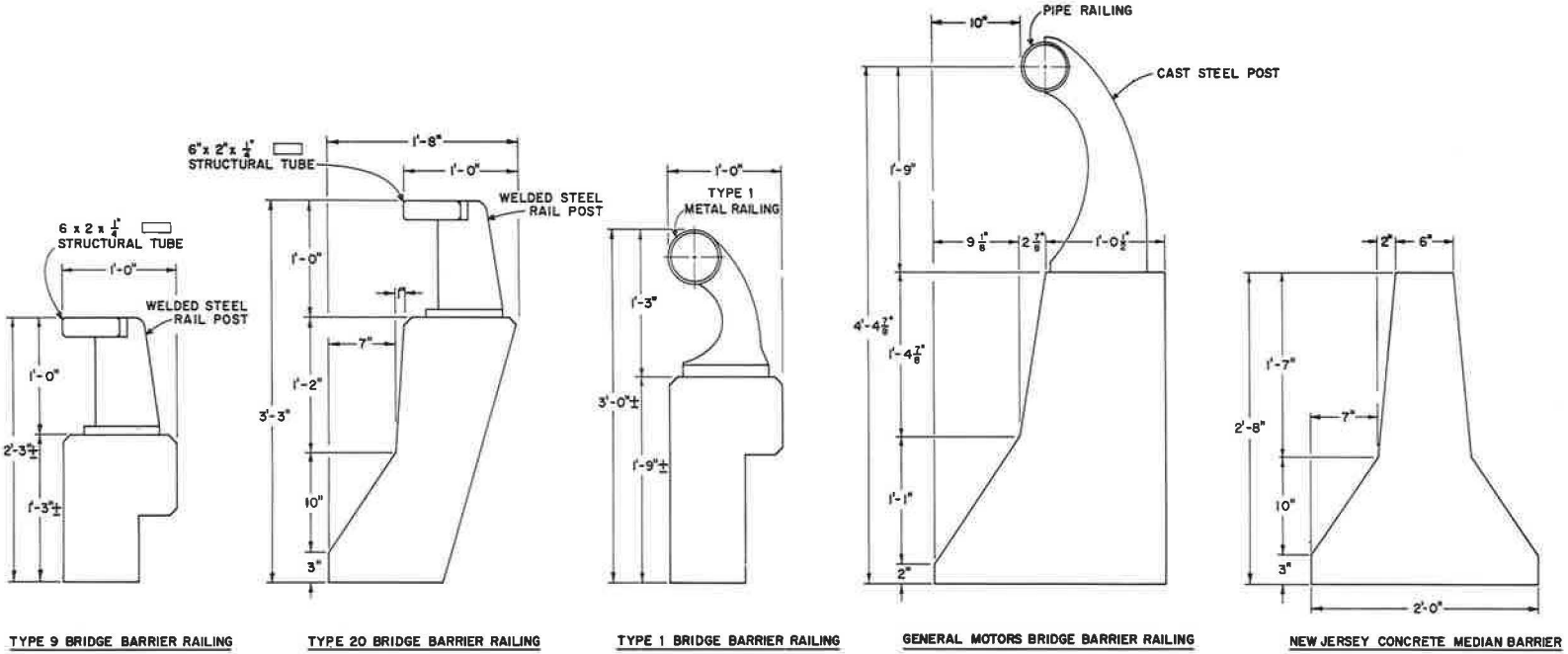
6 x 2 x 1/4 STRUCTURAL TUBE
1'-0"
WELDED STEEL RAIL POST
1'-0"
2'-3 1/2"±
1'-3"±
TYPE 9 BRIDGE BARRIER RAILING
6"x 2"x 1/4" STRUCTURAL TUBE
1'-8"
1'-0"
WELDED STEEL RAIL POST
1'-0"
1"
7"
1'-2"
3'-3"
10"
3"
TYPE 20 BRIDGE BARRIER RAILING
1'-0"
TYPE 1 METAL RAILING
1'-3"
3'-0"±
1'-9"±
TYPE 1 BRIDGE BARRIER RAILING
10"
PIPE RAILING
CAST STEEL POST
1'-9"
9 1/8"
2 1/8"
1'-0 1/2"
4'-4 1/8"
1'-4 7/8"
1'-1"
2"
GENERAL MOTORS BRIDGE BARRIER RAILING
2"
6"
1'-7"
2'-8"
7"
10"
3"
2'-0"
NEW JERSEY CONCRETE MEDIAN BARRIER

Figure 20.

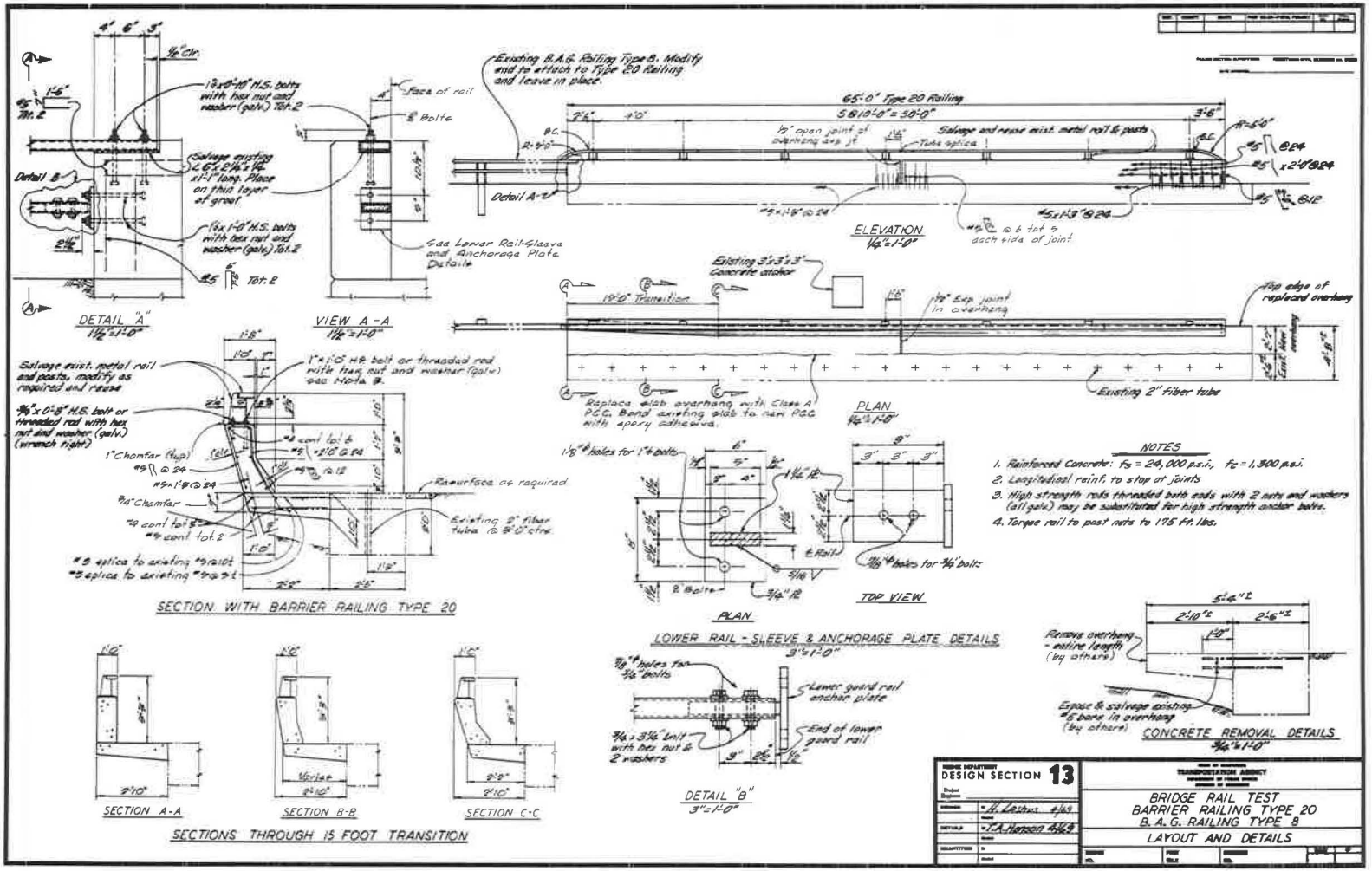
DETAIL "A"
VIEW A-A
ELEVATION
PLAN
SECTION WITH BARRIER RAILING TYPE 20
TOP VIEW
PLAN
LOWER RAIL - SLEEVE & ANCHORAGE PLATE DETAILS
DETAIL "B"
CONCRETE REMOVAL DETAILS
SECTION A-A
SECTION B-B
SECTION C-C
SECTIONS THROUGH 15 FOOT TRANSITION
NOTES
1. Reinforced Concrete: fs = 24,000 p.s.i., fc = 1,300 p.s.i.
2. Longitudinal reinf. to stop at joints
3. High strength rods threaded both ends with 2 nuts and washers (all galv.) may be substituted for high strength anchor bolts.
4. Torque rail to post nuts to 175 Ft. lbs.
DESIGN SECTION 13
BRIDGE RAIL TEST
BARRIER RAILING TYPE 20
B.A.G. RAILING TYPE 8
LAYOUT AND DETAILS

Figure 21.

CALIFORNIA DIVISION OF HIGHWAYS

VEHICLE INSTRUMENTATION

TYPE 20 BRIDGE BARRIER RAIL TESTS

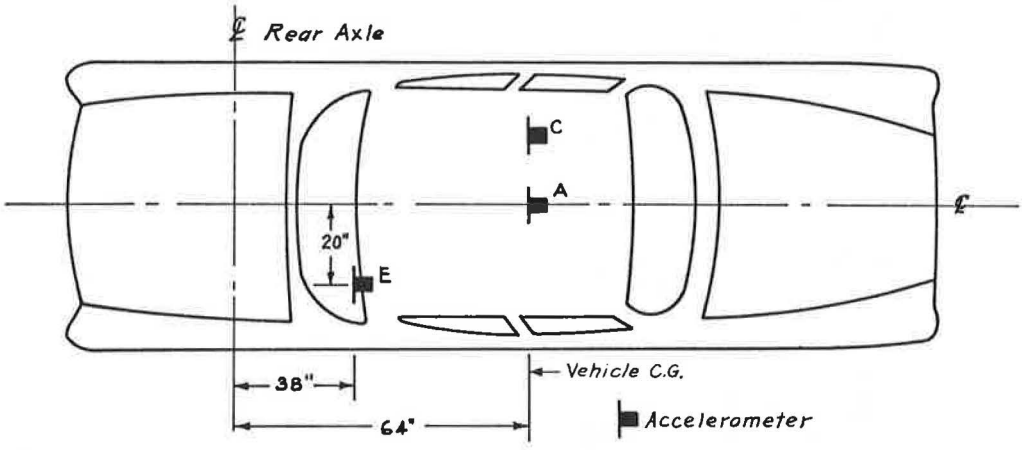

Test #232

CHANNEL NO.	LOCATION[1]	DESCRIPTION[2,3]
1	A	100 "G" longitudinal accelerometer (T)
2	A	100 "G" lateral accelerometer (T)
3	E	100 "G" longitudinal accelerometer (T)
4	E	50 "G" lateral accelerometer (T)
5	C	50 "G" longitudinal accelerometer (T)
6	C	50 "G" lateral accelerometer (T)
7	C	50 "G" vertical accelerometer (T)
8	E	100 "G" longitudinal accelerometer (U)
9	E	100 "G" lateral accelerometer (U)

Tests #234 & #235

1	A	100 "G" longitudinal accelerometer (T)
2	A	100 "G" lateral accelerometer (T)
3	E	100 "G" longitudinal accelerometer (T)
4		Same as Channel 3
5	E	50 "G" lateral accelerometer (T)
6	C	50 "G" lateral accelerometer (T)
7	C	50 "G" longitudinal accelerometer (T)
8	E	100 "G" longitudinal accelerometer (U)
9	E	50 "G" lateral accelerometer (U)

Notes:

[1] A and E on vehicle floor; C on back of dummy's chest cavity.

[2] (T) = telementry, (U) = umbilical cord.

[3] All transducers were unbonded strain gage type accelerometers. Channels 1-7 were Statham Model A514TC and Channels 8 and 9 were Statham Model A400TC.

Figure 22.

Impact +0.02 Sec.

I +0.21 Sec.

I +0.53 Sec.

I +0.62 Sec

TEST 231

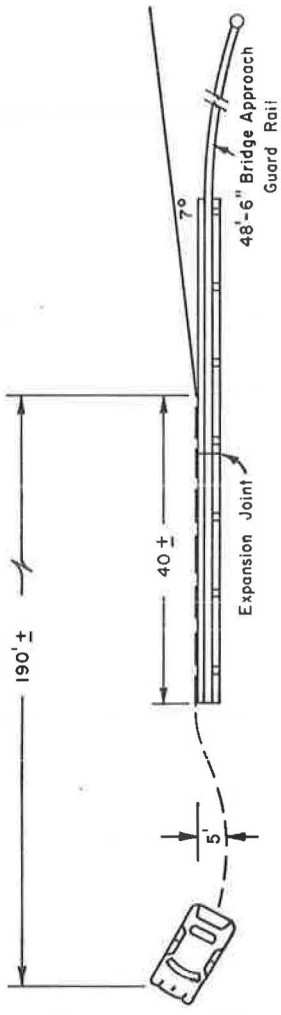

TEST NO.	231
DATE	10-2-69
VEHICLE	1966 Dodge Sedan
SPEED	45 mph
IMPACT ANGLE	7°
VEHICLE WEIGHT (Incl./ dummys & instrumentation)	4980 Lbs
DUMMY RESTRAINT	Lap Belt

BARRIER TESTED	Type 20 Bridge Rail
LENGTH OF INSTALLATION	67' ±
PASSENGER COMPARTMENT DECEL. (Highest 50 ms average) Long.	*
Lat.	*
MAXIMUM VEHICLE RISE	16"
EXIT ANGLE	0°
BARRIER DAMAGE	Negligible

*EXCESSIVE INTERFERENCE IN SIGNAL.

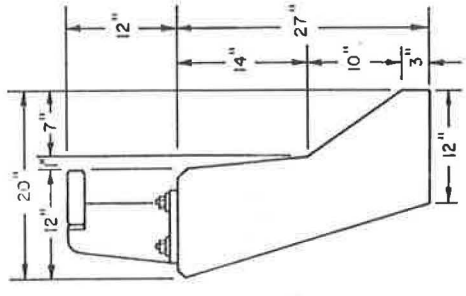

Figure 23.

Impact + 0.03 Sec.

I + 0.17 Sec.

I + 0.30 Sec.

I + 0.44 Sec.

TEST 232

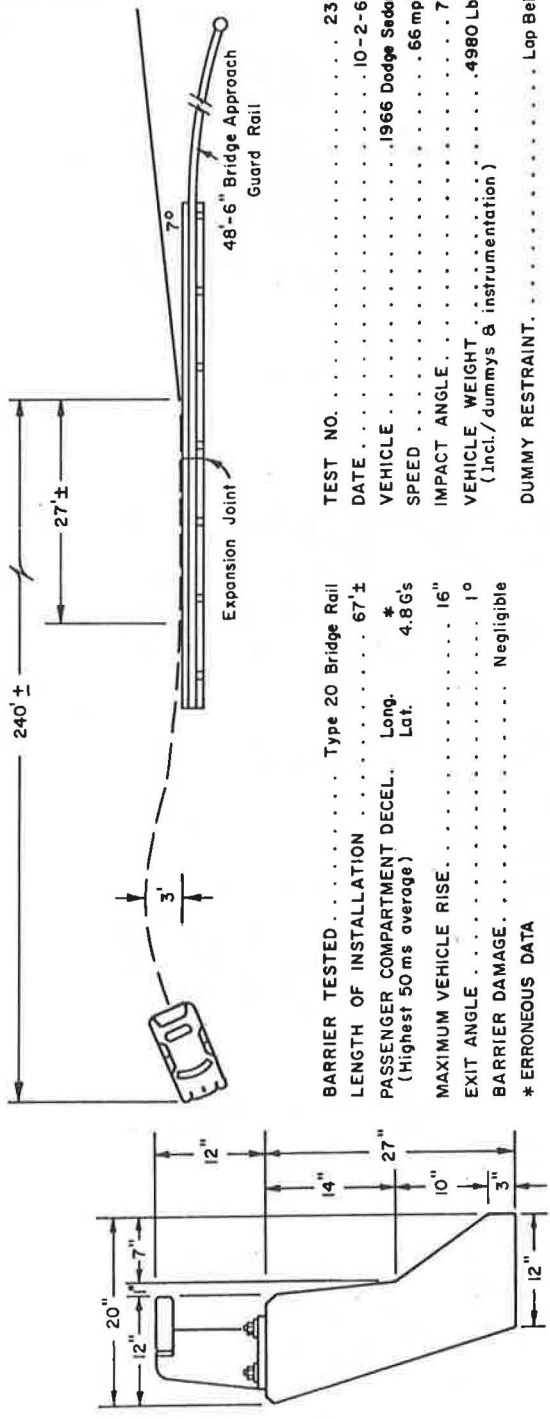

BARRIER TESTED	Type 20 Bridge Rail
LENGTH OF INSTALLATION	67'±
PASSENGER COMPARTMENT DECEL. (Highest 50 ms average)	Long. * Lat. 4.8 G's
MAXIMUM VEHICLE RISE	16"
EXIT ANGLE	1°
BARRIER DAMAGE	Negligible
* ERRONEOUS DATA	

TEST NO.	232
DATE	10-2-69
VEHICLE	1966 Dodge Sedan
SPEED	66 mph
IMPACT ANGLE	7°
VEHICLE WEIGHT (Incl./dummys & instrumentation)	4980 Lbs
DUMMY RESTRAINT	Lap Belt

Figure 24.

IMPACT

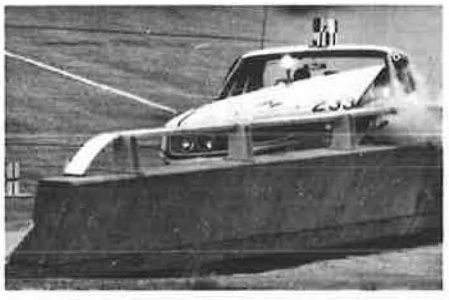

I + 0.09 Sec.

I + 0.23 Sec.

I + 0.46 Sec.

TEST 233

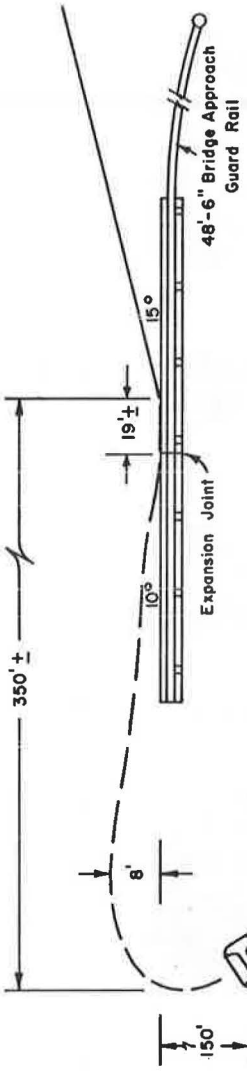

BARRIER TESTED	Type 20 Bridge Rail
LENGTH OF INSTALLATION	67'±
PASSENGER COMPARTMENT DECEL. (Highest 50 ms average) Long.	*
PASSENGER COMPARTMENT DECEL. (Highest 50 ms average) Lat.	*
MAXIMUM VEHICLE RISE	Negligible
EXIT ANGLE	10°
BARRIER DAMAGE	Negligible

* INSTRUMENTATION MALFUNCTION
† VEHICLE GAS TANK REMOVED

TEST NO.	233
DATE	10-8-69
VEHICLE	1966 Dodge Sedan
SPEED	64 mph
IMPACT ANGLE	15°
VEHICLE WEIGHT (incl./ dummys & instrumentation)	4900 Lbs.†
DUMMY RESTRAINT	Lap Belt

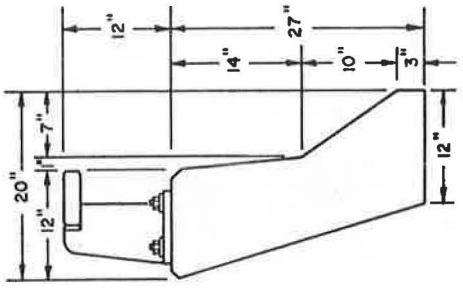

Figure 25.

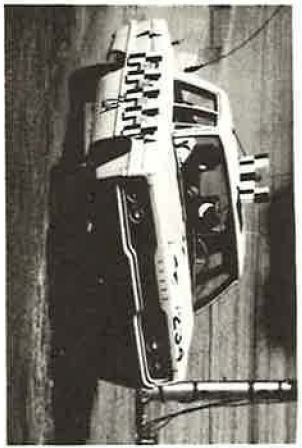

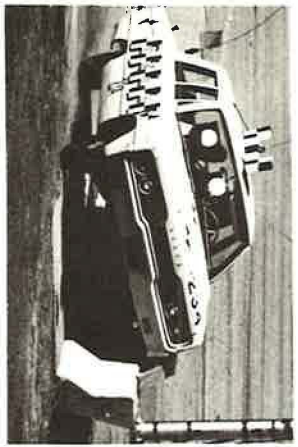

TEST 234

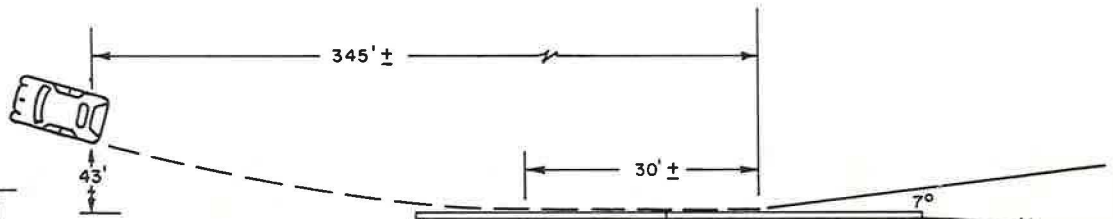

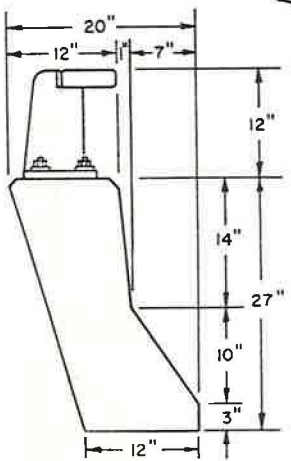

BARRIER TESTED		Type 20 Bridge Rail
LENGTH OF INSTALLATION		67' ±
PASSENGER COMPARTMENT DECEL. (Highest 50 ms average)	Long.	*
	Lat.	4.8 G's
MAXIMUM VEHICLE RISE		18"
EXIT ANGLE		1°
BARRIER DAMAGE		Negligible

* LESS THAN 1 G

TEST NO.	234
DATE	10-29-69
VEHICLE	1966 Dodge Sedan
SPEED	64 mph
IMPACT ANGLE	7°
VEHICLE WEIGHT (Incl. / dummys & instrumentation)	4980 Lbs
DUMMY RESTRAINT	Lap Belt

Figure 26.

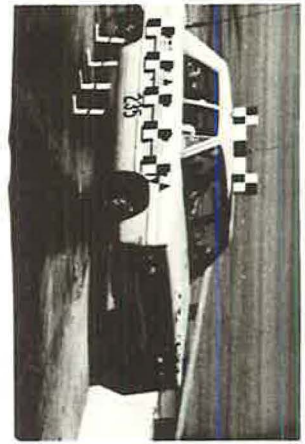

TEST 235

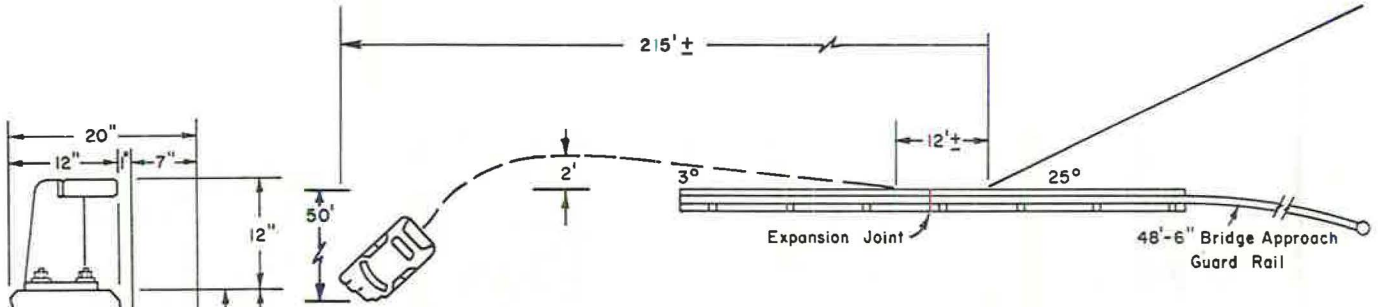

BARRIER TESTED	Type 20 Bridge Rail	
LENGTH OF INSTALLATION	67'±	
PASSENGER COMPARTMENT DECEL. (Highest 50 ms average)	Long.	14.8 G's
	Lat.	9.1 G's
MAXIMUM VEHICLE RISE	Negligible	
EXIT ANGLE	3°	
BARRIER DAMAGE	Minor	

† VEHICLE GAS TANK REMOVED

TEST NO.	235
DATE	10-29-69
VEHICLE	1966 Dodge Sedan
SPEED	66 mph
IMPACT ANGLE	25°
VEHICLE WEIGHT (Incl./ dummys & instrumentation)	4900 Lbs†
DUMMY RESTRAINT	Lap belt

Figure 27.

SCALE-MODEL TEST OF AN ENERGY-ABSORBING BARRIER

Richard J. Fay and Edward P. Wittrock,
Denver Research Institute, University of Denver

A scale-model test of the "Texas barrel barrier" was conducted to demonstrate the great utility of scale modeling in the study of energy-absorbing highway barriers. This barrier consists of an array of empty 55-gal drums attached together and fastened in place so that energy from an impacting automobile is absorbed in the plastic deformation of the drums. The results of this test were found to agree very well with results from a full-scale test that was modeled. The modeling techniques are presented, and the similitude requirements for the scale modeling of the car and the barrier are developed.

•A SCALE-MODEL TEST of the "Texas barrel barrier" was conducted at the Denver Research Institute (DRI). The test was restricted to a head-on collision of a model car impacting an array of scale-model 55-gal drums. The results were compared to the results of the actual tests conducted by the Texas Transportation Institute (1, 2). Specifically, the test modeled by DRI was test 1146-5 (2), which used a Dodge sedan weighing 3,360 lb, impacting head-on at 52.5 mph into a modular crash cushion. This cushion or barrier consisted of a rectangular array of 16-gage, 55-gal drums, 9 drums long by 3 drums wide, with a tenth row, 2 drums wide, placed at the impact point.

The scaling laws were determined using standard techniques discussed in the following section. For the specific test conducted, emphasis was placed on accurately scaling the dimensions, weight, and velocity of the car and the dimensions, weight, and static force-deflection curve for the drums. Briefly, it was found that, if the linear dimensions were scaled in the ratio of

$$\frac{\text{Model dimensions}}{\text{Prototype dimensions}} = n_1$$

the velocity would scale as

$$\frac{\text{Model velocity}}{\text{Prototype velocity}} = (n_1)^{1/2}$$

and the forces would scale as

$$\frac{\text{Forces on model}}{\text{Forces on prototype}} = (n_1)^3$$

The results of the test are shown in a later section. It is apparent from these results that even a simplified model, such as that used in this test, can give valid results provided strict attention is paid to the governing parameters.

DIMENSIONAL ANALYSIS

The variables assumed to be sufficient to describe the impact problem under discussion are given in Table 1. Using standard techniques, the variables may be com-

Sponsored by Committee on Traffic Safety Barriers and Sign, Signal and Lighting Supports and presented at the 50th Annual Meeting.

TABLE 1

IMPACT VARIABLES

Variable	Name	Basic Dimensions
Dependent		
a	Deceleration	LT^{-2}
Independent		
V	Velocity (initial)	LT^{-1}
w	Rotational velocity (initial)	T^{-1}
I	Polar moment of inertia of automobile	ML^2
θ	Obliquity angle at impact	—
u_1	Coefficient of friction between tires and road surface	—
γ_i	Characteristic dimensions of automobile	L
F_i	Force to operate barrier over the ith increment of stroke	MLT^{-2}
L	Stroke of barrier	L
u_2	Coefficient of friction between the barrier and the roadway	—
λ_i	Characteristic dimension of barrier	L
M	Mass of automobile	M
ρ	Density of the barrier material	ML^{-3}
g	Acceleration due to gravity	LT^{-2}
ϕ	Yaw angle at impact	—
k	Percent springback of barrier	—

bined into 13 dimensionless groups. For the present purpose, these have been taken as follows:

$$\pi_1 = aM/F_i \qquad \pi_8 = u_2$$

$$\pi_2 = \omega L/V \qquad \pi_9 = \rho V^2 \gamma_i^2/F_i$$

$$\pi_3 = I/M\lambda_i^2 \qquad \pi_{10} = \phi$$

$$\pi_4 = \theta \qquad \pi_{11} = gM/F_i$$

$$\pi_5 = u_1 \qquad \pi_{12} = \lambda_i F_i/V^2 M$$

$$\pi_6 = \gamma_i/L \qquad \pi_{13} = k$$

$$\pi_7 = L/\lambda_i$$

The design conditions for a true model are that the π terms for the model equal the corresponding π terms for the prototype; i.e., $(\pi_n)_m = (\pi_n)_p$, where the m and p subscripts refer to the model and prototype respectively.

There are three basic dimensions (mass, length, and time) for the variables considered and, therefore, three scale factors may be chosen arbitrarily that scale these basic dimensions. The scale factors chosen for the present case are $n_1 = (\lambda_i)_m/(\lambda_i)_p$ (scales length), $n_2 = g_m/g_p$ (scales time), and $n_3 = (F_i)_m/(F_i)_p$ (scales mass).

For our laboratory, a desirable linear scale for the model is $(\lambda_i)_m/(\lambda_i)_p = n_1 = 1/25$, while the most practical value for the ratio of the gravitational constants is $g_m/g_p = n_2 = 1$. The force ratio is conveniently chosen as $(F_i)_m/(F_i)_p = n_3 = n_1^3$, thus preserving the natural relationship between the length, volume, and weight or mass of the model. Using these scale factors and equating the terms gives the following complete similitude requirements:

$$a_m = a_p \qquad L_m = n_1 L_p$$

$$V_m = n_1^{1/2} V_p \qquad u_{2m} = u_{2p}$$

$$\omega_m = n_1^{-1/2} \omega_p \qquad \lambda_{im} = n_1 \lambda_{ip}$$

$$I_m = n_1^5 I_p \qquad M_m = n_1^3 M_p$$

$$\theta_m = \theta_p \qquad \rho_m = \rho_p$$

$$u_{1m} = u_{1p} \qquad g_m = g_p$$

$$\gamma_{im} = n_1 \gamma_{ip} \qquad \phi_m = \phi_p$$

$$F_{im} = n_1^3 F_{ip} \qquad k_m = k_p$$

These values (with $n_1 = 1/25$) were used in the model test described in the following sections.

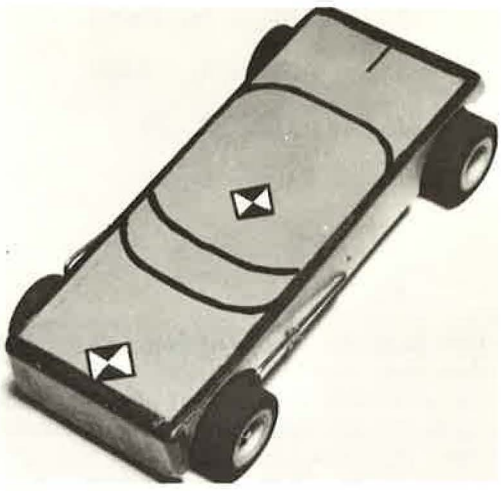

Figure 1. Scale-model car measures 6⅜ by 2½ in. The targets on the car (black and white triangles) were added after the test described in this paper to facilitate more accurate measurements from the high-speed film.

FACILITIES

Model Car

The car used in these tests (Fig. 1) was modeled to a scale of 1:25 and was specifically weighted to simulate the 3,360-lb Dodge used in test 1146-5 (2). The scale factors for the car mass, length, width, and velocity were

$$M_m = n_1^3 M_p = M_p/15{,}600$$

$$L_m = n_1 L_p = L_p/25$$

$$W_m = n_1 W_p = W_p/25$$

$$V_m = n_1^{1/2} V_p = V_p/5$$

As a first trial at the problem of modeling the impact on a modular crash barrier, the linear dimensions, the weight, and the velocity of the car were given primary consideration. Other factors such as tire friction, tire spring constant, ground pressure, and center of gravity were not considered significant because the test was confined to a straight, head-on impact where it could be assumed that these factors would play a negligible role. It was believed that this model was the simplest one that could be relied on to produce valid data and would therefore require the least expenditure of time and money to construct and operate.

One factor that was deemed to be of significance was the resistance of the car to motion with the motor turned off and the gear shift lever in the drive position (automatic transmission) or in high gear (standard transmission). In the actual test (2), the motor is turned off (brakes not applied) just prior to impact causing the rear wheels to run against the compression of the motor down to about 20 mph for an automatic and all the way down to a dead stop for a standard drive. How far the car rebounds depends on these factors because a car with automatic transmission in drive, for example, will roll backward rather easily, whereas a car with standard transmission engaged in third gear, say, offers a very great resistance to any force trying to accelerate it backwards. Thus, it was felt that for purposes of initial testing some method of braking the model in the direction of rebound should be incorporated. This was done by fastening a wire to each side of the car (Fig. 1) in such a way that the front wheels could not rotate backward. This also took into account some of the differences in the road surface used in the two tests, which in the case of the model was simply a wooden table top covered with grid paper.

The car was constructed of a solid block of redwood with axle holes drilled completely through the block front and rear. To model the weight correctly it was necessary to hollow out a large portion of the underside. The axles were one piece and threaded on both ends. The wheels were a common type used for "slot cars" and were attached directly to the axles.

Drums

Using the similitude requirements discussed earlier, models of the 16-gage, 55-gal drums were constructed (Fig. 2). The mass, static peak load, diameter, height, density, and springback of the model drum were respectively given as follows:

$$M_m = n_1^3 M_p = M_p/15{,}600$$

$$P_m = n_1^3 P_p = P_p/15{,}600$$

$$D_m = n_1 D_p = D_p/25$$

$$H_m = n_1 H_p = H_p/25$$

$$\rho_m = \rho_p$$

$$K_m = K_p$$

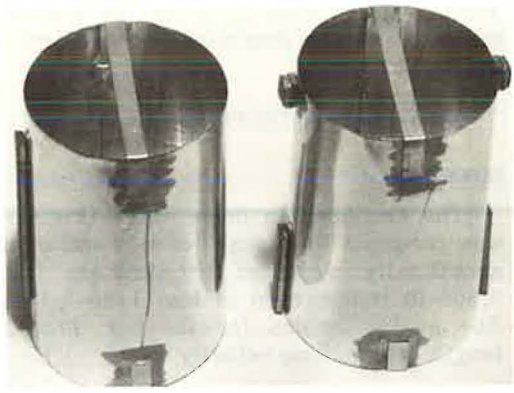

Figure 2. Scale models of the 55-gal drums used in the "Texas barrel barrier." A "center" drum is shown on the right and an "outside" drum on the left. Note small lead weights used as spacers on the center drum (photograph taken before painting the barrels).

The material selected was dead soft aluminum foil (since the springback characteristic of the real drums was not known but was assumed to be small) 0.003 in. thick. It was formed into cylinders (1-in. diameter by 1.4-in. long) by wrapping the material around a 1-in. diameter tube and gluing the seam with contact cement. The top was modeled by gluing an aluminum strip 0.005-in. thick by 0.1-in. wide over each end of the model barrel. The model was then compressed in a static testing machine to obtain the load deflection curve. The results of this test are shown in Figure 3, which also shows a plot of the load-deflection curve of an actual drum scaled down to model dimensions. The data in Figure 3 show that the load-deflection curve for the model has the same prominent features as the prototype, these being the sharp initial slope and the peaking effect with the subsequent rapid decrease in the load with continued increase in displacement. (Note that these curves were both obtained from only one test. To properly characterize the barrels, a statistical sample would be required.) It was found that considerable change in the peak load for the model could be achieved by varying the width of the end strip, making it possible to simulate a large number of designs. Furthermore, as indicated by the results of the present work, the load-deflection curve for the model drum need not be an exact duplicate of the prototype

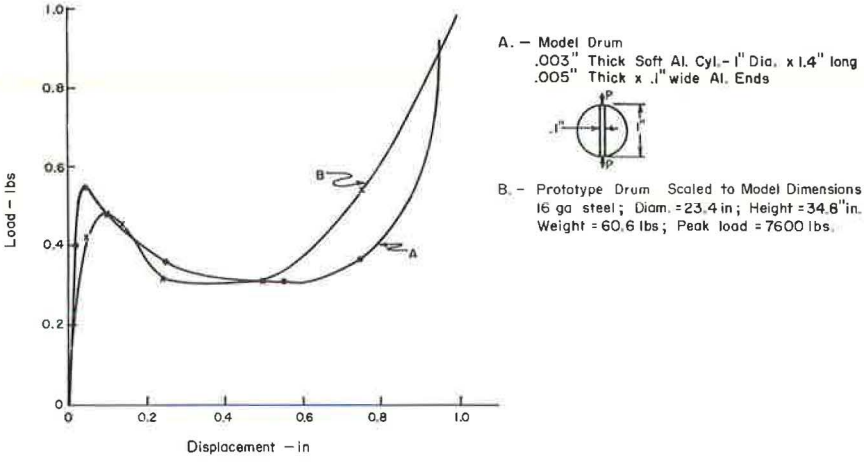

Figure 3. Relationship of the load versus deformation curves for the model and prototype drum.

curve, but must retain the essential character of the curve. It is, therefore, reasonable to assume that the top of the model drum need not duplicate physically the top of the prototype.

The drums used in the model test incorporated spacers that simulated rolling hoops. These were formed by gluing lead weights to each side of the center barrel in each row. This provided the necessary space between the center and outside drums for the wire used to simulate the steel cable used in the actual test. Also, the lead weights were necessary to bring the weight of the models up to the necessary values because the aluminum alone was too light. The weights used on the outside drums also served to raise them off the table in a manner similar to that of the "Re-Bar" chairs used in the actual test. Thus, the model 55-gal drums, individually as well as collectively, showed a close similarity to the actual drums.

Model Car Launching Facilities

The model car discussed previously impacted the barrier at 10.6 mph (equivalent to 53 mph for the prototype). This velocity was attained by a compressed air launcher operating at 150-psi air pressure (Fig. 4). The car was maintained on course for the first 12 in. by two guide rails. On leaving the guides, the car passed through the timing station where it interrupted two light beams, starting and stopping a Beckley (100,000-cps) chronograph. The time required for the car to traverse the distance between the light beams was used to determine the velocity of the car.

The motion of the car and the barrier was recorded by a 16-mm high-speed camera. This camera, a Fairchild Model HS101A capable of film speeds up to 10,000 frames per second, is shown in Figure 4 mounted to take a plan view of the collision. From the film obtained in this fashion, an accurate analysis was made of the motion of the car and the barrier (Fig. 5). A mirror was used to give a side view of the event, making it possible to observe vertical motion of the car and drums. This side view is visible in Figures 5 and 6.

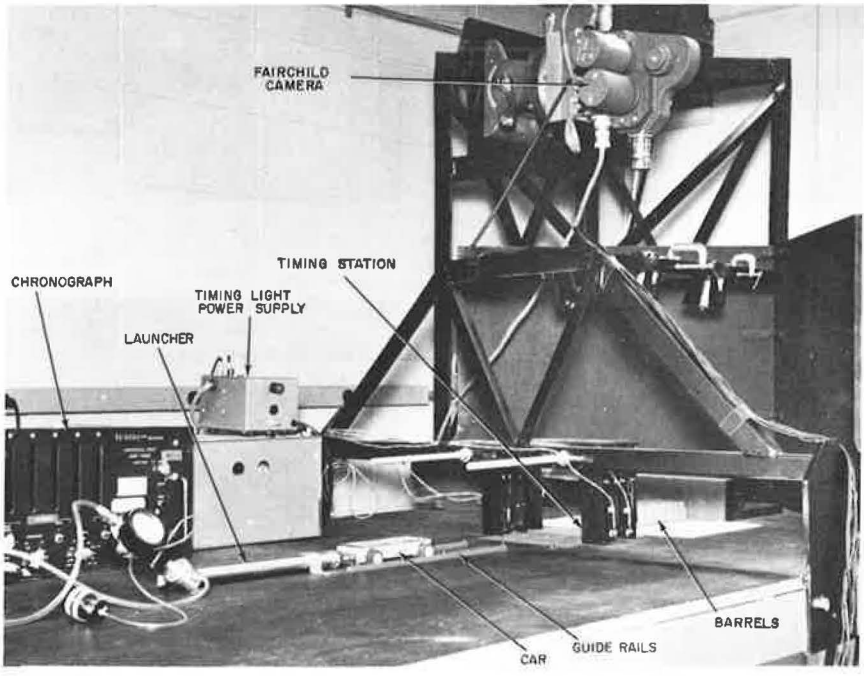

Figure 4. Overall view of model crash barrier test facilities.

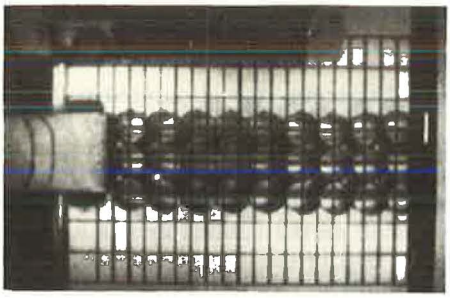

1

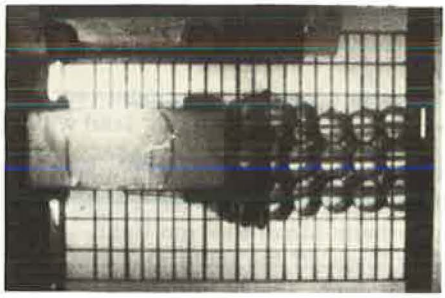

5

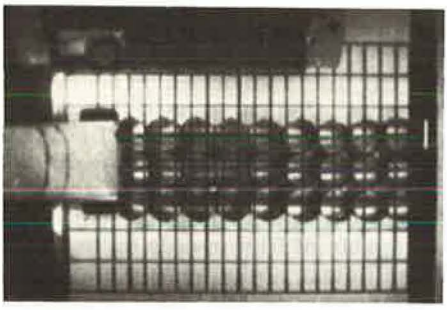

2

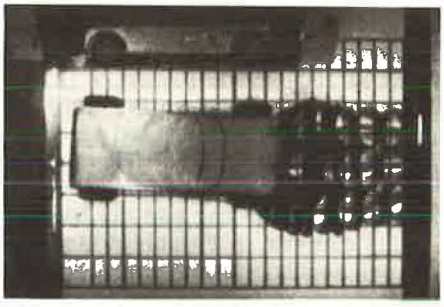

6

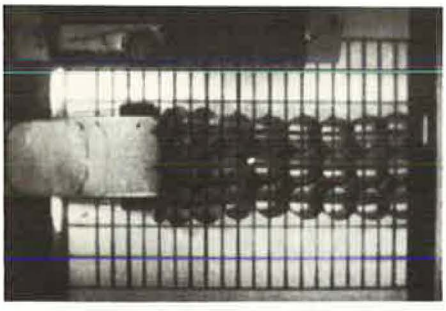

3

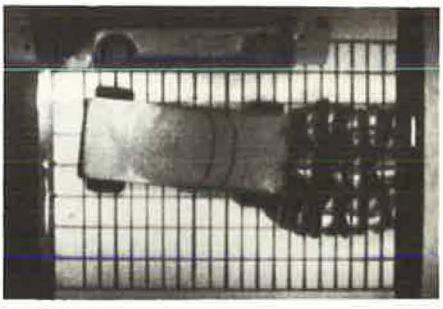

7

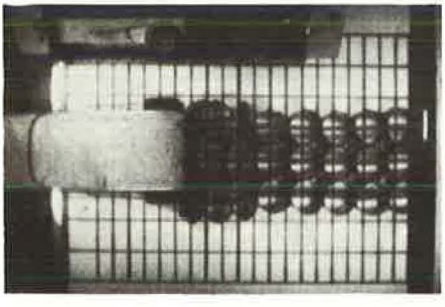

4

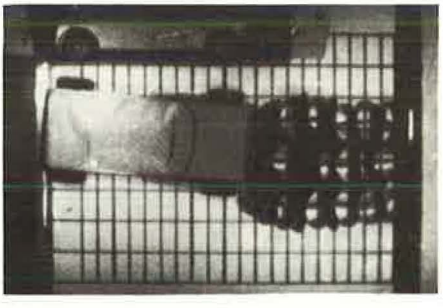

8

Figure 5. Sequence taken from 16-mm high-speed movie film (3,000 frames per second) during the scale-model test of the "Texas barrel barrier."

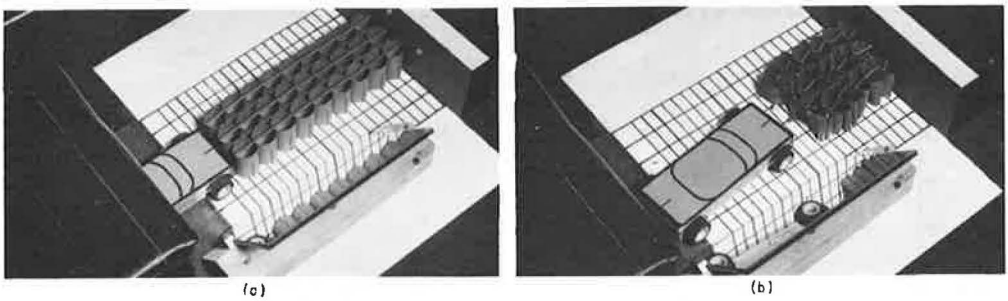

(a) (b)

Figure 6. Simulated car and barrier (a) at impact and (b) after impact.

RESULTS

The results obtained in the test are shown in Figure 7. The distance, velocity, and G curves are plotted as a function of time after impact for the model car. Also, the distance-time plot for the prototype (1964 Dodge, 3,360 lb) is shown to the scale of the model. Because of the good correlation of the model data with the prototype data, only the data for the model were actually differentiated to produce the velocity and G curves. The average deceleration in G for the model was computed (2) from the equation

$$G_{ave} = \frac{V_0^2}{2gS}$$

where

V_0 = initial velocity at time of impact,
S = movement of the vehicle center of gravity in feet from its position at first contact to its position when its longitudinal velocity is zero, and
g = 32.2 feet per second.

Thus, for the model, $(G_{ave})_m = 7.35$ while for the prototype the value was given (2) as $(G_{ave})_p = 7.6$. A further indication of the validity of the test can be obtained from a visual comparison of the barrier after the test to the after photograph of the prototype barrier (both cases are for the rectangular array of 3 by 9). In these photographs (Fig. 6 in this report, photograph on p. 10 of reference 1, and Figs. 6 and 11 of reference 2), the first two rows appear to crush somewhat uniformly, while thereafter there is a distinctive pattern wherein alternate rows do not crush uniformly. This behavior is very evident in the high-speed movie (3,000 frames per second) taken during the model test. An explanation for this nonuniform behavior lies in the manner in which the force is applied to successive elements of the barrier. The first two rows undergo catastrophic deformation due to the relatively high impact velocity. By the time the car travels approximately the distance equivalent to these two drum diameters, the second row has wrapped back around the third row, causing the load to be spread out over a much greater area. This row, having a more distributed load, is not as easily crushed. (Note that the kinetic energy of the car at this time has decreased by about 30 percent.) The fact that the third row is not crushing as rapidly implies that the fourth row is now being affected by a more concentrated load and therefore deforms more readily. This chain of events continues until, in the end, it appears that every other row is affected in this manner. Similar behavior, but to a lesser extent, was reported in test 1146-3 (2, Fig. 9). However, this last set of barrels was originally a slightly different array, which may account for the more uniform deformation.

The fact that the drums behave in this nonuniform manner clearly indicates an important role that modeling can play in barrier design. That is, a modular crash cushion can be studied experimentally to determine changes in design required to obtain uniform deformation, thereby applying the most uniform decelerating force to the

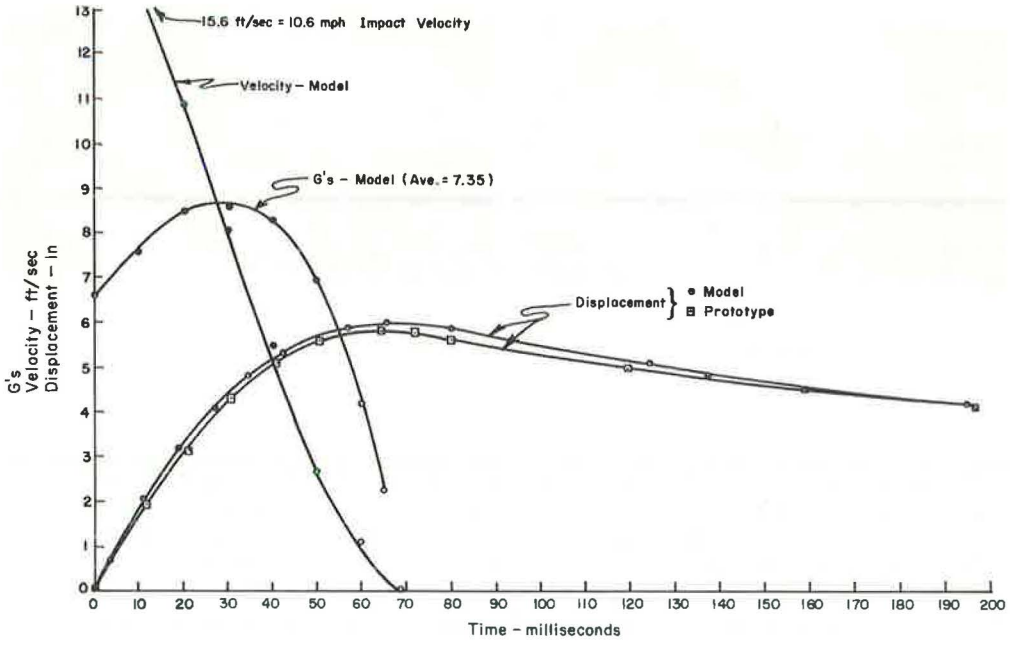

Figure 7. Results of the scale-model impact test compared to the results of the actual test (1146-5). The actual test data have been scaled down to the model dimensions of distance and time.

vehicle over the shortest distance. Simultaneously, the data from all tests may be compiled for use in developing and correlating analytical models. The same techniques may be applied to barriers of any design with the ultimate goal of designing a barrier that is optimized with regard to overall efficiency, including the cost of materials and labor to build and install the barrier. These points and others such as angle impacts and side impacts resulting in automobile redirection can be studied experimentally, using models, at a fraction of the cost of using full-size cars and barriers. For example, the cost of running a test such as that described in this paper is estimated to be less than $400, including direct labor, complete film coverage, materials, and data reduction. Some barrier tests would be expected to be considerably less expensive because, with the modular barrier, the largest expense is involved in construction of the individual elements. Simpler designs would cost less for labor and hence would be less expensive to test and evaluate.

REFERENCES

1. Hirsch, T. J. Barrel Protective Barrier. Texas A&M Research Foundation, Texas Transportation Institute, Tech. Memo. 505-1.
2. Hirsch, T. J., Ivey, D. L., and White, M. C. The Modular Crash Cushion: Research Findings and Field Experience. Texas Transportation Insitute, Texas A&M University.
3. Murphy, G. Similitude in Engineering. Ronald Press Co., New York, 1950.

WATER-PLASTIC CRASH ATTENUATION SYSTEM: TEST PERFORMANCE AND MODEL PREDICTION

Charles Y. Warner and Joseph C. Free, Department of Mechanical Engineering, Brigham Young University

This paper presents the results of a model performance study on the Hi-Dro Cushion Cell Barrier (water-plastic impact cushion). A digital computer model was constructed to represent the dynamic response of the cushion system. The model was verified by comparing with actual full-scale crash tests. The verified model was then exercised to provide prediction of response to extremes of vehicle mass and speed. The simulated performance of the barrier is presented and compared with the square-wave or "constant-force" cushion. Predictions show that the water-plastic unit provides good performance across the spectrum of impacting vehicle momenta, and that it provides a response that takes advantage of almost all of the available stopping distance for impacts between 30 and 70 mph, employing vehicles weighing from 2,000 to 6,000 lb.

•THE DESIGNER of highway systems in today's era of high-speed family transportation is faced with the enigma of the roadside hazard: "Shall I move it or protect it, and if I protect it, how?" Often the use of hardware such as guardrail aggravates rather than moderates the hazard. This study treats one technique for dealing with immovable objects and guardrail terminals. Considerations essential to a cost-effective design are discussed, and the behavior of the water-plastic cushion is compared to performance standards and to the hypothetical alternative of the "constant-force" cushion. Application of the principles discussed should help to solve the problem of obstacle protection effectively and economically.

CRITERIA FOR CUSHION PERFORMANCE

The rational design of an impact cushion device must take into account a large number of factors, of which the following are important:

1. Occupant loads during impact must be tolerable. Average occupant deceleration levels should not exceed 12 g; deceleration peaks should have a duration above 12 g of less than 40 milliseconds (msec), with magnitudes as low as possible. Onset rates should be limited at 500 g/sec. Overall success may be measured by the Gadd index of severity, assuming typical seat-belt restraint.
2. Occupants of vehicles weighing from 1,600 to 4,500 lb should be adequately protected in head-on or glancing impacts up to 60 mph, with vehicles in glancing blows at angles less than 25 deg being usually fendered rather than arrested.
3. The device should be reusable, insofar as possible; one impact should not destroy its capability. Some protection should remain for subsequent impacts, even without maintenance. Ease and rapidity of maintenance are essential; cost judgments should include maintenance and road-system downtime costs, as well as cost of initial hardware and right-of-way space.

In every engineering design, it is not always possible to meet all design criteria within the limitations imposed by cost and space considerations. A design study on the

Sponsored by Committee on Traffic Safety Barriers and Sign, Signal and Lighting Supports and presented at the 50th Annual Meeting.

water-plastic cushion used the preceding criteria in the development of cushion hardware (1). The following sections present the resulting design and its predicted performance.

DESCRIPTION OF CUSHION SYSTEM AND APPLICATIONS

The hydraulic-plastic protective barrier developed under this project utilized vertical cylindrical plastic cells as a primary building block (Fig. 1). These cells were closed at the bottom, equipped with orifices at the top as shown in Figure 2, and filled with water (2).

The functional characteristics of a single cell are controlled by selecting cell-wall material characteristics, size and number of orifices, water content, and cell geometry. Control of the characteristics of a cushion unit as a whole is accomplished by varying the number and distribution of various types of cells and cell spacing, and by including additional inertial or structural elements or both within the unit.

The prototype crash cushion consisted of clusters of water-filled plastic cells sandwiched between plywood-fiberglass plates. These were strung at 24-in. intervals along two heavy cables running parallel to traffic (Fig. 3). The main plates provided hinge points for overlapping deflector plates or "fish scales". The fish scales and main support cables provided a stiff but elastic redirection surface with low friction coefficient for glancing impacts, helping to avert pocketing. The cables also provide stability for absorbing head-on impacts.

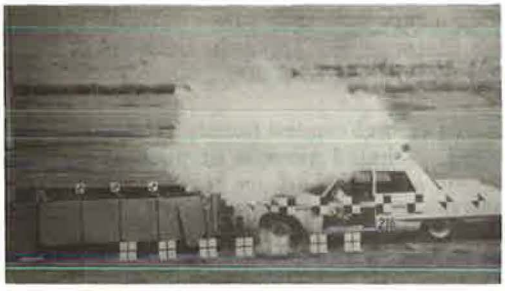

Figure 1. Crash test in progress.

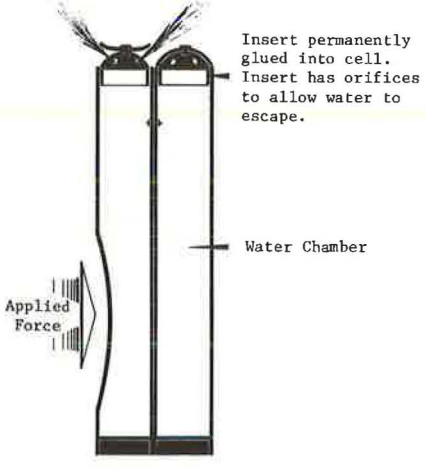

Figure 2. Cross section of typical polyvinyl chloride plastic cells. Typical dimensions of cells are 42 in. long by 6 in. outside diameter, with wall thickness varying.

The entire system was designed to provide capability for easy and rapid replacement of modules, ease of maintenance, and quick return to service after use. (Systems have been impacted repeatedly in engineering tests at conditions near design limits with only minor repairs between hits.) Usually only a simple reconfiguration and water-refilling procedure is required between crashes. Time required by a trained three-man crew to return test units to service after a 60-mph head-on impact has been less than 30 min.

For areas subject to freezing temperatures, the addition of calcium chloride to the water appears to solve the immediate freezing problem. The temperature-dependence of the plastic is, of course, another matter. The vinyl material used in the cells was compounded to maintain sufficient flexibility at -20 F, while maintaining sufficient rigidity at +110 F.

Most existing highway hazards associated with stationary structures could potentially be made safer by a properly designed water-plastic barrier. Figure 4 shows one hypothetical application. Other examples are given elsewhere (1).

COMPUTER MODEL AND VALIDATION

The mathematical model used for simulation of cushion behavior was a discrete-element representation, accounting for the

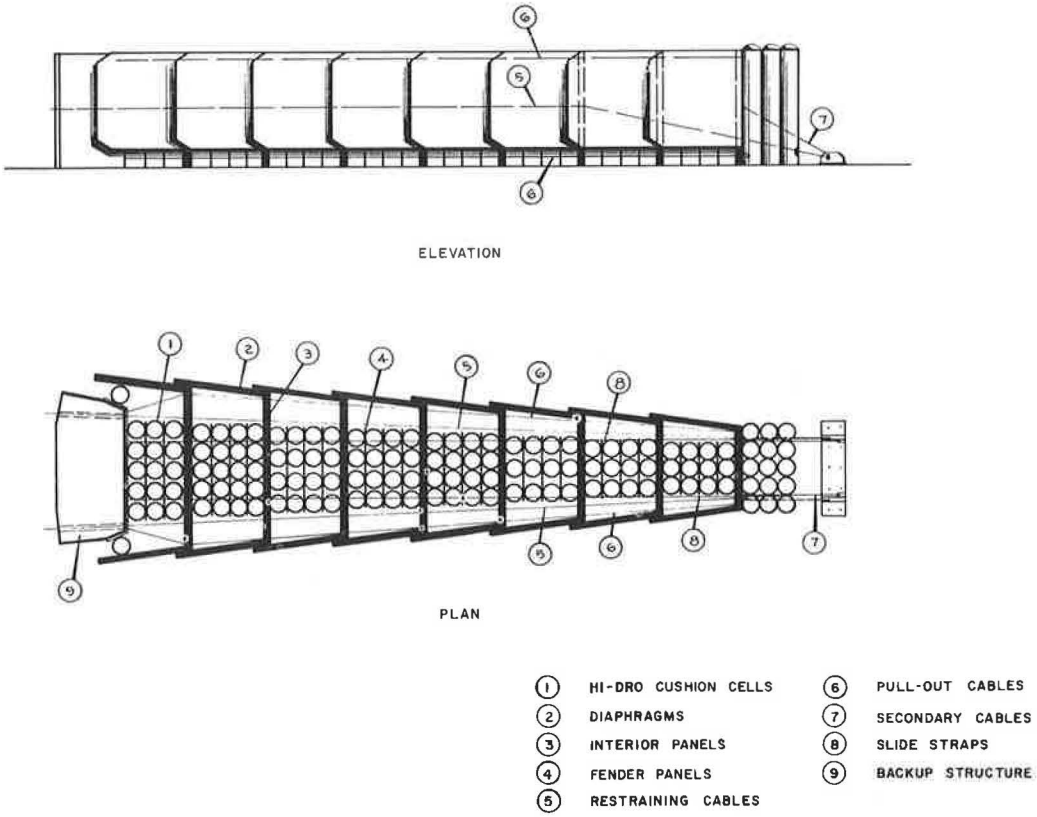

Figure 3. Cell sandwich unit of water-plastic cushion barrier.

essential characteristics of each component. The model took into account the strain-rate dependency of the plastic material, the nonlinear orifice resistance, the time-dependent mass, and the pressure-deflection dependency of the effective contact area between cells. The model parameters and functions were determined by dynamic tests in the laboratory, where actual loads and loading rates were simulated in a rapid-pressurization fixture. Occupant loads were predicted from a simple linear seat-belt model. The cushion model was constructed in such a way that either single-cell rows or effective-cell rows representing clusters of cells could be specified. It allowed inclusion of rigid beams of specified mass at the boundaries between cell cushions. The crushing behavior of the vehicle frontal structure was also simulated (3).

The accuracy of overall system behavior predicted by the computer model depended on the precision of the correspondence between model and experiment at the component level. Experimental verification of the various model subsystems was accomplished before the entire model was assembled. Full-scale crash tests conducted by various agencies have produced data showing good agreement with model predictions. Figure 5 shows the predicted vehicle deceleration pattern for a 4,720-lb_m, 60-mph impact compared with floor pan deceleration history recorded in a 4,690-lb_m, 61.8-mph impact by the California Division of Highways (unfiltered experimental data were hand-smoothed by the author). Figures 6, 7, and 8 show comparative predictions and test data for three different vehicle weights and speeds (test data were recorded by the Texas Transportation Institute, 4). The slight phase mismatch witnessed in some of the vehicle deceleration pulseforms may be attributed to the oversimplified representation

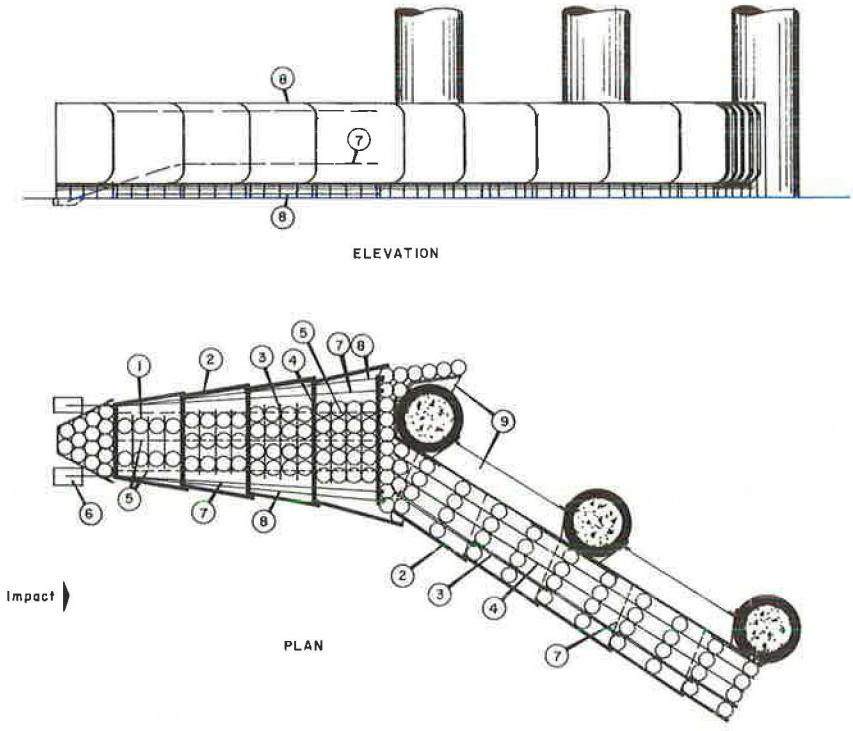

Figure 4. Specialized application of cell sandwich unit.

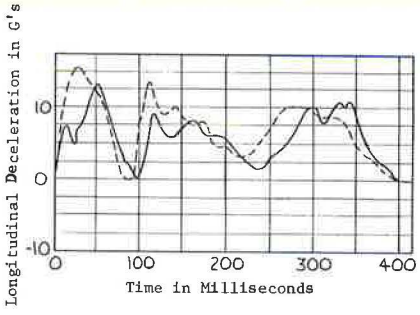

Figure 5. Full-scale crash test vs. simulation (California Division of Highways Test 216; head-on crash with Dodge). Solid line shows crash test with 4,690-lb vehicle at 61.8 mph; broken line shows simulated test with 4,720-lb vehicle at 60 mph.

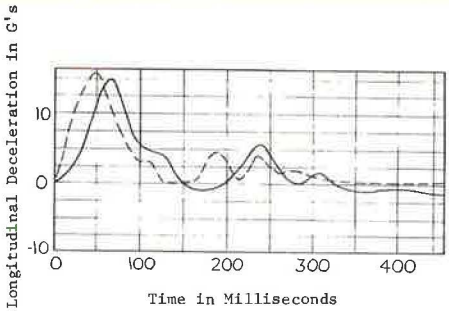

Figure 6. Full-scale crash test vs. simulation (Texas Transportation Institute Test 505R-A; head-on crash with Volkswagen). Solid line shows crash test with 1,820-lb vehicle at 40 mph; broken line shows simulated test with 1,500-lb vehicle at 40 mph.

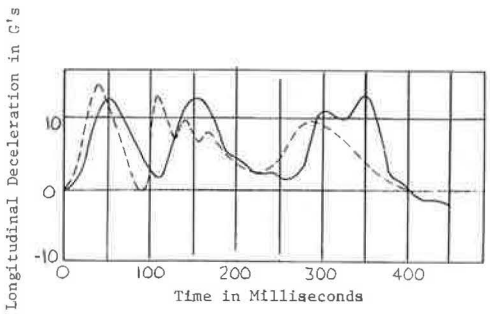

Figure 7. Full-scale crash test vs. simulation (Texas Transportation Institute Test 505R-B; head-on crash with Pontiac). Solid line shows crash test with 4,650-lb vehicle at 63 mph; broken line shows simulated test with 4,720-lb vehicle at 60 mph.

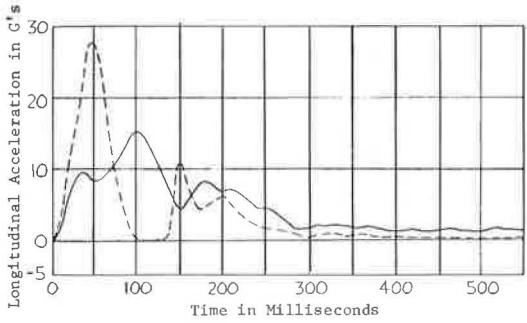

Figure 8. Full-scale crash test vs. simulation (Texas Transportation Institute Test 505R-D; head-on crash with Renault). Solid line shows crash test with 1,630-lb vehicle at 60 mph; broken line shows simulated test with 1,500-lb vehicle at 60 mph.

of the vehicle crush as a linear spring. Also, the very soft crush characteristic of the Renault vehicle was not simulated in the model for Figure 8, which may account for the mismatch in the early portion of the impact.

Table 1 gives a summary of data for the four tests shown in Figures 5, 6, 7, and 8. Gadd indexes for the tests were calculated from occupant model behavior (7). These comparisons with full-scale tests demonstrate acceptable validity for head-on impacts.

PERFORMANCE OF THE RESULTING DESIGN

The broad span of performance criteria discussed earlier pose a problem: Satisfactory system behavior under one or more of the conditions is changed. It is difficult to determine what the most cost-effective design point should be without a more complete definition of the average accidental collision. Conversely, evaluation test requirements plainly suggest that system performance be satisfactory at the most demanding conditions. Hence, the design point for the cushion system was chosen to be equivalent to the most critical energy-absorption case from the constraints given previously. It is the case of a 4,720-lb, 60-mph head-on impact. The total energy to be absorbed in this case is about 50,000 ft-lb_f.

It should be pointed out that, while this set of conditions probably is more severe than the average highway collision from the occupant's point of view, it does constitute

TABLE 1

COMPARISON OF PREDICTED AND ACTUAL BEHAVIOR

Predicted Results				Actual Results		
Nominal Vehicle Weight (lb_f)	Nominal Impact Speed (mph)	Peak Deceleration (g)	Gadd Index ($g^{5/2}$-sec)[a]	Agency and Number (weight, speed)	Peak Deceleration (g)	Gadd Index ($g^{5/2}$-sec)[a]
1,500	40	18	92	TTI505R-A (1,820, 40)	17	59.2
4,720	60	15	78	TTI505R-B (4,650, 63)	15	118
1,500	60	27	188	TTI505R-D[b] (1,630, 60)	18	92.3
4,720	60	15	78	CDH216 (4,690, 62)	14	75.4

[a]Occupant behavior simulated by one-dimensional dynamic model (Fig. 9) using either simulated or measured vehicle pulse forms.

[b]Soft frontal structure on vehicle.

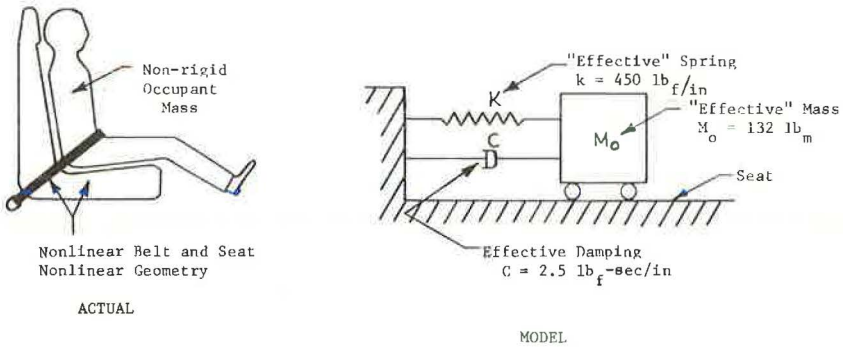

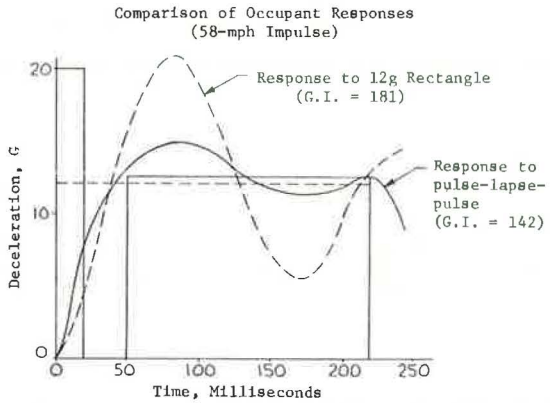

Figure 9. Idealized occupant restraint system.

a severe test of cushion system integrity. However, it is highly desirable that acceptance performance tests include an occupant-oriented test—one with a small car at high speed.

From a theoretical basis, the most efficient use of stopping distance is made by an energy absorber that gives a rectangular force-time response. Although this constant-force response optimizes energy absorption per unit length of cushion for one given mass and velocity, its response for other masses and velocities falls short of the optimum. Furthermore, the response of the seat-belted occupant to a square-wave vehicle response may be less than optimum (5, 6). Where the goal in the present work is to minimize occupant loads, some success may be realized by providing cushion characteristics that relieve vehicle loads after an initial impulse, taking advantage of the additional protection provided by the seat-belt restraints. Figure 9 shows a comparison of results of rectangular and two-pulse 60-mph vehicle deceleration waveforms on the simulated occupant responses. Occupant response is measurably improved by the two-pulse case, at the cost of a slight increase in stopping distance.

The design-point calculated performance of the water-plastic cushion is shown in Figure 10 in terms of the vehicle and occupant accelerations versus time. It may be seen that the occupant loads are within tolerable limits: 17 g peak, less than 8 g average. The Gadd severity index for this impact was 102. The stopping distance was approximately 15 ft. Figure 10 also shows data on pressures within the cushion and loads on the support structure.

Perhaps the most difficult demand on a highway energy absorber is the requirement that occupant response be tolerable regardless of vehicle mass. Hence, it is desirable

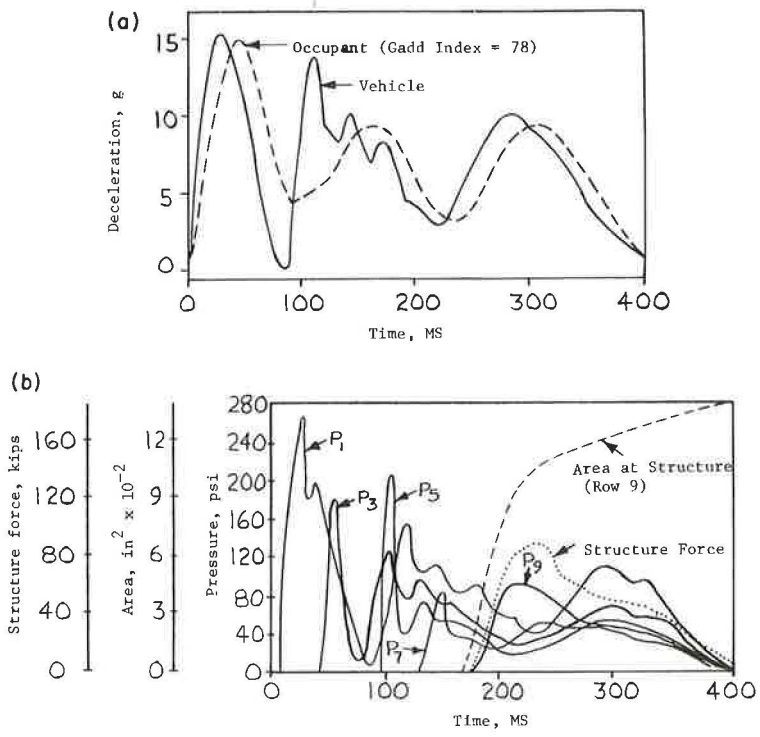

Figure 10. Predicted response for design point: (a) vehicle and occupant deceleration; and (b) pressures, area, and force.

to have a cushion that can somehow regulate its response to match the mass of the stopping vehicle. One way to do this is to provide low-energy and high-energy absorbers in tandem stages. This method may increase costs, however, by the inefficient use of stopping distance.

The simulated performance of the water-plastic cushion for the indicated spectrum of impact momentum is shown in Figures 11, 12, and 13 and given in Table 2. Occupant loads for 60-mph impacts are shown in Figure 11. Predicted peak occupant decelerations did not exceed 32 g for any case, and durations of peaks above 12 g were characteristically about 70 msec in the severe (light vehicle) cases. It may be noted that this violates the desired occupant protection criterion in some cases; however, occupant onset rates were less than 500 g/sec in all cases. The Gadd severity index ranged between 102 and 432 for the 60-mph simulated impacts compared to 113.5 for a 12-g rectangular pulse.

The ideal cushion is the one that gives a stopping force that is independent of mass. One comparison based on peak stopping forces is shown in Figure 12, where the peak force is shown as a function of the mass and velocity of the vehicle. Comparisons are drawn with simple linear-energy systems and the hypothetical constant-force system. The acceleration responses of the constant-force and linear cushions to vehicle mass (M) are approximately proportional to $1/M$ and $1/\sqrt{M}$ respectively. Thus for the constant-force cushion, a Volkswagen or Renault sedan would experience roughly double the deceleration of a Ford or Pontiac sedan. For the linear-spring cushion, it would experience about 1.4 times the heavier vehicle deceleration. As may be seen from the plotted points, the performance of the water-plastic cushion tends to follow that of an ideal linear spring; distributed mass and dissipative elements within the cushion provide a potential for mass-matching.

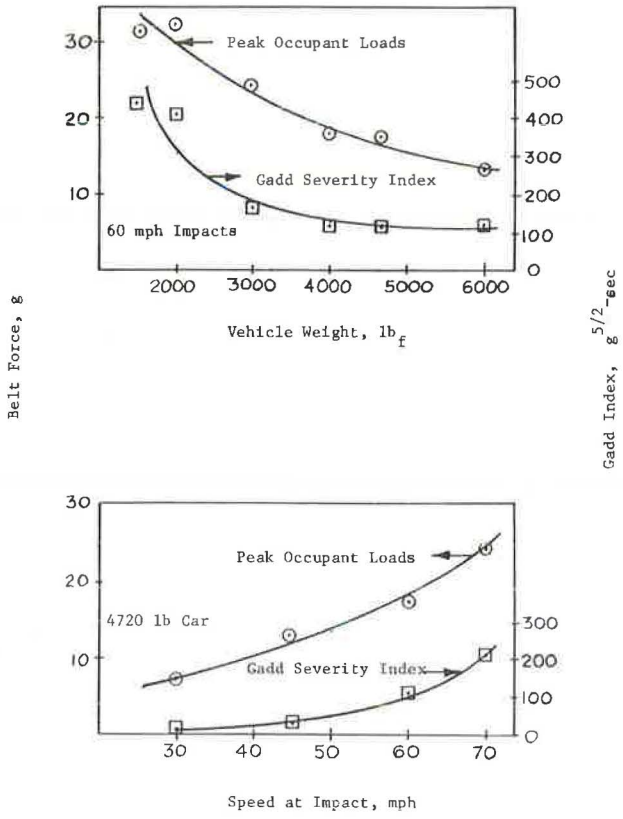

Figure 11. Occupant load and injury index predictions.

The lower part of Figure 12 shows the velocity sensitivity of the water-plastic cushion by comparison. The roughly linear velocity sensitivity causes the cushion to give a fairly uniform stopping distance.

The utilization of stopping distance is shown in Figure 13. Of course, the ideal case is that of uniform utilization, giving equally good response at all speeds and weights

TABLE 2

COMPARISON OF SIMULATED BEHAVIOR

Vehicle Mass (lb_m)	Initial Speed (mph)	Total Stopping Distance (in.)	Vehicle Crush (in.)	Vehicle Load				Occupant Load		Structure Load (kip)
				g		kip		Peak g	Gadd Index	
				Peak	Average	Peak	Average			
4,720	60	181	14	15.2	8.0	71.6	37.7	15	78.3	90
4,720	70	182	17	18.7	10.8	88	51	19	156	130
4,720	45	170	10	10.5	4.8	49.5	22.4	10	33	45
4,720	30	137	6.3	6.9	66	32.5	31	5	6	18
2,000	30	110	9.4	10	8.2	20	16.4	10	20	0
2,000	45	141	15.4	17	5.8	34	11.5	18	89	12
2,000	60	166	22	24.1	8.7	48.2	17.4	28	192	22
3,000	60	175	18	19.7	8.5	59	25.4	20	103	46
6,000	60	184	12	13	7.9	78	48	11	101	120
4,000	60	179	15	17	8.1	68	32.4	16	87	80
1,500	40	121	15	17	5.3	25.5	8.0	18	92	0
1,500	60	155	20	27.5	9.3	41.2	13.9	31	100	15

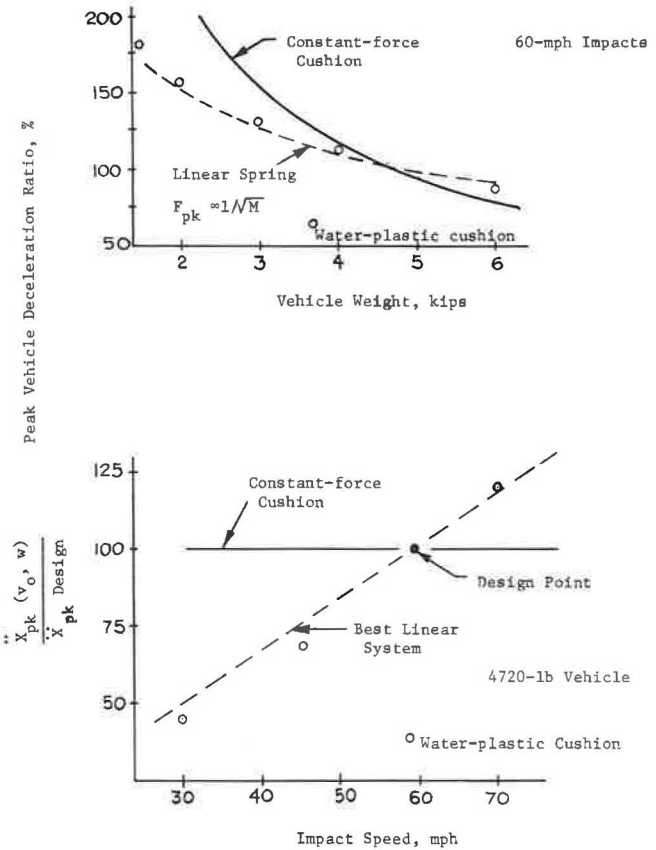

Figure 12. Peak deceleration ratio vs. vehicle weight and speed.

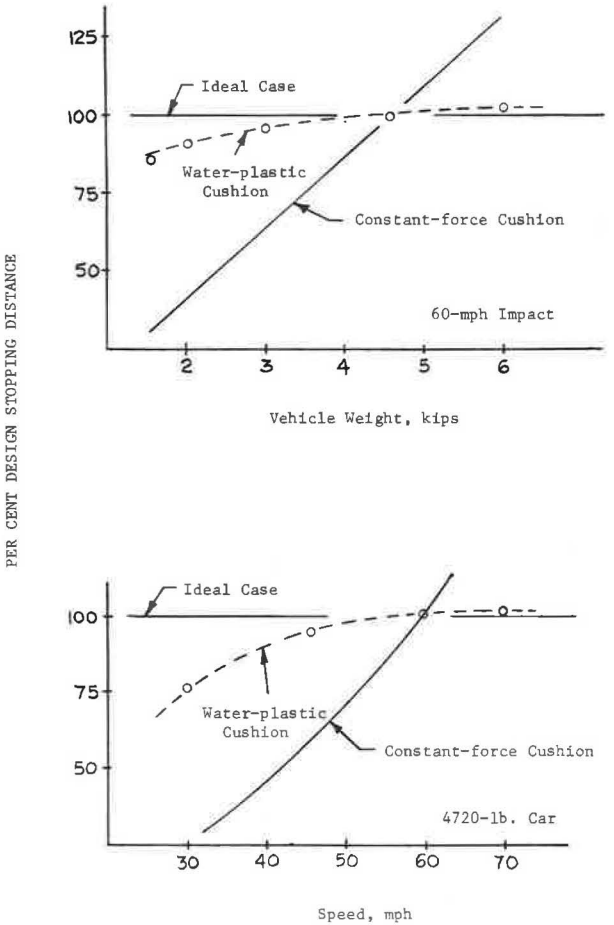

Figure 13. Stopping distance vs. weight and speed.

within the expected range. The water-plastic cushion gives an excellent performance, within ±8 percent of uniform space utilization over the entire mass range at 60 mph and only 25 percent reduction in effectiveness at half the design speed. The water-plastic cushion may be expected to provide good utilization of available stopping distance, producing resisting forces that compensate for vehicle mass and velocity. This attribute is particularly important for low-speed crashes, as the loads borne by the vehicle and occupants are considerably reduced from the constant-force case.

CONCLUSIONS

The mathematical model used for this study has been satisfactorily verified for head-on impacts by comparison with detailed full-scale crash results performed by several agencies. Behavior of the water-plastic cushion at the design condition provides an occupant response that is well within survivable limits.

An investigation of behavior for vehicle weights and velocities other than the design case shows that the water-plastic cushion provides survivable occupant responses over much of the range. This device is capable of a high degree of automatic self-adjustment, allowing it to satisfactorily match the resisting forces to the weight and speed of the impacting vehicle. Predicted stopping distances varied less than 10 percent for vehicle weights ranging from 2,000 to 6,000 lb and less than 25 percent for speeds ranging from 30 to 70 mph.

ACKNOWLEDGMENT

This paper is the result of research sponsored by the Federal Highway Administration, whose support is gratefully acknowledged. The opinions, findings, and conclusions expressed in this publication are those of the authors and not necessarily those of the Federal Highway Administration.

REFERENCES

1. Warner, C. Y., and Free, J. C. Development of a Hydraulic-Plastic Cushion for Impact-Energy Absorption. Brigham Young Univ., Provo, Utah, April 1, 1970, 131 pp.
2. Warner, C. Y. Hydraulic-Plastic Cushions for Attenuation of Roadside Barrier Impacts. Highway Research Record 259, 1969, pp. 24-34.
3. Emori, R. I. Analytical Approach to Automobile Collisions. Automotive Engineering Congress, Detroit, SAE Paper 680016, Jan. 8, 1968.
4. Hayes, G. G., Ivey, D. L., and Hirsch, T. J. Performance of the Hi-Dro Cushion Cell Barrier Vehicle-Impact Attenuator. Paper presented at the 50th Annual Meeting and included in this Record.
5. Kaufman, H., and Larson, D. B. Calculation of Deceleration Waveforms Using Optimal Control Theory. First Internat. Conf. on Vehicle Mechanics, Wayne State Univ., Detroit, 1967.
6. Rennecker, D. N. A Basic Study of Energy-Absorbing Vehicle Structure and Occupant Restraints by Mathematical Model. Automotive Safety Dynamic Modeling Symposium, SAE Conf. Proc., Anaheim, Calif., Oct. 1967.
7. Gadd, C. W. Use of a Weighted-Impulse Criterion for Estimating Injury Hazard. Proc. Tenth Stapp Car Crash Conf., SAE, New York, 1966.

PERFORMANCE OF THE HI-DRO CUSHION CELL BARRIER VEHICLE-IMPACT ATTENUATOR

Gordon G. Hayes, Don L. Ivey, and T. J. Hirsch, Texas Transportation Institute, Texas A&M University

The Hi-Dro Cushion Cell Barrier vehicle-impact attenuator consists basically of water-filled plastic tubes with orifices in the caps. A colliding vehicle forces the water out the orifices, thereby experiencing a restraining force that depends on orifice size and number, number of tubes being compressed, amount of water in the tubes, and other design considerations. Six full-scale crash tests were conducted to evaluate the effectiveness of the barrier as a vehicle-impact attenuator. The resulting test decelerations were substantially lower than those from a rigid wall test included for comparison purposes. Other full-scale tests have been conducted elsewhere. Data from a computer simulation model of the crash cushion developed at Brigham Young University showed excellent agreement with data from selected tests performed in this series.

•AS PART of its 4S program (Structural Systems in Support of Highway Safety), the Federal Highway Administration sponsored a series of vehicle crash tests to help evaluate the Hi-Dro Cushion Cell Barrier vehicle-impact attenuator. The testing was conducted in September, October, and November of 1969.

The impact attenuator has been analyzed and simulated by digital computer under another portion of the 4S program (1). This system is now handled by Energy Absorption Systems, Inc., of Chicago.

The crash cushion consists of an assembly of plastic, water-filled tubes with orifices in the caps. When the Hi-Dro Cushion Cell Barrier is struck by a vehicle, the water in the tubes is forced out the orifices. This reaction of individual tubes results in a predictable barrier deformation-force characteristic. Augmenting the vehicle-stopping force is the barrier inertia.

DESCRIPTION OF SYSTEM

The basic unit of the crash cushion is the Hi-Dro Cushion Cell, which is a hollow cylinder or envelope made of plastic material (Fig. 1). The cap contains orifices through which the water in the cell can be expelled. The stiffness of the cell is determined by the orifice areas. These cells were assembled as shown in Figure 2 for the first three tests.

The 138 cells were divided among eight "bays" separated by diaphragms as shown in Figure 2. The third bay from the front was void of cells due to design factors concerning the profile of the acceleration pulse produced during impact (1). The diaphragms separating the bays were made of 1½ in. fiberglass-coated plywood. The three diaphragms closest to the rigid barrier each had two ¼ in. steel plates attached. The rows of cells in each bay were separated by ¼ in. Duraply interior panels.

The fish-scale fender panels were designed to provide redirectional ability during angled impacts, while providing minimum interference during head-on crashes. These panels were hinged to the transverse diaphragms and were made of 1¼ in. fiberglass-coated plywood in the first three tests. The last three fender panels on the "off" side of the cushion were left off in order to avoid modification of the existing backup wall.

Sponsored by Committee on Traffic Safety Barriers and Sign, Signal and Lighting Supports and presented at the 50th Annual Meeting.

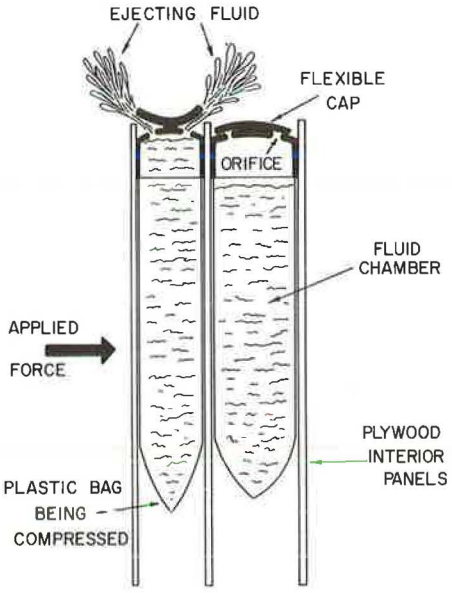

Figure 1. Function of Hi-Dro Cushion Cell.

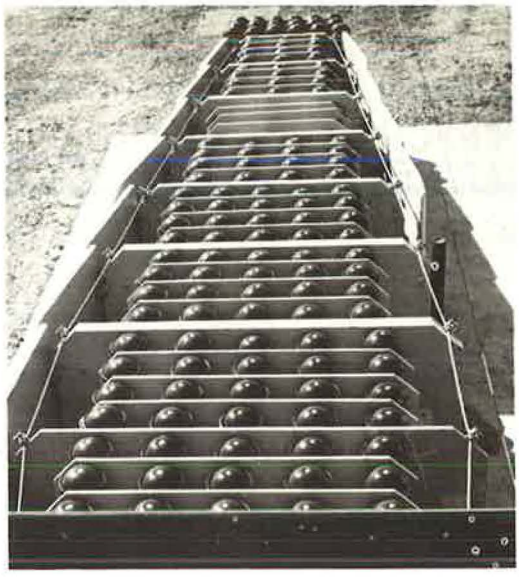

Figure 2. Top view of barrier.

In the final two tests, the five front fender panels on the impacted side were made of fiberglass-coated Hexcel, which is a lightweight, high-strength paper material resembling a honeycomb. In addition, the wood portions of the second and third diaphragms from the rear of the attenuator were removed and the 12-gage steel plate in the last diaphragm was eliminated in order to maintain the previous weight distribution after the modified fender panels had been installed. The $\frac{7}{8}$-in. diameter restraining cables were increased to 1 in., and the last diaphragm was increased in width to provide a constant diverging side slope.

TEST PROGRAM

The test conditions for the series are given in Table 1. For the angled tests, the impact point was approximately the rear edge of the first fender panel. The side of the unit diverged from the centerline by 6 deg 9 min, making an impact angle with the side of the cushion of about 26 deg.

Four accelerometers were used in each test vehicle, two on each longitudinal frame member. For head-on tests, all were mounted longitudinally, while in the angled tests, one on each side was mounted transversely. In addition, a mechanical Impactograph was mounted in the vehicle trunk as a secondary source of acceleration data.

TABLE 1

TEST CONDITIONS

Test	Vehicle	Weight (lb)	Initial Speed (mph)	Initial Angle With Barrier Centerline (deg)	Propulsion
A	1964 VW sedan	1,820	42	0	Self-powered
B	1961 Pontiac sedan	4,650	64	0	Self-powered
C	1963 Pontiac sedan	4,410	54	20	Self-powered
D	1962 Renault sedan	1,680	59	0	Towed
E	1964 Dodge sedan	3,710	59	20	Self-powered

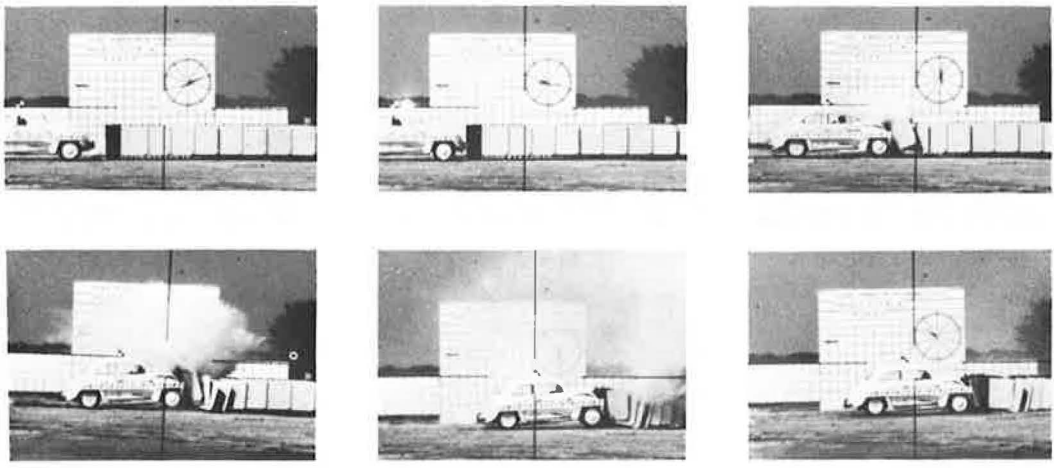

Figure 3. Sequential photographs of Test A.

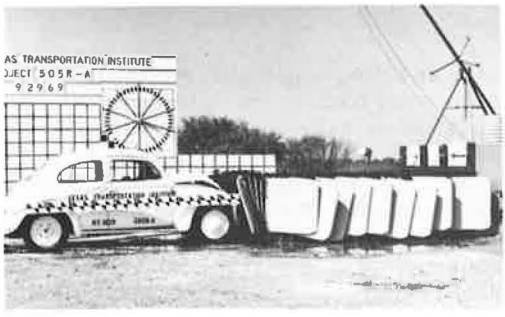

Figure 4. Vehicle and barrier after Test A.

An Alderson anthropometric dummy simulated a driver and was secured by a seat belt attached to a load cell for measuring seat-belt force. Redlakes Hycam cameras, operating at 500 frames per second, recorded the events for time-displacement analysis. A Photosonics camera (500 frames per second) was mounted over the barrier looking vertically downward. Much of the event was obscured in this view by the ejected water. Other cameras covered each test for documentary purposes.

The initial velocity and stopping distance, or distance in contact, can be measured accurately from the high-speed films, and an average deceleration can be calculated from these values. This average deceleration can be compared with that from the electromechanical accelerometers, which also indicate peak g.

DESCRIPTION OF TESTS

Table 2 gives the pertinent test data. In the first test, a Volkswagen sedan weighing 1,820 lb impacted the barrier head-on at 42 mph. The vehicle was stopped in 13.2 ft with an average deceleration of 4.5 g and a peak deceleration of 14.6 g. The vehicle damage was not severe (Figs. 3 and 4).

The second test used a Pontiac sedan weighing 4,650 lb that impacted head-on at an initial speed of 64 mph. The average deceleration over 17.3 ft and 0.34 sec was 7.9 g, while the maximum deceleration of 13.4 g was lower than that of the first test (Figs. 5 and 6).

In the third test, a Pontiac sedan weighing 4,410 lb struck the cushion at 54 mph and at an angle of 20 deg with the barrier centerline. The vehicle had begun to redirect and had rotated approximately 5 deg when the main restraining cables pulled out of their front anchorage connections. The left front of the vehicle went head-on into the rigid barrier, and the vehicle rolled over on its right side (Figs. 7 and 8).

The cables pulled out of their connectors due to an improper installation procedure. A lead filler was used instead of a more desirable babbitt metal. All cushion units in

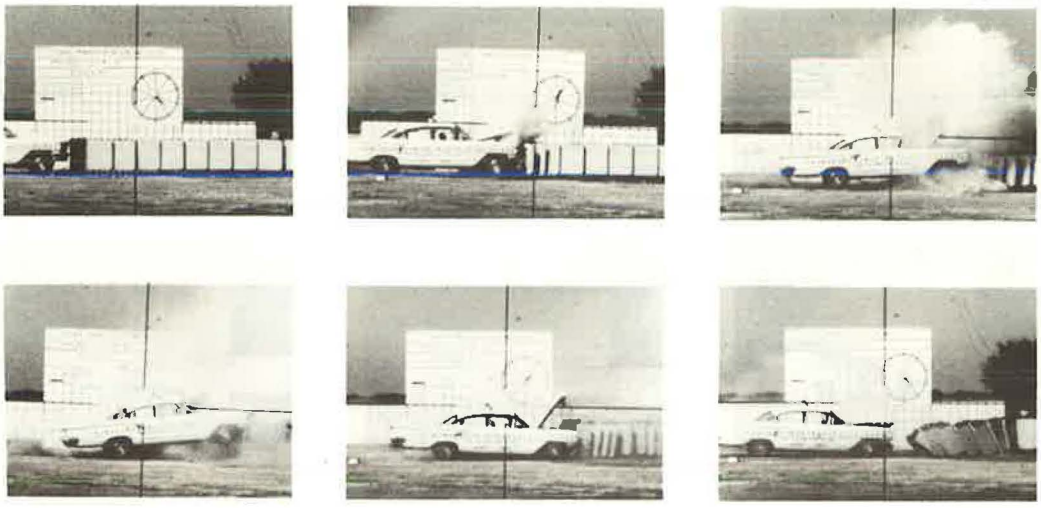

Figure 5. Sequential photographs of Test B.

Figure 6. Vehicle after Test B.

service are equipped with factory-fabricated cables and connectors. Because of this installation error, this test cannot be judged to be representative of the performance of the barrier. In spite of this, the films showed a very tolerable average deceleration of 5.8 g over 16.7 ft and 0.34 sec, while the accelerometers detected a peak of only 14.6 g.

Before the fourth test, the modifications mentioned earlier were made. The vehicle was powered by a towing system that disengaged from the vehicle before impact. In this test a 1,680-lb Renault was directed head-on into the cushion at 59 mph. The stopping distance of 16.3 ft gave an average deceleration of 7.1 g (over 0.58 sec), and the maximum deceleration was 15.6 g.

The vehicle apparently struck the front of the barrier about 1 ft off-center and started a yaw and roll motion, finally rolling over on its top after most of the kinetic energy had been absorbed (Figs. 9 and 10).

The final test was another 20 deg impact. A 3,710-lb Dodge sedan traveling at 59 mph was used. This was the only test in which the vehicle left the barrier with significant speed. The average longitudinal deceleration of 4.9 g was calculated over the distance in contact of 19.4 ft by noting the speeds at the beginning and end of this contact. The maximum deceleration was 8.9 g. Figure 11 shows the vehicle after the test.

In this last test, the vehicle began to ramp or climb up the side of the barrier. It became completely airborne by as much as 1.5 ft for about 20 ft and, upon recontacting the ground, rolled over on its left side before coming to rest upright. Examination of vehicle and barrier indicates that a slight contact was made with the upper corner of the rigid steel wall. The path of the vehicle contact up the side panels is shown in Figure 12.

The steel barrier in front of the concrete wall was pulled away from the concrete about 6 in. at the bottom and about 2 in. at the top. The restraining cables were fastened to this steel barrier so this could allow as much as 2 ft of additional localized lateral movement to the cushion.

Figure 7. Sequential photographs of Test C.

Figure 8. Vehicle after Test C.

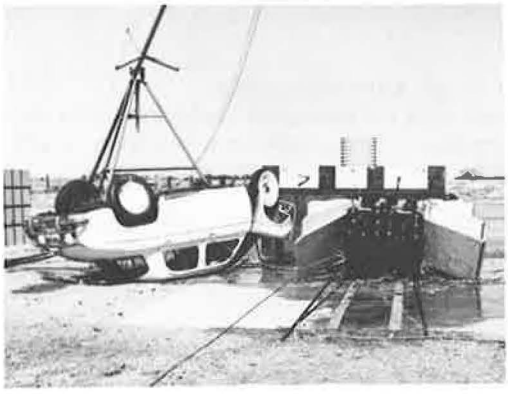

Figure 9. Vehicle and barrier after Test D.

Figure 10. Vehicle after Test D (righted).

Figure 11. Vehicle after Test E.

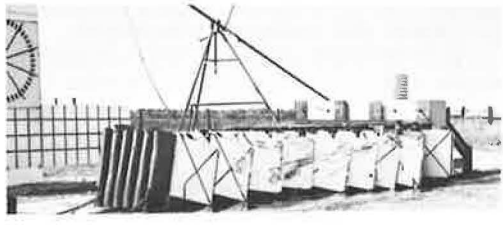

Figure 12. Barrier after Test E.

TABLE 2

SUMMARY OF DATA

Factor	Test					
	A	B	C	D	E	Rigid Wall
Vehicle weight, lb	1,820	4,650	4,410	1,680	3,710	3,270
Angle of impact, deg	0	0	20	0	20	0
Film data						
Initial speed, mph	42	64	54	59	59	53
Initial speed, fps	61.6	93.6	79.3	86.3	86.6	78.3
Average longitudinal deceleration, g	4.5	7.9	5.8	7.1	4.9	25.0
Stopping distance, ft	13.2	17.3	16.7	16.3	19.4[a]	3.8
Time in contact, sec	0.74	0.34	0.34	0.58	0.34	0.10
Longitudinal accelerometer data						
Maximum deceleration, g	14.6	13.4	14.6	15.6	8.9	35.0
Average deceleration, g	3.1	6.8	5.6	7.3	4.6	18.0
Time, sec	0.46	0.47	0.42	0.29	0.33	0.13
Transverse accelerometer data						
Maximum deceleration, g	—	—	5.7	—	9[b]	—
Average deceleration, g	—	—	1.1	—	2	—
Time, sec	—	—	0.42	—	0.33	—
Attenuation index[c]						
$AI_{(max)} = \frac{G_{max}\ (test)}{G_{max}\ (rigid\ wall)}$	0.4	0.2	0.3	0.3	0.2	0.7
$AI_{(avg)} = \frac{G_{avg}\ (test)}{G_{avg}\ (rigid\ wall)}$	0.2	0.2	0.2	0.2	0.1	0.7
Vehicle deformation, ft	1.04	1.83	3.33	2.33	0.83	3.82

[a]Distance in contact.
[b]From Impactograph (accelerometers malfunctioned).
[c]G (maximum rigid) = 0.9V, G (average rigid) = 0.574V, V in mph (2).

Pertinent data from a rigid wall test (3) conducted in March of 1969 are given in Table 2 and shown in Figure 13 for comparison purposes. This vehicle was a 1963 Plymouth sedan weighing 3,270 that was directed head-on into a rigid concrete wall at 53 mph. The vehicle stopped in 3.8 ft (vehicle deformation) with an average deceleration of 25 g and a peak deceleration of 35 g.

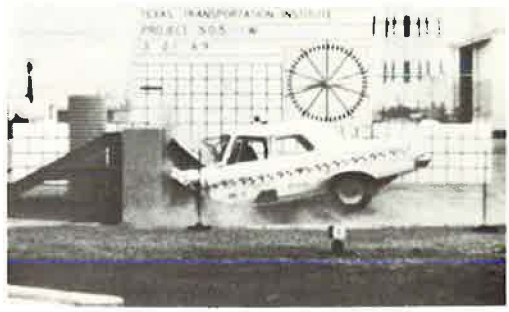

Figure 13. Rigid wall crash test.

The damage to the cushion in the head-on tests was relatively minor, usually in the form of torn plastic cells that were easily replaced. The following listing of parts replaced gives an idea of the severity of damage to the barrier in each test:

Test A—No parts were replaced.
Test B—25 cartridges were replaced, 19 of which were repairable.
Test C—Failure of anchorages caused damage that necessitated replacement of several fender panels, diaphragms, and interior panels. (Some replacements were made in the course of the previously mentioned modification of the barrier structure.)
Test D—No parts were replaced.
Test E—Damage occurred to fender panels only. No replacements were made because no further tests were planned.

FIELD EXPERIENCE

One severe collision with a Hi-Dro Cushion Cell Barrier located in New Orleans, Louisiana, has been reported recently (4). On April 2, 1970, a vehicle skidded sideways into the barrier on rain-slick pavement at an estimated speed of 70 mph. The driver's side of the vehicle impacted the barrier nose. The driver, who was unre-

strained, suffered cuts and bruises but was treated and released. The vehicle was towed to a garage, and then driven inside. The authors of the report feel that the collision would have undoubtedly been fatal if the impact attenuator had not been there.

DISCUSSION OF RESULTS

Table 2 gives a comparison of attenuation indexes, which are defined as the ratios of decelerations experienced in the cushioned impacts to those calculated for rigid barrier impacts. The values experienced in a rigid wall crash will depend in part on the crush characteristics of the impacting vehicle. For this reason the index for the rigid wall test is not unity. The more attenuation caused by the inclusion of a crash cushion, the smaller will be the attenuation index.

The predictions of the mathematical model developed at Brigham Young University showed very good agreement with the test data for the head-on tests (1). No predictions were made for the angled tests.

Great design flexibility is possible by varying orifice size and number, arrangement of cells, size of cells used, and amount of fluid in the cells.

The 4S program of the Federal Highway Administration uses the following criteria for development and testing of protective barriers (5):

Vehicle weight range—2,000 to 4,500 lb.
Vehicle speed—60 mph.
Impact angle—Up to 25 deg as measured from the direction of the roadway.
Average permissible vehicle deceleration—12 g maximum while preventing actual impacting or penetration of the roadside hazard.
Maximum occupant deceleration onset rate—500 g per sec.

The observed average deceleration levels were significantly below the 12-g level in all tests. The accelerometer traces showed that the 12-g level was exceeded by peak decelerations no longer than 0.03 sec except in Test D, which was a head-on test of a vehicle weighing less than the minimum weight specifications.

Other tests on this type of barrier have been conducted by Rich Enterprises, the California Division of Highways, and Brigham Young University. The results of these tests have, in general, shown acceptable performance of this vehicle-impact attenuator.

ACKNOWLEDGMENTS

This study was conducted by the Texas Transportation Institute under an interagency contract with the Federal Highway Administration and is part of the research program entitled "Structural Systems in Support of Highway Safety" (4S program) in the Office of Research and Development, Structures and Applied Mechanics Division. F. J. Tamanini is the Project Manager for the Federal Highway Administration. The work was carried out by personnel of the Highway Safety Research Center and the Structures Division of the Texas Transportation Institute.

The opinions, findings, and conclusions expressed in this publication are those of the authors and not necessarily those of the Federal Highway Administration.

REFERENCES

1. Warner, C. Y., and Free, J. C. Water-Plastic Crash Attenuation System: Test Performance and Model Prediction. Paper presented at the 50th Annual Meeting and included in this Record.
2. Emori, R. I. Analytical Approach to Automobile Collisions. Automotive Engineering Congress, Detroit, SAE Paper 680016, Jan. 1968.
3. Ivey, D. L., Buth, E., and Hirsch, T. J. Feasibility of Lightweight Cellular Concrete Vehicle Crash Cushion. Texas Transportation Institute, Tech. Memo. 505-9, Jan. 1970.
4. Walters, W. C., and Bokun, S. G. Performance Report of the HIDRO Cushion Crash Attenuation Devices. Louisiana Dept. of Highways, Highway Research Report, June 1970.
5. Tamanini, F. J., and Viner, J. G. Structural Systems in Support of Highway Safety. ASCE, Meeting Preprint 930, July 1969.

DYNAMIC TESTS OF AN ENERGY-ABSORBING BARRIER EMPLOYING WATER-FILLED CELLS

Eric F. Nordlin, James H. Woodstrom, and Robert N. Doty,
California Division of Highways

The results of four full-scale vehicle-impact tests into energy-absorbing barriers using water-filled plastic cells and cartridges are reported. This barrier absorbs the energy of an impacting vehicle through the movement of water horizontally as the barrier is shortened and vertically through orifices as the flexible water cells and cartridges are compressed. The recorded vehicle passenger-compartment decelerations indicated that, although unrestrained occupants would sustain moderate to severe injuries, in most cases, during 60-mph collisions with this barrier design, fully restrained (seat belt and shoulder harness) occupants would sustain little or no injuries during the majority of 60-mph impacts into the nose or side of the barrier. In addition, the barrier did not generate unstable vehicle behavior and, in conjunction with the bridge approach guardrail backstop, effectively redirected a vehicle impacting from the side. The overall barrier performance showed significant improvement over the concrete wedge-shaped deflectors currently in use in California on off-ramp gores.

•ACCIDENTS where vehicles ran off the road accounted for approximately 50 percent of the fatalities on the California freeway system during 1967 and 1968. More than 50 percent of the fatalities resulting from this type of accident involved collisions with fixed objects such as bridge abutments, bridge rail end posts, and large sign supports. Consequently, the California Division of Highways is now striving to provide a 30-ft wide recovery area alongside the traveled way free of unprotected fixed objects.

Providing protection for those fixed objects that cannot be removed or made "breakaway" has often been very difficult. One of the problems for which no satisfactory solution has been developed is providing protection from hazardous fixed objects located in the gore area at freeway off-ramps. Thus, the California Division of Highways has been involved in a research program for the last 2 years to develop energy-absorbing barriers for use in gore areas.

During 1967, 40 full-scale vehicle-impact tests of barriers incorporating water-filled cells were conducted and reported by Brigham Young University researchers (1). Based on the results of these tests and a few earlier unpublished tests by the original developer of this concept (John Rich Enterprises of Sacramento), the California Division of Highways undertook in 1968 a series of eight full-scale impact tests of barriers incorporating the water-filled cell concept. The results of the four tests of the second-generation barrier are reported here. The results of the four tests on the much less satisfactory first-generation barrier can be found elsewhere (2).

The California Division of Highways has also tested two other types of energy-absorbing barriers. The barriers utilized (a) 55-gal steel drums and (b) plastic drums containing sand. The results of the three tests of barriers using steel drums can be found elsewhere (3). The tests of the barrier using sand will be reported during the spring of 1971.

Sponsored by Committee on Traffic Safety Barriers and Sign, Signal and Lighting Supports and presented at the 50th Annual Meeting.

OBJECTIVES

The primary objectives of this research were as follows:

1. Test the ability of a barrier incorporating water-filled plastic cells to decelerate a 4,700-lb vehicle impacting at speeds up to 60 mph such that (a) the maximum average 40-millisecond (msec) deceleration sustained by the vehicle passenger compartment is no more than 12 g, and (b) the vehicle does not ramp, roll, or spin out in a manner that will result in additional damage to it, injury to its occupants, or hazards to oncoming traffic because of its final position.
2. Generate barrier modifications dictated by the barrier behavior during the tests to decrease the decelerations sustained by the vehicle, minimize the amount of barrier debris created during a collision, and minimize the on-site repairs that would be required to return the barrier to service.

DESCRIPTION OF TEST PROCEDURE

All four tests were conducted on a section of runway at an airport near Lincoln, California. The vehicles used for this series of tests were 1968 Dodge sedans weighing about 4,700 lb, including dummies and instrumentation, that impacted the barrier on the nose and side at speeds near 60 mph. Control of the vehicles was accomplished by a remote operator following 200 ft behind the test vehicle in a car equipped with a tone transmission system. A "trip line" placed in the vehicle path cut off the ignition just prior to impact. A study by Nordlin, Woodstrom, and Hackett (4) contains a description of this control equipment.

The test barriers were 19 ft 6 in. long and incorporated rows of flexible water-filled plastic cartridges placed between plywood panels oriented perpendicular to the barrier axis. Fiberglass-coated plywood diaphragms were used for every fourth panel. Overlapping fiberglass-coated plywood fender panels were attached to each end of each diaphragm so that they would telescope during head-on impacts but redirect a vehicle if oblique-angle impacts occurred. Lateral restraint was provided by two $\frac{7}{8}$-in. diameter main cables plus two $\frac{3}{8}$-in. diameter secondary cables.

All the tests were recorded with high-speed (250 to 400 frames per second), motor-driven Photosonic cameras that were manually actuated from a central control console. These cameras were located on both sides of the barrier and on a 30-ft light standard directly above the point of impact. Another Photosonic camera was located in the vehicle passenger compartment to film the movement of the dummies. This camera was started by means of a pin-actuated switch mounted on the rear bumper of the test vehicle.

A motor-driven Hulcher camera with a speed of approximately 20 frames per second was located on scaffolding and provided documentary coverage of the tests. High-speed and normal-speed cameras were hand-panned through impact. Still photographs, slides, and documentary movies of the test barrier and vehicle were also taken.

TEST RESULTS

The barrier used and its modifications are described in the following sections for each of the four tests reported. The primary variables were the impact speeds of the vehicles and the angles and locations of impact into the barrier. Table 1 gives these impact conditions.

TABLE 1

TEST PARAMETERS

Test No.	Impact Speed (mph)	Location on Barrier of Impact	Angle With Barrier Axis of Impact
215	57.5	Nose	Head-on
216	61.8	Nose	Head-on
217	57.0	Side[a]	9 deg
218	59.2	Nose	8 deg

[a] 13 ft behind the nose.

The decelerations included in the descriptions of each test are averages of the highest average decelerations sustained by the vehicle passenger compartment or the dummy over a 50-msec period unless otherwise noted. These measurements were taken using Statham strain-gage accelerometers mounted on the vehicle floor and on the back of the dummy. The decel-

eration curves are given in another study by the authors (2). A discussion of the processing and interpretation of these types of data is included elsewhere (3).

The effect of the measured vehicular decelerations was interpreted using the tolerance limits given in Table 2. Injury severity predictions are related only to the direction of deceleration that appears to be most critical (i.e., no vectorial addition of deceleration was accomplished). A discussion of deceleration tolerances and the reasoning behind the choice of these values is given elsewhere (4). These limits define what would be, in the opinion of the authors, a survivable environment under almost all circumstances.

TABLE 2

DECELERATION LIMITS

Occupant Restraint	Lateral	Longitudinal	Total
Unrestrained	3	5	6
Seat belt	5	10	12
Seat belt and shoulder harness	15	25	25

Note: Measured in g in passenger compartment—highest 50 msec average.

Test 215

Barrier Description—The overall dimensions of the test barrier used in test 215 were a 19-ft 6-in. length, a 3-ft width at the nose, and a 7-ft width at the back of the barrier (Fig. 1). The basic module of the barrier consisted of four rows of cells contained by 1½-in. fiberglass-coated plywood diaphragms; there were eight modules in the barrier plus a cluster of cells at the nose. Between diaphragms, the rows of cells were separated by a ½-in. interior panel of Duraply plywood. There were three to five water-filled cartridges in each row (Fig. 2). Along the sides of the barrier, fender panels of 1¼ in. fiberglass-coated plywood were hinged to each diaphragm at the nosewards side of the panel (Fig. 3). The length of these fender panels was such that they overlapped. Thus, backward movement (compression) of the barrier was not hindered. The back sides of the fender panels were attached with springs to the next rearward diaphragm. Fiberglass was used to provide not only additional strength but also a low-friction surface between the fender panels and the impacting vehicle. These fender panels were developed for the purpose of redirecting vehicles that impacted the side of the barrier without permitting pocketing into the barrier.

The cartridges used in the eight modules (126 total) were made of a thin vinyl-coated nylon fabric and were 24, 30, and 36 in. long (Figs. 3 and 4). Their outside diameter was 5½ in. These cartridges were slipped through ¼-in. thick vinyl supporting rings that were fastened to the interior panels or diaphragms. The water-filled cells used in the nose of the barrier (18 total) were 6 in. in diameter, 41 in. long, and consisted of ¼-in. thick vinyl walls.

The nose cells and the cartridges both had solid vinyl evaporation caps permanently attached with aluminum pop rivets. All the cartridges were filled with water, but only 6 of the 18 nose cells contained water.

Figure 1.

Figure 2.

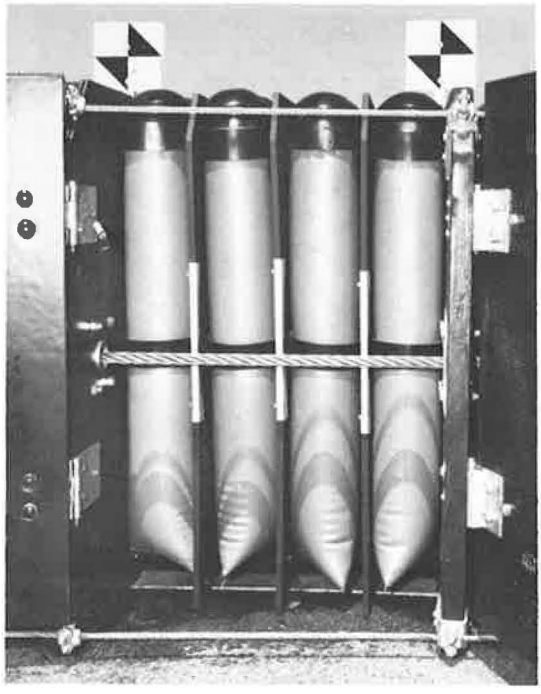

Figure 3.

Figure 4.

The third module back from the nose of the barrier contained no cells or cartridges. The developers advised the use of this empty, or void, space for better dynamic response of the barrier (6). The theoretical effect of the void bay is shown in Figure 20 of the Appendix.

Wire ropes were used to stabilize the entire barrier. Two parallel $\frac{7}{8}$-in. preformed galvanized 6 by 19 wire ropes with independent wire cores extended from steel plates attached to a concrete anchor block in front of the barrier nose back through fabricated steel guides in the diaphragms to the backup bridge rail at the rear of the barrier. These cables were designed to give the barrier lateral and vertical stability and limit pocketing during side-angle impacts. Two secondary cables of $\frac{3}{8}$-in. wire rope were used to stabilize the barrier nose during a side-angle impact (Fig. 5). They were attached to the anchor block and the first diaphragm; each cable anchor attachment included a pin that would shear when subjected to a 4,000-lb load. After the barrier had been

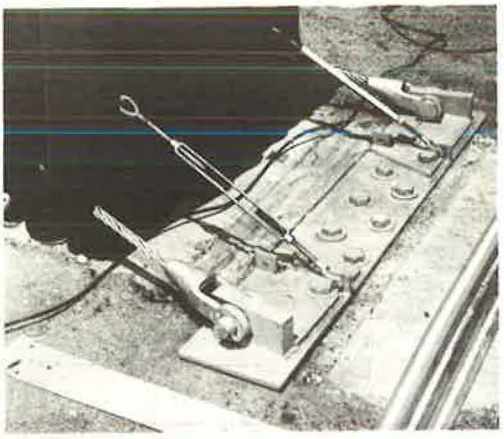

Figure 5.

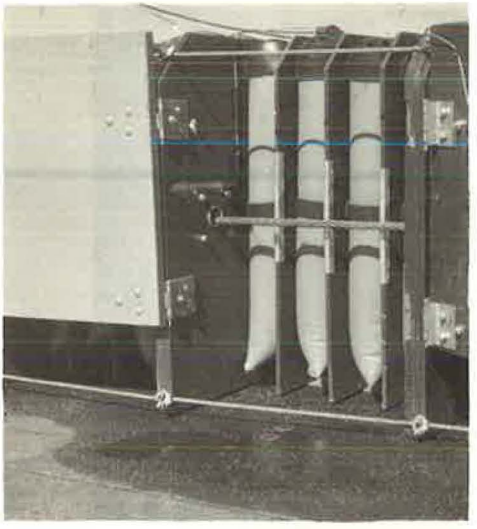

Figure 6.

compressed due to an impact, ⅜-in. wire ropes were used to stretch out the barrier and reposition it. These wire ropes were attached to the upper and lower corners of each end of each diaphragm (Fig. 6).

Diaphragms 6 and 7 contained two ¼-in. steel plates in addition to the 1½-in. fiberglass-coated plywood. Diaphragm 8 consisted of two ¼-in. steel panels and one 12-gage steel sheet. This additional weight was also suggested by the developer to improve the barrier's dynamic response (6).

The test barrier required a rigid backup structure. Thus, a bridge approach guardrail nose structure typical of a gore installation was constructed. In addition, a fabricated steel plate backup panel was attached to the nose of the bridge rail to provide a large bearing area for the barrier during impact (Fig. 7). (See Figs. 21 and 22 in the Appendix for additional barrier details.)

Results of Test 215—Figure 23 in the Appendix shows a summary of the test results. The 1968 Dodge impacted the barrier head-on at a speed of 57.5 mph. As rearward displacement of the barrier began, the fender panels rotated downward so that their lower rear corners penetrated into the asphalt concrete runway and restricted barrier compression. This, plus an 18-in. vehicle offset at impact, resulted in a lifting, rolling motion being imparted to the test vehicle. The vehicle traversed a 360-deg roll off to the right side of the barrier and came to rest several feet behind and to the right of the barrier (Fig. 8). Front-end crush varied from 0 to 20 in.; maximum crush was on the left side (Appendix Fig. 24). The top caved in, the windshield was broken, the left-

Figure 7.

Figure 8.

rear wheel was bent, the left-rear door was jammed, and there were scrapes over much of the surface of the vehicle.

The barrier itself remained intact (Fig. 9). However, some damage was sustained as many of the fender panels were scarred, and most were damaged on the rear-bottom corners where they were thrust into the ground as the barrier was compressed (Fig. 10). The edges of several diaphragms were broken or showed delamination of the plywood; hinges between fender panels and diaphragms were bent or broken in several locations. Damage was less severe toward the rear of the barrier. There was no damage to the steel backup structure. Static barrier displacement was 9.3 ft.

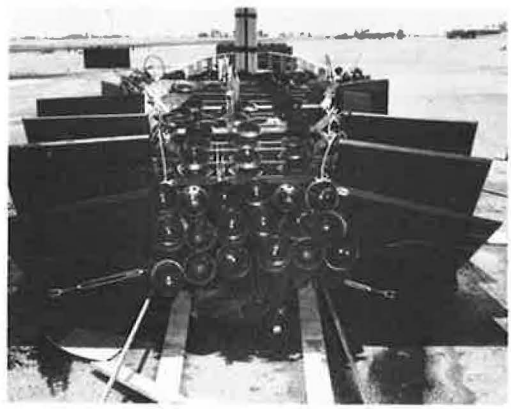

Figure 9.

Data From Instrumentation—An instrumentation system on loan from the Federal Highway Administration was used for test 215 and the succeeding tests (7). This system (the Wyle system) consisted of seven channels of FM telemetry for use on the barrier. The system included seven accelerometers and two seat-belt force transducers and all the necessary signal-conditioning equipment for their use. The dynamic data from these transducers were recorded on a 14-channel analog magnetic tape recorder.

In addition to the FHWA system, there were six channels of data transmitted through a Visicorder oscillograph. However, this did not produce usable results. The data included results from load cells on the two $\frac{7}{8}$-in. cables and four pressure transducers in selected cartridges. (See Figs. 25 and 26 in the Appendix for the locations of the instrumentation.)

The maximum compressive stress in the bridge approach guardrail tubular members was 4,500 psi. Maximum seat-belt load for the dummy driver was 513 lb; maximum load on the dummy's chest was 470 lb.

The peak vehicular decelerations were 10 to 12 g in the longitudinal direction. The highest 50-msec average vehicle deceleration (longitudinal) was 7.0 g (average of two accelerometers). Thus, in most cases unrestrained vehicle occupants would have sustained minor to moderate injuries under this longitudinal deceleration; restrained occupants would probably have sustained little or no injuries. The peak longitudinal deceleration for the dummy was more than 25 g; the lateral and vertical decelerations were 10 to 12 g. These decelerations were sustained for relatively short 5-msec periods.

Figure 10.

Test 216

Barrier Description—In test 216, the barrier used for test 215 was modified by cutting off the lower 6 in. of all the fender panels and cutting the lower rear corner of the panels on a diagonal to eliminate penetration of these trailing corners into the runway, as had occurred during test 215 (Figs. 11 and 12). Also, metallic shoes (or skids) were added to the lower edge of interior panels, heavier hinges were used to attach the fender panels to the diaphragms, and all the evaporation flaps were removed to lessen, at least to some extent, the lateral discharge of the water and danger of loss of telemetry signal.

Figure 11.

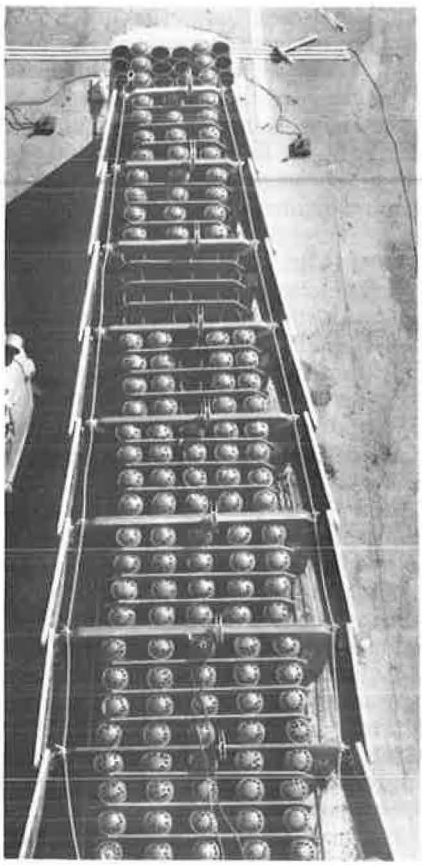

Figure 12.

Results of Test 216—Figure 27 in the Appendix contains a summary of the test results. A 4,690-lb 1968 Dodge impacted the barrier head-on at a speed of 61.8 mph. Deceleration of the impacting vehicle was relatively smooth and the vehicle remained stable. Vehicle rise was a little more than 1 ft.

The maximum crush of the vehicle forestructure was 20 in.; it occurred at the center of the vehicle (Fig. 13; Appendix Fig. 24). Buckling of the car body was indicated by a crimp in the roof over the door post on both sides of the car. The engine deflected the firewall back 1 to 2 in. Steering wheel deformation was 1¼ in. The steering column collapsed 2.9 in.

Fender panels on the left side of the first three modules were scarred. The bottoms or top inserts or both were blown out of 16 cartridges. The barrier moved straight back with negligible lateral movement or buckling. Maximum vehicular displacement of the barrier was 16.3 ft, but the at-rest displacement of the barrier nose was only 10.7 ft (Fig. 14).

Figure 13.

Figure 14.

Data From Instrumentation—Instrumentation was nearly identical to that used for test 215 (Appendix Figs. 25 and 26).

The maximum pressure transducer reading from the cartridges was 110 psi. The maximum loads on the two $\frac{7}{8}$-in. wire ropes were 14,750 lb on the left and 18,750 lb on the right. The bridge-approach guardrail experienced compressive stresses from 3,060 psi on the bottom left to 12,200 psi on the top left. Seat-belt loads up to 533 lb were measured for the dummy driver along with a maximum chest load of 530 lb.

The vehicle longitudinal deceleration included three distinct 5 to 10 msec peaks. The highest 50-msec average vehicle deceleration (longitudinal) was 9.8 g. Thus, moderate to severe injuries would be sustained by unrestrained vehicle occupants in most cases. Little or no injury would be sustained by restrained vehicle occupants. These magnitudes and the general shape of the curve are in excellent agreement with those reported by the Texas Transportation Institute for a 64-mph, head-on impact of a 4,650-lb vehicle (8).

The longitudinal dummy trace had a shape very similar to that for the vehicle except that the peaks were higher (above 14 g for 5 to 10 msec). The first dummy peak occurred about 25 msec after the first vehicle peak, but the later peaks occurred at about the same time, presumably after the dummy was positioned against the seat belt or vehicle interior. The lateral vehicle trace was somewhat erratic; however, it appears as though the peaks coincide with the longitudinal vehicle peaks. The vertical dummy trace was similar in shape to the longitudinal dummy trace but with mostly lower peaks (8 to 12 g). This reflects the probability that the main motion of the dummy had strong components in both the vertical and longitudinal direction as it was decelerated along a diagonal path.

Test 217

Results of Test—The barrier used in test 217 was the same as that used for test 216. Figure 28 in the Appendix shows a summary of the test results. A 4,760-lb 1968 Dodge impacted along the side of the barrier 13 ft behind the barrier nose at a speed of 57.0 mph and an angle of 9 deg. After the vehicle struck the barrier, it was slightly redirected by the barrier fender panels. However, significant redirection was not achieved until the solid resistance of the bridge approach guardrail was utilized. There was virtually no rise of the vehicle forestructure. The right-front side of the car was severely crushed; there was no crush on the left side (Fig. 15; Appendix Fig. 24). The right-front door was jammed and the right doorpost was partially torn loose at the roof connection. The right side of the hood cracked the windshield. Near the end of the collision, the right-rear quarter panel of the car slapped the barrier. This damaged the right-rear fender and the right end of the rear bumper. A crimp in the roof over the doorposts was sustained on both sides of the car; the radiator was buckled back toward the engine on the right side. The steering wheel had a slight deformation, but the steering column did not collapse.

Figure 15.

Several fender panels were torn off the barrier on the left side, mainly because of hinge failures. Two panels were thrown 8 ft beyond the final position of the car and two panels were lodged in the crushed front end of the car. The five cells on the left side of the bridge approach guardrail were all torn off and scattered along the path of the car. Shear pins in the secondary cables sheared off. Permanent displacement of the barrier nose was 1.5 ft (Figs. 16 and 17).

Data From Instrumentation—The instrumentation consisted of the FHWA system plus six extra channels recorded directly on the Visicorder oscillograph. (See Figs. 29 and 30 in the Appendix for the type and location of this instrumentation.)

Figure 16.

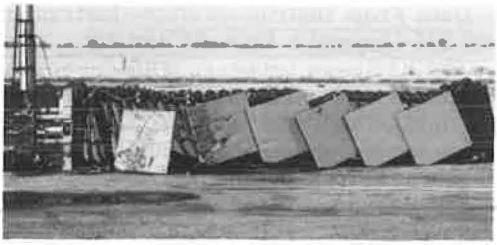

Figure 17.

The maximum pressure transducer reading was 50 psi. The maximum loads on the two ⅞-in. cables were 14,300 lb on the left and 11,500 lb on the right. The bridge approach guardrails sustained compressive stresses from 3,540 psi on the top right to 9,850 psi on the bottom left.

Two accelerometer traces were produced in test 217 for both the longitudinal and lateral motions of the vehicle (4 total) and were filtered at 100 Hz. The two longitudinal traces were very similar with thin peaks above 15 g. The highest 50-msec average passenger-compartment deceleration was 8.4 g (average of two accelerometers). The two lateral traces were also similar. The highest 50-msec passenger-compartment average (average of two accelerometers) was 5.2 g. Thus, unrestrained vehicular occupants would have sustained moderate to severe injuries in most cases. If restraints were used, no more than moderate injury would usually occur. The lateral traces were similar in shape to the longitudinal ones. The highest peaks (9 g for 5 msec) occurred on all four traces at about 190 msec after impact. At 430 msec after impact, all four records showed evidence of a deceleration pulse caused by the rear of the car slapping the barrier.

The filtered traces for the longitudinal and lateral dummy motions appeared to be distorted by the noise; they showed large, somewhat erratic peaks.

Test 218

Test Results—The barrier used in test 218 was the same as that used for tests 216 and 217. Figure 31 in the Appendix shows a summary of the test results. A 4,760-lb 1968 Dodge impacted the nose of the barrier at an angle of 8 deg and a speed of 59.2 mph. The vehicle struck the barrier, rotated until it was nearly on line with the barrier axis, and continued to a stop in a manner similar to that of Test 216 (62-mph head-on impact). The crush in the vehicle forestructure formed an arc (plan view) with least crush at the fenders. Maximum crush at the center was 20 in. (Fig. 18; Appendix Fig. 24). Once again, a crimp was noted in the roof over the door posts on both sides of the car. The left-front door was jammed, and the radiator buckled back around the engine. Vehicle rise was 1 ft 4 in.

Maximum vehicular penetration was 15.3 ft, and permanent displacement of the barrier nose was 11.7 ft. There were delamination and splitting of some of the interior panels and diaphragms, bent and broken hinges, and gouging of some of the fender panels. However, no parts became detached from the barrier (Fig. 19).

Data From Instrumentation—The FHWA instrumentation system was used in addi-

Figure 18.

tion to nine channels of information that were transmitted through a hardwire system to a second magnetic tape recorder (Appendix Figs. 29 and 30).

The maximum pressure transducer reading from the cells was 64.0 psi. The maximum loads on the two $\frac{7}{8}$-in. cables were 20,900 lb on the left and 5,450 lb on the right. The bridge approach guardrails sustained compressive stresses from 4,800 psi on the bottom left to 12,000 psi on the top right. The maximum chest load on the dummy was 175 lb.

Figure 19.

The longitudinal deceleration sustained by the vehicle included three distinct peaks greater than 13 g (5-msec duration). The average 50-msec passenger compartment deceleration (three accelerometers) was 10.2 g. This magnitude of deceleration would cause moderate to severe injuries in most cases if the vehicle occupants were not fully restrained. The fact that the vehicle impacted the nose of the barrier at an angle did not appear to cause large lateral decelerations.

Accelerometer records were obtained for the motion of the chest of the driver dummy in the longitudinal, lateral, and vertical directions. Only the longitudinal record was transmitted by hardwire. It had a shape very similar to the longitudinal vehicle records, with two peaks exceeding 12 g for as much as 30 msec. The first dummy peak lagged the vehicle peak by about 40 msec; the other two peaks lagged about 20 msec.

The lateral dummy record of motion showed a thin 20-g spike (5-msec duration), three or four other thin spikes with magnitudes of 8 to 10 g (also 5-msec duration), and low values elsewhere. The peaks occurred at the same time as the longitudinal dummy peaks, but the shape of the two curves was totally dissimilar. The vertical dummy record of deceleration was similar to that for longitudinal motion, except that the first, vertical peak was opposite in direction to the second and third vertical peaks. There was one thin (5-msec duration) 23-g spike; the second and third peaks (also 5 msec) were about 13 g. If the second and third longitudinal and vertical peaks are resolved vectorially, the resultant is about 18 to 19 g for each peak.

CONCLUSIONS

The following conclusions are based on an analysis of the results of the full-scale impact tests conducted during this test series:

1. The passenger-compartment decelerations measured indicate that passengers will have a good chance of sustaining little or no injury during high-speed collisions if fully restrained (with seat belt and shoulder harness). However, even unrestrained occupants will have a much better chance of surviving an impact with the barrier than they would if colliding with a fixed object. This is particularly true at impact speeds less than 60 mph.
2. The post-collision trajectory of impacting vehicles will be acceptable in most cases. The final position of the vehicle may, however, be hazardous to adjacent traffic after oblique-angle impacts.
3. During test 217, the vehicle was effectively redirected when it struck near the rear of the barrier; however, redirection appeared to be due more to the action of the bridge railing than to the fendering ability of the energy-absorbing barrier. Despite this observation, the fendering system is recommended on the basis of several unpublished tests by the developer in which test vehicles weighing around 4,500 lb and traveling 50 to 60 mph impacted the side and the nose of the barrier at angles of 10 to 20 degrees with the barrier axis and were effectively redirected.
4. The effort and number of barrier components required to place the barrier back in service will be minimal after the head-on and nearly head-on tests in most cases.

A significantly greater effort may be required to repair the barrier after the oblique-angle collision with the side of the barrier because of the amount of debris that is created during this type of collision.

5. Minor drawbacks to this barrier system include the problems that might arise in protecting water in the cells from leakage, vandalism, and freezing. Also, the barrier is more complex than most other highway barriers and, as such, would require skilled construction and maintenance personnel as well as a relatively large number of maintenance components compared with most other highway barriers.

6. Because most of the test objectives were successfully met using a moderately heavy passenger vehicle impacting at relatively high speeds, this barrier should perform with reasonable effectiveness under the range of conditions that constitute the majority of gore-area impacts.

ACKNOWLEDGMENT

This work was accomplished in cooperation with the Federal Highway Administration. The opinions, findings, and conclusions expressed are those of the authors and not necessarily those of the Federal Highway Administration.

REFERENCES

1. Engineering Evaluation of Water-Filled Plastic Cells in Fixed Barrier Automobile Impacts. Dept. of Mechanical Engineering, Brigham Young Univ., Rept. RSCB-2.
2. Nordlin, E. F., Woodstrom, J. H., and Doty, R. N. Dynamic Tests of an Energy-Absorbing Barrier Employing Water-Filled Cells, Series 21. California Division of Highways, Nov. 1970.
3. Nordlin, E. F., Woodstrom, J. H., and Doty, R. N. Dynamic Tests of an Energy-Absorbing Barrier Employing Steel Drums, Series 22. California Division of Highways, Oct. 1970.
4. Nordlin, E. F., Woodstrom, J. H., and Hackett, R. P. Dynamic Tests of the California Type 20 Bridge Barrier Rail, Series 23. California Division of Highways, Oct. 1970.
5. Nordlin, E. F., Field, R. N., and Prysock, R. H. Dynamic Full Scale Impact Tests of Double Blocked-Out Metal Beam Barriers and Metal Beam Guard Railing, Series 10. California Division of Highways, Feb. 1965.
6. Development of a Hydraulic-Plastic Barrier for Impact-Energy Absorption. Dept. of Mechanical Engineering, Brigham Young Univ.
7. Nordlin, E. F., Ames, W. H., Kubel, L. G., and Chow, W. Evaluation of a Telemetry System for Use in Vehicle-Barrier Impact Tests. Materials and Research Dept., California Division of Highways, Res. Rept. 636405-1, July 1969.
8. Hayes, G. G., Ivey, D. L., and Hirsch, T. J. Performance of the "Hi-Dro Cushion" Vehicle-Impact Attenuator. Texas Transportation Institute, Tech. Memo. 505-11, Aug. 1970.

Appendix

DETAILS OF BARRIER DESIGN AND PERFORMANCE

The following figures contain pertinent data and photographs of the impact tests discussed in this report.

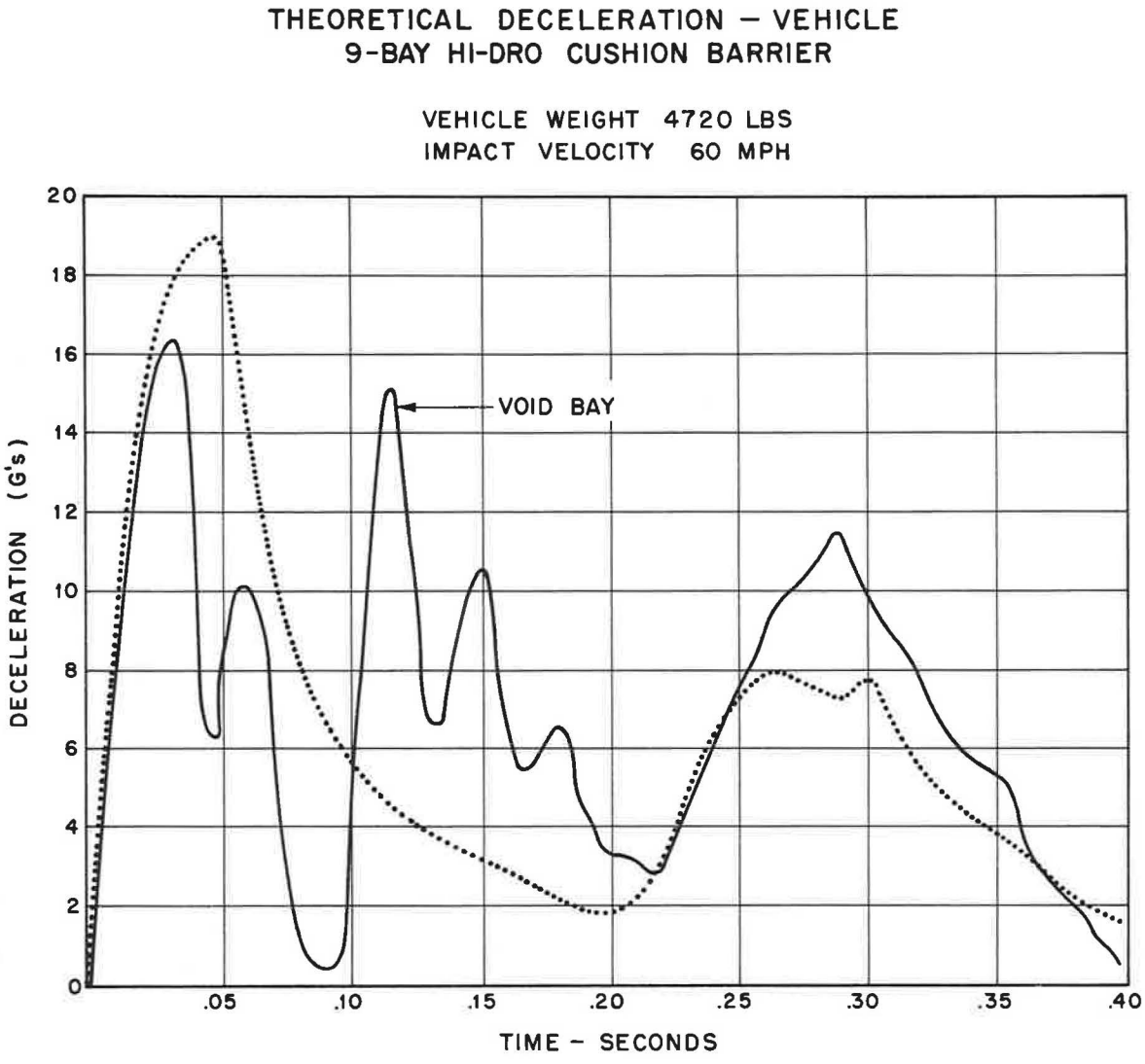
THEORETICAL DECELERATION – VEHICLE
9-BAY HI-DRO CUSHION BARRIER
VEHICLE WEIGHT 4720 LBS
IMPACT VELOCITY 60 MPH
VOID BAY
DECELERATION (G's)
TIME – SECONDS
0
2
4
6
8
10
12
14
16
18
20
.05
.10
.15
.20
.25
.30
.35
.40

Figure 20.

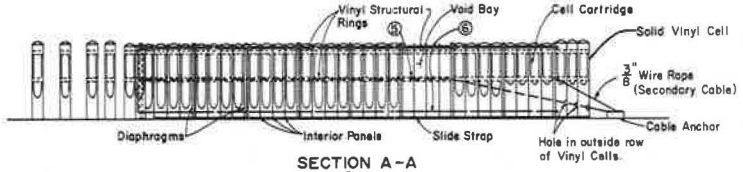

SECTION A-A
1/2" = 1'-0

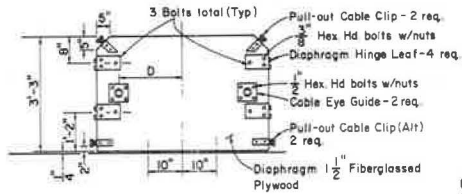

DIAPHRAGM - ELEVATION
3/4" = 1'-0"

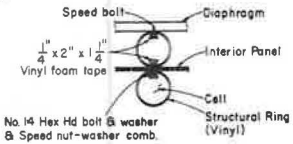

CELL - PLAN
No Scale

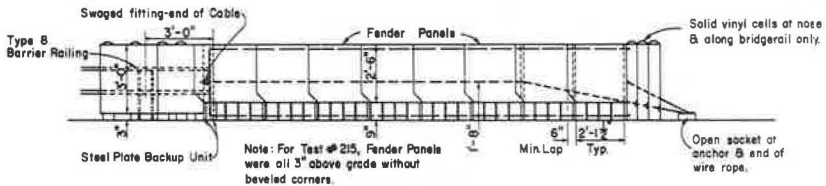

ELEVATION
1/2" = 1'-0"

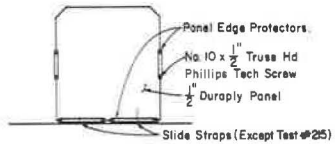

INTERIOR PANEL
3/4" = 1'-0"

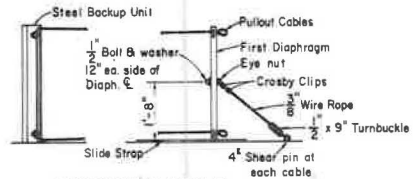

SECONDARY CABLE
3/4" = 1'-0"

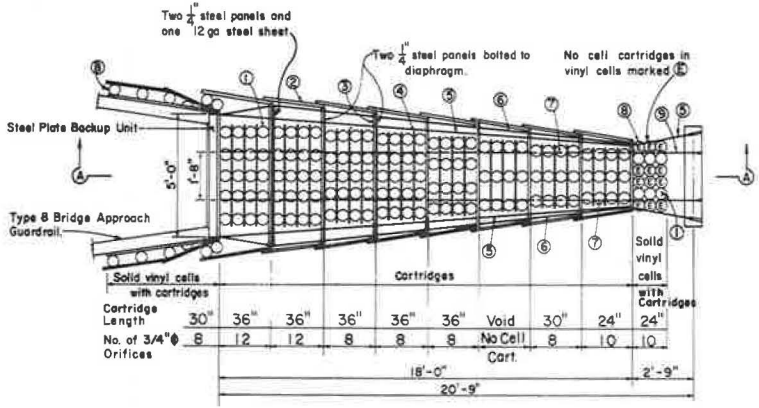

PLAN

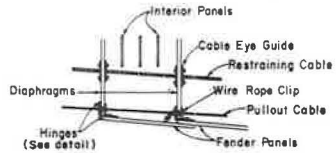

HINGE PLAN

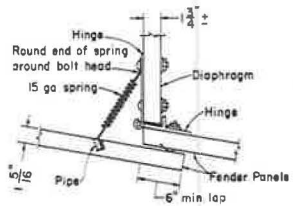

HINGE DETAIL

LEGEND

① - Hi-Dro Cushion Cell Cartridge (Vinyl coated nylon fabric) 126 total.
② - Fender Panel - 1 1/16" fiberglassed plywood.
③ - Diaphragm - 1 1/2" fiberglassed plywood.
④ - Interior Panel - 1/2" duraply plywood.
⑤ - Restraining Cable - 7/8" wire rope.
⑥ - Pullout Cable - 3/8 wire rope.
⑦ Slide Straps - 4" x 1/4" steel straps (on ground.)
⑧ Hi-Dro Cushion Cells - solid vinyl. (28 total)
⑨ Secondary Cable 3/8" wire rope with 4" shear pin.

BARRIER DETAILS - TEST NO. 215 - 218

Figure 21.

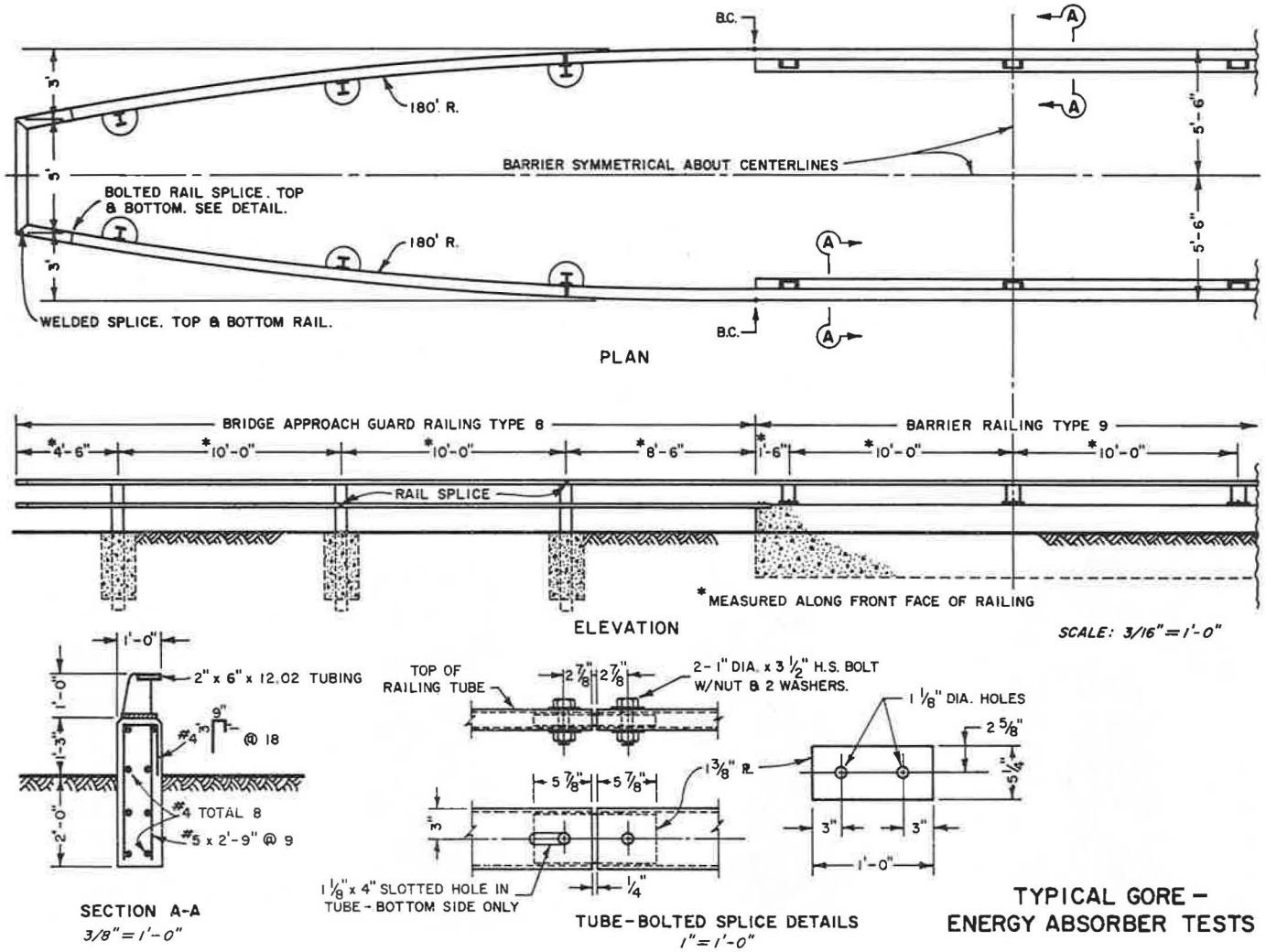
B.C.
180' R.
BARRIER SYMMETRICAL ABOUT CENTERLINES
BOLTED RAIL SPLICE. TOP & BOTTOM. SEE DETAIL.
WELDED SPLICE. TOP & BOTTOM RAIL.
5'-6"
PLAN
BRIDGE APPROACH GUARD RAILING TYPE 8
BARRIER RAILING TYPE 9
RAIL SPLICE
*MEASURED ALONG FRONT FACE OF RAILING
ELEVATION
SCALE: 3/16"=1'-0"
2" x 6" x 12.02 TUBING
#4 TOTAL 8
#5 x 2'-9" @ 9
SECTION A-A
3/8"=1'-0"
TOP OF RAILING TUBE
2- 1" DIA. x 3 1/2" H.S. BOLT W/NUT & 2 WASHERS.
1 1/8" DIA. HOLES
1 1/8" x 4" SLOTTED HOLE IN TUBE - BOTTOM SIDE ONLY
TUBE-BOLTED SPLICE DETAILS
1"=1'-0"
TYPICAL GORE - ENERGY ABSORBER TESTS

Figure 22.

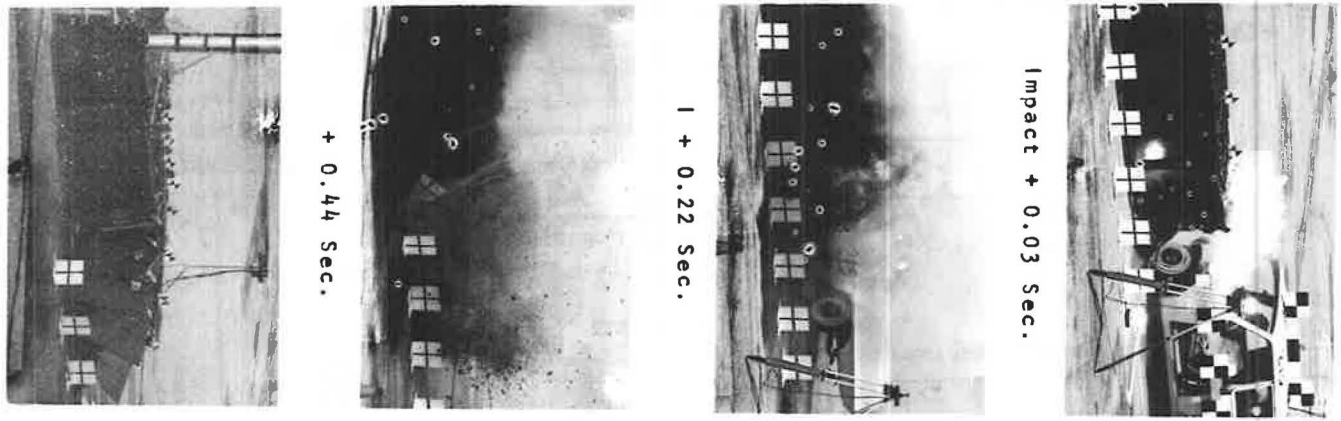

Figure 23.

Barrier Depth	19.5 Ft.	Test No.	215
No. of Water-Filled Cells	126	Date	7-16-69
Permanent Displacement of Barrier Nose	9.3 Ft.	Vehicle	1968 Dodge
Deceleration Distance-Passenger Compartment	-	Vehicle Weight (W/Dummy and Instrumentation)	4690 Lbs.[1]
Maximum Vehicular Deformation	20 In.	Impact Velocity	57.5 mph
Passenger Compartment Deceleration (Highest 50 ms avg. - accelerometer)	7.0 G's (long.)	Impact Angle	Head-on
Vehicle Average Deceleration-Calculated	Rolled	Dummy Restraint	Lap belt

[1] Left front door removed.

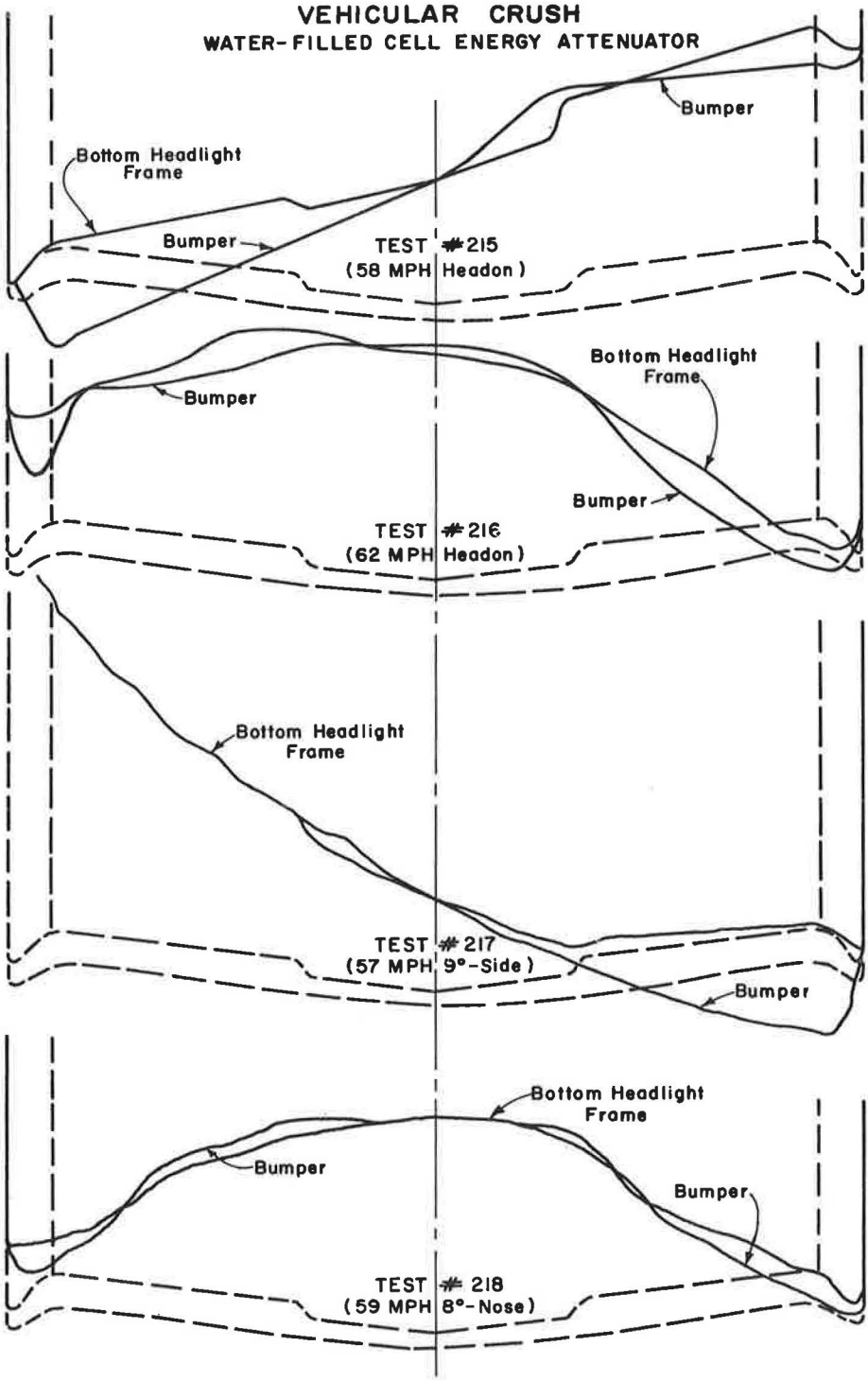
VEHICULAR CRUSH
WATER-FILLED CELL ENERGY ATTENUATOR
Bumper
Bottom Headlight Frame
Bumper
TEST #215
(58 MPH Headon)
Bottom Headlight Frame
Bumper
Bumper
TEST #216
(62 MPH Headon)
Bottom Headlight Frame
TEST #217
(57 MPH 9°-Side)
Bumper
Bottom Headlight Frame
Bumper
Bumper
TEST #218
(59 MPH 8°-Nose)

Figure 24.

CALIFORNIA DIVISION OF HIGHWAYS

VEHICLE INSTRUMENTATION

WATER-FILLED CELL ENERGY ATTENUATOR TESTS

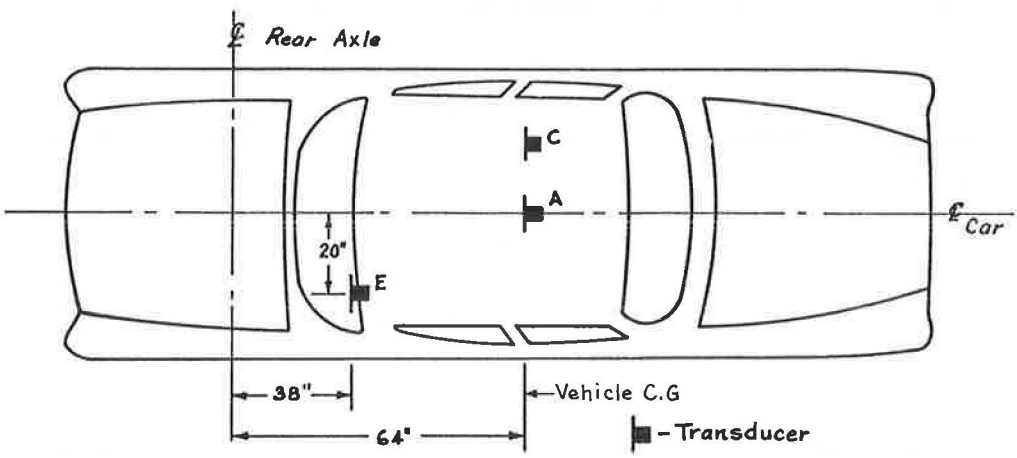

Tests #215 & 216

CHANNEL NO.	LOCATION[1]	DESCRIPTION
1	A	100 "G" longitudinal accelerometer
2	E	100 "G" longitudinal accelerometer
3	C	50 "G" longitudinal accelerometer
4	C	50 "G" lateral accelerometer
5	C	50 "G" vertical accelerometer
6	C	Force meter in dummy's chest
7	C	Lap belt tension transducer

Notes:

[1] A and E on vehicle floor; C on back of dummy's chest cavity.

Figure 25.

BARRIER INSTRUMENTATION
TESTS 215 & 216

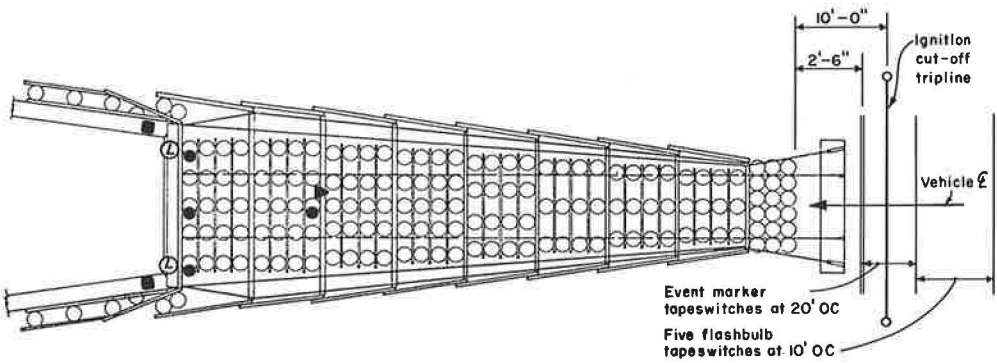

TEST 215

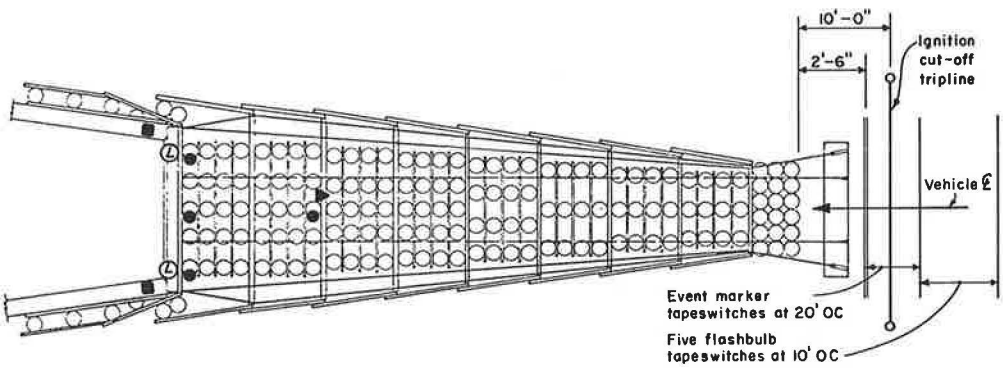

TEST 216

LEGEND:
- ■ = Strain gage - on top of top and bottom bridgerails (Total 4)
- ● = Pressure transducer in water cells.
- Ⓛ = Load cell on main cables
- ▶ = Accelerometer.

Figure 26.

Figure 27.

Barrier Depth	19.5 Ft.	Test No.	216
No. of Water-Filled Cells	126	Date	9-3-69
Permanent Displacement of Barrier Nose	10.7 Ft.	Vehicle	1968 Dodge
Deceleration Distance-Passenger Compartment	18.0 Ft.	Vehicle Weight (W/Dummy and Instrumentation)	4690 Lbs.[1]
Maximum Vehicular Deformation	20 In.		
Passenger Compartment Deceleration (Highest 50 ms avg. - accelerometer)	9.8 G's (long.)	Impact Velocity	61.8 mph
		Impact Angle	Head-on
Vehicle Average Deceleration-Calculated	7.1 G's	Dummy Restraint	Lap belt

[1] Left front door removed.

Figure 28.

Barrier Depth	19.5 Ft.
No. of Water-Filled Cells	126
Permanent Displacement of Barrier Nose	1.5 Ft.
Deceleration Distance-Passenger Compartment	-
Maximum Vehicular Deformation	-
Passenger Compartment Deceleration (Highest 50 ms avg. - accelerometer)	8.4 G's (long.)
Vehicle Average Deceleration-Calculated	Redirected

Test No.	217
Date	9-25-69
Vehicle	1968 Dodge
Vehicle Weight (W/Dummy and Instrumentation)	4760 Lbs.
Impact Velocity	57.0 mph
Impact Angle	9° (side)
Dummy Restraint	Lap belt

CALIFORNIA DIVISION OF HIGHWAYS

VEHICLE INSTRUMENTATION

WATER-FILLED CELL ENERGY ATTENUATOR TESTS

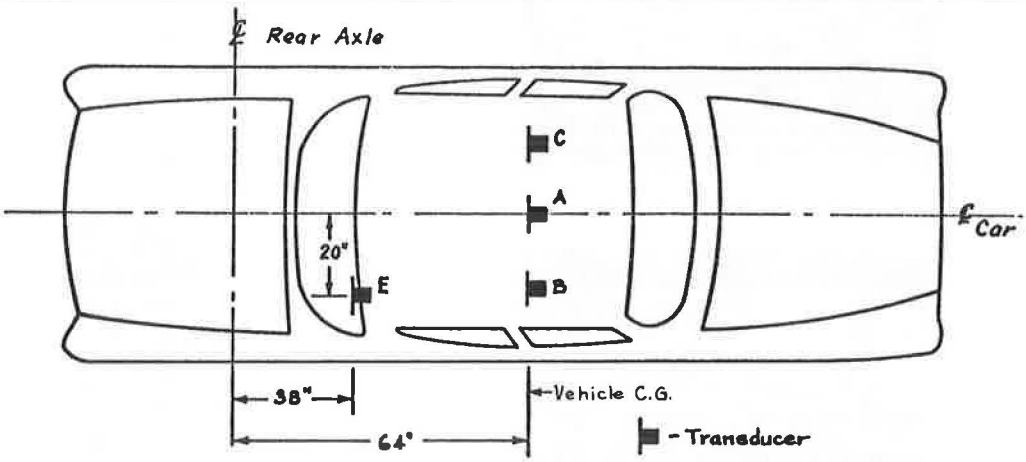

Test #217

CHANNEL NO.	LOCATION[1]	DESCRIPTION[2]
1	A	100 "G" longitudinal accelerometer (T)
2	A	100 "G" lateral accelerometer (T)
3	E	100 "G" longitudinal accelerometer (T)
4	E	50 "G" lateral accelerometer (T)
5	C	50 "G" longitudinal accelerometer (T)
6	C	50 "G" lateral accelerometer (T)
7	C	50 "G" vertical accelerometer (T)

Test #218

1	A	100 "G" longitudinal accelerometer (T)
2	A	100 "G" lateral accelerometer (T)
3	E	100 "G" longitudinal accelerometer (T)
4	E	50 "G" lateral accelerometer (T)
5	C	50 "G" vertical accelerometer (T)
6	C	Force meter (In dummy's chest cavity)
7	C	50 "G" lateral accelerometer (T)
G	E	50 "G" lateral accelerometer (U)
H	B	50 "G" longitudinal accelerometer (U)
I	E	100 "G" longitudinal accelerometer (U)

Notes:

[1] A and E on vehicle floor; C on back of dummy's chest cavity, B in dummy's chest cavity.

[2] (T) = telementry, (U) = umbilical cord.

Figure 29.

BARRIER INSTRUMENTATION
TESTS 217 & 218

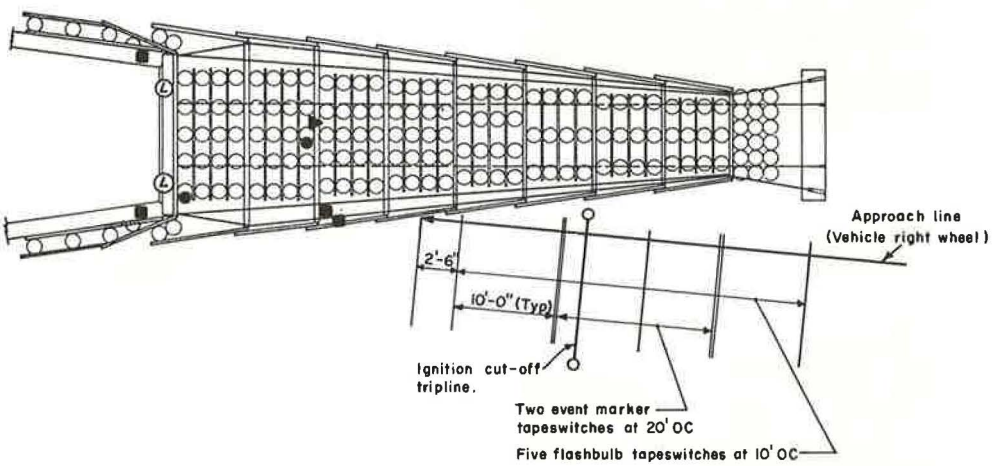

TEST 217

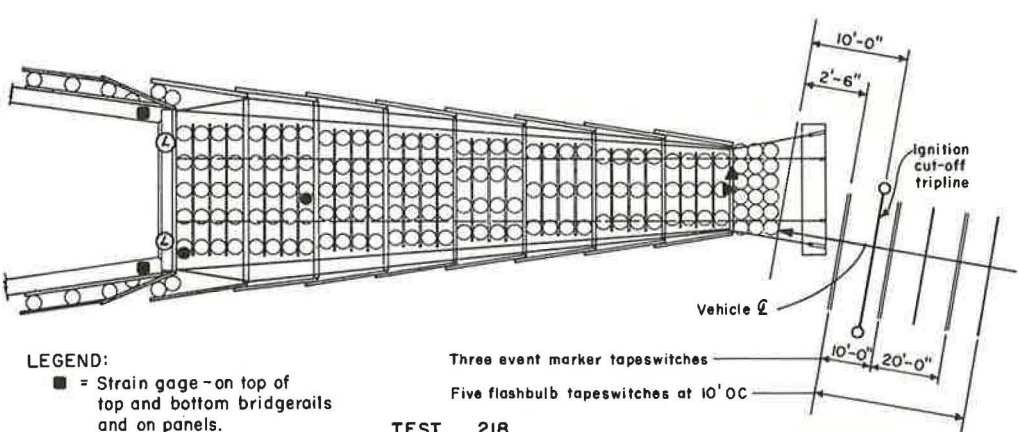

TEST 218

LEGEND:
- ■ = Strain gage - on top of top and bottom bridgerails and on panels.
- ● = Pressure transducer in water cells.
- Ⓛ = Load cell on main cables.
- ▶ = Accelerometer

Figure 30.

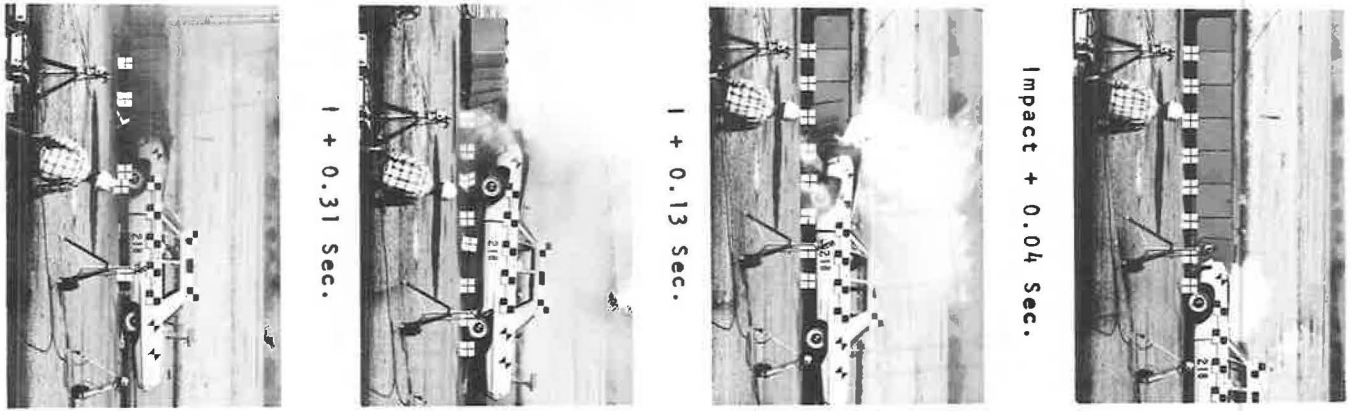

Figure 31.

Barrier Depth	19.5 Ft.
No. of Water-Filled Cells	126
Permanent Displacement of Barrier Nose	11.7 Ft.
Deceleration Distance-Passenger Compartment	16.9 Ft.
Maximum Vehicular Deformation	20 In.
Passenger Compartment Deceleration (Highest 50 ms avg. - accelerometer)	10.2 G's (long.)
Vehicle Average Deceleration-Calculated	6.9 G's

Test No.	218
Date	11-12-69
Vehicle	1968 Dodge
Vehicle Weight (W/Dummy and Instrumentation)	4760 Lbs.
Impact Velocity	59.2 mph
Impact Angle	8° (nose)
Dummy Restraint	Lap belt

DYNAMIC TESTS OF AN ENERGY-ABSORBING BARRIER EMPLOYING STEEL DRUMS

Eric F. Nordlin, James H. Woodstrom, and Robert N. Doty,
California Division of Highways

The results of three full-scale vehicle impact tests of an energy-absorbing barrier employing 55-gal tight-head steel drums are reported. The 19.6-ft long test barriers were designed as gore installations. The tests were conducted with 1968 sedans weighing approximately 4,700 lb and traveling at speeds of from 54 to 64 mph. The tests were run head-on and at 9 deg with the barrier axis into the barrier nose, and at 11 deg with the barrier axis midway along the side of the barrier.

The head-on and angle impacts into the nose of the barrier resulted in vehicle passenger-compartment decelerations less than the 12-g limit suggested by the Federal Highway Administration. Vehicle damage was moderate. The vehicle remained stable and upright during impact. The impact into the side of the barrier did not produce completely satisfactory results. The vehicle was redirected but by the bridge approach guardrail behind the barrier.

The results of the three tests indicate that the barrier effectiveness in reducing the severity of most impacts is such that it should be used operationally on an experimental basis. However, future refinements in the design need to be made, particularly with regard to redirection of vehicles that collide with the side of the barrier. A study of accident statistics and human tolerance to deceleration is also summarized. This study indicated that the deceleration imparted to the impacting vehicle should be as low as possible, perhaps lower than in some current criteria.

•ABOUT HALF of all the fatalities on the California freeway system in 1967 and 1968, an average of 430 a year, were caused by vehicles that ran off the road. Of this number, 225 fatalities (over 25 percent of all freeway fatalities) were the result of hitting a fixed object. The types struck most frequently were abutments and piers, bridge rails, guardrails at fixed objects, steel sign poles, light poles, and cable types of median barriers.

In an attempt to decrease the frequency of these relatively severe accidents, the California Division of Highways is now striving to provide a minimum of 30 ft of recovery area alongside the traveled way into which an out-of-control vehicle can intrude without striking an immovable or unprotected fixed object. Every effort is first being made to eliminate the fixed object. If it cannot be eliminated, an attempt is then made to incorporate breakaway features. In cases where the fixed object can neither be eliminated nor made to yield, protection in the form of guardrails is now being provided.

Recent improvements in bridge approach guardrailing, confirmed by full-scale tests (1, 2), should minimize the probability of impact into the ends of bridge barrier rails. However, one of the remaining problems, for which no satisfactory solution has been developed, is protection from hazardous fixed objects located in the gore area

Sponsored by Committee on Traffic Safety Barriers and Sign, Signal and Lighting Supports and presented at the 50th Annual Meeting.

at freeway off-ramps. Collisions with the concrete wedge-shaped deflectors or large overhead sign supports or both, often found in these gores, are usually very severe. In an effort to alleviate this problem, the California Division of Highways has been involved for the last 2 years in a research program to investigate and develop energy-absorption barriers for use in gore areas. Three types of energy-absorption barriers have been tested to date. These barriers used (a) water-filled plastic cells, (b) 55-gal tight-head steel drums, and (c) plastic drums containing sand. The results of tests of barriers employing water-filled plastic cells are documented in a report included in this Record (4). The testing of a barrier employing sand-filled plastic containers has just been completed and will be reported. The three tests reported here were of barriers containing 55-gal tight-head steel drums as the primary energy-absorbing mode.

The results of research at the Texas Transportation Institute (TTI) indicated that the resistance to deformation of modified 55-gal tight-head steel drums could be effectively utilized to decelerate a standard-size vehicle traveling 60 mph (3). A series of tests at TTI consisted of three 50 to 60 mph head-on tests and three 40 to 50 mph tests at angles of 20 deg (one test) and 30 deg (two tests) with the barrier axis. The weights of the test vehicles varied from 3,200 to 4,400 lb. Although the results of these six TTI tests were generally favorable, additional testing using heavier vehicles (4,700 lb) impacting head-on and at 10 to 15 deg angles into the front and side of the barrier were felt to be more representative of the conditions encountered on California highways. The utilization of a fendering system similar to that employed for the water-filled cell barrier (4) was also considered advisable. Consequently, the series of three tests reported herein was conducted.

OBJECTIVE

The objective of this research was to conduct instrumented vehicular impact tests of energy-absorbing barriers incorporating 55-gal tight-head steel drums and, based on the results of these tests, determine the degree to which these barriers would minimize the hazards created by many existing gore-separation structures and other fixed objects. The following criteria were used to evaluate the barrier design:

1. The impact severity for the occupants of errant vehicles involved in head-on collisions into fixed objects located in gores must be reduced to a survivable level at impact velocities of 60 mph and less.
2. The energy-absorbing barrier should be at least as effective as the anchored W-beam guardrail currently used in California to redirect vehicles impacting at oblique angles into the side of the barrier.
3. The barrier components should not be susceptible to dislodgment or ejection onto the traveled way such that they become a hazard to adjacent traffic when an impact occurs.
4. First cost and maintenance costs should be economically feasible.
5. On-site repair time should be minimal because of the safety hazards to maintenance personnel and adjacent traffic when field repairs are in progress.

DESCRIPTION OF TEST BARRIER

As stated previously, the records of the California Highway Patrol for the years 1967 and 1968 show that about 25 percent of all California freeway fatalities occurred when vehicles ran off the road and collided with fixed objects. Another tabulation of California freeway fixed-object fatal accidents for the years 1965 through 1967 contains a total of 640 for this 3-year period. Of this number, 548 involved a vehicle traveling at an estimated speed of over 50 mph at impact, with 171 of these 548 traveling over 70 mph. A further breakdown of this total of 640 accidents indicates that 376 standard-size cars, 159 compact cars, and 105 other miscellaneous vehicles were involved. These results indicate that energy-absorbing barriers must be designed to cushion impacts of standard-size cars traveling at high speeds.

In an effort to determine the most prevalent impact angle, 47 California Highway Patrol (CHP) accident reports involving fatalities at gore installations during 1965-

Figure 2.

Figure 3.

component of the impact forces. The trailing edge of each fender panel overlapped the leading edge of the next rearward panel in a fish-scale manner such that barrier crush would not be restricted during a head-on impact. Light springs were used to maintain the fender panels in the closed position (Fig. 2).

Lateral and vertical restraint was provided by four ¾-in. wire ropes attached to fabricated steel T-sections embedded in cast-in-place concrete anchors. The wire rope was threaded between the drums so that the drums would be free to slide backward during impact and then attached to the bridge approach guardrail using swaged fittings. A slight pre-impact tensile force was applied to the cables, which were aligned in a straight line to minimize the slack, and subsequent lateral movement that develops during an oblique-angle impact. The concrete anchors were located so that the front drums would receive as much lateral support as possible from cables placed low enough to minimize the possibility of snagging the impacting vehicle (Fig. 3).

The barrier was elevated 4 in. above the ground with U-bolts bolted to the bottom of each drum. The drums were bolted together at all points of contact. For test 221, bolts were placed 2 in. below the drum tops and 2 in. above the drum bottoms; wood spacer blocks were used between drums. For tests 222 and 223, the bolts were located at the two rolling hoops, and a steel washer was placed between the drums so that the cable could be threaded between the drums easily. Because the drums were bolted together in a relatively rigid assembly, some of the U-bolt chairs were not in contact with the slightly irregular ground surface at all times. (Bolts were used in lieu of the welded connections used in the TTI test barriers because, although slightly more expensive initially, it was felt that the bolted connections would simplify and accelerate barrier repairs.)

DESCRIPTION OF TESTING

All of the tests reported were conducted on an unused portion of a runway at the Lincoln Municipal Airport, Lincoln, Calif. The test vehicles used for this series were 1968 Dodge sedans. The test vehicles were operated remotely from a control car that followed them along the approach line. A trip switch cut off the ignition in the test vehicle 10 ft prior to impact. A more complete description of the control system is given elsewhere (6).

1967 were examined and classified (Table 1). These data were based on the sketches of the accident site included in the CHP officers' reports. In many cases, no barriers were present so the impact angle was estimated assuming an energy-absorbing barrier was in place. Also, funds were not available to locate and examine all the police reports involving gores. Thus, the sample was small and the accuracy of the data definitely subject to question. In any event, the study indicated that a number of collisions were side-angle impacts (most less than 10 deg); hence, energy-absorbing barriers should be capable of redirecting vehicles impacting at oblique angles in addition to effectively decelerating vehicles impacting head-on.

TABLE 1

ANALYSIS OF 47 FREEWAY FATAL ACCIDENTS INVOLVING GORES

Category	Fatalities			
	1965	1966	1967	Total
Angle of Impact[a, b]				
Head-on[c]	6	5	8	19
Flat angle (> 10 deg)	4	8	6	18
Large angle (> 10 deg)	3	4	1	8
Location[a]				
Nose	11	12	12	35
Side	2	6	4	12
Barrier or object				
Concrete	2	11	5	18
Guardrail	8	6	8	22
Pole[d]	2	1	2	5
Concrete curb	1	0	1	2

Note: The 1966 and 1967 accidents all involved one fatality per accident.

[a]When a pole was impacted, an imaginary barrier was assumed in front of it, and the vehicle path was studied to determine the location and angle of a hypothetical barrier impact.

[b]No estimate was made on two accidents.

[c]Includes broadside impacts.

[d]Includes both sign posts and lighting standards.

Thus, the test barrier was designed to decelerate a 4,700-lb vehicle impacting head-on or at an angle of 10 deg with the barrier axis at an impact velocity of 60 mph without subjecting the passenger compartment to an average deceleration greater than 10 g. (This choice of a relatively shallow 10-deg angle has since been justified, at least to some extent, by reports from several other states indicating that in-service energy-absorbing barriers are being impacted head-on in almost all cases.) The construction details for the barrier are shown in Figure 17 of the Appendix.

The primary energy-absorbing media used for the test barrier were 55-gal tight-head steel drums. Forty-one of these drums, which were approximately 24 in. in diameter and weighed 38 lb each, were used for each barrier. The drums contained 18-gage tops and bottoms and 20-gage sides. The tops and bottoms each contained one 7-in. diameter hole to decrease the magnitude of the force required to crush the drum (Fig. 1). The barrier design procedure used was developed and reported by the Texas Transportation Institute (3). The design calculations are given elsewhere (5).

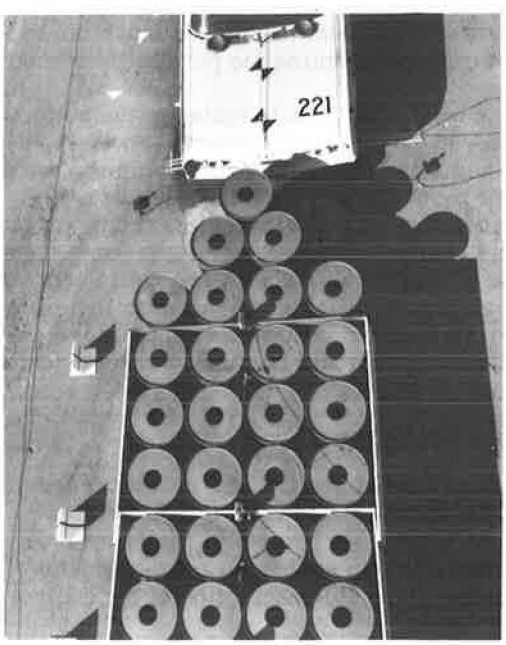

Figure 1.

In an effort to provide an effective redirective capability, a system consisting of three 1-in. thick plywood diaphragms and eight 1-in. thick plywood fender panels was used for the first test barrier. The diaphragms were intended to provide support for the fender panels and to transmit the lateral component of the impact force to the cable system when oblique-angle impacts occurred. Although not of primary importance, it was felt that the lateral distribution of the impact forces provided by the diaphragms during an offset head-on impact would also be of some benefit.

The fender panels, attached to the diaphragms using steel hinges, were intended to act as beams when resisting the lateral

and 6). Maximum vehicular crush was 16.5 in.

All the drums in the barrier were deformed (Figs. 7 and 8). The cables were slack but undamaged. The plywood fender panels were badly cracked and splintered but remained attached to the barrier as it was deformed around the nose of the bridge approach guardrail. The drums crushed one row at a time, in successive order, as had been assumed in the design procedure. Figure 20 in the Appendix shows additional test data.

Figure 5.

Test 222

The barrier used for test 222 was identical to that used for the first test with the following exceptions: (a) the length of the fender panels was decreased to minimize contact of the bottom corner of the trailing edge of these panels with the ground (this required an increase in the number of diaphragms used); and (b) the drum-to-drum bolted connections were made at the rolling hoops to eliminate the need for wood spacers and make it easier to tighten the lower bolts from the top of the barrier.

The 4,760-lb 1968 Dodge sedan impacted the left side of the barrier 10.2 ft in front of the bridge approach guardrail at a speed of 59.8 mph and an angle of 11 deg with the barrier. The vehicle was redirected, but minimal redirectional forces were provided by the drums as the vehicle axis was displaced 12 in. laterally from its location at impact before any redirection began (i.e., crabbing occurred). At this time, solid contact with the bridge approach guardrail had been established.

Figure 6.

Figure 7.

Instrumentation

For tests 221 and 222, a telemetry instrumentation system on loan from the Federal Highway Administration was used (7). It consisted of seven channels of FM telemetry for use in the crash vehicle or dummies and seven hardwire channels for use on the test barrier and backup bridge approach guardrail. The system included seven accelerometers and two seat-belt force transducers and all the necessary signal-conditioning equipment. The dynamic data from these transducers were recorded on a 14-channel analog magnetic tape recorder. For tests 222 (partial) and 223, data from instrumentation on the test vehicle were transmitted through an umbilical cord (hardwire) system. All the accelerometers in the test vehicle and the dummies were of the unbonded strain-gage type. Additional data regarding the vehicular and barrier instrumentation are shown in Figures 18 and 19 of the Appendix.

Impactographs (mechanical stylus devices designed to measure acceleration) were placed in the chest cavity of the dummy in the passenger position and also on the floor of the test vehicle.

Photography

High-speed photography was used to study the vehicular, dummy, and barrier kinematics for all three tests. Eight Photosonic cameras operating at frame rates of 200 to 400 frames per second were placed as shown in Figure 19 of the Appendix. Cameras 1 and 2 were mounted overhead. Camera 8 was placed in the crash car to record the movement of the dummies. Red-orange pips were placed on the edge of the film at a rate of 1,000 ± 5 pips per second, using Adtrol timing light generators, to provide a means of determining the frame rate of each camera.

The authors' original study (5) contains a discussion of the data obtained with the photographic, mechanical, and electrical data-acquisition systems described here.

TEST RESULTS

Test 221

A 4,690-lb 1968 Dodge sedan impacted the barrier head-on at a speed of 64.2 mph. Deceleration was relatively constant. However, the record of the accelerometers on the floor of the vehicle indicated that the barrier bottomed out. The maximum average 50-millisecond (msec) passenger-compartment deceleration, based on accelerometer data, was 10.3 g and occurred at the end of the collision. The average deceleration (based on impact velocity and the total passenger-compartment stopping distance) was 8.4 g.

This magnitude of deceleration exceeds the tolerable limits for unrestrained occupants, as discussed later. Thus, unrestrained occupants probably would have sustained moderate to severe injuries. Occupants restrained by seat belts or seat belts and shoulder harnesses would have sustained no more than moderate injuries in most cases.

Figure 4.

There was a noticeable vertical force imparted to the vehicle as shown by the vehicular rise in Figure 4. The rise was caused at least in part by the right-front wheel riding up on the cable. There was virtually no vehicular rebound.

Vehicular damage consisted of some bumper deformation, a cracked windshield, a jammed door on the right-front side, damage to both front quarter panels, 3.4 in. of steering column collapse (energy-absorbing steering column), and some dashboard deformation (Figs. 5

Figure 8.

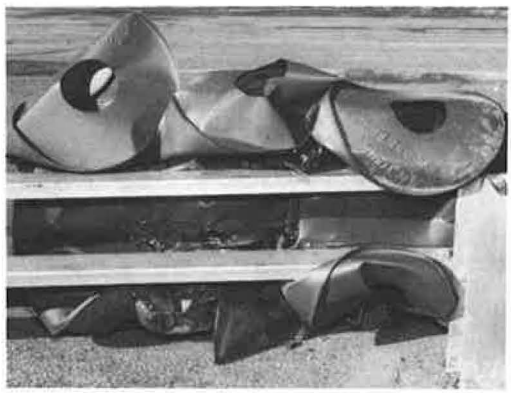

Figure 9.

The force of the impact caused a clamping action to take place between the rear drums and the bridge approach guardrail, thus preventing drum ejection (Fig. 9). Additional barrier damage consisted of crushing of the outside drums in the back half of the barrier on the impacted side. All the fender panels beyond the point of impact were torn off the barrier. There were some failures of hinge pins; the ends of the last few diaphragms were broken off on the impact side. There was an unacceptable amount of debris deposited in what would be the adjacent traveled way. Some of the fender-panel fragments were thrown approximately 155 ft from the point of impact (Figs. 10 and 11).

The maximum 50-msec average passenger-compartment decelerations recorded were 5.3 g laterally and 6.6 g longitudinally. Thus, unrestrained occupants would probably have sustained moderate injuries. Although the lateral deceleration was slightly in excess of the tolerance limits for seat-belt restrained occupants, little or no injury would probably be sustained in most collisions of this severity if any occupant restraints were in use at the time of the collision.

Vehicle damage included severe crushing of the right-front quarter panel, jamming of the right-front door, scars on the right doors and right-rear panel, and displacement of the radiator to the point of touching one fan blade (Fig. 12). Figure 21 in the Appendix shows additional test data.

Figure 10.

Figure 11.

Figure 12.

Figure 13.

Test 223

Test 223 consisted of a 4,740-lb 1968 Dodge sedan impacting the same barrier design used for the previous test. The vehicle impacted the left corner of the barrier nose at a speed of 53.6 mph and an angle of 9 deg. At impact, the center of the front of the vehicle was offset 3.5 ft from the barrier axis. Significant elastic lateral deflection of the barrier took place as the vehicle penetrated 13.2 ft, rotated clockwise, and then rebounded 2.5 ft. The maximum 50-msec average passenger-compartment deceleration, based on accelerometer data, was 10.9 g longitudinally. The average passenger-compartment longitudinal deceleration was 7.2 g. Deceleration of this magnitude would, in most cases, result in moderate to severe injury for an unrestrained occupant, minor to moderate injury for an occupant restrained by a seat belt, and little or no injury for an occupant using both a seat belt and a diagonal shoulder harness. The position of the vehicle after the collision was such that it would have been a hazard to adjacent traffic (Fig. 13).

Vehicle damage consisted of a crimp in the roof on the passenger side, extensive hood deformation, slight displacement of the left-front quarter panel, and 3.6 in. of energy-absorbing steering column collapse (Figs. 14 and 15). There was a slash high on the cheek of the dummy driver, and the windshield was broken in front of the dummy passenger. The dummy passenger was badly cut on the tip of the bridge of his nose, over his right eye and on his forehead, and on the right side of his face and cheek. (The removal of this dummy's lower legs before the crash may have contributed to some excessive movement of his upper body during the collision.)

Figure 14.

Figure 15.

All but two drums were damaged. The left-front and the right-rear plywood fender panels were the only ones damaged. It appeared that the impact force was transmitted somewhat diagonally from the left-front to the right-rear portion of the barrier (Fig. 16). The left-front portion of the barrier was crushed much more than the right-front side. The film record shows the drums crushing one row at a time in successive order with the exception of the back row, which was deformed soon after impact. This was very similar to the dynamic barrier compression sequence observed during test 221.

Figure 16.

The movies showed the car being ejected outward from the barrier due to the elastic energy stored within the barrier. The clockwise rotation of the car was probably caused by a moment couple consisting of the vehicular momentum, acting through the vehicle center of gravity, and this elastic energy, acting through the centroid of the vehicle-barrier contact interface. Figure 22 of the Appendix shows additional test data.

DISCUSSION OF RESULTS

In addition to studying accident records, it is necessary to investigate the various aspects of human and vehicle tolerance to deceleration before an energy-absorbing barrier can be designed effectively.

Longitudinal decelerations (Appendix Fig. 23) as high as 40 g have been tolerated by fully restrained, healthy young male volunteers for up to 100 msec with no ill effects (8). Acceleration above this level caused extreme chest pain, difficulty in breathing, and visual malfunctions such as blurred vision, pain, headache, and retinal hemorrhage. The deceleration of a 160-lb driver in a head-on rigid barrier crash at 22 mph is about 25 g (9). The same reference reported that few serious injuries occurred in vehicle collisions at 20 mph. This would indicate that a tolerable occupant longitudinal deceleration of 25 g would be appropriate.

A 12-g maximum deceleration is permitted for devices classified as satisfactory when evaluated under the 4S program of the Federal Highway Administration (10). This 4S criterion is intended to provide a survivable environment and, as such, applies to the decelerations sustained by the passenger compartments of 2,000- to 4,500-lb vehicles. This criterion was based on the tentative tolerable limits of deceleration proposed by Cornell Aeronautical Laboratory in 1961 (11) given in Table 2. The duration of impact must be less than 200 msec and the rate of onset less than 500 g per second.

Table 2, although helpful as a rough guide for vehicle decelerations, does not give completely the shape of the deceleration pulse, which can vary considerably and still satisfy the 12-g average limitation.

TABLE 2

DECELERATION LIMITS

Occupant Restraint	Maximum Deceleration (g)		
	Lateral	Longitudinal	Total
Unrestrained	3	5	6
Seat belt	5	10	12
Seat belt and shoulder harness	15	25	25

A small but detailed accident study has been conducted at Cornell University to determine the benefits of seat belts in other than the prevention of ejection (12). The study showed no significant reduction in the severity of injuries due to the wearing of seat belts. It did determine that the type of injury varied; namely, whereas unbelted occupants impacted the windshield, belted occupants jackknifed toward and hit the steering wheel or instru-

ment panel and received head injuries in a slightly different manner. This suggests that the deceleration of the vehicle by the protective barrier may need to be almost as low for seat-belted passengers as for unrestrained passengers in order to minimize head injuries during a collision in which ejection would be quite unlikely even if no restraint were used.

Another study has been completed in which average longitudinal vehicular deceleration was related to the proportion of those vehicles in which unrestrained occupants sustained injuries (13). This study indicated that a 12-g vehicular deceleration will result in occupant injuries in the majority of cases. When this study is tied to one regarding general use of seat belts (12), one can conclude that, even with energy-absorbing barriers designed for maximum vehicle decelerations of 12 g (60-mph impact velocity), the 65 to 70 percent of the public who disdain the use of seat belts will probably be injured in a major collision with these barriers (10). Consequently, for the purposes of this study, the deceleration limits established by Cornell Laboratory (Table 2) were applied to the maximum average vehicle passenger-compartment deceleration measured over a 50-msec period. It is acknowledged that higher decelerations could be safely tolerated for shorter time intervals.

An injury study by UCLA indicated that impact into the steering wheel and column is the most common and also most dangerous cause of injuries during nonfatal accidents. Therefore, it would be well to adjust the design of the energy-absorbing barrier, with due consideration given to the energy-absorbing properties of steering columns in current vehicle models.

A paper from a General Motors seminar (14) includes information on energy absorption in steering columns. This type of column was first installed in 1967 in cars made by General Motors, American Motors, and Chrysler. This column was designed to collapse a maximum of $8\frac{1}{4}$ in. under loads no greater than 1,000 to 1,500 lb. The Federal Motor Vehicle Safety Standards limit the impact force of a simulated body traveling at a relative velocity of 15 mph to 2,500 lb when impacting the steering control system (15). Accident statistics from 257 cases involving the steering column in 1967 model cars traveling at speeds of 10 to 125 mph show that the column collapsed more than 5 in. in only six cases. A more detailed study of 88 head-on accidents out of the total 257 cases revealed two fatalities. This study also indicated that, at 60 mph, the maximum column compression for all 88 cases was slightly less than 8 in. and the average compression was about $3\frac{1}{2}$ in. There were numerous cases of steering column compression with closure speeds of 50 to 60 mph that resulted in no injury to the chest.

The main conclusions that can be drawn from this limited review of the effect of energy-absorbing steering columns is that recent improvements to the steering column are probably reducing fatalities and serious injuries. The severity of those chest injuries being sustained will decrease even more if the passenger-compartment longitudinal deceleration is decreased. (This conclusion is based on the assumption that no occupant ejection occurs.) The steering column collapse of 3.4 in. for test 221 and 3.6 in. for test 223 indicates that there would be a good possibility of little or no chest injuries being sustained during 60-mph head-on or nearly head-on collisions with the drum type of energy attenuator. This correlates well with the predicted severity based on passenger-compartment decelerations.

CONCLUSIONS

The results of the three full-scale tests reported herein indicate that the hazards presented by many existing gore-separation structures and other fixed objects can be significantly reduced by providing protection with energy-absorbing barriers incorporating 55-gal tight-head steel drums. Occupants of full-size vehicles (4,700 lb. including occupants) impacting these barriers at 60 mph will, in most cases, sustain little or no injury if wearing a seat belt and shoulder harness, minor injuries if wearing only a seat belt, and moderate injuries if unrestrained.

The fendering system tested did not satisfactorily redirect a vehicle impacting midway along the side of the barrier at an 11-deg angle with the barrier axis. Also, the

debris that resulted from this collision would definitely have been hazardous to adjacent traffic. Consequently, the fendering system included on the test barriers should not be used for an operational installation.

The reported average first cost of each of three freeway installations of energy-absorbing barriers incorporating 55-gal drums near Houston, Texas, was $3,600. As would be the case with most barriers, some on-site preparation was included in this cost. These barriers contained no fendering systems.

The maintenance costs for this barrier would probably be relatively high. Although no routine maintenance should be required, with the possible exception of checking the cable tension, relatively mild impacts will probably necessitate considerable repair work to restore the barrier's effectiveness. However, on-site repair time could be relatively short if prefabricated modules were used.

ACKNOWLEDGMENT

This work was accomplished in cooperation with the Federal Highway Administration. The opinions, findings, and conclusions expressed are those of the authors and not necessarily those of the Federal Highway Administration.

REFERENCES

1. Nordlin, E. F., Ames, W. H., Hackett, R. P., and Folsom, J. J. Dynamic Tests of Type 9 Bridge Barrier Rail and Type 8 Bridge Approach Guardrail. Highway Research Record 302, 1970, pp. 1-20.
2. Michie, J. D., Calcote, L. R., and Bronstad, M. E. Guardrail Performance and Design. NCHRP Final Rept., Phase I, Project No. 15-1(2), Southwest Research Institute, Jan. 1970.
3. Hirsch, T. J., and Ivey, D. L. Vehicle Impact Attenuation by Modular Crash Cushion. Texas Transportation Institute, Texas A&M Univ., Res. Rept. 146-1, June 1969.
4. Nordlin, E. F., Woodstrom, J. W., and Doty, R. N. Dynamic Tests of an Energy-Absorbing Barrier Employing Water-Filled Cells, Series 21. California Division of Highways, Nov. 1970.
5. Nordlin, E. F., Woodstrom, J. H., and Doty, R. N. Dynamic Tests of an Energy-Absorbing Barrier Employing Steel Drums, Series 21. California Division of Highways, Oct. 1970.
6. Nordlin, E. F., Ames, W. H., and Hackett, R. P. Dynamic Tests of the California Type 20 Bridge Barrier Rail, Series 23. California Division of Highways, Sept. 1970.
7. Nordlin, E. F., Ames, W. H., Kubel, L. G., and Chow, W. Evaluation of a Telemetry System for Use in Vehicle-Barrier Impact Tests. California Division of Highways, July 1969.
8. Damon, A., Stoudt, H. W., and MacFarland, R. A. The Human Body in Equipment Design. Harvard Univ. Press, 1966.
9. Vanderstempel, T. M. A Device to Lessen Injuries in Fixed Object Collisions. Traffic Engineering, Nov. 1966.
10. Tamanini, F. J., and Viner, J. G. Structural Systems in Support of Highway Safety. Office of Research and Development, Federal Highway Administration, paper presented at the ASCE National Meeting on Transportation Engineering, Washington, D.C., July 21-25, 1969.
11. Highway Barrier Analysis and Test Program, Summary Report for Period July 1960-July 1961. Cornell Aeronautical Laboratory, Inc., Rept. VJ-1472-V-3, July 1969.
12. Severy, D. N., ed. The Seventh Stapp Car Crash Conference Proceedings. Charles S. Thomas, publisher.
13. Olson, R. M., Post, E. R., and MacFarland, W. F. Tentative Service Requirements for Bridge Rail Systems. NCHRP Rept. 86, 1970.

14. Proceedings, General Motors Corporation Automotive Safety Seminar. General Motors Safety Research and Development Lab., July 11-17, 1968.
15. Federal Motor Vehicle Safety Standards. National Highway Safety Bureau, U.S. Department of Transportation, with amendments and interpretations through August 6, 1968.

Appendix

DETAILS OF HIGHWAY GORE DESIGN AND PERFORMANCE

The following figures contain pertinent data and photographs of the impact tests discussed in this report.

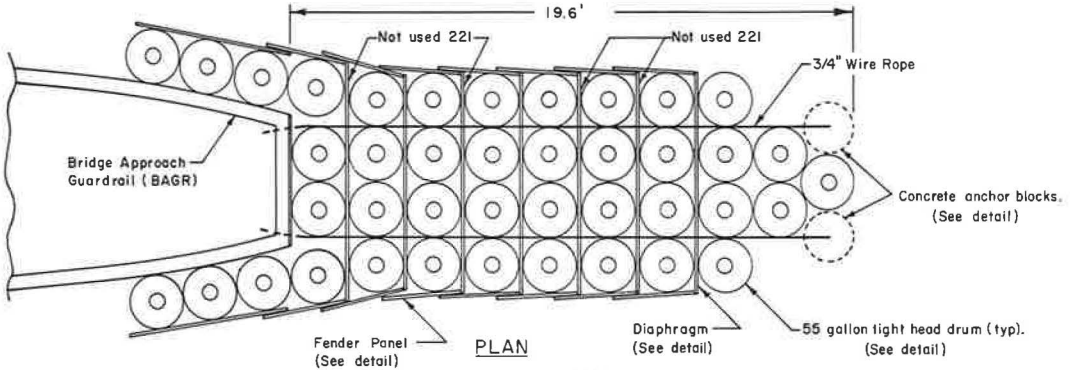

TEST BARRIER

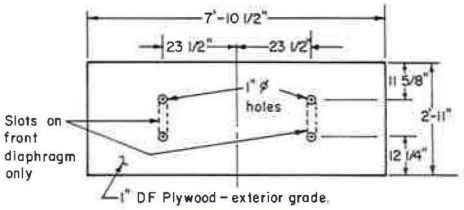

DIAPHRAGMS

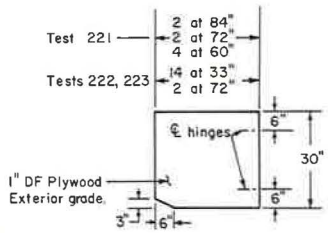

FENDER PANELS

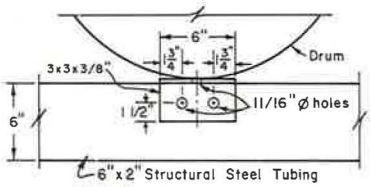

Attachment of rear drums to BAGR.

ENERGY ABSORBING BARRIER DETAILS

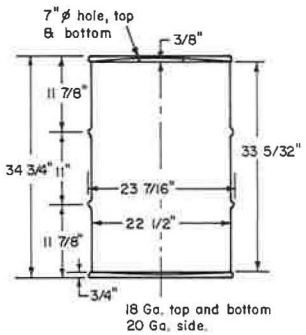

55 GALLON TIGHT HEAD DRUM

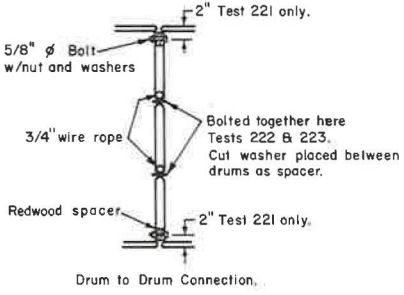

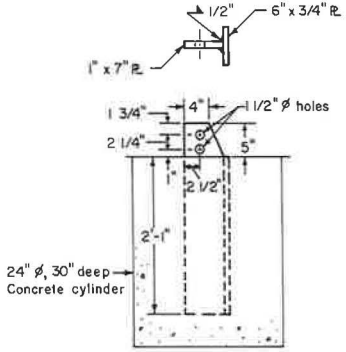

NOSE CABLE ANCHOR

Figure 17.

CALIFORNIA DIVISION OF HIGHWAYS

VEHICLE INSTRUMENTATION

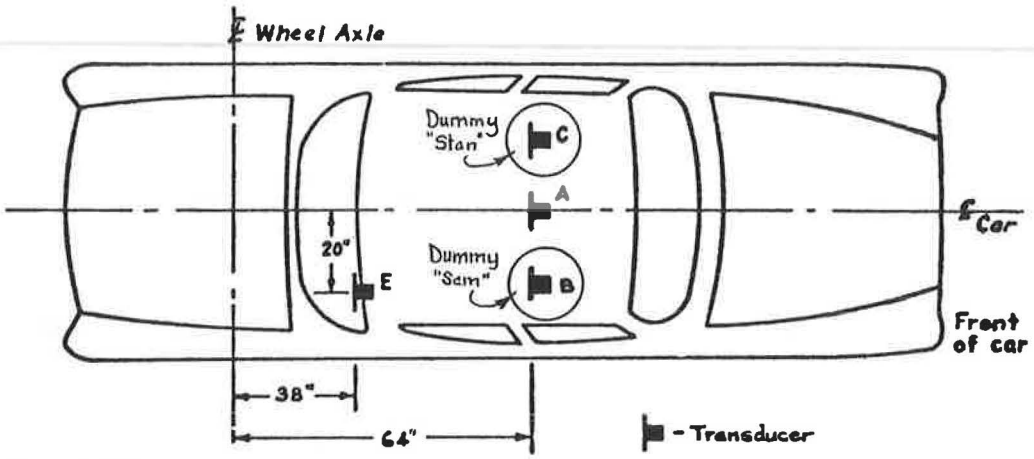

Test #221

CHANNEL NO.	LOCATION[1]	DESCRIPTION[2]
1	A	100 "G" longitudinal accelerometer (T)
2	E	100 "G" longitudinal accelerometer (T)
3	C	50 "G" longitudinal accelerometer (T)
4	C	50 "G" lateral accelerometer (T)
5	C	50 "G" vertical accelerometer (T)
6	C	Force meter in "Stan's" chest (T)
7	C	Lap belt tension transducer, "Stan" (T)

Test #222

1	A	100 "G" longitudinal accelerometer (T)
2	A	50 "G" lateral accelerometer (T)
3	E	100 "G" longitudinal accelerometer (T)
4	E	100 "G" lateral accelerometer (T)
5	C	50 "G" longitudinal accelerometer (T)
6	C	50 "G" lateral accelerometer (T)
7	C	50 "G" vertical accelerometer (T)
A	A	50 "G" lateral accelerometer (U)
B	E	100 "G" longitudinal accelerometer (U)
C	E	50 "G" lateral accelerometer (U)
D	B	50 "G" longitudinal accelerometer (U)

Test #223

1	A	100 "G" longitudinal accelerometer (U)
2	A	50 "G" lateral accelerometer (U)
3	C	50 "G" longitudinal accelerometer (U)
4	C	50 "G" lateral accelerometer (U)
5	E	50 "G" longitudinal accelerometer (U)

Notes:

[1] A and E on vehicle floor; B and C on back of dummy's chest cavity.

[2] (T) = FM telemetry, (U) = umbilical cord.

Figure 18.

CAMERA AND INSTRUMENTATION LOCATIONS AT BARRIER

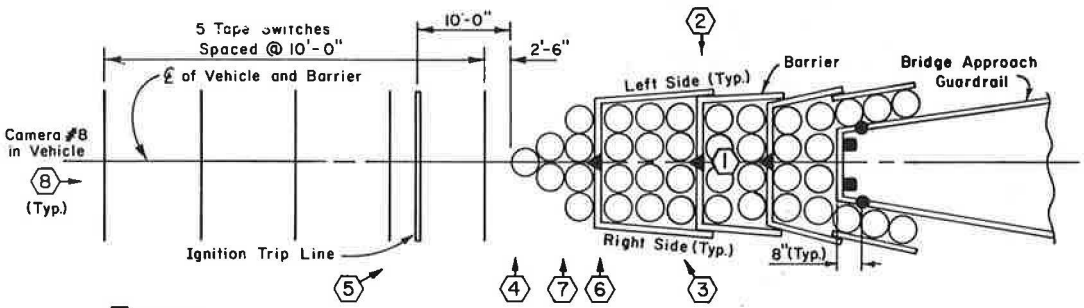

Cameras
Accelerometer (200 G's) Total 3.
Load cell (50 Kip min. capacity) Total 4.
Strain gage (℄ top surface, upper & lower rails, ℄ 8" behind nose of steel barrier) Total 4.

TEST 221

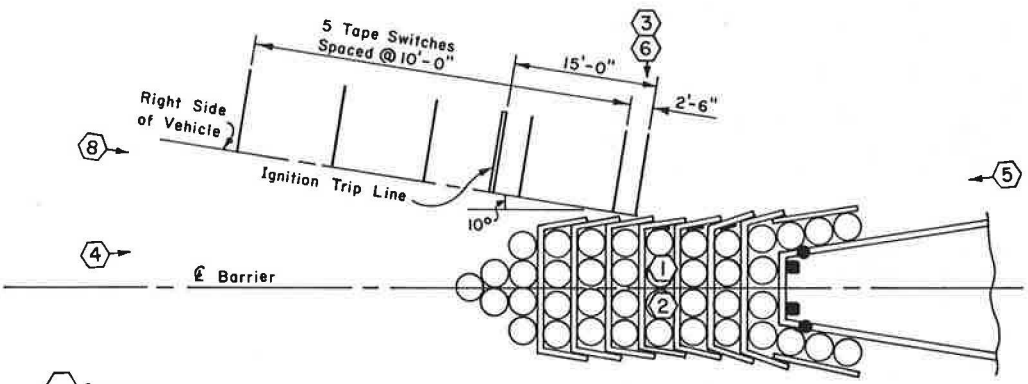

Cameras
Load cell (50 Kip min. capacity) Total 4.
Strain gage (℄ top surface, upper & lower rails. ℄ 8" behind nose of steel barrier) Total 4.
Strain gage on Fender Panel, Total 3.

TEST 222

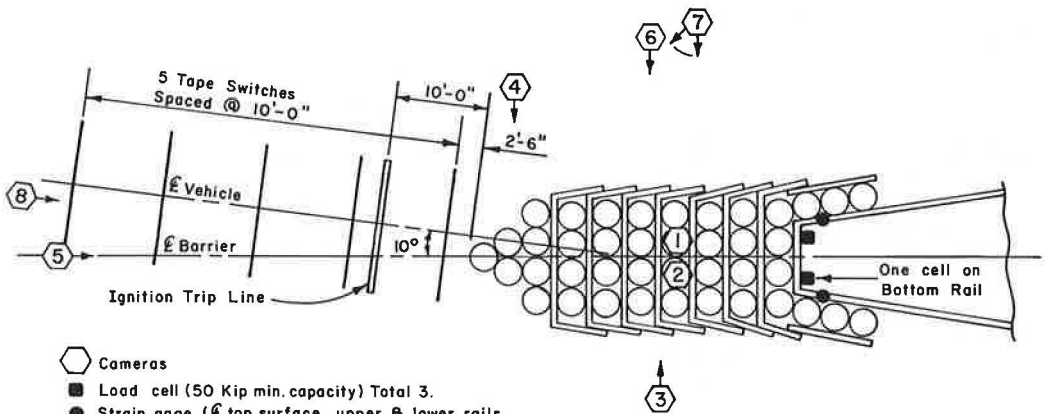

Cameras
Load cell (50 Kip min. capacity) Total 3.
Strain gage (℄ top surface, upper & lower rails.
℄ 8" behind nose of steel barrier) Total 4.

TEST 223

Figure 19.

Figure 20.

Barrier Depth	19.6 Ft.	Test No.	221
No. of Drums	41	Date	9-11-69
Permanent Displacement of Barrier Nose	10.7 Ft.	Vehicle	1968 Dodge
Deceleration Distance-Passenger Compartment	16.5 Ft.	Vehicle Weight	4690 Lbs.[2]
Maximum Vehicular Deformation	16.5 In.	(W/Dummy and Instrumentation)	
Steering Column Collapse[1]	3.4 In.	Impact Velocity	64.2 MPH
Passenger Compartment Deceleration (Highest 50 ms avg.)	10.3 G's	Impact Angle	Head-On
		Dummy Restraint	Lap Belt
Vehicle Average Deceleration-Calculated	8.4 G's		

[1] Energy Absorbing Steering Column - 1500 lb. design axial force required to initiate collapse.

[2] Left front door removed.

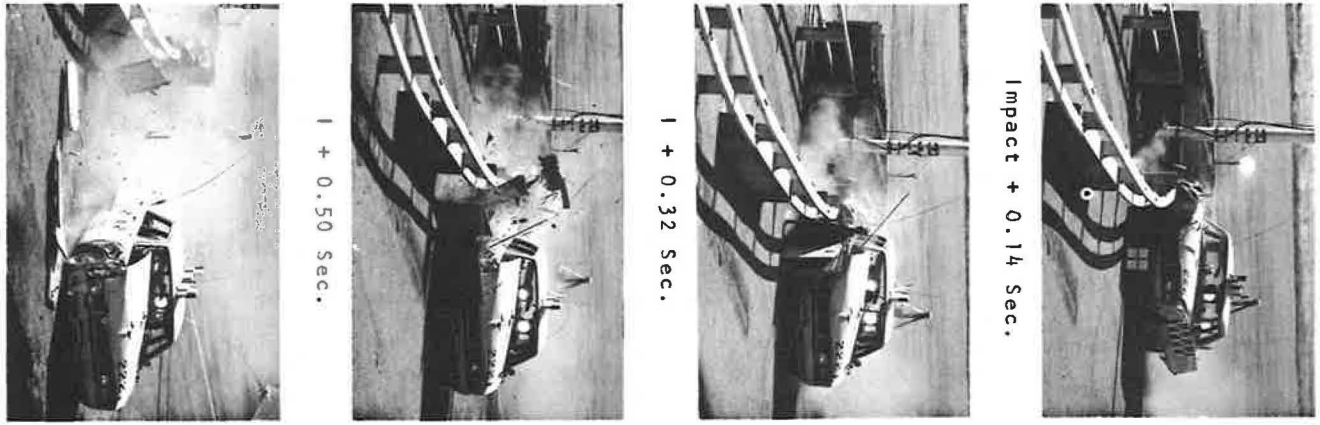

Figure 21.

Barrier Depth	19.6 Ft.	Test No.	222
No. of Drums	41	Date	11-21-69
Permanent Displacement of Barrier Nose	None	Vehicle	1968 Dodge
Deceleration Distance-Passenger Compartment	Redirected	Vehicle Weight (W/Dummy and Instrumentation)	4760 Lbs.
Maximum Vehicular Deformation	27 In.		
Steering Column Collapse[1]	None	Impact Velocity	59.8 MPH
Passenger Compartment Deceleration (Highest 50 ms avg.)	6.6 G's Long. 5.3 G's Lat.	Impact Angle	11° (Side)
		Dummy Restraint	Lap Belt
Vehicle Average Deceleration-Calculated	-		

[1] Energy Absorbing Steering Column - 1500 lb. design axial force required to initiate collapse.

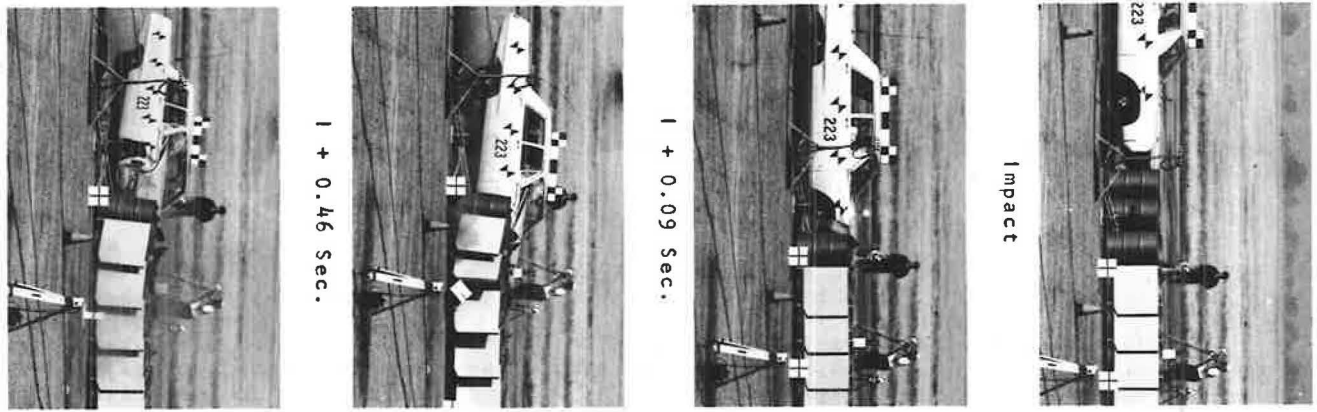

Figure 22.

Barrier Depth	19.6 Ft.	Test No.	223
No. of Drums	41	Date	12-5-69
Permanent Displacement of Barrier Nose	5.5 Ft.	Vehicle	1968 Dodge
Deceleration Distance-Passenger Compartment	13.2 Ft.	Vehicle Weight (W/Dummy and Instrumentation)	4740 Lbs.[3]
Maximum Vehicular Deformation	14.5 In.		
Steering Column Collapse[1]	3.6 In.	Impact Velocity	53.6 MPH
Passenger Compartment Deceleration (Highest 50 ms avg.)	10.9 G's Long.	Impact Angle	9° (Nose)
		Dummy Restraint	Lap Belt
Vehicle Average Deceleration-Calculated	7.2 G's[2]		

[1] Energy Absorbing Steering Column - 1500 lb. design axial force required to initiate collapse.

[2] Lateral components of deceleration not included.

[3] Lower legs removed from dummy placed in passenger location to facilitate handling of dummy.

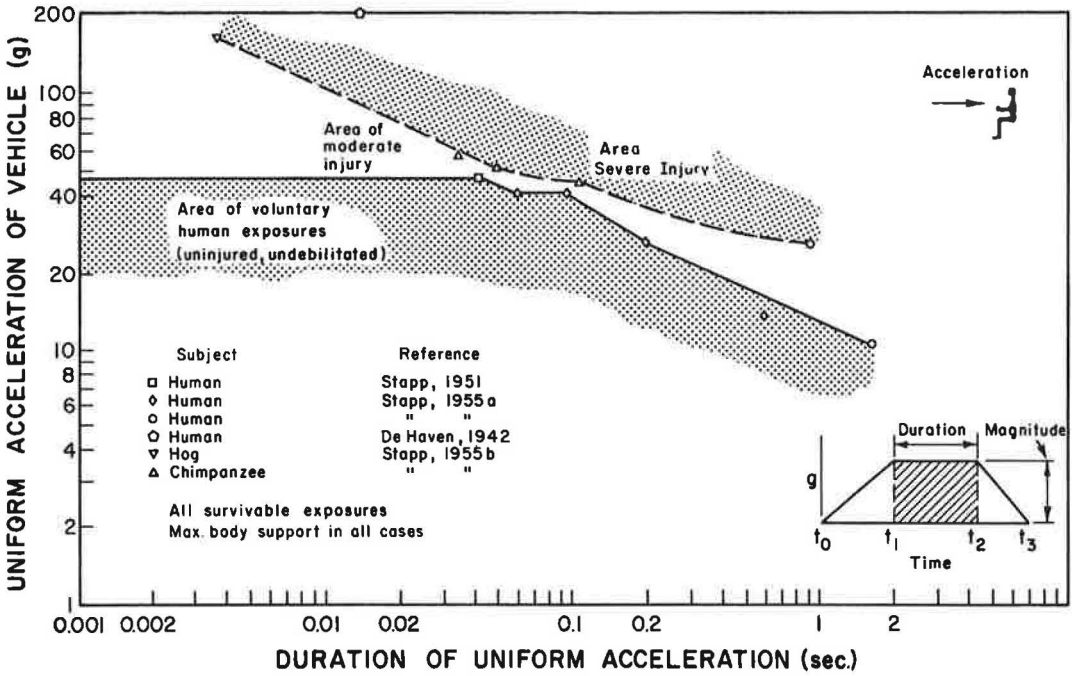
UNIFORM ACCELERATION OF VEHICLE (g)
200
100
80
60
40
20
10
8
6
4
2
1
0.001
0.002
0.01
0.02
0.1
0.2
1
2
DURATION OF UNIFORM ACCELERATION (sec.)
Area of moderate injury
Area Severe Injury
Area of voluntary human exposures (uninjured, undebilitated)
Acceleration
Subject
Reference
Human
Stapp, 1951
Human
Stapp, 1955a
Human
"
"
Human
De Haven, 1942
Hog
Stapp, 1955b
Chimpanzee
"
"
All survivable exposures
Max. body support in all cases
Duration
Magnitude
g
t_0
t_1
t_2
t_3
Time

Figure 23.